UNIVERSITY OF ALBERTA

FORECASTING OPEN WATER AND ICE RELATED FLOOD EVENTS USING HYDRAULIC MODELLING TECHNIQUES

by

JULIA L. BLACKBURN ©

A THESIS
SUBMITTED TO THE FACULTY OF GRADUATE STUDIES AND RESEARCH
IN PARTIAL FULFILLMENT OF THE REQUIREMENTS FOR THE DEGREE OF
MASTER OF SCIENCE

IN

WATER RESOURCES ENGINEERING

DEPARTMENT OF CIVIL & ENVIRONMENTAL ENGINEERING

EDMONTON, ALBERTA
FALL 2000

National Library
of Canada

Acquisitions and
Bibliographic Services

395 Wellington Street
Ottawa ON K1A 0N4
Canada

Bibliothèque nationale
du Canada

Acquisitions et
services bibliographiques

395, rue Wellington
Ottawa ON K1A 0N4
Canada

Your file Votre référence

Our file Notre référence

The author has granted a non-exclusive licence allowing the National Library of Canada to reproduce, loan, distribute or sell copies of this thesis in microform, paper or electronic formats.

L'auteur a accordé une licence non exclusive permettant à la Bibliothèque nationale du Canada de reproduire, prêter, distribuer ou vendre des copies de cette thèse sous la forme de microfiche/film, de reproduction sur papier ou sur format électronique.

The author retains ownership of the copyright in this thesis. Neither the thesis nor substantial extracts from it may be printed or otherwise reproduced without the author's permission.

L'auteur conserve la propriété du droit d'auteur qui protège cette thèse. Ni la thèse ni des extraits substantiels de celle-ci ne doivent être imprimés ou autrement reproduits sans son autorisation.

0-612-59780-6

Canada

UNIVERSITY OF ALBERTA

LIBRARY RELEASE FORM

Name of Author: Julia L. Blackburn

Title of Thesis: Forecasting Open Water and Ice Related Flood Events Using Hydraulic Modelling Techniques

Degree: Master of Science

Year this Degree Granted: 2000

Permission is hereby granted to the University of Alberta Library to reproduce single copies of this thesis and to lend or sell such copies for private or scientific purposes only.

The author reserves all other publication and other rights in association with the copyright in the thesis, and except as herein before provided, neither the thesis not any substantial portion thereof may be printed or otherwise reproduced in any material form whatever without the author's prior written permission.

Julia Blackburn

R. R. # 1
Long Sault, ON
K0C 1P0

Date: September 29, 2000

UNIVERSITY OF ALBERTA

Faculty of Graduate Studies and Research

The undersigned certify that they have read, and recommend to the Faculty of Graduate Studies and Research for acceptance, a thesis entitled **Forecasting Open Water and Ice Related Flood Events Using Hydraulic Modelling Techniques** by **Julia L. Blackburn** in partial fulfillment of the requirements for the degree of **Master of Science** in **Water Resources Engineering**.

FE Hicks
F. E. Hicks

P. M. Steffler

RB Rains
R. B. Rains

Date: September 29, 2000

ABSTRACT

Traditional *hydrologic* flood routing models are difficult to calibrate, cannot handle dynamic events such as ice jam release surges, and provide no information about associated flood levels. In contrast, *hydraulic* flood routing models are able to calculate water levels and model dynamic events. In this investigation, a hydraulic flood routing model was developed based on the Saint Venant equations adapted for flow in natural channels. This model was used to simulate two flood events: a summer flood event on the Peace River, Alberta and an ice jam release surge on the Saint John River, New Brunswick. The results of these two case studies indicate that use of natural channel geometry in a hydraulic flood routing model produces a flood forecasting tool that provides accurate water levels forecasts for both diffusive and dynamic flood events.

ACKNOWLEDGEMENTS

The author gratefully acknowledges the encouragement and support provided by her supervisor, Dr. Faye E. Hicks. Her enthusiasm and patient guidance throughout the research and particularly the writing of this thesis are most greatly appreciated.

The author would like to thank Dr. Sayed Ismail, New Brunswick Electric Power Commision, Dr. Spyros Beltaos, National Water Research Institute, Mr. Brian Burrell, and Mr. Pat Tang for providing the data for the Saint John River ice jam release event. Thanks are also extended to Mr. Jim Choles, River Engineering Branch, Alberta Environment, who supplied the data for the Peace River summer flood event.

The author sincerely thanks Dr. Bruce Rains and Dr. Peter Steffler for taking the time to review this thesis. In addition, Dr. Peter Steffler provided valuable input regarding the implementation of the numerical scheme used in this study. His advice is most gratefully appreciated.

The author would also like to thank Mr. Perry Fedun and Mr. Sheldon Lovell for their ongoing technical support throughout the course of this study. In addition, special thanks are extended to Mr. Lovell for his continual encouragement and support.

This thesis was financially supported through scholarships from the Natural Sciences and Engineering Research Council of Canada and the University of Alberta (Faculty of Graduate Studies and Faculty of Engineering). It was also supported through a grant from the Natural Sciences and Engineering Research Council of Canada. All are most gratefully acknowledged.

Finally, I would like to thank my parents, Hilary and Ian Blackburn, for their love, support and encouragement through the many, many years of studies.

TABLE OF CONTENTS

1. **INTRODUCTION** 1

2. **MODEL IMPLEMENTATION** 5

2.1 INTRODUCTION 5

2.2 EQUATIONS OF UNSTEADY OPEN CHANNEL FLOW 6

2.2.1 Introduction 6

2.2.2 General Form of the Saint Venant Equations 7

2.2.2.1 Other forms of the Saint Venant equations for rectangular channels 9

2.2.3 The Saint Venant Equations for Natural Channels 12

2.2.3.1 Determination of the longitudinal boundary friction slope 13

2.2.3.2 Determination of the momentum correction coefficient 16

2.2.3.3 Determination of the sinuosity factor 16

2.2.3.4 Other forms of the Saint Venant equations for natural channels 17

2.2.4 Boundary and Initial Conditions 20

2.3 APPPROXIMATIONS TO THE SAINT VENANT EQUATIONS 21

2.3.1 Introduction 21

2.3.2 The Kinematic Wave Approximation 21

2.3.3 The Diffusive Wave Approximation 23

2.3.4 Application of the Various Approximations of the Saint Venant Equations 25

2.3.5 Comparison of the Various Waves 27

2.4 DEVELOPMENT OF THE NATURAL CHANNEL HYDRAULIC FLOOD ROUTING MODEL 29

3. **OPEN CHANNEL FLOOD EVENT: PEACE RIVER, ALBERTA** 37

3.1 INTRODUCTION 37

3.2 DESCRIPTION OF THE STUDY REACH 38

3.3 AVAILABLE GEOMETRIC DATA 38

3.3.1 Geometric Database Developed from Limited Geometry 38

3.3.2 Natural Channel Data 40

3.3.3 Channel Resistance 41

3.4 AVAILABLE HYDROLOGIC DATA 42

3.4.1 WSC Gauge Data Available on the Peace River 42

3.4.2 WSC Gauge Data Available on Peace River Tributaries 42

3.5 NUMERICAL SIMULATION 44

3.5.1 Development of the input data sets 45

3.5.1.1 Boundary and initial conditions 45

3.5.1.2 Selection of the spatial and temporal discretization 46

3.5.2 Model Application 48

3.5.2.1 Discharge hydrographs 48

3.5.2.2 Water levels 50

3.5.2.3 Model blending issues 52

3.6 CONCLUSIONS 53

4. ICE RELATED FLOOD EVENT: SAINT JOHN RIVER, NEW BRUNSWICK 64

4.1 INTRODUCTION 64

4.2 MODELLING ICE JAM RELEASE SURGES 65

4.2.1 Introduction 65

4.2.2 Previous Studies 65

4.2.2.1 Henderson and Gerard (1981) 65

4.2.2.2 Beltaos and Krishnappan (1982) 68

4.2.2.3 Joliffe and Gerard (1982) 70

4.2.2.4 Wong, Beltaos and Krishnappan (1985) 71

4.2.2.5 Hicks, Steffler and Gerard (1992) 71

4.2.2.6 Saadé, Sarraf, and El-Jabi (1993) 74

4.2.2.7 Hicks, McKay, and Shabayek (1997) 76

4.2.2.8 Khan, Steffler, and Gerard (2000) 78

4.2.3 Need for Further Studies 79

4.3 DESCRIPTION OF THE STUDY REACH 79
4.4 DETAILS OF THE DOCUMENTED ICE JAM RELEASE EVENT 81
4.5 MODEL DATA REQUIREMENTS 82
- 4.5.1 Introduction 82
- 4.5.2 Geometric Data 82
- 4.5.3 Resistance 83
- 4.5.4 Boundary Conditions 84
  - *4.5.4.1 Upstream boundary condition* 84
  - *4.5.4.2 Downstream boundary condition* 84
  - *4.5.4.3 Lateral inflows* 85
- 4.5.5 Initial Conditions 85
- 4.5.6 Verification Data 86

4.6 MODEL APPLICATION 87
- 4.6.1 Introduction 87
- 4.6.2 Model Results 88
  - *4.6.2.1 Run No. 1* 89
  - *4.6.2.2 Run No. 2* 89
  - *4.6.2.3 Run No. 3* 91
  - *4.6.2.4 Run No. 4* 92
- 4.6.3 Discussion of Results 93

5. CONCLUSIONS AND RECOMMENDATIONS **106**

5.1 MODEL IMPLEMENTATION 106
5.2 OPEN CHANNEL FLOOD EVENT 107
5.3 ICE RELATED FLOOD EVENT 108
5.4 RECOMMENDATIONS TO FIELD RESEARCHERS 111
5.5 RECOMMENDATIONS TO NUMERICAL MODELLERS 111

REFERENCES **113**

APPENDIX A – IMPLEMENTATION OF THE CDG SCHEME TO THE SAINT VENANT EQUATIONS FOR NATURAL CHANNELS 117

A.1 INTRODUCTION 117

A.2 THE CHARACTERISTIC-DISSIPATIVE-GALERKIN FINITE ELEMENT SCHEME (HICKS AND STEFFLER, 1990) 117

A.3 WEAK STATEMENT, UPWINDING MATRIX AND JACOBIAN FOR THE cdg1-D MODEL (HICKS AND STEFFLER, 1990) 121

A.4 WEAK STATEMENT, UPWINDING MATRIX AND JACOBIAN FOR THE cdg1-Dn MODEL 129

A.5 HANDLING OF BOUNDARY CONDITIONS AND TRIBUTARIES IN BOTH THE cdg1-D AND cdg1-Dn MODELS 135

A.6 SELECTION OF NUMERICAL PARAMETER VALUES 136

A.6.1 Introduction 136

A.6.2 Selection of Convergence Tolerance 136

A.6.3 Selection of ω 136

A.6.4 Selection of θ 137

A.6.5 Approach to Updating the Upwinding Matrix 137

A.6.6 Summary 138

APPENDIX B – IMPLEMENTATION OF THE CDG SCHEME TO THE SAINT VENANT EQUATIONS FOR NATURAL CHANNELS 139

B.1 INTRODUCTION 139

B.2 STEADY FLOW TEST 139

B.3 UNSTEADY FLOW TEST 140

APPENDIX C – HANDLING OF NATURAL CHANNEL GEOMETRY IN THE cdg1-Dn MODEL 150

APPENDIX D – CROSS SECTIONS ALONG THE PEACE RIVER 156

LIST OF TABLES

Table 3.1 Location of key sites along the Peace River (after Hicks, 1996). 40

Table 3.2 Manning's *n* values used in this investigation (after Hicks, 1996). 42

Table 3.3 Peace River tributaries considered in this investigation 43

Table 3.4 Comparison of mass conservation properties of the natural and approximate channel models. 48

Table 3.5 Comparison of peak discharge accuracy of the natural and approximated channel models. 49

Table 4.1 Location of key sites along the Saint John River (adapted from Hicks *et al.*, 1997). 80

Table A.1 Numerical parameter values for unsteady and steady flow. 138

Table B.1 Test results: transition from a mild to a steep channel. 140

Table B.2 Comparison of conservation properties of cdg1-D and cdg1-Dn. 143

LIST OF FIGURES

Figure 2.1 Definition of stage in open channel flow. 35

Figure 2.2 Relationship between main channel and floodplain (after Delong, 1986). 35

Figure 2.3 Sketch of a single –valued rating curve (uniform flow) and a looped rating curve (dynamic waves). 36

Figure 3.1 Location map of the Peace River study reach. 54

Figure 3.2 Dunvegan subreach showing the location of available cross sections. 55

Figure 3.3 Town of Peace River subreach showing the location of available cross sections. 56

Figure 3.4 Fort Vermilion subreach showing the location of available cross sections. 57

Figure 3.5 Variation in the initial discharge over the Dunvegan subreach. 58

Figure 3.6 Comparisons of measured and computed discharge hydrographs for the 1987 flood event. 59

Figure 3.7 Comparison of measured and computed water levels for the 1987 flood event. 60

Figure 3.8 Computed rating curves for the 1987 event using the cdg1-Dn model. 61

Figure 3.9 Comparison of the peak stage calculated using HEC-RAS and cdg1-Dn along the Town of Peace River subreach. 62

Figure 3.10 Comparison of computed hydrographs at the location of the downstream ends of the natural subreaches. 63

Figure 4.1 The ice jam release problem treated as a classic dam break. 96

Figure 4.2 Comparison of hydrographs produced downstream of an ice jam release. 97

Figure 4.3 Location map of the study reach along the Saint John River. 98

Figure 4.4 Measured ice jam profile and an example of the water levels used in one of the ice jam release simulations. 99

Figure 4.5 Comparison of measured and computed flows and stages for run No.1. 100

Figure 4.6 Comparison of measured and computed flows and stages for run No.2. 101

Figure 4.7 Comparison of measured and computed flows and stages for run No.3. 102

Figure 4.8 Comparison of measured and computed flows and stages for run No.4. 103

Figure 4.9 Computed discharge profiles for (a) run No.1 and (b) run No.4. 104

Figure 4.10 Computed water level profiles for (a) run No.1 and (b) run No.4. 105

Figure B.1 Transition from a mild to a steep slope, cdg1-Dn, at 4000 time steps. 144

Figure B.2 Transition from a mild to a steep slope, cdg1-D, at 4000 time steps. 145

Figure B.3 Dam break, $H_1/H_0 = 0.5$, initial conditions. 146

Figure B.4 Dam break, $H_1/H_0 = 0.5$. 147

Figure B.5 Dam break, $H_1/H_0 = 0.05$, initial conditions. 148

Figure B.6 Dam break, $H_1/H_0 = 0.05$. 149

Figure C.1 Composite sections used to determine the number of topwidths required to adequately define a composite section in cdg1-Dn. 152

Figure C.2 Area versus stage curves for all four composite sections, where n is the number of topwidths defining a section. 153

Figure C.3 Compound sections used to determine the number of topwidths required to adequately define a compound section in cdg1-Dn. 154

Figure C.4 Area versus stage curves for all four compound sections, where n is the number of topwidths defining a section. 155

Figure D.1 Cross section on the Peace River at 293.60 km downstream of the Bennett Dam (Dunvegan subreach). 157

Figure D.2 Cross section on the Peace River at 294.50 km downstream of the Bennett Dam (Dunvegan subreach). 158

Figure D.3 Cross section on the Peace River at 295.20 km downstream of the Bennett Dam (Dunvegan subreach). 159

Figure D.4 Cross section on the Peace River at 295.90 km downstream of the Bennett Dam (Dunvegan subreach). 160

Figure D.5 Cross section on the Peace River at 296.70 km downstream of the Bennett Dam (Dunvegan subreach). 161

Figure D.6 Cross section on the Peace River at 297.30 km downstream of the Bennett Dam (Dunvegan subreach). 162

Figure D.7 Cross section on the Peace River at 298.10 km downstream of the Bennett Dam (Dunvegan subreach). 163

Figure D.8 Cross section on the Peace River at 298.90 km downstream of the Bennett Dam (Dunvegan subreach). 164

Figure D.9 Cross section on the Peace River at 299.10 km downstream of the Bennett Dam (Dunvegan subreach). 165

Figure D.10 Cross section on the Peace River at 299.70 km downstream of the Bennett Dam (Dunvegan subreach). 166

Figure D.11 Cross section on the Peace River at 369.80 km downstream of the Bennett Dam (Town of Peace River subreach). 167

Figure D.12 Cross section on the Peace River at 375.20 km downstream of the Bennett Dam (Town of Peace River subreach). 168

Figure D.13 Cross section on the Peace River at 377.90 km downstream of the Bennett Dam (Town of Peace River subreach). 169

Figure D.14 River at 380.85 km downstream of the Bennett Dam (Town of Peace River subreach). 170

Figure D.15 Cross section on the Peace River at 382.35 km downstream of the Bennett Dam (Town of Peace River subreach). 171

Figure D.16 Cross section on the Peace River at 384.85 km downstream of the Bennett Dam (Town of Peace River subreach). 172

Figure D.17 Cross section on the Peace River at 386.05 km downstream of the Bennett Dam (Town of Peace River subreach). 173

Figure D.18 Cross section on the Peace River at 390.00 km downstream of the Bennett Dam (Town of Peace River subreach). 174

Figure D.19 Cross section on the Peace River at 391.80 km downstream of the Bennett Dam (Town of Peace River subreach). 175

Figure D.20 Cross section on the Peace River at 393.50 km downstream of the Bennett Dam (Town of Peace River subreach). 176

Figure D.21 Cross section on the Peace River at 394.40 km downstream of the Bennett Dam (Town of Peace River subreach). 177

Figure D.22 Cross section on the Peace River at 394.72 km downstream of the Bennett Dam (Town of Peace River subreach). 178

Figure D.23 Cross section on the Peace River at 395.10 km downstream of the Bennett Dam (Town of Peace River subreach). 179

Figure D.24 Cross section on the Peace River at 395.58 km downstream of the Bennett Dam (Town of Peace River subreach). 180

Figure D.25 Cross section on the Peace River at 395.65 km downstream of the Bennett Dam (Town of Peace River subreach). 181

Figure D.26 Cross section on the Peace River at 395.95 km downstream of the Bennett Dam (Town of Peace River subreach). 182

Figure D.27 Cross section on the Peace River at 396.35 km downstream of the Bennett Dam (Town of Peace River subreach). 183

Figure D.28 Cross section on the Peace River at 396.95 km downstream of the Bennett Dam (Town of Peace River subreach). 184

Figure D.29 Cross section on the Peace River at 397.65 km downstream of the Bennett Dam (Town of Peace River subreach). 185

Figure D.30 Cross section on the Peace River at 398.40 km downstream of the Bennett Dam (Town of Peace River subreach). 186

Figure D.31 Cross section on the Peace River at 400.40 km downstream of the Bennett Dam (Town of Peace River subreach). 187

Figure D.32 Cross section on the Peace River at 404.00 km downstream of the Bennett Dam (Town of Peace River subreach). 188

Figure D.33 Cross section on the Peace River at 405.95 km downstream of the Bennett Dam (Town of Peace River subreach). 189

Figure D.34 Cross section on the Peace River at 408.58 km downstream of the Bennett Dam (Town of Peace River subreach). 190

Figure D.35 Cross section on the Peace River at 411.20 km downstream of the Bennett Dam (Town of Peace River subreach). 191

Figure D.36 Cross section on the Peace River at 412.39 km downstream of the Bennett Dam (Town of Peace River subreach). 192

Figure D.37 Cross section on the Peace River at 412.84 km downstream of the Bennett Dam (Town of Peace River subreach). 193

Figure D.38 Cross section on the Peace River at 415.65 km downstream of the Bennett Dam (Town of Peace River subreach). 194

Figure D.39 Cross section on the Peace River at 804.30 km downstream of the Bennett Dam (Fort Vermilion subreach). 195

Figure D.40 Cross section on the Peace River at 806.00 km downstream of the Bennett Dam (Fort Vermilion subreach). 196

Figure D.41 Cross section on the Peace River at 807.00 km downstream of the Bennett Dam (Fort Vermilion subreach). 197

Figure D.42 Cross section on the Peace River at 809.50 km downstream of the Bennett Dam (Fort Vermilion subreach). 198

Figure D.43 Cross section on the Peace River at 810.80 km downstream of the Bennett Dam (Fort Vermilion subreach). 199

Figure D.44 Cross section on the Peace River at 804.30 km downstream of the Bennett Dam (Fort Vermilion subreach). 200

LIST OF SYMBOLS

A	cross sectional area perpendicular to the flow
A_c	main channel cross sectional area perpendicular to the flow
A_l	left floodplain cross sectional area perpendicular to the flow
A_o	inactive cross sectional flow area or off-channel storage
A_r	right floodplain cross sectional area perpendicular to the flow
$[\mathbf{A}]_r$	convection matrix for the Saint Venant equations, applicable to rectangular channels
$[\mathbf{A}]_c$	convection matrix for the Saint Venant equations, applicable to natural channels
B	channel width (and ice pack width)
$[\mathbf{B}]$	coefficient matrix for the Saint Venant equations, applicable to natural channels
C	Courant number
C_c	conservation form of the continuity equation
C_{nc}	non-conservation form of the continuity equations
c	celerity of a small gravity wave
d	depth to the phreatic surface within an equilibrium jam
$\{F\}_n$	'pseudo' flux vector for the Saint Venant equations, applicable to natural channels

$\{F\}_r$	flux vector for the Saint Venant equations, applicable to rectangular channels
ΔF	net force (in calculation of percent error in momentum conservation for dam break test)
f_i, f_j	interpolation function
$\{f\}_{n,c}$	source terms for the Saint Venant equations, applicable to natural channels, 'pseudo' conservation form
$\{f\}_{n,nc}$	source terms for the Saint Venant equations, applicable to natural channels, non-conservation form
$\{f\}_{r,c}$	source terms for the Saint Venant equations, applicable to rectangular channels, conservation form
$\{f\}_{r,nc}$	source terms for the Saint Venant equations, applicable to rectangular channels, non-conservation form
g	acceleration due to gravity
H	elevation of the water surface above a specified datum, also called stage
h	depth of flow
i	integer indices
$[J]$	Jacobian matrix
J,k	depth index
K	conveyance factor
K_c	conveyance factor for the main channel
K_l	conveyance factor for the left floodplain

K_r	conveyance factor for the right floodplain
$[K]$	stiffness matrix
k	composite roughness height
k_i	ice roughness height
k_b	bed roughness height
L	length of the domain
M_c	conservation form of the momentum equation
M_{nc}	non-conservation form of the momentum equation
M	mass
$\dot{M}$	rate of change of momentum
m	any known function
N	number of computational nodes
n	Manning's roughness coefficient
n_c	Manning's roughness coefficient for the main channel
n_l	Manning's roughness coefficient for the left floodplain
n_r	Manning's roughness coefficient for the right floodplain
n	integer index
P	wetted perimeter
P_c	wetted perimeter for the main channel

P_l	wetted perimeter for the left floodplain
P_r	wetted perimeter for the right floodplain
p	integer index
Q	discharge
Q_o	uniform flow discharge
q	unit discharge
R	hydraulic radius
R_c	hydraulic radius for the main channel
R_l	hydraulic radius for the left floodplain
R_r	hydraulic radius for the right floodplain
$\{R\}$	Residual
$[S]$	stiffness matrix
S_f, S_{fx}	longitudinal boundary friction slope
S_{fy}	transverse boundary friction slope
S_i	specific gravity of ice
S_o, S_{xo}	longitudinal channel bed slope
S_{yo}	transverse channel bed slope
s	sinuosity factor to account for channel meandering
T	top width of the active cross sectional flow area

T_o	top width of the inactive cross sectional flow area
t	temporal coordinate
U	cross sectional averaged longitudinal velocity
u	depth averaged longitudinal velocity
V_n	speed of the negative wave
V_w	speed of the wave
v	depth averaged transverse velocity
$[\mathbf{W}]$	upwinding matrix
x	longitudinal coordinate
y	transverse coordinate
y_b	is the elevation of the channel bottom above some datum
$\bar{y}$	depth from the surface to the centroid of the cross section
β	momentum flux correction coefficient to account for a non-uniform velocity distribution
Φ	solution vector
ϕ	angle between the channel bed and the horizontal
η	non-dimensional depth to the phreatic surface at an equilibrium section of a fully developed ice jam
φ	conversion factor for the employed system of units (1.00 for SI units or 1.49 for Imperial units)

λ	eigenvalues
μ	ice jam internal friction-porosity coefficient
θ	implicitness, ice cover thickness
ω	upwinding coefficient

CHAPTER 1

INTRODUCTION

Historically, water has been the most expedient and common medium for travel or transportation of goods. Consequently, many urban and rural centres are adjacent to rivers. In these areas, it is essential that engineers are able to predict the timing and magnitude of an incoming flood wave in order to provide ample time to warn or evacuate the populace who may be in danger. This is known as real-time flood forecasting. The propagation of a flood wave is also of interest to engineers with regards to the design and operation of structures such as culverts, dams, pipelines, water intakes and bridges. The process of calculating the propagation of this unsteady phenomenon is known as channel routing or flood routing. As a flood wave travels downstream, channel storage and friction effects attenuate the flood peak (lengthen and flatten the flood wave). Therefore, knowing the streamflow at one site (known as a gauging station), a 'routing model' serves to determine by how much the shape of the flood hydrograph has changed at a downstream station.

There are two possible approaches to the flood routing problem available to engineers, namely, hydrologic and hydraulic flood routing techniques. Hydrologic models are based on conservation of mass and an empirical storage-flow relation to approximate momentum effects (Watt, *et al.*, 1989). These models are very economical from the data perspective, as they only require streamflow hydrographs as input. Hydraulic models are based on the laws of physics and require physical data. Therefore, in addition to streamflow data, hydraulic models require a sophisticated mathematical model of mass and momentum conservation and adequate information describing the channel geometry and resistance characteristics (Hicks, 1996).

The main disadvantage of hydrologic models is that output is limited to the discharge hydrographs and only at the gauging stations used in their calibration. In contrast, hydraulic routing models have the ability to produce output describing stage (water level), and discharge hydrographs *at* and *between* gauge stations. In addition, because they do not have any terms to handle dynamic effects, the application of hydrologic models to dynamic problems, such as dam breaches or ice jam release events, is not suitable. Despite these disadvantages, many flood forecasters continue to use hydrologic models over hydraulic models. This is because flood routing problems typically involve reaches that are hundreds of kilometres long for which the cross-sectional data requirements for a hydraulic model would be too costly to obtain.

Recent investigations (Hicks, 1996; Hicks *et al.*, 1994; Hicks and McKay, 1995; McKay *et al.*, 1996) have revealed that hydraulic routing can be used successfully to determine discharge hydrographs in reaches where few channel geometry data are available. This was achieved by approximating the modelled reach by a rectangular channel. The rectangular geometric database for the hydraulic model was developed using limited cross section data supplemented with channel slope and top width data obtained from topographic maps. Although a hydraulic routing model was used in those investigations, which can technically calculate discharges and water levels, they found that the 'limited geometry model' could accurately determine discharges but not water levels. They speculated that the poor water level accuracy was attributable to the use of approximate geometry when a detailed 'natural channel model' is essential to accurately predict flood stages and to ultimately delineate the floodplain.

In practice, it is too costly to obtain data everywhere along the types of reaches involved in flood routing problems. However, it is typically only of interest to the engineer to be able to predict flood levels at a few key sites, such as populated areas, not along an entire reach. Therefore, the first objective of this study was to determine whether it is possible to blend the 'limited geometry model' and the 'natural channel model' into one model so that, operationally, flood forecasting could include the determination of accurate flood levels. In practical applications, floodplain delineation involves two steps. First, a flood routing model (usually hydrologic) is used to obtain the flood peak. This flood peak would then provide the input for a steady gradually varied flow model based on detailed geometry (such as the HEC-RAS model) in order to determine flood levels at key sites.

Therefore, the ability to blend approximate and detailed geometry would reduce floodplain delineation to one step.

All Water Survey of Canada (WSC) gauge sites are placed at locations along a river to measure water levels where there is a unique relationship between stage (water level) and discharge. This relationship is called a rating curve. Rating curves are very reliable during open water conditions. However, during the winter when a river is covered with ice, the relationship between stage and discharge is no longer unique, as stage is also dependent on the thickness and roughness of the ice cover. It is generally unsafe to measure discharge directly and so, since only water levels are known during ice related events, flood routing during these periods warrants the use of natural channel geometry and hence the use of a hydraulic model. Therefore, the second objective is to assess whether a hydraulic flood routing model based on detailed natural channel geometry can be used to route an ice related flood event.

Chapter 2 presents the details associated with the development of the natural channel hydraulic model, used in this study, which is called the cdg1-Dn model. These details include the one-dimensional equations of open channel flow, known as the Saint Venant equations, and the numerical technique employed to solve them. Approximations to these equations, called the kinematic wave and the diffusive wave, are presented to illustrate their applicability in the context of flood routing. Due to the form of the Saint Venant equations for natural channels, some difficulties arose in the implementation of the chosen numerical scheme, which are also discussed in Chapter 2.

In Chapter 3, the first objective of this study is investigated using an open water event that occurred on the Peace River, Alberta in the summer of 1987. The chapter describes the numerical and river hydraulic issues that had to be addressed to accomplish this objective. The computed results are compared to those obtained using the 'limited geometry approach' and the observed data for the event.

Chapter 4 investigates the second objective using an ice jam release event that occurred on the Saint John River in New Brunswick, in the spring of 1993. This ice related event was chosen because it is the type of dynamic event that flood forecasters may encounter that requires the use of a hydraulic flood routing model. Chapter 5 presents the summary and conclusions, along with recommendations for further research.

CHAPTER 2

MODEL IMPLEMENTATION

2.1 INTRODUCTION

In order to investigate the objectives of this study, a hydraulic model capable of modelling natural channels was required. The hydraulic flood routing studies that employed the 'limited geometry approach' used the cdg1-D model, which solves the one-dimensional unsteady open channel flow equations, also called the Saint Venant equations. However, the cdg1-D model is limited to the case where the channel is approximated by a rectangular channel of varying width (Hicks and Steffler, 1990; 1992). The cdg1-D model solves the Saint Venant equations in a conservation form (to be explained later) using the Characteristic Dissipative Galerkin (CDG) finite element scheme (Hicks and Steffler, 1990; 1992).

Comparisons of the CDG scheme with finite difference schemes and other finite element schemes have demonstrated the superiority of this finite element scheme with respect to solution accuracy and numerical stability for open channel flow problems (Hicks and Steffler, 1990, 1992). Because of its robustness and its success in the limited geometry hydraulic flood routing studies, it was decided to employ the CDG scheme in the current investigation to solve the Saint Venant equations for natural channels.

In implementing the CDG for natural channels, a number of issues arose. The first is due to the inability to manipulate the natural channel equations into a fully conservation formulation, which inhibits both mass and momentum from being perfectly conserved. The second stems from the fact that it is not possible to correctly implement the dissipative component of the CDG scheme, which may prevent the appropriate dampening of numerical oscillations. The CDG scheme uses a Newton-Raphson iteration to advance the solution to the next time step. Due to these two issues, it is more difficult for the solution to converge and therefore stability problems arise.

In order to explain these issues, this chapter first presents the equations of one-dimensional unsteady open channel flow, including both rectangular channel and natural channel forms. This is followed by a discussion of the various flow approximations to the Saint Venant equations and their applicability in the context of flood routing. Lastly, the issues of implementing the CDG scheme to solve natural channel equations are discussed in detail.

2.2 EQUATIONS OF UNSTEADY OPEN CHANNEL FLOW

2.2.1 Introduction

The flow in an open channel, artificial or natural, varies in all three spatial dimensions. For example, in a river, the velocity varies along its length (longitudinal direction), across its width (transverse direction), and also from the river bed to the water surface (vertical direction). However, for many practical purposes including flood routing, the spatial variation in the velocity in the transverse and vertical directions can be neglected, so that the overall flow can be approximated as varying in only one spatial dimension: the longitudinal direction (Chow, 1959). Sediment transport also plays a role in the flow in natural channels. However, it is an extremely complex problem that depends on the three dimensional and turbulent aspects of the flow. Therefore, the use of the one-dimensional flow approximation does not warrant the quantification of mobile bed hydraulics. In using the Saint Venant equations for flood routing, the effects of sediment transport are not entirely neglected but instead incorporated into the roughness characteristics of a channel.

2.2.2 General Form of the Saint Venant Equations

The Saint Venant equations can be formulated by applying the principles of mass and momentum conservation to a one-dimensional control volume with a rigid boundary. The equations are comprised of one equation of mass conservation and one equation of momentum conservation where discharge, Q, and water cross sectional area, A, are the dependent variables.

Conservation of Mass:

$$\frac{\partial A}{\partial t}+\frac{\partial Q}{\partial x}=0 \qquad [2.1]$$

Conservation of Momentum:

$$\frac{\partial Q}{\partial t}+\frac{\partial (Q^2/A)}{\partial x}+gA\frac{\partial h}{\partial x}-gAS_o+gAS_f=0 \qquad [2.2]$$

where:

A = cross sectional area perpendicular to the flow;

g = acceleration due to gravity;

h = depth of flow;

Q = discharge;

S_f = longitudinal boundary friction slope;

S_o = longitudinal channel bed slope;

t = temporal coordinate; and

x = longitudinal coordinate.

The following assumptions were made in the derivation of these equations:

1) the flow varies only in the longitudinal direction;
2) the pressure distribution is hydrostatic;
3) the velocity distribution is uniform across the channel;
4) the friction formulae for steady flow are applicable to unsteady flow;
5) the channel is straight with a horizontal water surface across the width (no flow superelevation);
6) the fluid (water) is incompressible;
7) the channel slope is small enough that $\phi \cong \sin\phi$ where ϕ is the angle the bed makes with the horizontal;
8) both dependent variables, Q and A, are continuous differentiable functions (i.e. the flow and cross sectional area vary gradually).

Equation [2.1] is also referred to as the continuity equation. The continuity equation states that the change in flow per unit length (in the flow direction) into a control volume is equal to the change in flow area per unit time (Ponce, 1989). In equation [2.2], the momentum equation, the first and second terms represent the temporal and local acceleration, respectively. Together, they describe the effects of inertial forces on the flow. The third term is often referred to as the "pressure term" and represents the net longitudinal pressure force as a result of changes in channel width and water depth in the longitudinal direction.

2.2.2.1 Other forms of the Saint Venant equations for rectangular channels

If the cross sectional area, A, may be approximated as a rectangular section using

$$A = Bh \tag{2.3}$$

where B is the channel width, then the pressure term in equation [2.2] can described using,

$$gA\frac{\partial h}{\partial x} = gBh\frac{\partial h}{\partial x} = \frac{\partial}{\partial x}\left(\frac{gAh}{2}\right) - \frac{gAh}{2B}\frac{dB}{dx} \tag{2.4}$$

to obtain:

$$\frac{\partial Q}{\partial t} + \frac{\partial(Q^2 / A)}{\partial x} + \frac{\partial}{\partial x}\left(\frac{gAh}{2}\right) - \frac{gAh}{2B}\frac{dB}{dx} - gAS_o + gAS_f = 0 \tag{2.5}$$

In equation [2.4], the change in channel width, B, per unit length, x, is a total derivative rather than a partial derivative because B is only a function of x and not of t. Because no dependent variables appear outside of the partial derivatives, equation [2.5] is called the conservation form of the momentum equation (Liggett, 1975) for a rectangular channel.

Still approximating the cross sectional area by a rectangular section, the momentum equation can also be written in non-conservation form by manipulating the pressure term in equation [2.2] using:

$$gh\frac{\partial A}{\partial x} = g\frac{A}{B}\frac{\partial(Bh)}{\partial x} = g\frac{A}{B}\left(B\frac{\partial h}{\partial x} + h\frac{dB}{dx}\right) = gA\frac{\partial h}{\partial x} + \frac{gAh}{B}\frac{dB}{dx} \tag{2.6}$$

The discharge, Q, and the cross sectional area, A, are related by the following equation:

$$Q = AU \tag{2.7}$$

where U is the cross sectionally averaged longitudinal velocity. Knowing this relationship, the local acceleration term can be described using:

$$\frac{\partial(Q^2/A)}{\partial x}=\frac{\partial(AU^2)}{\partial x}=U\frac{\partial(AU)}{\partial x}+AU\frac{\partial U}{\partial x}=U\left(\frac{\partial Q}{\partial x}+A\frac{\partial U}{\partial x}\right)$$
$$=U\left(\frac{\partial Q}{\partial x}+\frac{\partial(AU)}{\partial x}-U\frac{\partial A}{\partial x}\right)=2U\frac{\partial Q}{\partial x}-U^2\frac{\partial A}{\partial x} \qquad [2.8]$$

Substituting equations [2.6] and [2.8] into equation [2.2], results in:

$$\frac{\partial Q}{\partial t}+2U\frac{\partial Q}{\partial x}+\left(gh-U^2\right)\frac{\partial A}{\partial x}-\frac{gAh}{B}\frac{dB}{dx}-gAS_o+gAS_f=0 \qquad [2.9]$$

When equation [2.9] is combined with the continuity equation ([2.1]), the two can be presented in matrix form,

$$\frac{\partial}{\partial t}\begin{Bmatrix}A\\Q\end{Bmatrix}+\begin{bmatrix}0 & 1\\gh-U^2 & 2U\end{bmatrix}\frac{\partial}{\partial x}\begin{Bmatrix}A\\Q\end{Bmatrix}+\begin{Bmatrix}0\\gA\left(S_f-S_o-\dfrac{h}{B}\dfrac{dB}{dx}\right)\end{Bmatrix}=\{0\} \qquad [2.10]$$

or as,

$$\frac{\partial\{\Phi\}}{\partial t}+[\mathbf{A}]_r\frac{\partial\{\Phi\}}{\partial x}+\{f\}_{r,nc}=\{0\} \qquad [2.11]$$

where:

$$\{\Phi\}\equiv\begin{Bmatrix}A\\Q\end{Bmatrix} \qquad [2.12]$$

is the called the solution vector;

$$[\mathbf{A}]_r=\begin{bmatrix}0 & 1\\gh-U^2 & 2U\end{bmatrix}=\begin{bmatrix}0 & 1\\c^2-U^2 & 2U\end{bmatrix} \qquad [2.13]$$

is known as the convection matrix where

$$c=\sqrt{gh} \qquad [2.14]$$

is the celerity of a small gravity wave; and

$$\{f\}_{r,nc} = \begin{Bmatrix} 0 \\ gA\left(S_f - S_o - \dfrac{h}{B}\dfrac{dB}{dx}\right) \end{Bmatrix} \qquad [2.15]$$

represents the source terms.

Neglecting terms associated with variations in the channel width (in time and space), the Saint Venant equations may be written for a rectangular prismatic channel (Henderson, 1966):

$$\frac{\partial h}{\partial t} + \frac{\partial (Uh)}{\partial x} = 0 \qquad [2.16]$$

$$\frac{\partial U}{\partial t} + U\frac{\partial U}{\partial x} + g\frac{\partial h}{\partial x} = g\left(S_o - S_f\right) \qquad [2.17]$$

Substituting equation [2.14] into equations [2.16] and [2.17], knowing

$$\partial(gh) = \partial(c^2) = 2c\partial c \qquad [2.18]$$

will yield the symmetric form of the Saint Venant equations for a rectangular prismatic channel:

$$\frac{\partial (2c)}{\partial t} + U\frac{\partial (2c)}{\partial x} + c\frac{\partial U}{\partial x} = 0 \qquad [2.19]$$

$$\frac{\partial U}{\partial t} + c\frac{\partial (2c)}{\partial x} + U\frac{\partial U}{\partial x} = g\left(S_0 - S_f\right) \qquad [2.20]$$

The symmetric aspect of the above equations becomes more apparent when they are in matrix form:

$$\frac{\partial}{\partial t}\begin{Bmatrix} 2c \\ U \end{Bmatrix} + \begin{bmatrix} U & c \\ c & U \end{bmatrix}\frac{\partial}{\partial x}\begin{Bmatrix} 2c \\ U \end{Bmatrix} + \begin{Bmatrix} 0 \\ g(S_f - S_0) \end{Bmatrix} \qquad [2.21]$$

The two above equations can be expressed in yet another form by first obtaining their sum and then their difference to produce (Henderson, 1966):

$$(U+c)\frac{\partial(U+2c)}{\partial x}+\frac{\partial(U+2c)}{\partial t}=g(S_0-S_f) \qquad [2.22]$$

$$(U-c)\frac{\partial(U-2c)}{\partial x}+\frac{\partial(U-2c)}{\partial t}=g(S_0-S_f) \qquad [2.23]$$

Recognizing the above as total derivatives, equations [2.22] and [2.23] can also be rewritten as:

$$\frac{D(U\pm 2c)}{Dt}=\frac{\partial(U\pm 2c)}{\partial t}+\begin{bmatrix}U+c & 0\\ 0 & U-c\end{bmatrix}\frac{\partial(U\pm 2c)}{\partial x}=g(S_0-S_f) \qquad [2.24]$$

Here, the total derivative operators represent the rate of change of $U+2c$ and $U-2c$ from the viewpoint of observers moving with velocities $U+c$ and $U-c$ respectively. This is the basis of the graphical solution technique of the Saint Venant equations known as the method of characteristics (Henderson, 1966).

2.2.3 The Saint Venant Equations for Natural Channels

The general form of the Saint Venant equations was derived for a straight channel where the velocity distribution is uniform across the channel. Flow in natural rivers is often complicated due to channel meandering and a non-uniform velocity distribution across the flow cross section. Some rivers may have areas where the flow velocity in the longitudinal direction is negligible. These are called inactive flow areas or off-channel storage. In order to model natural rivers, the Saint Venant equations must be modified to consider channel sinuosity, off channel storage, non-uniform velocity distributions, floodplain flow, and storage effects. With these considerations, the Saint Venant equations become (adapted from Fread, 1988, and Delong, 1986):

$$\frac{\partial(s(A+A_o))}{\partial t}+\frac{\partial Q}{\partial x}=0 \qquad [2.25]$$

$$\frac{\partial(sQ)}{\partial t}+\frac{\partial(\beta Q^2/A)}{\partial x}+gA\frac{\partial H}{\partial x}+gAS_f=0 \qquad [2.26]$$

where:

A_o = inactive cross sectional flow area or off-channel storage;

β = momentum flux correction coefficient to account for a non-uniform velocity distribution;

H = elevation of the water surface above a specified datum, also called stage; and

s = sinuosity factor to account for channel meandering.

In equation [2.23], depth of flow, h, has been replaced by stage, H, using the following relationship:

$$\frac{\partial H}{\partial x}=\frac{\partial h}{\partial x}-S_o=\frac{\partial h}{\partial x}+\frac{\partial y_b}{\partial x}=\frac{\partial(h+y_b)}{\partial x} \qquad [2.27]$$

where y_b is the elevation of the channel bottom above some datum as illustrated in Figure 2.1. Because the bottom of a natural channel can be irregular, the depth of flow will vary across a section. Therefore, stage becomes a more appropriate way to define water level when modelling natural channels as it is constant across a section.

2.2.3.1 Determination of the longitudinal boundary friction slope

In this study, Manning's n is used to describe channel resistance. Manning's n is a bulk empirical channel resistance parameter used to account for surface resistance and form drag resistance associated with bed features. To account for the fact that Manning's n is dependent on the flow depth, the natural channel hydraulic flood routing model was developed to allow input for n as function of stage. With n representing the channel resistance, the boundary friction slope is determined from Manning's equation for uniform, steady flow such that,

$$S_f = \frac{|Q|Q}{K^2} \qquad [2.28]$$

where K is a conveyance factor. When Manning's roughness is constant across a channel cross section for any given water elevation, the channel is called a composite channel. If a channel is classified as composite, then the conveyance factor is defined by:

$$K = \frac{\varphi}{n} A R^{2/3} \qquad [2.29]$$

where:

n = Manning's roughness coefficient;

R = hydraulic radius; and

φ = conversion factor for the employed system of units (1.00 for SI units or 1.49 for Imperial units).

The hydraulic radius is given by:

$$R = \frac{A}{P} \qquad [2.30]$$

where P is the wetted perimeter of the channel, i.e. the portion of the channel cross section that is in contact with the fluid (water). The conveyance factor is also defined by equations [2.29] and [2.30] if the channel is approximated by a rectangular channel.

If the cross section of a channel is composed of several distinct subsections, each having different values of roughness, then the channel is known as a compound channel (Chow, 1959). In this investigation, compound channels are defined by three subsections: the left floodplain, the main channel, and the right floodplain. In the case of a compound channel, the conveyance factor is computed using the following equations:

$$K_l = \frac{\varphi}{n_l} A_l R_l^{2/3} \qquad [2.31]$$

$$K_c = \frac{\varphi}{n_c \sqrt{s}} A_c R_c^{2/3} \qquad [2.32]$$

$$K_r = \frac{\varphi}{n_r} A_r R_r^{2/3} \qquad [2.33]$$

$$K = K_l + K_c + K_r \qquad [2.34]$$

where s is the sinuosity and the subscripts l, r, and c denote left floodplain, right floodplain, and main channel, respectively.

The hydraulic radii for the left floodplain, the main channel, and the right floodplain are defined by the following formulae.

Left floodplain:

$$R_l = \frac{A_l}{P_l} \qquad [2.35]$$

Main channel:

$$R_c = \frac{A_c}{P_c} \qquad [2.36]$$

Right floodplain:

$$R_r = \frac{A_r}{P_r} \qquad [2.37]$$

In the above formulae, P_l, P_c, and P_r refer to the wetted perimeters for the left floodplain, the main channel, and the right floodplain, respectively.

2.2.3.2 Determination of momentum correction coefficient

The momentum correction coefficient, β, appears in the momentum equation to account for the effect of a non-uniform velocity distribution across the channel section in the calculation of momentum. β cannot be less than unity. For a uniform velocity distribution β is equal to one. The more non-uniform the velocity becomes, the greater the value of β. For fairly straight prismatic channels, Chow (1959) reported β to vary from 1.01 to 1.12. For this study, based on values used by Fread (1988),

$\beta = 1.0$ for rectangular channels; and [2.38]

$\beta = 1.06$ for natural channels. [2.39]

However, if the channel is classified as a compound channel, the momentum correction coefficient is defined as (Fread, 1988):

$$\beta = \frac{1.06(K_l^2 / A_l + K_c^2 / A_c + K_r^2 / A_r}{(K_l + K_c + K_r)^2 / (A_l + A_c + A_r)} \qquad [2.40]$$

2.2.3.3 Determination of the sinuosity factor

Figure 2.2 illustrates a meandering river, where the length of the main channel is longer than the length of the floodplain or river valley. Therefore, the length of the flow path will decrease as the water surface elevation increases. The degree of meandering of a river is typically described by the sinuosity factor, defined as the ratio of the channel length to the valley length. For this study, the sinuosity factor is described as a function of the water surface elevation using (Fread, 1988):

$$s = \frac{\sum_{k=2}^{k=J} (\Delta A_{l_k} + \Delta A_{c_k} s_k + \Delta A_{r_k})}{A_l + A_c + A_r} \qquad [2.41]$$

where k is a depth index, ΔA is the difference in cross sectional area between two flow depths k and $k+1$; s_k is the sinuosity factor for the flow between these two flow depths;

and J is a depth index which represents the water surface elevation. The use of this equation requires a channel cross section to be broken down into a number of differential portions each having a sinuosity factor represented by s_k. Equation [2.41] assumes that the main channel is meandering in a straight floodplain. If the water surface elevation falls between two of the depths specified by the depth indices, then the sinuosity factor is linearly interpolated according to:

$$s = s_J + \left(\frac{s_{J+1} - s_J}{\Delta H} \right) \Delta H_1 \qquad [2.42]$$

where ΔH is the depth between J and $J+1$; and ΔH is the depth between J and the location of the water surface elevation.

2.2.3.4 Other forms of the Saint Venant equations for natural channels

When a channel is rectangular or is well approximated by a rectangular section, then the cross sectional area may be described by equation [2.3], reproduced here for convenience:

$$A = Bh \qquad [2.3]$$

However, in many cases (i.e. floodplain delineation) this rectangular approximation is not reasonable. For an irregularly shaped channel, A is a function of h. However, this function cannot be described by a simple mathematical relationship such as that in equation [2.3]. This makes it very difficult to obtain the conservation form of equation [2.26]. However, the pressure term can be rewritten using,

$$gA \frac{\partial H}{\partial x} = \frac{\partial (gAH)}{\partial x} - gH \frac{\partial A}{\partial x} \qquad [2.43]$$

to obtain:

$$\frac{\partial (sQ)}{\partial t} + \frac{\partial (\beta Q^2 / A)}{\partial x} + \frac{\partial (gAH)}{\partial x} - gH \frac{\partial A}{\partial x} + gAS_f = 0 \qquad [2.44]$$

This equation looks similar to the conservation formulation of the momentum equation for rectangular channels (reproduced here for convenience):

$$\frac{\partial Q}{\partial t}+\frac{\partial(Q^2/A)}{\partial x}+\frac{\partial}{\partial x}\left(\frac{gAh}{2}\right)-\frac{gAh}{2B}\frac{dB}{dx}-gAS_o+gAS_f=0 \qquad [2.5]$$

Nevertheless, equation [2.44] is not fully conservative as the dependent variable H appears outside of the partial derivative in the fourth term.

Assuming that the variation of sinuosity with time is small,

$$\frac{\partial s}{\partial t}\approx 0 \qquad [2.45]$$

equations [2.25] and [2.44] can also be rewritten as:

$$s\left(1+\frac{T_o}{T}\right)\frac{\partial A}{\partial t}+\frac{\partial Q}{\partial x}=0 \qquad [2.46]$$

$$s\frac{\partial Q}{\partial t}+\frac{\partial(\beta QU)}{\partial x}+\frac{\partial(gAH)}{\partial x}-gH\frac{\partial A}{\partial x}+gAS_f=0 \qquad [2.47]$$

where, T and T_o are the top widths of the active and inactive cross sectional flow areas, respectively.

Equation [2.23] can be written in non-conservation form using:

$$\begin{aligned}\frac{\partial(\beta Q^2/A)}{\partial x}&=\frac{\partial(\beta AU^2)}{\partial x}=\beta U\frac{\partial(AU)}{\partial x}+AU\frac{\partial(\beta U)}{\partial x}=U\left(\beta\frac{\partial Q}{\partial x}+A\frac{\partial(\beta U)}{\partial x}\right)\\&=U\left(\beta\frac{\partial Q}{\partial x}+\frac{\partial(\beta AU)}{\partial x}-\beta U\frac{\partial A}{\partial x}\right)=U\left(\beta\frac{\partial Q}{\partial x}+Q\frac{\partial\beta}{\partial x}+\beta\frac{\partial Q}{\partial x}-\beta U\frac{\partial A}{\partial x}\right)\\&=2\beta U\frac{\partial Q}{\partial x}-\beta U^2\frac{\partial A}{\partial x}+QU\frac{\partial\beta}{\partial x}\end{aligned} \qquad [2.48]$$

to obtain:

$$\frac{\partial(sQ)}{\partial t} + 2\beta U\frac{\partial Q}{\partial x} - \beta U^2\frac{\partial A}{\partial x} + QU\frac{\partial \beta}{\partial x} + gA\frac{\partial H}{\partial x} + gAS_f = 0 \qquad [2.49]$$

This is a non-conservation form of the momentum equation for natural channels.

Using equation [2.45], the above expression can be rewritten as:

$$\frac{s\partial Q}{\partial t} + 2\beta U\frac{\partial Q}{\partial x} - \beta U^2\frac{\partial A}{\partial x} + QU\frac{\partial \beta}{\partial x} + gA\frac{\partial H}{\partial x} + gAS_f = 0 \qquad [2.50]$$

Equations [2.46] and [2.50] can be presented in matrix form,

$$[\mathbf{B}]\frac{\partial\{\Phi\}}{\partial t} + [\mathbf{A}]_n\frac{\partial\{\Phi\}}{\partial x} + \{f\}_{n,nc} = \{0\} \qquad [2.51]$$

where:

$$\{\Phi\} \equiv \begin{Bmatrix} A \\ Q \end{Bmatrix} \qquad [2.12]$$

$$[\mathbf{A}]_n = \begin{bmatrix} 0 & 1 \\ -\beta U^2 & 2\beta U \end{bmatrix} \qquad [2.52]$$

$$[\mathbf{B}] = \begin{bmatrix} s\left(1 + \frac{T_o}{T}\right) & 0 \\ 0 & s \end{bmatrix} \qquad [2.53]$$

$$\{f\}_{n,nc} = \begin{Bmatrix} 0 \\ gA\left(\frac{\partial H}{\partial x} + S_f\right) + QU\frac{\partial \beta}{\partial x} \end{Bmatrix} \qquad [2.54]$$

Equation [2.50] looks similar to equation [2.9] (reproduced here for convenience):

$$\frac{\partial Q}{\partial t} + 2U\frac{\partial Q}{\partial x} + \underbrace{\left(gh - U^2\right)\frac{\partial A}{\partial x}}_{\text{pressure term}} - \frac{gAh}{B}\frac{dB}{dx} - gAS_o + gAS_f = 0 \qquad [2.9]$$

However, because of the lack of an expression to describe the area as a function of depth, the pressure term in equation [2.50] cannot be manipulated into two new terms as in equation [2.9]. As a result, the convection matrix for the natural channels equations, equation [2.52], is missing the celerity term ($c = gh$) that appears in the convection matrix for the rectangular channel equations ([2.13]), shown again below.

$$[\mathbf{A}]_r = \begin{bmatrix} 0 & 1 \\ gh - U^2 & 2U \end{bmatrix} = \begin{bmatrix} 0 & 1 \\ c^2 - U^2 & 2U \end{bmatrix} \qquad [2.13]$$

2.2.4 Boundary and Initial Conditions

Depending on the flow regime (subcritical, supercritical, or mixed), certain boundary conditions are necessary in order to obtain a unique solution of the Saint Venant equations. If the flow is subcritical throughout the domain, one boundary condition must be specified at each end of the domain. In most flood routing applications, the upstream boundary condition is simply a specified inflow (discharge) hydrograph while the downstream boundary is a stage-discharge relationship (rating curve) or a constant stage. If the flow is supercritical, two boundary conditions are required at the upstream end and none are required at the downstream end. These two conditions usually take the form of an inflow (discharge) hydrograph and a stage-discharge relationship. If the flow regime is mixed, then the required boundary condition will depend on the flow regime at the boundary. For example, if the flow is subcritical at the upstream end of the domain but supercritical at the downstream end of the domain, then one boundary condition would be required at the upstream end due to the subcritical flow. However, no boundary conditions would be necessary at the downstream end, as the flow is supercritical at this boundary. In any numerical model that solves the Saint Venant equations, the user must provide the model with the necessary boundary conditions in order to obtain a solution for the flow situation being modelled.

In addition to the boundary conditions, initial conditions must be provided at every node within the computational domain as a starting place from which the solution can proceed in time. In the case of flood routing, there are two methods to obtain the initial conditions if they are not known. In the first method, the initial conditions are obtained from a steady flow model, such as the US Corp of Engineers' HEC-RAS computer program, that can generate a gradually varied flow profile at every point in the computational domain for a given discharge. In the second method, the unsteady flow model is used to calculate a gradually varied flow profile. This is achieved by arbitrarily choosing a set of initial conditions and running the model with constant inflows until a steady state solution is obtained.

2.3 APPROXIMATIONS TO THE SAINT VENANT EQUATIONS

2.3.1 Introduction

The momentum equation of the Saint Venant equations is also described as the dynamic equation (Henderson, 1966). By neglecting certain terms in the momentum equation, various flow approximations to the Saint Venant equations can be obtained. Those relevant to flood routing are the kinematic wave and the diffusive wave. As both of these approximations are easier to solve, they provide a convenient and practical alternative for the hydraulic engineer when use of the full dynamic equation is unwarranted.

2.3.2 The Kinematic Wave Approximation

The various flow approximations may be derived by considering equations, which are the Saint Venant equations written for a rectangular prismatic channel (reproduced here for convenience).

$$\frac{\partial h}{\partial t} + \frac{\partial (Uh)}{\partial x} = 0 \qquad [2.16]$$

$$\frac{\partial U}{\partial t} + U\frac{\partial U}{\partial x} + g\frac{\partial h}{\partial x} = g(S_o - S_f) \qquad [2.17]$$

If the friction and slope terms become much larger than the inertial and pressure terms, then the above form of the Saint Venant equations can be approximated as:

$$\frac{\partial h}{\partial t} + \frac{\partial (Uh)}{\partial x} = 0 \qquad [2.16]$$

and

$$S_o = S_f \qquad [2.55]$$

This is known as the "kinematic wave approximation" (Henderson 1966). In this situation, the momentum equation has been replaced with a statement of uniform flow (friction slope is equal to the slope of the channel bed). For this reason, the kinematic wave is also described as "unsteady, uniform flow".

Substituting Manning's equation, where,

$$S_f = \frac{U^2 n^2}{\varphi^2 R^{4/3}} \qquad [2.56]$$

into equation [2.55] yields:

$$S_o = \frac{U^2 n^2}{\varphi^2 R^{4/3}} \qquad [2.57]$$

For a wide, rectangular channel, the hydraulic radius is well approximated by the flow depth, $R \sim h$, so that equation [2.57] can be rearranged to:

$$U = \frac{\varphi}{n} S_o h^{2/3} \qquad [2.58]$$

Multiplying by h,

$$Uh = \frac{\varphi}{n} S_o h^{5/3} \qquad [2.59]$$

Assuming n is not a function of x, equation [2.59] can be differentiated with respect to x as follows:

$$\frac{\partial (Uh)}{\partial x} = \frac{5}{3}\frac{\varphi}{n} S_o h^{2/3} \frac{\partial h}{\partial x} \qquad [2.60]$$

Replacing equation [2.60] in equation [2.16] results in the kinematic wave equation:

$$\frac{\partial h}{\partial t} + \frac{5}{3}\frac{\varphi}{n} S_o h^{2/3} \frac{\partial h}{\partial x} = 0 \qquad [2.61]$$

or

$$\frac{\partial h}{\partial t} + \alpha U \frac{\partial h}{\partial x} = 0 \qquad [2.62]$$

where,

$$\alpha = \frac{5}{3} \qquad [2.63]$$

when Manning's equation is used. If the friction slope is defined by Chezy's equation then α has a value of 3/2. Because the speed of a kinematic wave is a function of the depth, the peak of the wave will travel faster than the lower depths out in front. Therefore, a kinematic disturbance steepens as it propagates downstream.

2.3.3 The Diffusive Wave Approximation

Including the pressure term in the approximation to the momentum equation is the basis to the diffusive wave approximation. For the diffusive wave, only the inertial terms are neglected in the momentum equation. This reduces the momentum equation to a statement of nonuniform flow. Therefore, the Saint Venant equations for a rectangular prismatic channel can be expressed as:

$$\frac{\partial h}{\partial t} + U \frac{\partial h}{\partial x} + h \frac{\partial U}{\partial x} = 0 \qquad [2.64]$$

$$\frac{\partial h}{\partial x} = S_o - S_f \tag{2.65}$$

Substituting Manning's equation into equation [2.65], assuming *R*~*h*, and rearranging:

$$U = \frac{\varphi h^{2/3}}{n}\sqrt{S_o - \frac{\partial h}{\partial x}} \tag{2.66}$$

This illustrates that for a diffusive wave, the velocity is a function of the water surface slope as well as a function of flow depth. Differentiating equation [2.66] with respect to *x*, assuming S_o and *n* are not functions of *x*:

$$\frac{\partial U}{\partial x} = \frac{2}{3}\frac{\varphi}{nh^{1/3}}\frac{\partial h}{\partial x}\sqrt{S_o - \frac{\partial h}{\partial x}} - \frac{1}{2}\frac{\varphi h^{2/3}}{n}\left(S_o - \frac{\partial h}{\partial x}\right)^{-1/2}\frac{\partial^2 h}{\partial x^2} \tag{2.67}$$

Simplifying this becomes:

$$\frac{\partial U}{\partial x} = -\frac{\varphi^2 h^{4/3}}{2n^2 U}\frac{\partial^2 h}{\partial x^2} + \frac{2U}{3h}\frac{\partial h}{\partial x} \tag{2.68}$$

Substituting the above equation into the continuity equation ([2.64]) results in:

$$\frac{\partial h}{\partial t} + U\frac{\partial h}{\partial x} + \frac{2U}{3}\frac{\partial h}{\partial x} = \frac{\varphi^2 h^{7/3}}{2n^2 U}\frac{\partial^2 h}{\partial x^2} \tag{2.69}$$

or

$$\frac{\partial h}{\partial t} + \alpha U\frac{\partial h}{\partial x} = D\frac{\partial^2 h}{\partial x^2} \tag{2.70}$$

which is called the "diffusive wave equation", where:

$$\alpha = \frac{5}{3} \tag{2.63}$$

and

$$D = \frac{\varphi^2 h^{7/3}}{2n^2 U} \qquad [2.71]$$

Equation [2.70] is a second order partial differential equation describing convection-diffusion in a wide rectangular channel. Contrary to a kinematic wave, as it propagates downstream, it will attenuate at a rate governed by the magnitude of the diffusion term D.

2.3.4 Application of the Various Approximations of the Saint Venant Equations

The kinematic wave equation ([2.61]) is a first order partial differential equation describing convection in a wide rectangular channel. Waves defined by this convection equation experience pure translation at a speed of αU without any attenuation. Wave attenuation can only be described by a diffusion term, which is a second order partial differential term. Since there are no such terms in the kinematic wave approximation, it cannot account for wave attenuation. Consequently, in calculating the propagation of a kinematic disturbance the wave will steepen and will eventually want to break. The 'breaking' wave will cause the solution to break down.

The diffusive wave approximation, by neglecting the inertial (or dynamic) terms but not the pressure term in the momentum equation, introduces a diffusion term that prevents the indefinite steepening problem. The diffusion term also causes the wave to attenuate as in travels downstream, which is a characteristic behaviour of actual flood waves. Therefore, the diffusive wave approximation can be used quite readily for modelling flood wave propagation. However, like a kinematic wave, the diffusive wave neglects the dynamic aspects of the wave and therefore has only one convective velocity, which propagates in the downstream direction. This becomes more apparent when the symmetric form of the Saint Venant equations are compared to kinematic and diffusive wave equations (reproduced below for convenience).

Kinematic wave:

$$\frac{\partial h}{\partial t} + \alpha U \frac{\partial h}{\partial x} = 0 \qquad [2.61]$$

Diffusive wave:

$$\frac{\partial h}{\partial t}+\alpha U\frac{\partial h}{\partial x}=D\frac{\partial^2 h}{\partial x^2} \qquad [2.70]$$

Dynamic wave:

$$\frac{\partial(U\pm 2c)}{\partial t}+\begin{bmatrix} U+c & 0 \\ 0 & U-c \end{bmatrix}\frac{\partial(U\pm 2c)}{\partial x}=g\left(S_0-S_f\right) \qquad [2.24]$$

The Saint Venant equations take into account the complete momentum equation, including the dynamic terms. Therefore the disturbances defined by these equations have *two* convective velocities ($U \pm c$), in contrast to kinematic or diffusive disturbances which only have *one* convective velocity (αU). The progressive wave ($U+c$) travels in the direction of the flow while the regressive wave ($U-c$) may travel upstream, downstream, or remain stationary, depending on the flow regime (supercritical, subcritical, or critical).

For most flood routing problems, a diffusive wave model is more than adequate except when a dynamic event occurs. A dambreak is a dynamic event; however, it is not generally a flood forecasting issue since simulation of this type of event would occur when the dam in question is designed, as part of the dam safety requirements. The type of situation a flood forecaster may encounter, where flood wave dynamics cannot be neglected, occurs in cold regions where an ice jam releases and creates a dynamic disturbance.

2.3.5 Comparison of the Various Waves

An illustrative way of comparing the various wave models is by examining the rating curve produced by each type of disturbance. In general, the flow rate is given by Manning's equation as:

$$Q = KS_f^{1/2} = \frac{\varphi}{n}ARS_f^{1/2} \qquad [2.72]$$

By definition, for uniform flow the friction slope is equal to the slope of the bed, and Manning's equation is given by:

$$Q_o = \frac{\varphi}{n} A R S_o^{1/2} \qquad [2.73]$$

Combining equations [2.72] and [2.73] yields:

$$Q = Q_o \sqrt{\frac{S_f}{S_o}} \qquad [2.74]$$

Substituting the momentum equation ([2.17]) into the above expression results in:

$$Q = Q_o \sqrt{1 - \frac{1}{S_0}\left(\frac{\partial h}{\partial x} + \frac{U}{g}\frac{\partial U}{\partial x} + \frac{1}{g}\frac{\partial U}{\partial t}\right)} \qquad [2.75]$$

Equation [2.75] describes a loop-rating curve (Henderson, 1966) for the complete Saint Venant equations for the case of a rectangular prismatic channel. It defines the stage discharge relationship experienced by the progressive wave of a dynamic disturbance. When the progressive wave propagates downstream, a looped rating curve occurs at every cross section, and at any given stage the discharge is greater on the rising limb of the hydrograph than it is on the receding limb, as shown in Figure 2.3. Also, the point of maximum depth does not correspond with the point of maximum discharge.

For a kinematic wave, the momentum equation simplifies to:

$$S_o = S_f \qquad [2.55]$$

and, therefore equation [2.74] becomes,

$$Q = Q_o \qquad [2.76]$$

which, for the case when $R \sim h$, can be written as:

$$Q = Q_o = \frac{\varphi}{n} B h^2 S_0^{1/2} \qquad [2.77]$$

which indicates that a kinematic wave is defined by a unique relationship between stage and discharge, this is known as a single valued (or uniform flow) rating curve, and is illustrated in Figure 2.3.

For a diffusive wave, the momentum equation reduces to:

$$\frac{\partial h}{\partial x} = S_o - S_f \qquad [2.65]$$

Substituting this expression into equation [2.74] yields:

$$Q = Q_o \sqrt{1 - \frac{1}{S_0} \frac{\partial h}{\partial x}} \qquad [2.78]$$

which defines the rating curve for a diffusive wave. Like the dynamic wave, the diffusive wave also produces a looped rating curve. Again, a diffusive wave model is adequate for most flood routing problems. However, for a dynamic disturbance, the flow depth at maximum discharge can be significantly less than the maximum flow depth of the event. Therefore, the use of a diffusive wave to model a dynamic event may result in a significant underestimation of the peak stage.

2.4 DEVELOPMENT OF THE NATURAL CHANNEL HYDRAULIC FLOOD ROUTING MODEL

In order to develop the natural channel hydraulic flood routing model, a numerical scheme was required. It is important to recognize that there are many numerical schemes that could have been used to solve the governing equations. The Characteristic Dissipative Galerkin (CDG) finite element scheme (Hicks and Steffler, 1990, 1992) was chosen for the current investigation for two main reasons. First, the CDG scheme is numerically very robust. It is successful at selectively damping the high frequency wavelengths associated with numerical instabilities (Hicks and Steffler, 1990). It has also been shown to handle the transition from subcritical to supercritical flow and provide stable solutions for extremely-dynamic, diffusive, and kinematic events, including the transition between these (Hicks, *et al.*, 1992). Second, the cdg1-D model, which employs the CDG scheme, has been applied successfully as a flood routing model in a number of investigations (Hicks, 1996; Hicks *et al.*, 1994; Hicks and McKay, 1995; McKay *et al.*, 1996).

The details on implementing the CDG scheme to the Saint Venant equations for natural channels to create the cdg1-Dn flood routing model are presented in Appendix A. The following is provided to highlight the main issues that arose in the implementation of the CDG scheme for natural channels and to discuss how these issues may affect the performance of the cdg1-Dn model.

In the cdg1-D model, the CDG scheme is used to solve the conservation form of the Saint Venant equations for the case when the channel is approximated by a rectangular channel of varying width. That is, equations [2.1] and [2.5], reproduced here for convenience.

$$\frac{\partial A}{\partial t}+\frac{\partial Q}{\partial x}=0 \qquad [2.1]$$

$$\frac{\partial Q}{\partial t}+\frac{\partial(Q^2/A)}{\partial x}+\frac{\partial}{\partial x}\left(\frac{gAh}{2}\right)-\frac{gAh}{2B}\frac{dB}{dx}-gAS_o+gAS_f=0 \qquad [2.5]$$

The CDG scheme does not require the use of the conservation formulation. However, in a comparison of the conservation, non-conservation (equations [2.1] and [2.9]), and symmetric (equations [2.19] and [2.20]) formulations of the Saint Venant equations, Hicks and Steffler (1990) found that only the conservation formulation was able to perfectly conserve both mass and longitudinal momentum. It was therefore desirable to implement CDG scheme for the Saint Venant equations for natural channels using a conservation formulation. Unfortunately, at present, it is not possible to manipulate the natural channel equations into a fully conservation formulation, as previously shown.

Consequently, in the cdg1-Dn model, the CDG scheme was implemented using the following form of the natural channel equations:

$$s\left(1+\frac{T_o}{T}\right)\frac{\partial A}{\partial t}+\frac{\partial Q}{\partial x}=0 \qquad [2.46]$$

$$s\frac{\partial Q}{\partial t}+\frac{\partial(\beta QU)}{\partial x}+\frac{\partial(gAH)}{\partial x}-gH\frac{\partial A}{\partial x}+gAS_f=0 \qquad [2.47]$$

Because this form of the equations is not fully conservative, the cdg1-Dn model is not capable of conserving mass and momentum under all circumstances. In a numerical analysis, presented in Appendix B, it was found that for a particularly challenging dambreak test (supercritical dambreak), the cdg1-Dn could only conserve mass and momentum to two decimal places. For the same test, the cdg1-D model was able to conserve both mass and momentum to five decimal places.

The ability of dissipative schemes, such as the CDG, to selectively dampen spurious (numerically generated) oscillations is through the introduction of numerical diffusion into the system of equations being solved. In the CDG scheme, the distribution of the numerical dissipation is controlled by an upwinding matrix, which takes the form:

$$[\mathbf{W}]=\frac{[\mathbf{A}]}{|[\mathbf{A}]|}=[\mathbf{M}]\begin{bmatrix}\lambda_1/|\lambda_1| & 0\\ 0 & \lambda_2/|\lambda_2|\end{bmatrix}[\mathbf{M}]^{-1} \qquad [2.79]$$

where:

[A] = convection matrix for non-conservation form;

λ_i = eigenvalues of **[A]**; and

[M] = matrix having as its columns, the eigenvectors of **[A]**.

In the cdg1-D model, the convection matrix takes the form:

$$[\mathbf{A}]_r = \begin{bmatrix} 0 & 1 \\ gh-U^2 & 2U \end{bmatrix} = \begin{bmatrix} 0 & 1 \\ c^2-U^2 & 2U \end{bmatrix} \qquad [2.13]$$

which is based on the non conservation for of the Saint Venant equations for rectangular channels, presented in equations [2.1] and [2.9]. For this form of the convection matrix, the upwinding matrix becomes:

$$\begin{aligned} [\mathbf{W}]_r &= \begin{bmatrix} 1/2c & -1/2c \\ (U+c)/2c & -(U+c)/2c \end{bmatrix} \begin{bmatrix} \dfrac{U+c}{|U+c|} & 0 \\ 0 & \dfrac{U-c}{|U-c|} \end{bmatrix} \begin{bmatrix} -(U-c) & 1 \\ -(U+c) & 1 \end{bmatrix} \\ &= \frac{1}{2c} \begin{bmatrix} \left(c^2-U^2\right)\left(\dfrac{1}{|U+c|}-\dfrac{1}{|U-c|}\right) & \dfrac{U+c}{|U+c|}-\dfrac{U-c}{|U-c|} \\ \left(c^2-U^2\right)\left(\dfrac{U+c}{|U+c|}-\dfrac{U-c}{|U-c|}\right) & \dfrac{(U+c)^2}{|U+c|}-\dfrac{(U-c)^2}{|U-c|} \end{bmatrix} \end{aligned} \qquad [2.80]$$

which demonstrates that the eigenvalues for this convection matrix are the characteristic velocities, $U+c$ and $U-c$. The above decomposition also illustrates the use of both characteristic velocities in the determination of the upwinding matrix for the cdg1-D model.

As was demonstrated previously, it is not possible to manipulate the Saint Venant equations for natural channels into a non-conservation formulation that has a convection matrix of the form in equation [2.13]. In the non-conservation formulation of the natural channel equations that was presented previously, the convection matrix appears as:

$$[\mathbf{A}]_n = \begin{bmatrix} 0 & 1 \\ -\beta U^2 & 2\beta U \end{bmatrix} \qquad [2.52]$$

Because this convection matrix is missing the celerity term, *gh*, the eigenvalues of this matrix are not the characteristic velocities. In addition, when equation [2.80] is implemented using equation [2.52], the resulting expression is a very complex upwinding matrix that is indeterminate if $\beta=1$, that is, if the velocity distribution is uniform. For these reasons, the dissipative component of the CDG scheme in the cdg1-Dn model uses the upwinding matrix in the cdg1-D model, except that for natural channels, the celerity is defined by:

$$c = \sqrt{g\frac{A}{T}} \tag{2.81}$$

where A/T is known as the hydraulic depth. As will be demonstrated in the following chapter, the cdg1-Dn model is far less stable than the cdg1-D model. Therefore, the fact that the upwinding matrix is not based upon the natural channel equations that are solved by the cdg1-Dn model may be preventing the appropriate damping of the numerical oscillations that lead to numerically generated instabilities.

In both the cdg1-D and cdg1-Dn models, the CDG scheme is used to discretize the problem in space. The problem is discretized in time using a semi-implicit finite difference approximation. Once the problem is discretized in both space and time, the complete set of equations to be solved can be abbreviated as (Hicks and Steffler, 1990):

$$\{m_p(\Phi)\} = \{0\} \tag{2.82}$$

where m is a function of Φ which represents the vector of unknowns $\{Q, A\}$, and p is the number of equations which is equal to the number of unknowns (2N, where N is the number of computational nodes). Because the temporal discretization is implicit, an iterative solution technique is required to solve for the vector of unknowns at every time step. In both the cdg1-D and the cdg1-Dn models, a Newton-Raphson iteration was employed to solve the system of non-linear equations. In the Newton-Raphson iteration, the first guesses of the unknown values at the new time step, Φ^{n+1}, are based on the solution at the previous time step, Φ^{n}. Unless the guesses are correct, the right hand sides of the equations represented by [2.82] will not be zeros. These non-zero values are termed the residual, $\{R\}$. The next and subsequent guesses are obtained by applying corrections, $\Delta\Phi$, to the old guess, which are determined using:

$$[J]\{\Delta\Phi\} = \{R\} \quad [2.83]$$

where [*J*] is called the Jacobian matrix and is given by:

$$[J] = \left[\frac{\partial\{R\}}{\partial\{\Phi\}}\right] \quad [2.84]$$

The Jacobian matrix can be evaluated numerically or analytically. In both the cdg1-D and cdg1-Dn models, an analytical Jacobian matrix is used. Because the dependence of the upwinding matrix on the solution is neglected, that is,

$$\frac{\partial[\mathbf{W}]}{\partial\{\Phi\}} \approx [0] \quad [2.85]$$

the Jacobian matrix in both models is approximate. The approximate nature of the Jacobian matrix does not seem to affect the convergence of the cdg1-D model at every time step, even for particularly difficult problems. However, this is not the case for the cdg1-Dn model. As will be demonstrated in the following chapter, when the cdg1-D and cdg1-Dn models were used to simulate the same problem, a significantly larger time step increment could be used in the cdg1-D model compared to the cdg1-Dn model. It is likely that the instabilities that arise while running the cdg1-Dn model are the result of problems with equation formulation and the upwinding component of the scheme. However, the stability problems of the cdg1-Dn model are possibly exacerbated by the lack of a full analytical Jacobian matrix. In theory, the closer the Jacobian matrix is to the full Jacobian matrix, the better equipped it will be to determine the solution at the next time step and, as a result, a larger time step interval should be permissible without the model 'blowing up'.

In summary, due to its stability problems, the cdg1-Dn model is not an entirely practical tool at this time. Expanding the Jacobian matrix to the full analytical Jacobian may improve the stability of the cdg1-Dn model. However, the lack of a fully conservation formulation and a convection matrix based on the characteristic velocities indicate that perhaps the CDG scheme is not the best scheme for solving the Saint Venant equations for natural channels. Although the cdg1-Dn model is not currently an operationally useful model, it can still be used to determine the feasibility of using hydraulic flood routing techniques based on natural geometry for forecasting water levels. This is accomplished in the two following chapters.

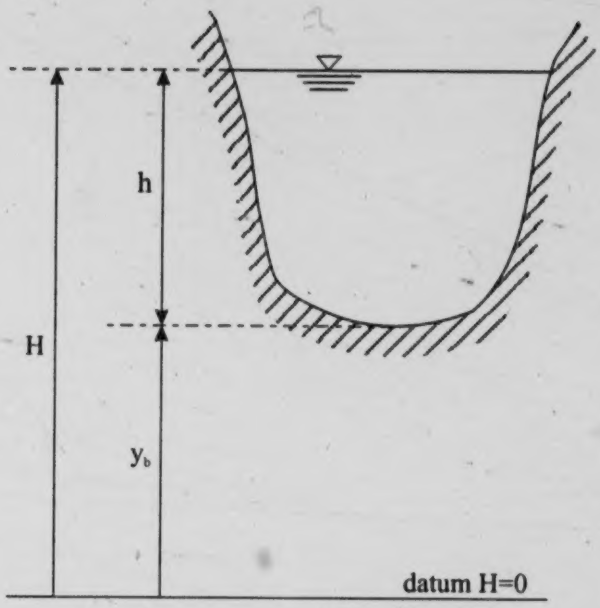

Figure 2.1 Definition of stage in open channel flow.

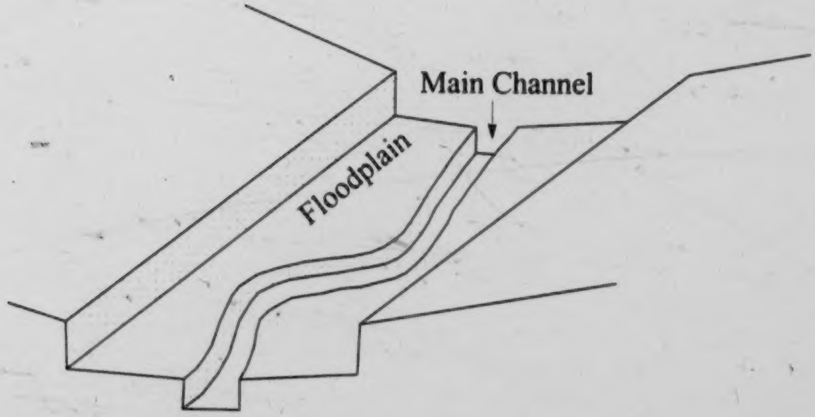

Figure 2.2 Relationship between main channel and floodplain (after Delong, 1986).

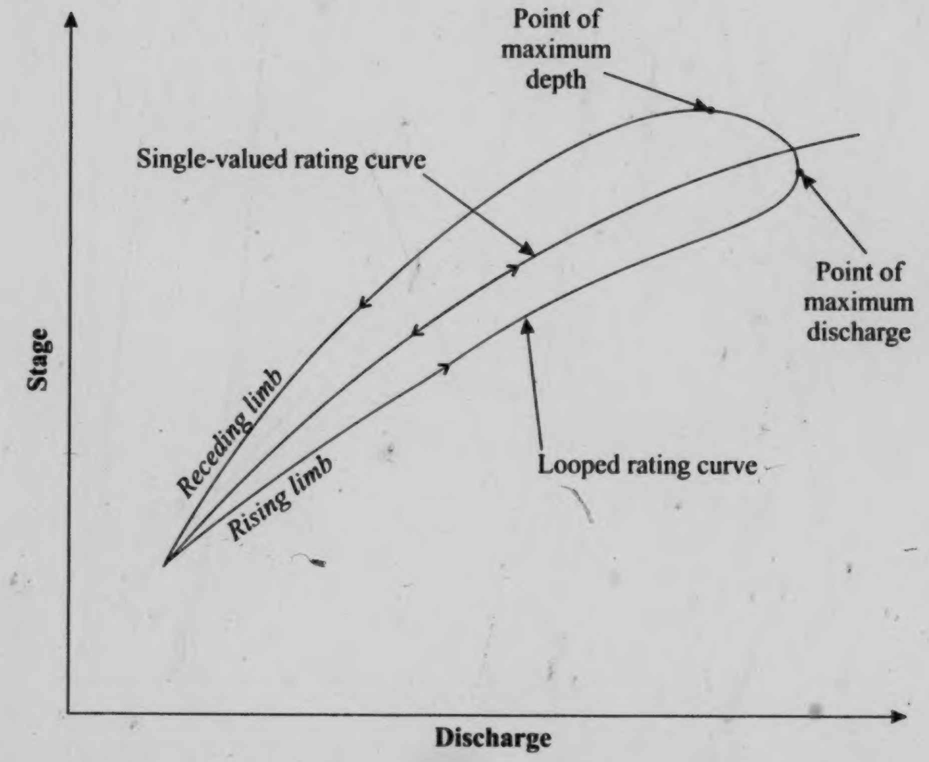

Figure 2.3 Sketch of a single-valued rating curve (uniform flow) and a looped rating curve (dynamic waves).

CHAPTER 3

OPEN CHANNEL FLOOD EVENT: PEACE RIVER, ALBERTA[1]

3.1 INTRODUCTION

In this chapter, the first objective of this study is addressed. To reiterate, the objective was to determine whether it is possible to blend the 'limited geometry model' and the 'natural channel model' into one model so that, operationally, flood forecasting could include the determination of accurate flood levels. In order to accomplish this objective two issues must be addressed. The first issue is one of river hydraulics. That is, will changing from approximate geometry to natural geometry in the short reaches, where water levels are desired, produce accurate water levels? The second is a numerical issue: is it possible to blend the geometry types, approximate and detailed, into one flood routing model? This would be operationally desirable.

To address the first issue, a reach of the Peace River was used, which extends from Hudson Hope, British Columbia to Peace Point, Alberta. The reach was chosen for a number of reasons. First, the reach had already been modelled by Hicks (1996) using the limited geometry approach, and therefore a geometric database of the reach was available for use in the current investigation. Second, for the event modelled in this investigation, the 1987 summer event, Water Survey of Canada (WSC) water level data were available at a few natural channel subreaches, which could be used to validate the proposed method. Third, the 1987 summer event was also modelled by Hicks (1996), thus facilitating a comparison between the limited geometry approach to the proposed hybrid approach of using both natural and approximate geometry.

---

[1] An abridged version of this chapter will be submitted for publication in the Canadian Journal of Civil Engineering.

To assess the second issue the cdg1-Dn and cdg1-D models are employed. The cdg1-Dn model was used to route the event through the natural channel subreaches while the cdg1-D model was used to route the event through the approximate channel subreaches.

3.2 DESCRIPTION OF THE STUDY REACH

Figure 3.1 illustrates the study reach which extends from Hudson Hope, British Columbia (28 km downstream of the W.A.C. Bennett Dam) to Peace Point, Alberta in Wood Buffalo National Park, a distance of 1107 km in terms of length along the channel centreline. The geomorphic features of the Peace River vary along the length of the study reach. Kellerhals *et al.*, (1972) provide excellent details of these features from which the following description is drawn.

In the upper portion of the study reach, the river is defined by a straight channel with the occasional island and mid-channel bar where the channel bed is a shallow alluvium of gravel over shale and some sandstone. Near Dunvegan the river become slightly sinuous defined by point bars and by Fort Vermilion the river displays an irregular meandering pattern characterized by a mid-channel and point bars and a channel bed consisting predominately of sand. Throughout the entire reach the river is partly entrenched and confined to the river valley. The entire river is described as having a stream cut valley, that is to say, fluvial rather than glacial processes were responsible for the valley's formation.

3.3 AVAILABLE GEOMETRIC DATA

3.3.1 Geometric Database Developed from Limited Geometry

As mentioned previously, Hicks (1996) developed the geometric database of the Peace River using available cross section data supplemented by topographic map data. In this database, the study reach was defined using an effective bed profile and channel widths at 1 km intervals, where the effective bed level is defined as the bed elevation of an equivalent rectangular section approximating the actual channel geometry (Hicks *et al.*, 1997). To define the effective bed profile, the effective bed level at each surveyed cross section was computed by first determining the hydraulic mean depth (flow area/top width) at the 1:2 year flood level and then subtracting this depth from 1:2 year flood stage. The effective bed profile was established by drawing a best-fit line through the effective bed points established from the surveyed sections. Between surveyed reaches, the water surface slope, obtained by identifying locations where topographic contours intersected the river channel on 1:250 000 scale National Topographic Series (NTS) maps, was used to estimate the gradient of the effective bed profile. The channel widths were obtained entirely by measuring the channel top widths from 1:250 000 NTS maps. These widths were then smoothed using 4 point moving mean widths to develop the widths that were put in the database.

In the database, the effective bed profile and channel width are defined at 1 km intervals along the channel centreline with the downstream face of the W.A.C. Bennett specified as the origin. All of the available surveyed cross sections and all major tributaries were also referenced to this stationing system. Table 3.1 presents the location of key sites in terms of their distances downstream of the origin.

Table 3. 1. Location of key sites along the Peace River (after Hicks, 1996).

Location	Station (km)
Peace River at Hudson Hope	***28***
Halfway River confluence	65
Moberly River confluence	103
Peace River at Fort St. John	110
Pine River confluence	120
Peace River at Taylor	121
Beaton River confluence	141
Kiskatinaw River confluence	154
British Columbia-Alberta Border	166
Clear River confluence	186
Peace River at Dunvegan Bridge	**295**
Smoky River confluence	388
Heart River confluence	394
Peace River at Peace River	**395**
Notikewin River confluence	558
Peace River near Carcajou	650
Peace River at Fort Vermilion	**808**
Boyer River confluence	819
Wabasca River confluence	865
Peace River at Peace Point	**1107**

3.3.2 Natural Channel Data

In order to assess whether a flood can be routed down a channel using an approximate channel where data are lacking and using natural channel data where flood level quantification is desired, two things are required. First, data describing the channel cross section are necessary along the subreaches where the flood levels are to be calculated. Second, measured water levels must be available at these subreaches to compare with computed water levels. Although there are cross section surveys at a number of locations along the Peace River, for the chosen event, water level data were only available at three locations, namely, the towns of Dunvegan, Peace River, and Fort Vermilion. Figures 3.2, 3.3. and 3.4 illustrate the details of these subreaches. The availability of surveyed cross sections varied in each of these three subreaches: 10 cross sections in Dunvegan between km 293.6 and km 299.7; 28 cross sections at Peace River (town) between km 369.8 and km 415.7; and only 6 at Fort Vermilion between km 804.3 and km 812.0. The details of these cross sections are presented in Appendix D.

To input a natural channel cross section into the cdg1-Dn model, it must be in the form of a table of topwidths defined at a specific number of elevations. Based on an analysis presented in Appendix C, 8 topwidths (defined at evenly spaced elevations) are recommended to adequately describe a cross section that is defined by the main channel only. Since the available cross section data in the three subreaches define the main channel only, they were all converted into topwidth tables defined by 8 topwidths.

3.3.3 Channel Resistance

The only calibration parameter required by the cdg1-Dn model is channel resistance, specifically Manning's *n*. As it was desirable to compare the results of the current analysis with those obtained by Hicks (1996), it was decided to use the Manning's *n* values used by Hicks (1996). Table 2.3 presents the values used in the various subreaches of the Peace River, which were estimated based on the values presented by Kellerhals *et al.*, (1972).

Table 3. 2. Manning's *n* values used in this investigation (after Hicks, 1996). *

Location (km)	Manning's *n*
28 to 75	0.030
75 to 210	0.045
210 to 345	0.025
345 to 1107	0.020

* Based on the values from Kellerhals, *et al.*, 1972.

3.4 AVAILABLE HYDROLOGIC DATA

3.4.1 WSC gauge data available on the Peace River

The event used in this analysis was the 1987 summer flood on the Peace River. During this event a number of streamflow gauges were operational including the Peace River at Hudson Hope at station 28 km; the Peace River above Pine River at station 120 km; the Peace River near Taylor at station 122 km; the Peace River at Dunvegan Bridge at station 295 km; the Peace River at Peace River at station 395 km; and the Peace River at Peace Point at station 1107 km. The gauge at Hudson Hope provided the inflow at the upstream boundary for the routing computations while the data from the other gauges provided a means of assessing the model performance. Flow data were unavailable at Carcajou (650 km) and Fort Vermilion (808 km) as these gauges were discontinued in 1967 and 1978, respectively. In this analysis, the model inflow at Hudson Hope was based on the WSC records on the HYDAT CD-ROM. WSC only publishes mean daily flows. However, it is important to realize that in practice flood forecasting is performed with 6-hour flow data.

3.4.2 WSC gauge data available on Peace River tributaries

To facilitate a consistent comparison with the results obtained by Hicks (1996), the tributary inflows used in this investigation are those used by Hicks (1996). In the investigation by Hicks (1996), the limited geometry hydraulic flood routing model was compared to Alberta Environment's SSARR (hydrologic) model. Therefore, the tributaries used by Hicks (1996) were identical to those used by Alberta Environment (AE). Table 3.3 presents the tributaries considered in the current investigation, the WSC gauges from which the data were obtained, and the multiplication factor used by Alberta Environment (AE) to transpose the tributary gauge data downstream to the confluence with the Peace River (Taggart, 1995). The multiplication factor is simply a linear adjustment based on the ratio of the catchment area at the confluence to the catchment area at the gauge. Other tributary data were available; however, no multiplication factors were available from AE to transpose these data downstream to the confluence with the Peace River. Therefore, these additional tributary data were not used by Hicks (1996) nor were they used in the current investigation.

Table 3. 3 Peace River tributaries considered in this investigation (after Hicks, 1996).

Location	WSC	Factor
Halfway River near Farrell Creek	07FA006	1.00
Moberly River near Fort St. John	07FB008	1.40
Pine River at East Pine	07FB001	1.00
Beaton River near Fort St. John	07FC001	1.03
Kiskatinaw River near Farmington	07FD001	1.26
Clear River near Bear Canyon	07FD009	1.00
Smoky River near Watino	07GJ001	1.02
Heart River near Mampa	07HA003	1.00
Notikewin River at Manning	07HC001	1.39
Boyer River near Fort Vermilion	07JF002	1.00
Ponton River above Boyer River	07JF003	1.26
Wabasca River at Walden Lake Road	07JD002	1.10

3.5 NUMERICAL SIMULATION

Since the cdg1-Dn model can accommodate cross sections of any shape, it was thought at first, that the cdg1-Dn model could be used to route the entire event with the natural channel data incorporated into the approximate channel database. In the investigation by Hicks (1996), the limited channel geometry flood technique was applied using the cdg1-D model. Therefore, before inserting the natural channel geometry into the approximate geometry database, the cdg1-Dn model was used to simulate the 1987 event using only the approximate geometry, to provide a means of comparing the two models for a practical problem. The cdg1-D model simulated the entire event, which extended from July 29 to September 1 (35 days), using a time step increment of 6 hours (Hicks, 1996). This translates to 140 time steps to complete the entire simulation. When the cdg1-Dn model was employed to model the same situation (approximate geometry only), a time step increment of no greater than 1 minute could be used or the model would 'blow up'. This required 504, 000 time steps for the 35 day simulation period. For the sizes of reaches and simulation periods that are commonly seen in flood routing problems, this sort of time step limitation is impractical. Therefore, it was concluded that the cdg1-Dn model, in its current version, is not stable enough to be used as practical tool for routing floods.

It is the author's opinion that the stability issue of the cdg1-Dn is due to a number of factors. These are described in Chapter 2 but reiterated here for convenience. The first has to do with the inability to manipulate the natural channel equations into a fully conservation formulation, which affects the model convergence at every time step. The second is related to the inability to properly implement the dissipative component of the CDG scheme, which may prevent the appropriate dampening of numerical oscillations. Perhaps a Jacobian matrix closer to the actual Jacobian for the problem would mitigate this stability issue.

It would be beneficial if the cdg1-Dn could be used as a practical flood routing tool as flood routing and floodplain delineation could potentially be accomplished using one model. However, the issue here was to determine whether it is indeed *feasible* to blend the approximate geometry and natural channel geometry into one hydraulic flood routing model. To accomplish this, the 1987 summer flood event was modelled accordingly. First, the entire event was simulated with the approximate geometry database using the cdg1-D model as was done by Hicks (1996). However, in this simulation discharge output were requested at the upstream ends of the three natural channel reaches in addition to the gauge locations. These extra hydrographs were then used as the input to route the flood through each of the three townsites using the natural geometry and the cdg1-Dn model. In order to perform these three simulations, input data sets had to be created for each subreach.

3.5.1 Development of the input data sets

3.5.1.1 Boundary and initial conditions

To simulate the event in each of the three subreaches, they all had to be provided with two boundary conditions and all tributary inflows in order to solve the Saint Venant equations. Since all three subreaches experience subcritical flow, they all required one upstream and one downstream boundary condition. In practical flood routing situations for subcritical flow, the upstream boundary condition typically takes the form of a discharge hydrograph while the downstream boundary condition may be a stage or discharge hydrograph, or a rating curve. The flow conditions at the downstream boundary may be unknown, especially in unsteady situations. However, if the downstream boundary is located far enough downstream of the site of interest, then a constant stage may be used for the downstream boundary condition. In this case, the distance between site of interest and the downstream boundary must be sufficient to ensure that backwater and drawdown effects from the assumed boundary condition do not affect the model output at the site of interest.

For the Dunvegan subreach, the upstream boundary of the computational domain was taken as the furthermost upstream cross section (293.6 km) and the downstream boundary was specified 30 km downstream of the last cross section in the subreach (299.7 km). Between the last surveyed cross section and the downstream boundary, the domain was defined using approximate (rectangular) geometry. The domain was extended to minimize the influence of the downstream boundary on the calculations at the gauge at Dunvegan. The downstream boundary condition was specified as a constant stage and the cdg1-D model provided the discharge hydrograph to supply the upstream boundary condition.

The boundaries and boundary conditions for the two other subreaches, Town of Peace River and Fort Vermilion, were specified in the same manner as those for the Dunvegan subreach. The only exception was that two tributary inflows had to be specified in the Peace River (town) subreach, namely, the Smoky River (km 388) and the Heart River (km 394), which were obtained as mean daily flows from the HYDAT CD-ROM.

As input to the unsteady flow simulation, initial conditions (stage and discharge) had to be specified at every computational node in each subreach. This was accomplished using the cdg1-Dn model to calculate a gradually varied flow profile for each subreach for constant incoming and tributary inflows, based on the mean daily flows observed at the beginning of the simulation period, July 29, 1987

3.5.1.2 Selection of the spatial and temporal discretization

In each of the subreaches, the cross sections were surveyed with an uneven spacing. The CDG scheme, being a finite element scheme, can accommodate variable spacing between the computational nodes (cross sections), though evenly spaced nodes and or gradual changes in geometry are preferred for better accuracy. Therefore, in each subreach, cross sections were linearly interpolated between the original surveyed sections. To minimize the possibility of error due to insufficient discretization and to obtain very gradual changes in geometry, it was decided to interpolate cross sections at every 0.2 km in each subreach. However, since the Dunvegan and Fort Vermilion subreaches were very short, it was found that cross sections could be interpolated at every 0.1 km without adding significantly to the computational time. Figure 3.5 provides a comparison of the steady state discharge obtained along the Dunvegan subreach with and without interpolation of cross sections, to illustrate the benefit of interpolation. Although the model was supplied with a constant incoming discharge of 1995 m^3/s, the discharge output oscillated between 1900 m^3/s and 2100 m^3/s when only the surveyed cross sections were used to define the computational domain. With cross sections interpolated at every 0.1 km, the oscillations significantly diminished. In both cases, the Dunvegan subreach is shown with the 30 km extension of approximate geometry.

For the CDG scheme, Hicks and Steffler (1990, 1992) found that it produces the most accurate results over a range of Courant number values up to $C = 0.5$, remembering that C is defined as:

$$C = \frac{V_w \Delta t}{\Delta x} \qquad [3.1]$$

where V_w is the speed of the wave ($U+c$ for dynamic disturbances and αU for diffusive or kinematic disturbances); Δt is the temporal discretization; and Δx is the spatial discretization. However, this recommendation of a Courant number less than or equal to 0.5 is for dynamic waves. For a diffusive wave, such as that in the Peace River event, very large Courant numbers can be used with little or no effects on the accuracy of the solution (Hicks and Steffler, 1990). This can be explained in terms of spatial resolution, which is defined as the ratio of the wavelength of the disturbance to the spatial discretization. When the spatial resolution of the wave is greater than 20, which is the case for the diffusive wave in the current investigation, the accuracy of the CDG scheme is good regardless of the Courant number. In the investigation by Hicks (1996), the time step increment of 6 hrs corresponds to a Courant number of about 49, based upon the time of travel of the flood peak from Taylor to Peace Point. For the same situation, the cdg1-Dn model required a time step increment of 1 minute, which corresponds to a Courant number of a 0.14. Although, this is not a problem in terms of accuracy, since the accuracy of the CDG scheme increases with decreasing Courant number (Hicks and Steffler, 1990). This illustrates that for the cdg1-Dn model, increasing the time step increment will affect the model stability far before it affects the model accuracy, especially for diffusive waves. In each subreach (with interpolated sections), the event was simulated using a time step increment of 10 s, again, to maintain stability. This time step increment corresponds to a Courant numbers of 0.002 and 0.001 for the spatial discretizations of 0.1 km and 0.2 km, respectively.

3.5.2 Model Application

3.5.2.1 Discharge hydrographs

Figure 3.6 shows the discharge hydrographs obtained for the natural channel models (cdg1-Dn), as compared to the WSC gauge data and the approximate geometry model (cdg1-D). At each location, the results from both models were analyzed in terms of mass conservation and peak discharge accuracy. Mass conservation of the models was determined using:

$$\% error = \frac{M_{in} - M_{out}}{M_{in}} \qquad [3.2]$$

where M_{in} and M_{out} are the masses entering and leaving a subreach, respectively. These masses were determined by integrating the direct runoff (total discharge minus baseflow) entering and leaving a subreach over the simulation period. Table 3.4 shows the mass conservation properties for both models at each of the three subreaches.

Table 3.4 Comparison of mass conservation properties of the natural and approximate channel models.

Location	natural geometry (cdg1-Dn)	approximate geometry (cdg1-D)
Dunvegan Bridge	2.35 %	0.365 %
Town of Peace River	-1.90 %	-3.71 %
Fort Vermilion	-4.54 %	-1.74 %

The conservation formulation of the Saint Venant equations in the cdg1-D model has been found to conserve mass perfectly (Hicks and Steffler, 1990). Consequently, the error in mass conservation displayed by the approximate geometry model (cdg1-D) must be due to the approximate nature of the baseflow separation. As shown in Appendix B, the formulation of the Saint Venant equations in the cdg1-Dn model does not conserve mass under all circumstances. Therefore, it is more likely, that percent error in mass conservation of the approximate geometry model is zero at every subreach and that the error of the natural geometry model is the relative error between the two models at each subreach. This translates to a mass conservation error of 1.99%, 1.81%, and –2.80% at the Dunvegan subreach, the Town of Peace River subreach, and the Fort Vermilion subreach, respectively. The mass conservation errors displayed by the natural channel model reflect both mass conservation errors in the numerical solution as well as errors associated with the approximate nature of the baseflow separation. As Table 3.4 indicates, these errors can be either cumulative (e.g. at Dunvegan and Fort Vermilion) or might tend to cancel each other out (e.g. Peace River). In either case, the total error is small (<5%).

The percent error in peak discharge was calculated at the Dunvegan Bridge and at the Town of Peace River using:

$$\%\,error = \frac{observed\ peak\ discharge - calculated\ peak\ discharge}{observed\ peak\ discharge} * 100 \qquad [3.3]$$

These errors are presented in Table 3.5. As there were no gauge data published at Fort Vermilion, the peak discharge accuracy could not be evaluated at this location.

Table 3. 5 Comparison of peak discharge accuracy of the natural and approximate channel models.

Location	natural geometry (cdg1-Dn)	approximate geometry (cdg1-D)
Dunvegan Bridge	14.9 %	15.6 %
Town of Peace River	6.91 %	2.10 %

Since the natural channel geometry did not really improve the peak accuracy or change the peak discharge at the Dunvegan Bridge, the inaccuracies displayed by both models are likely to do with the neglected tributary inflows. Using natural geometry, the error in peak discharge increased at the Town of Peace River in comparison to the error obtained when the approximate geometry was used. Based on the results of the mass conservation analysis, this error is probably partly numerical.

3.5.2.2 Water levels

Figure 3.7 shows the stage hydrographs obtained for the natural channel models (cdg1-Dn), as compared to the WSC data and the approximate geometry model (cdg1-D). For the Dunvegan subreach, the stage hydrograph did not change much in using the natural geometry. However, this subreach was only defined by 10 cross sections, which spanned 6.1 km. Therefore, it is probable that this subreach was too short with too few cross sections to produce more accurate water level in comparison to the approximate channel geometry. The accuracy of the approximate geometry model is likely due to the fact that the actual cross sections are well approximated by rectangular sections, as shown in Appendix D.

For the Town of Peace River subreach, the use of natural geometry (cdg1-Dn) significantly improved the stage accuracy, with a 0.38 m (-18 % error, based on the ratio between the difference of the measured and computed peaks and the measured stage increase for the event) difference between the observed and computed peak stage in comparison to 1.1 m difference (-31 % error) when the approximate geometry was used (cdg1-D). This is remarkable when one considers that channel resistance was based on very preliminary values and, no calibrating adjustments were made.

At Fort Vermilion, the use of natural channel geometry did nothing to improve the stage accuracy in comparison to the results obtained in using the approximate geometry. In fact, the available natural geometry produced worse results than the approximate geometry, as shown in Figure 3.7. As was the case for the Dunvegan subreach, it is probable that there the available data at Fort Vermilion were insufficient to adequately define the subreach in terms of subreach length and number of cross sections. Also, one might suspect that the data provided had a different datum than the original gauge (which was discontinued at the time the stage data were obtained by AE).

Figure 3.8 presents the rating curves at each subreach. At each location, a very tight (i.e. almost single valued) rating curve was produced. The tight curve illustrates that the wave did indeed display the behaviour of a diffusive wave.

In practice, floodplain delineation requires two steps. A flood routing model (usually hydrologic) is first used to obtain the flood peak. This flood peak would then provide the input for a steady, gradually varied flow model based on detailed natural geometry, such as the US Army Corp of Engineers' HEC-RAS model, to determine flood levels at important sites. As this is the method currently used in practice, it was of interest to see whether this method produced results at the Town of Peace River, comparable to those obtained using the natural channel geometry hydraulic flood routing model (cdg1-Dn). This comparison was only performed for the Town of Peace River subreach, as it was felt that the poor results obtained at the two other sites were a result of the lack of geometry.

Using the same natural channel geometry and channel resistance values that were used in the natural channel model (cdg1-Dn) of the Peace River subreach, HEC-RAS was used to generate a gradually varied profile. The profile was based on the peak discharge flowing into the reach obtained using the cdg1-D model and the peak discharges entering the reach at the Smokey and Heart Rivers obtained from the HYDAT CD-ROM. The profile is presented in Figure 3.9 along with the computed peak stages obtained at the surveyed cross sections using the natural channel model (cdg1-Dn). Using these two methods, the computed water surface profiles are visually very similar. Along the entire reach, the maximum difference in water level between the two sets of results was 29 cm. At the gauge, the difference in water level between the two methods was only 2 cm. Both underestimated the peak stage by about 50 cm; however, it is important to remember that no attempt was made to calibrate channel roughness here. In all, the results illustrate that the natural channel hydraulic model (cdg1-Dn) produces results that are at least as good as those obtained by using the more conventional approach involving a routing model followed by a gradually varied flow model. For this event, there was only a 4% difference between the inflow to and the outflow from the subreach when the peak stage arrived at the Town of Peace River gauge, which illustrates the validity of the using the steady, gradually varied flow approximation to delineate a 'non-dynamic' open water runoff events such as this one.

3.5.2.3 Model blending issues

In this chapter, part of the objective was to determine whether it would be operationally possible to blend the approximate and natural geometry models into one model. In a blended model, the event would be routed in one step using a database comprised of approximate and natural geometry. Essentially, this would be the same as breaking the reach into approximate and natural subreaches and modelling the approximate geometry subreaches with cdg1-D and the natural channel subreaches with cdg1-Dn. In this case, the output from an approximate geometry subreach would provide the input for a succeeding natural geometry subreach and vice versa. In this investigation, because of the time step constraint experienced with the cdg1-Dn model, the event was not modelled in this manner. Instead, the event was simulated using the approximate geometry model of the entire study reach with the output from this model providing the input at the upstream end of each of the three natural channel subreaches. Because the natural channel models were not used to provide the succeeding approximate channel subreaches with input hydrographs, it was necessary to compare the discharge hydrographs produced by both models at the location of the last cross section in each natural geometry subreach. Figure 3.10 presents these comparisons. Since the hydrographs produced by both models at the end of each natural channel subreach are visually very similar, it is clear that for this event, a blended model would have produced the same result as the method used in this investigation. However, if the natural subreaches had been longer or if overbank flow had occurred, then the wave may have experienced more attenuation in the natural model. In that case, it would have been necessary to use the discharge hydrograph from the natural geometry models to continue to the routing, as the approximate model, without the detailed geometry, would not be able to produce the correct wave attenuation within the town reaches.

3.6 CONCLUSIONS

Based on the results from the current investigation, it is concluded that it would be possible to blend approximate and natural geometry models to expedite water level forecasts during flood events. The results from the three subreach models indicate that a natural subreach requires a minimum length and a minimum number of cross sections in order to produce accurate water levels. However, it is difficult to conclude what these minimum values should be except that it appears as though both the Dunvegan (6 cross sections) and Fort Vermilion (10 cross sections) subreaches were insufficiently defined while the Town of Peace River subreach (28 cross sections) was quite well defined. Therefore, more investigations of this sort are required to evaluate the minimum natural geometry data requirements to accurately predict water levels.

The results also suggest that it would be operationally possible to blend the two geometry types into one model. However, the model used in this investigation, the cdg1-Dn model, although capable of handling approximate and natural channel geometry, is not stable enough to be used as a practical flood routing tool. Use of a better Jacobian matrix in the iterative solution technique of the CDG scheme may improve the stability. Ideally, the stability of the cdg1-Dn could be improved to a level commensurate with the stability of the cdg1-D model.

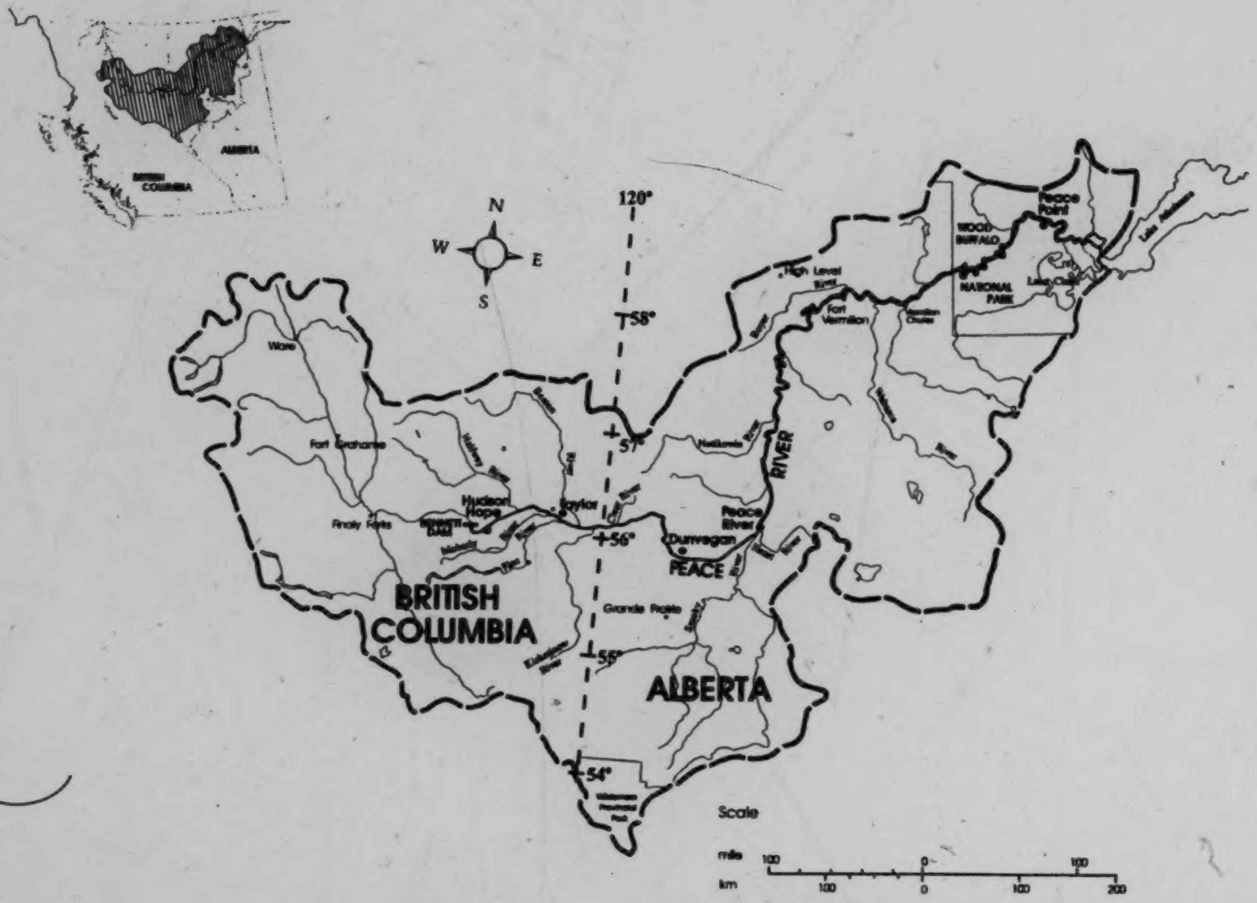

Figure 3.1 Location map of the Peace River study reach.

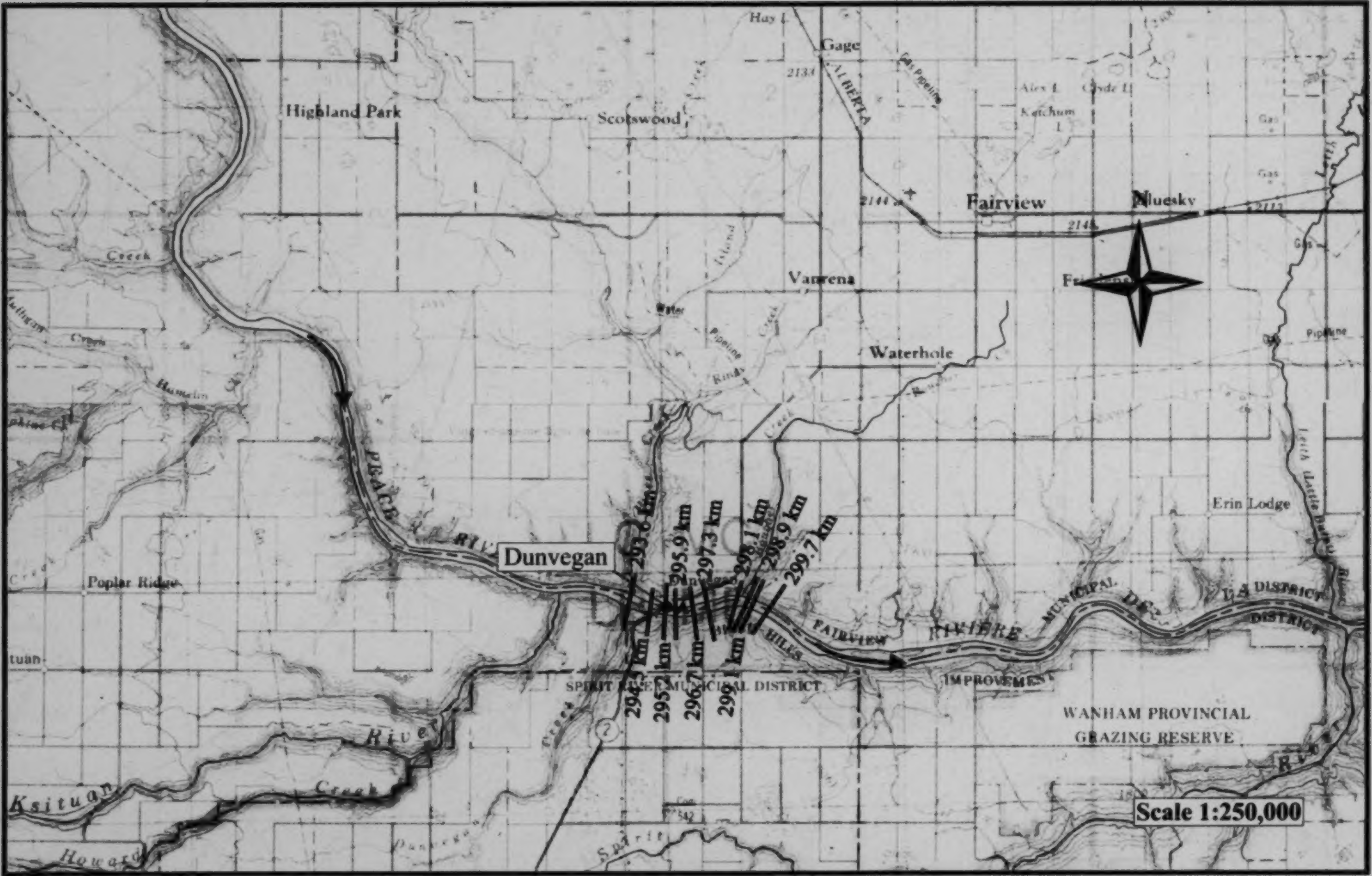

Figure 3.2 Dunvegan subreach showing the location of available cross sections.

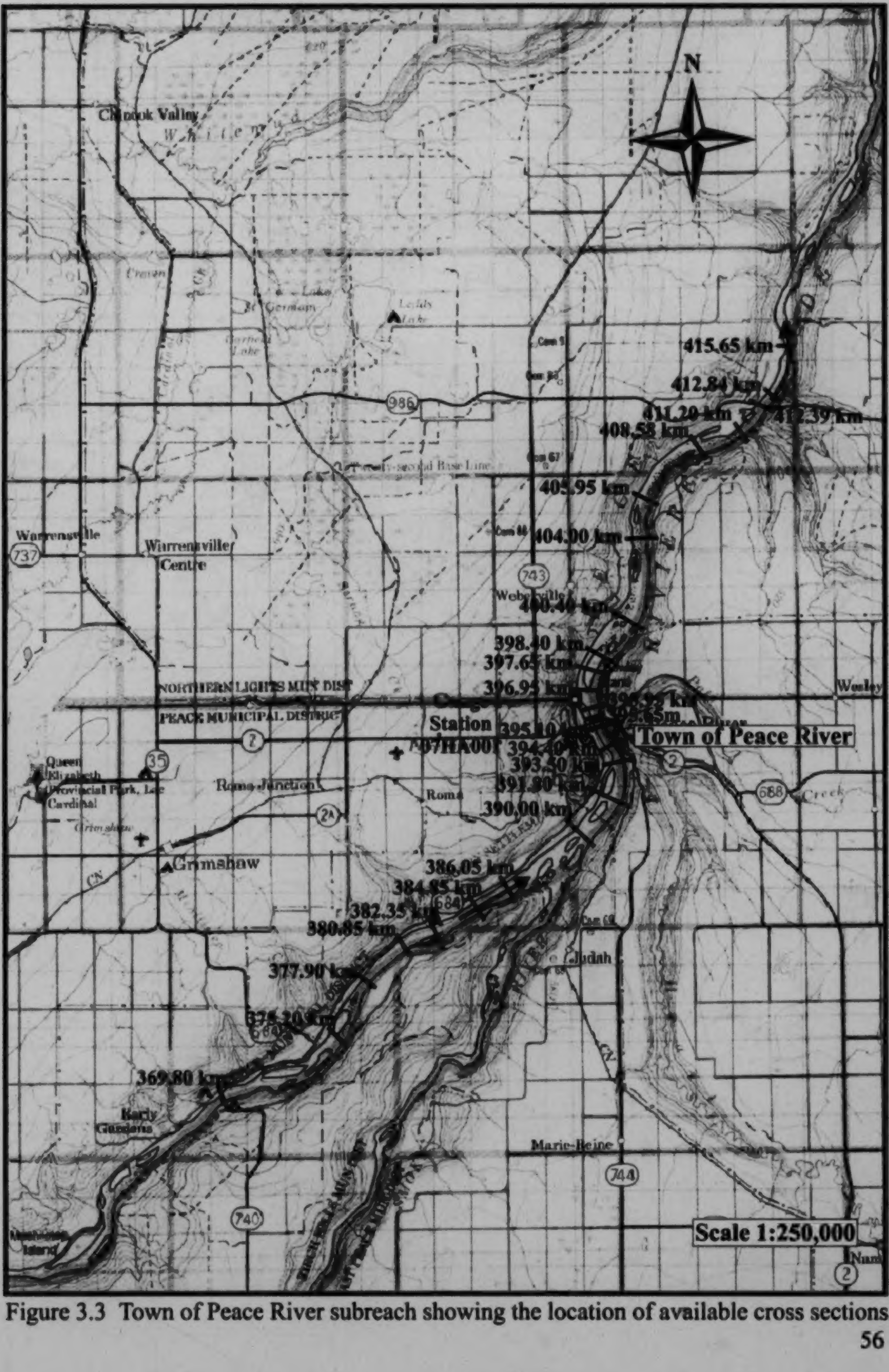

Figure 3.3 Town of Peace River subreach showing the location of available cross sections.

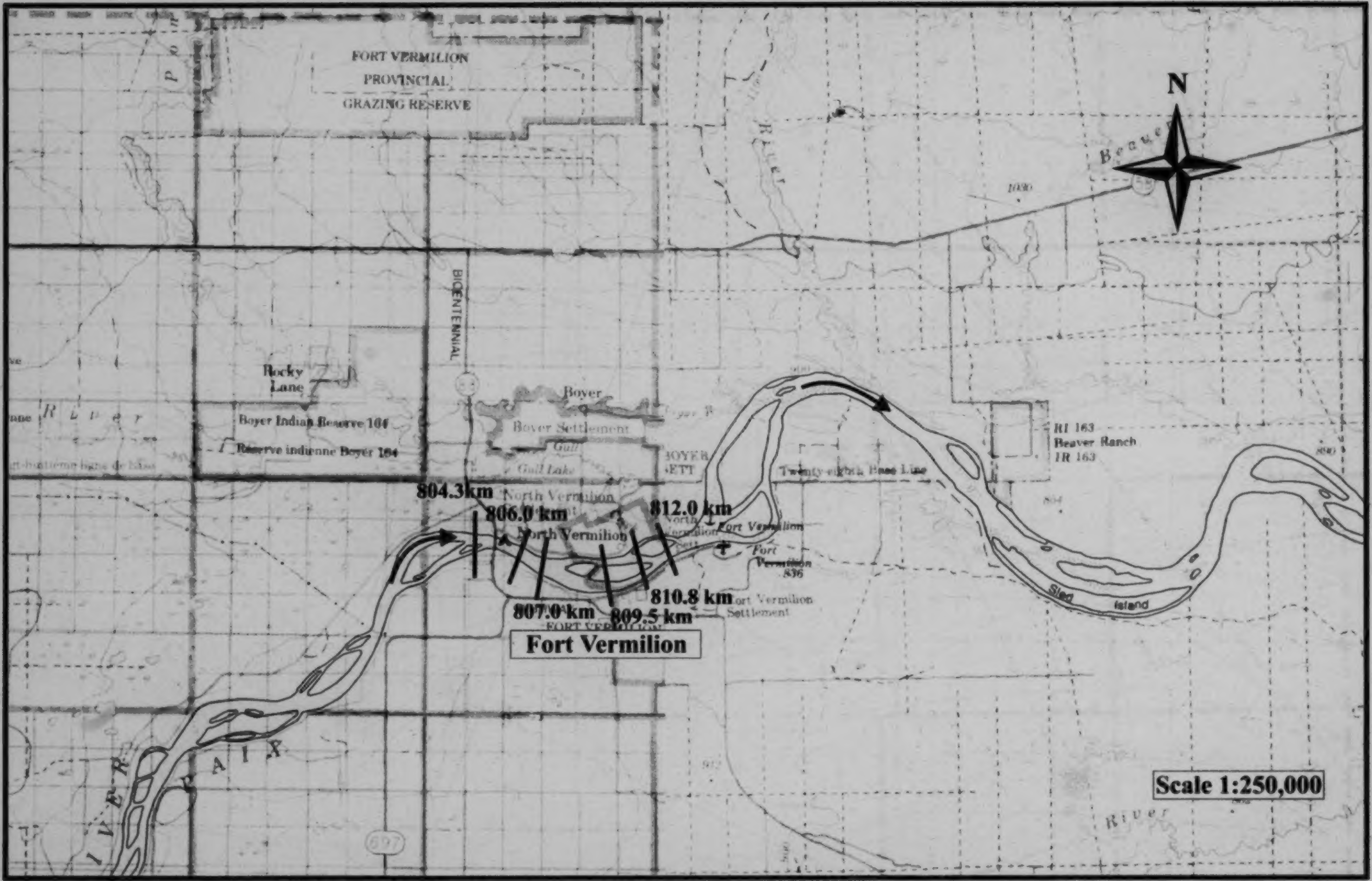

Figure 3.4 Fort Vermilion subreach showing the location of available cross sections.

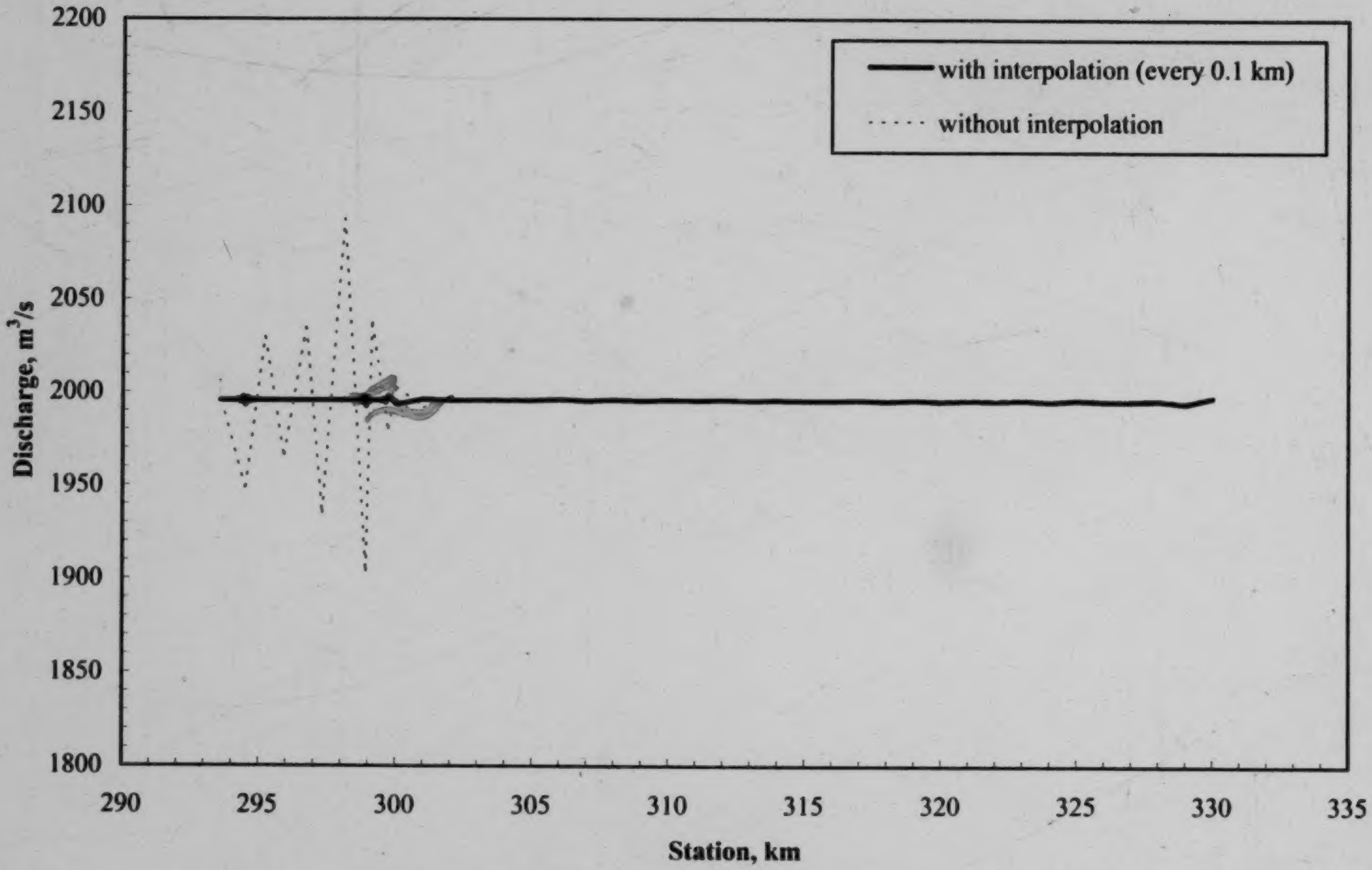

Figure 3.5 Variation in the initial discharge over the Dunvegan subreach.

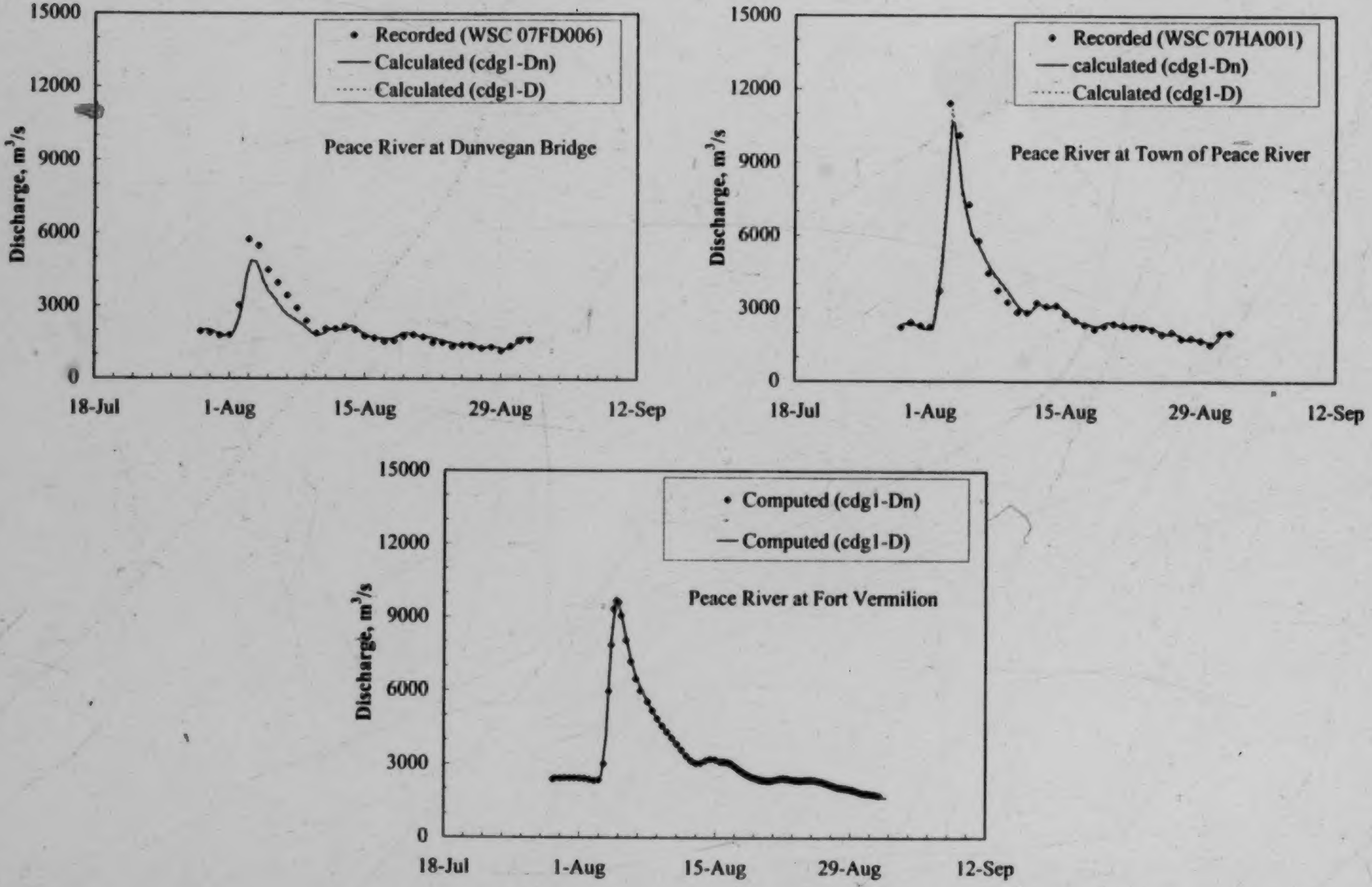

Figure 3.6 Comparisons of measured and computed discharge hydrographs for the 1987 flood event.

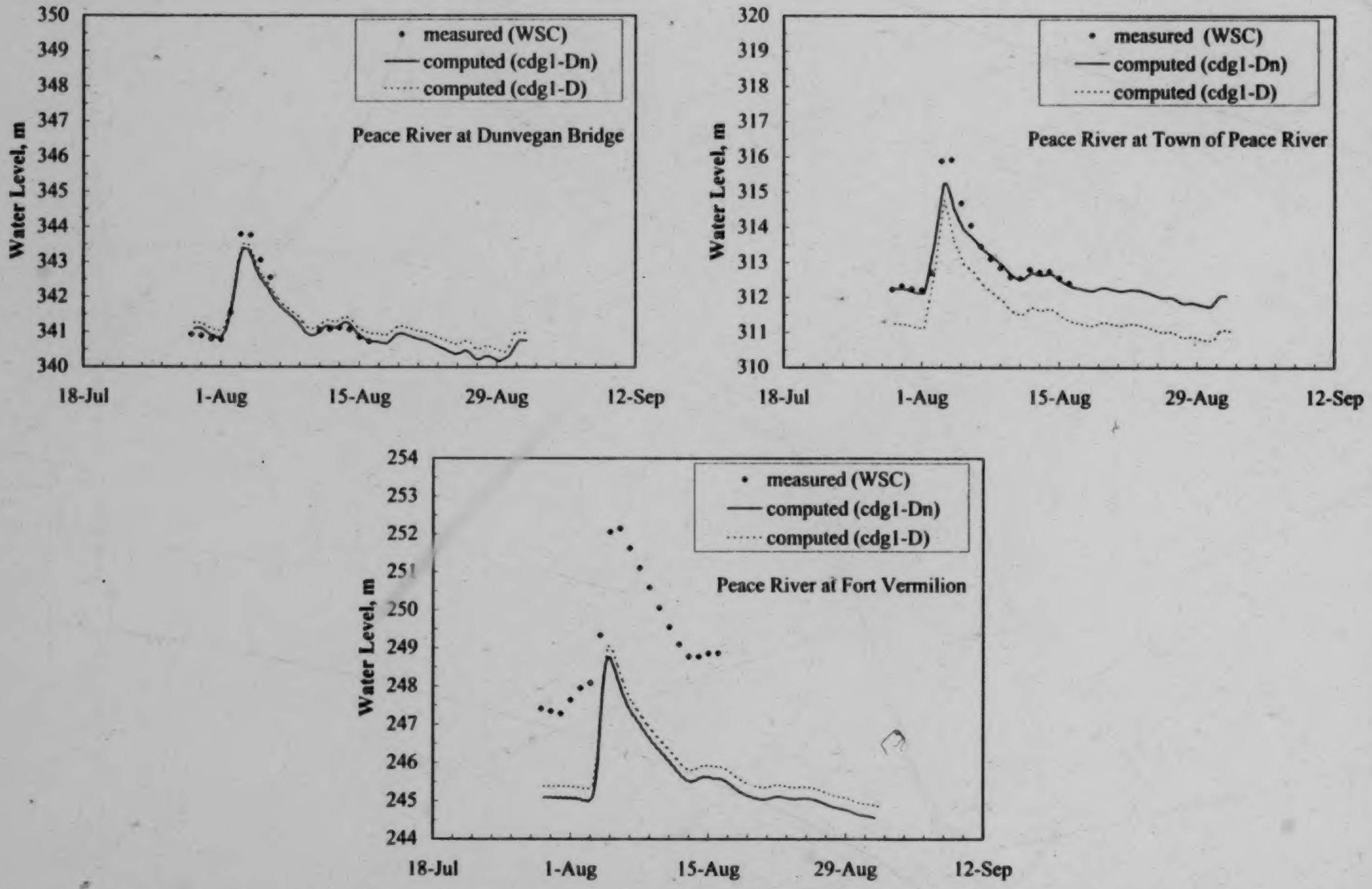

Figure 3.7 Comparison of measured and computed water levels for the 1987 flood event.

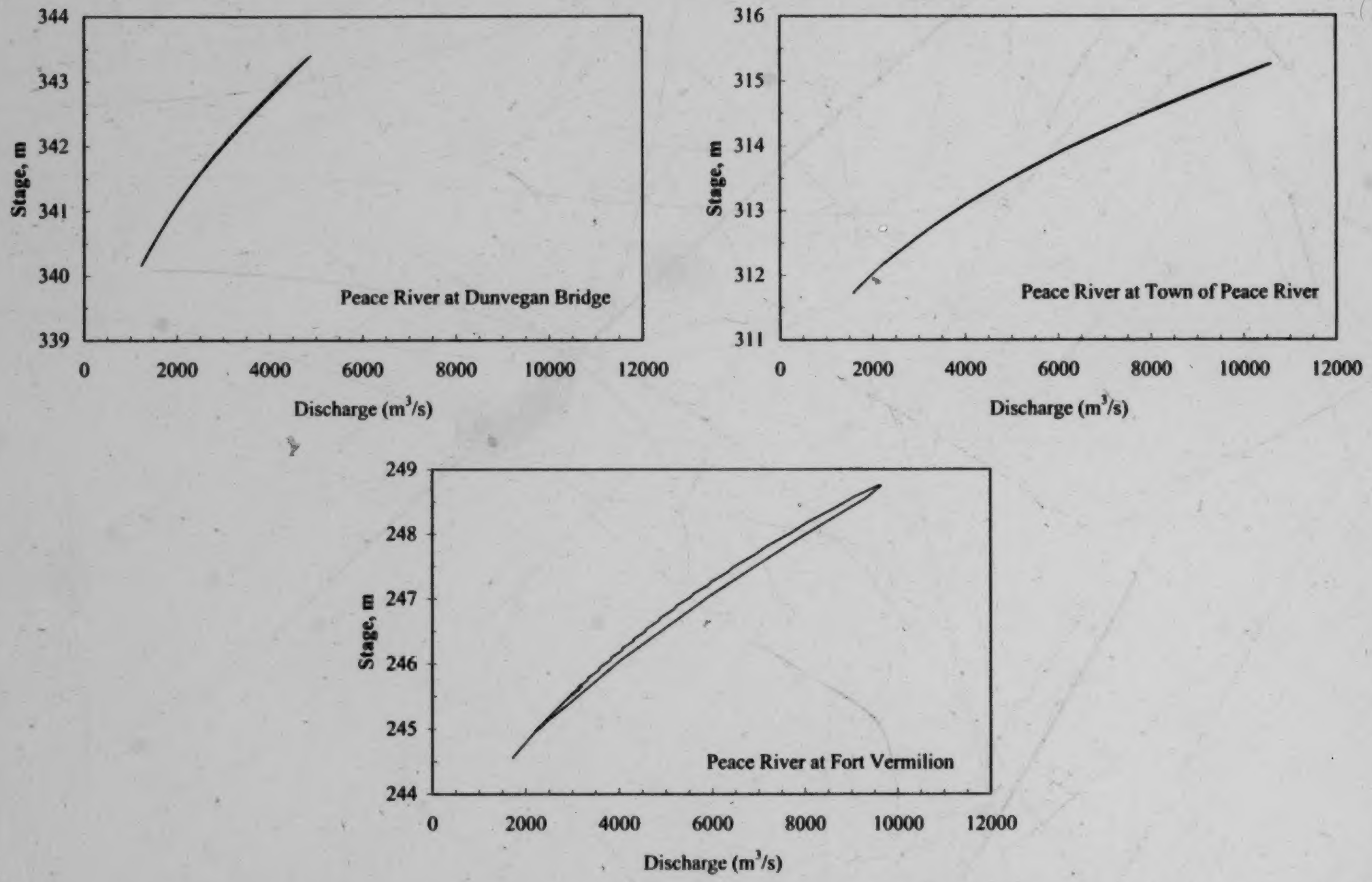

Figure 3.8 Computed rating curves for the 1987 event using the cdg1-Dn model.

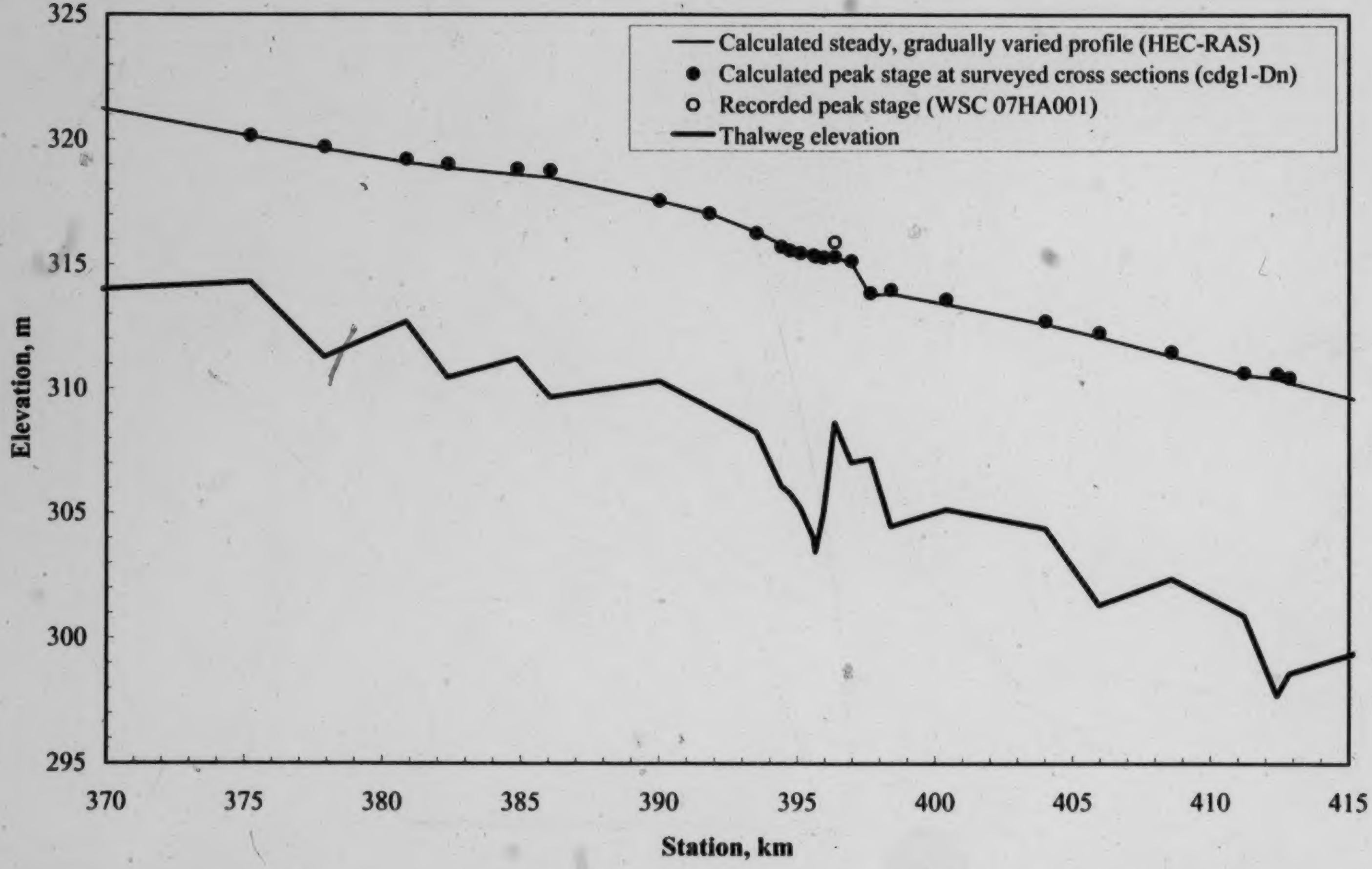

Figure 3.9 Comparison of the peak stage calculated by using HEC-RAS and cdg1-Dn along the Town of Peace River reach.

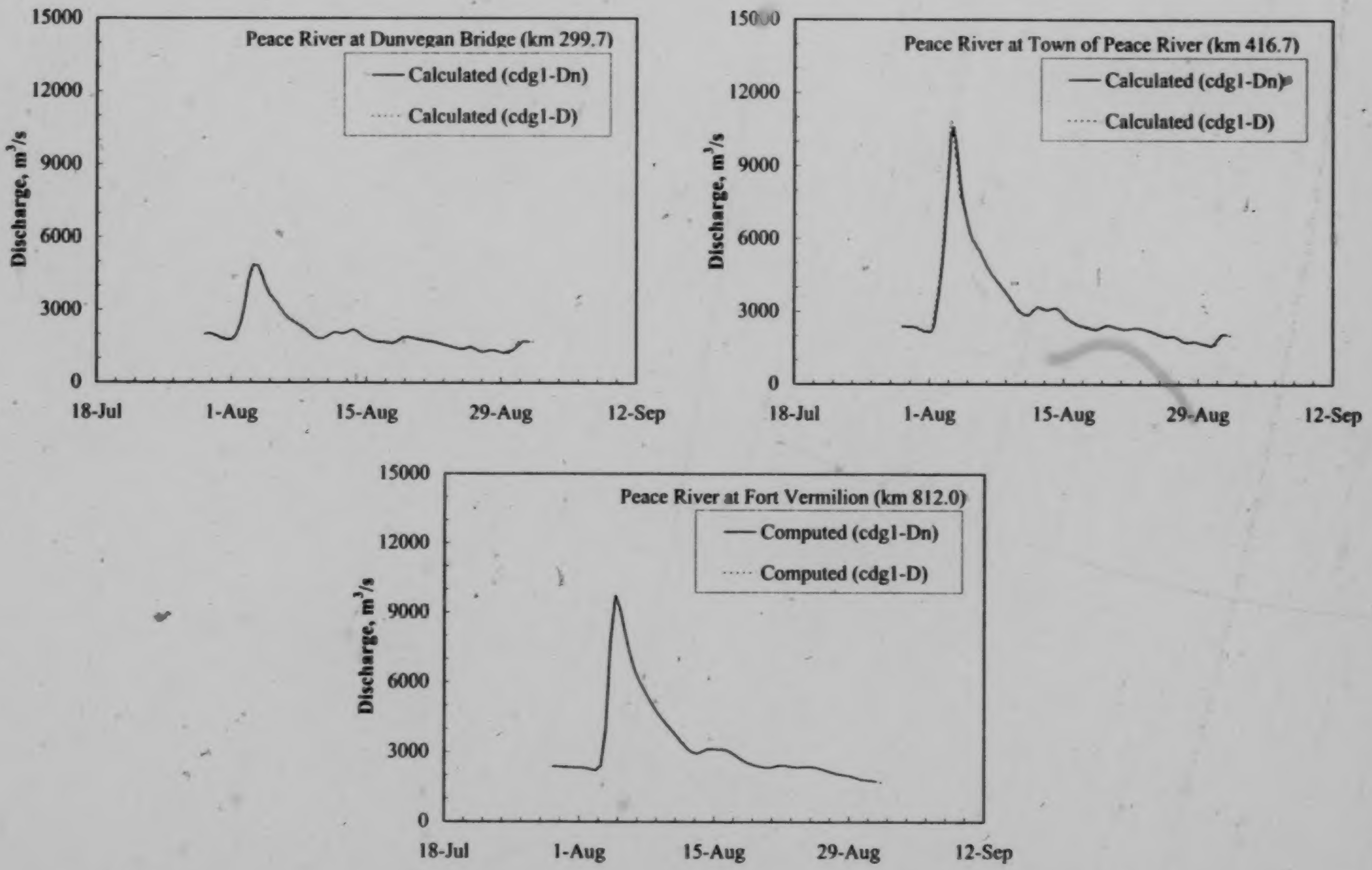

Figure 3.10 Comparison of computed hydrographs at the location of the downstream ends of the natural subreaches.

CHAPTER 4

ICE RELATED FLOOD EVENT: SAINT JOHN RIVER, NEW BRUNSWICK[2]

4.1 INTRODUCTION

During the spring breakup, warm weather can lead to rapid snowmelt and increases in water level. These rising water levels can lift and fracture an ice cover resulting in ice floes being transported downstream. If these floes are halted by an obstruction such as a resistant, solid ice cover, or if the ice transport capacity of the river is locally reduced, an ice jam may form (Beltaos, 1995). Depending on the size, an ice jam has the ability to store a substantial volume of water. If the ice jam suddenly releases, the resulting high velocity surge of water and ice can lead to significant rises in water level which pose a risk to human life and could potentially damage property (Beltaos, 1995).

The purpose of this chapter is to assess whether a hydraulic flood routing model based on detailed natural geometry can be used to route an ice related flood event effectively. This is accomplished through the simulation of an ice jam release which occurred on the Saint John River upstream of Grand Falls Dam in the spring of 1993. This event was chosen for two reasons. One, the event was well documented and therefore the model results could be verified. Two, an ice jam release is a dynamic event that a flood forecaster may encounter which requires the use a dynamic flood routing model such as the cdg1-Dn model. A review of previous ice jam release surge modelling efforts, presented in this chapter, reveals that many investigators suggest that ice jam release surges can be modelled using one-dimensional unsteady open channel models. Therefore, a second objective of this chapter is to further verify the application of one-dimensional unsteady flow models to the problem of ice jam releases. A third objective is to study what effects the ice in, and downstream of, the ice jam has on the resulting surge. Lastly, some conclusions will be drawn about what data are important for modelling ice jam release surges in order to provide advice to field researchers.

---

[2] An abridged version of this chapter will be submitted for publication in the American Society of Civil Engineer's Journal of Cold Regions Engineering.

4.2 MODELLING ICE JAM RELEASE SURGES

4.2.1 Introduction

A number of investigators have attempted to model the surges that can result from an ice jam release. These efforts include modelling ice jam release surges in the laboratory setting, the development of an analytical solution, and the application of numerical models. The following section presents a review of these previous studies.

4.2.2 Previous Studies

4.2.2.1 Henderson and Gerard (1981)

Henderson and Gerard (1981) proposed an analytical solution for an ice jam release. They assumed "that the formation of an ice jam is equivalent to the sudden insertion of an resistant baffle (of zero volume) into the river and that its breakup is equivalent to the sudden removal of the baffle", implying that the effects of ice are negligible after the jam releases. Their approach involves, in essence, a classic dam break solution which assumes:

1. one-dimensional flow;
2. a channel section of rectangular and constant width; and
3. the effects of bed slope and channel resistance are negligible.

The assumed situation is shown in Figure 4.1 (a). Initially the channel is occupied by an ice jam with a steady flow condition upstream and downstream of the ice jam. Figure 4.1 (b) illustrates the solution after it has progressed to some time, t_1, which assumes a positive surge propagates downstream and a negative wave moves upstream while a region of uniform flow develops between the two. In the figure:

h_o = depth of flow downstream of the ice jam prior to the release and downstream of the disturbed region once the jam releases;

h_2 = depth of flow upstream of the ice jam prior to the release and upstream of the disturbed region once the jam releases;

h_1 = depth of flow in the region of uniform flow that develops as the surge forms;

U_o = average flow velocity downstream of the ice jam prior to the release and downstream of the disturbed region once the jam releases;

U_2 = average flow velocity upstream of the ice jam prior to the release and upstream of the disturbed region once the jam releases;

U_1 = average flow velocity in the region of uniform flow that develops as the surge forms;

q_2 = unit discharge upstream of the ice jam;

q_1 = unit discharge downstream of the ice jam;

V_w = speed of the positive surge wave; and

V_n = speed of the negative wave.

Assuming the initial conditions upstream and downstream of the ice jam are known, there are only three unknowns to the problem: V_w, U_1, and h_1. Therefore, three equations are required to determine a solution. As presented by Henderson and Gerard (1981), these equations are as follows.

The first equation is for the negative wave:

$$U_2 + 2\sqrt{gh_2} = U_1 + 2\sqrt{gh_1} \tag{4.1}$$

The second and third equations are the equations of momentum and continuity for the surge, which are developed by changing the frame of reference to one in which the observer is moving at the speed of the surge, V_w.

$$\text{Momentum: } \frac{(V_w - U_0)^2}{gh_0} = \frac{1}{2}\frac{h_1}{h_0}\left(\frac{h_1}{h_0} + 1\right) \tag{4.2}$$

$$\text{Continuity: } V_w(h_1 - h_0) = U_1 h_1 - U_0 h_0 \tag{4.3}$$

Once the equations are solved, the progression of the solution in time can be traced on a phase diagram, provided the propagation of the negative wave and positive surge is uninhibited. The phase diagram for this situation is presented in Figure 4.1 (c) which shows the path of the solution on the x-t plane, and illustrates how the location of the positive and negative wave front can be determined at time, t_I. In the figure:

x = longitudinal coordinate;

t = time coordinate;

t_I = some time t after the ice jam has release ($t = 0$);

Zone I = an undisturbed region upstream of the influence of the negative wave;

Zone II = a region of varying depth and velocity;

Zone III = a region of constant depth and velocity (uniform flow); and

Zone IV = an undisturbed region downstream of the influence of the positive surge wave.

Based on this analytical solution, an observer standing downstream of an ice jam at the time of its release would see a step-like increase in stage, as shown in Figure 4.2(a). In reality, the observer would see something more like the stage-time relationship presented in Figure 4.2(b) where the stage would rise more gradually and would eventually decrease as an ice jam can only store a finite volume of water. Therefore, at best, this solution technique can be used to predict the peak stage of an ice jam release event at a location close to the toe of an ice jam. As a surge propagates downstream the effect of bed slope and channel resistance (neglected in this model) become more prominent, at which point the analytical solution is longer applicable due to the violation of its assumptions.

Using ice jam release data collected by Doyle and Andres (1979) on the Athabasca River at Fort McMurray, Alberta, during the 1979 breakup, Henderson and Gerard (1981) tested the applicability of their proposed theory. They found that the surge height determined using the theory was in close agreement with the observations of the peak height. However, they found that there was a large discrepancy between the observed and theoretical speed of the surge, with the observed speed being considerably less than the predicted value. Ice floes carried by the surge, which are neglected in the theory, were presumed by Henderson and Gerard (1981) to slow the surge and increase its height. As a result, Henderson and Gerard (1981) recommended further investigation of the effect of the ice floes on surge attenuation.

4.2.2.2 Beltaos and Krishnappan (1982)

Beltaos and Krishnappan (1982) considered the problem of an ice-water surge subsequent to the release of an ice jam as an unsteady system with two flow layers: an upper layer of fragmented ice with water contained in the voids, and a lower layer consisting of only water. Through the development of the equations, they deduced that the problem could be handled by one dimensional open water unsteady hydraulic models provided that (i) the 2 layer flow system could be treated as one-dimensional and (ii) the upper ice-water layer developed the same speed as the lower water layer quickly after the release. From an order of magnitude analysis, assuming a constant water speed and ice thickness, they deduced that the fragmented ice cover developed a speed equal to 95% of the water speed within a few minutes. Consequently, they suggested that, as a first approximation, the acceleration time of the ice-water layer could be neglected and therefore the solution of an ice jam release surge could be based on the open water equations.

In order to assess the applicability of open channel unsteady models to the problem of an ice jam release surge, documentation of actual ice jam releases is essential. Beltaos and Krishnappan (1982) described the necessary data as follows. First, the longitudinal water surface profile along and downstream of an ice jam must be documented just prior to its release, to supply initial conditions. Second, a stage hydrograph capturing the passing surge is essential at one or more locations downstream of the ice jam, in order to assess model results. Third, channel geometry and flow conditions are necessary in order to define the computational domain and the boundary condition for the mathematical model.

Using an implicit finite difference scheme developed by Krishnappan and Snider (1977) to solve the Saint Venant equations, Beltaos and Krishnappan (1982) modelled the 1979 Athabasca River breakup data that were previously modelled by Henderson and Gerard (1981). Their model handled channel roughness through a global friction factor (one value for the whole domain for all values of time) which was assumed to account for bed and ice roughness. Although the model was capable of handling natural channel cross sections, it was deemed sufficient to approximate the known channel cross sections by rectangular sections when applying the model.

For the 1979 event, breakup in the town of Fort McMurray was triggered by the release of an ice jam that had formed a few kilometres upstream of town (Doyle and Andres 1979). Both the longitudinal water surface profile of the ice jam prior to its release (initial conditions) and a stage hydrograph downstream of the ice jam release (verification data) were reasonably well documented. As did Henderson and Gerard (1981), Beltaos and Krishnappan (1982) found that the peak height of the surge produced by their model was in good agreement with the observations. However, their model had some difficulties matching the shape of observed stage hydrograph. This was attributed to two factors. First, the model used a constant value to represent channel roughness, when in reality it would be a function of discharge and location along the channel and therefore variable in space and time. Second, after the ice jam released, a new ice jam formed downstream, which could not be handled by the model since it did not take dynamic ice processes (such as the formation of an ice jam) into consideration.

4.2.2.3 Joliffe and Gerard (1982)

Joliffe and Gerard (1982) performed laboratory studies to investigate whether ice released from an ice jam modified surge characteristics. Laboratory ice jams were formed by placing polyethylene pellets upstream of a sluice gate in a 1.2 m wide flume. This configuration simulated the step-like initial conditions assumed by Henderson and Gerard (1981) in their analytical solution. Ice jam failure was simulated by suddenly lifting the sluice gate. Hydrographs were recorded 150 mm upstream of the sluice gate for variable ice thicknesses and flow depths, and the results were found to agree well with the predictions from Henderson and Gerard's (1981) theoretical solution. Model ice was observed to travel at the average flow velocity, which was much slower than the surge velocity and, as a result, it was deemed that the ice from the jam should not affect the propagation of a surge. They concluded that, in the absence of large amounts of friction along the banks, the ice in a jam has negligible effect on the post-release flow.

Joliffe and Gerard (1982) also conducted a numerical analysis using the Saint Venant equations to assess the effect of bed slope, channel resistance and ice jam profile on ice jam release surges. The equations used in their analysis were:

$$\frac{\partial A}{\partial t}+\frac{\partial Q}{\partial x}=0 \qquad [2.1]$$

$$\frac{\partial Q}{\partial t}+\frac{\partial (Q^2/A)}{\partial x}+gA\frac{\partial h}{\partial x}-gAS_o+gAS_f=0 \qquad [2.2]$$

For this analysis they assumed a very flat ice jam profile in a rectangular channel with significant bed slope and channel resistance, which was in contrast to the assumptions made in Henderson and Gerard's (1981) simple dam break analysis. Their computational model predicted larger maximum flow depths and lower maximum velocities compared to the simple dam break analysis. They therefore concluded that the dam break analysis should only be used when the assumptions inherent in the analysis represent the ice jamming conditions at hand, that is: minimal bed slope and channel resistance; and, a discontinuity in the water surface profile at the ice jam toe.

4.2.2.4 Wong, Beltaos and Krishnappan (1985)

Wong *et al.*, (1985) conducted laboratory experiments in order to investigate the validity of the ice jam release models of Henderson and Gerard (1981), and Beltaos and Krishnappan (1982). In the experiments, ice jams were simulated by delivering polyethylene blocks into the upstream end of a 1m wide rectangular flume, impeding their movement downstream using a porous retaining gate (Wong *et al.*, 1983). The ice jams were then released by suddenly removing the retaining gate. Stage hydrographs were recorded at a number of stations along the length of the flume and the results were compared to the model predictions. In total five experimental runs were conducted. The water levels predicted by the method of Beltaos and Krishnappan (1982) agreed well with the measured levels at all stations. In addition to accurately predicting the initial surge, the model was also capable of capturing the wave reflected of the downstream end of the flume. In contrast, the analytical solution of Henderson and Gerard (1981) was only able to predict the peak water level at every station. Like previous investigators, Wong *et al.*, (1985) concluded that moving ice has minimal effect on post ice jam release surges.

4.2.2.5 Hicks, Steffler and Gerard (1992)

To facilitate the development of a flood forecasting model, Hicks *et al.*, (1992) applied the cdg1-D model to the of the propagation of ice jam release surges on a 500 km reach of the Hay River in Alberta and the Northwest Territories. The Hay River study reach presented significant challenges to the model because there are several supercritical and subcritical flow transitions and was therefore a practical test of the CDG scheme.

To model the reach using the cdg1-D model, the channel had to be approximated using an equivalent rectangular channel, defined by an 'effective bed profile' and varying channel top widths along the study reach. This was achieved using limited available survey data and supplemented with National Topographic Series (N.T.S.) maps. The effective bed elevations at the surveyed cross sections were determined by dividing the flow area by the top width at the 1:2 year flood level, and then subtracting this mean depth value from the 1:2 year water level. Water surface slopes obtained from the N.T.S. maps were then used to extend the bed elevations throughout the entire computational domain in order to define the effective bed profile for the model. Between surveyed cross sections, channel top widths in the model were measured from the N.T.S. maps.

The initial conditions for the ice jam release simulation were obtained by superimposing an ice jam profile on a gradually varied flow profile calculated for a carrier discharge of 500 m^3/s. To develop the ice jam profile for the simulation, a number of assumptions were used. At the downstream end of the jam profile, it was assumed the ice jam had a toe length equal to the grid spacing in the model (1000 m). Upstream of the jam, the gradually varied flow profile, which would be an M1 backwater curve, was approximated by extending a horizontal line back from the jam head to its intersection with the initial gradually varied flow profile. Within the jam, the flow depths were based on those for an equilibrium reach of a fully developed jam using the following relationship as presented by Beltaos (1983, 1995):

$$\eta = 0.38\zeta + \frac{5.75}{\mu}\left\{1 + \sqrt{1 + 0.07\mu\zeta\left(\frac{k_i}{k}\right)^{\frac{1}{4}}}\right\} \qquad [4.4]$$

where

$$\eta \equiv \frac{d}{S_f B} \qquad [4.5]$$

and

$$\zeta \equiv \frac{\left(qk^{\frac{1}{6}} / \sqrt{gS_f}\right)^{\frac{3}{5}}}{S_f B} \qquad [4.6]$$

in which

μ = an internal friction - porosity coefficient;

d = the depth to the phreatic surface;

S_f = the slope of the water surface (approximating the friction slope); and

B = the pack width, and q the discharge per unit width of channel.

The composite roughness k, is based on the ice roughness, k_i, and the bed roughness, k_b, such that[3]:

$$k = \left(\frac{k_i^{1/4} + k_b^{1/4}}{2}\right)^4 \qquad [4.7]$$

Beltaos (1995) defines an equilibrium reach as the region within a fully developed jam where the thickness of the jam is relatively uniform and the water surface slope is essentially equal to the channel bed slope. Current knowledge regarding ice jams suggests that the maximum ice thickness and flow depth occur within this equilibrium section. Therefore, Hicks *et al.*, (1992) used an equilibrium jam to provide a 'worst-case' scenario for flood forecasting on the Hay River.

For the jam release simulation, it was assumed that the jam failed instantaneously and that the ice in the jam had no resistance effect on the flow once the jam released. It was also assumed that downstream of the toe of the jam, open water conditions existed (i.e.

---

[3] Note that the form of the equation presented here corrects a typographical error in Hicks and Steffler, 1990 and repeated in Hicks *et al.*, 1992.

absolutely no ice cover). Although these assumptions represented a simplification of the actual physical processes, they had the effect of reducing the amount of attenuation of the released wave. Therefore, Hicks *et al.*, (1992) chose to use these assumptions as they delineate a worst case scenario for flood risk from ice jam release surges.

Their results illustrated the ability of the CDG scheme to handle the propagation of surges through subcritical and supercritical flow transitions, and to deliver stable solutions when a dynamic wave transforms into a diffusive wave and then into a wave that is essentially kinematic. Unfortunately, due to the lack of documented ice jam release events on the Hay River, it was not possible to verify the model results. Nevertheless, as the assumptions for the ice jam simulation provided conservative results, Hicks *et al.*, (1992) used the model results to report an upper bound on the severity of possible ice jam release events on the Hay River.

4.2.2.6 Saadé, Sarraf, and El-Jabi (1993)

Saadé *et al.*, (1993) developed a numerical model that solves the two-dimensional shallow water equations for open channel flow using the Modified MacCormack explicit finite-difference scheme. They modified the equations to include the effects of an ice jam on the flow by considering an ice jam as a simple ice cover such that the conservation of mass and momentum can be given as follows:

Continuity

$$\frac{\partial h}{\partial t}+\frac{\partial uh}{\partial x}+\frac{\partial vh}{\partial y}=0 \qquad [4.8]$$

Momentum in the x-direction

$$\frac{\partial uh}{\partial t}+\frac{\partial u^2 h}{\partial x}+\frac{\partial uvh}{\partial y} = g\frac{\partial}{\partial x}\left(\frac{1}{2}h^2+S_i\theta h\right)+g\left(h+S_i\theta\right)_{ave}\left(S_{xo}-S_{fx}\right)+gS_i\theta_{ave}\frac{\partial H}{\partial x} \qquad [4.9]$$

Momentum in the y-direction

$$\frac{\partial uh}{\partial t}+\frac{\partial v^2 h}{\partial y}+\frac{\partial uvh}{\partial x} = g\frac{\partial}{\partial y}\left(\frac{1}{2}h^2+S_i\theta h\right)+g\left(h+S_i\theta\right)_{ave}\left(S_{xo}-S_{fy}\right)+gS_i\theta_{ave}\frac{\partial H}{\partial y} \qquad [4.10]$$

where:

u = depth averaged longitudinal velocity;

v = depth averaged transverse velocity;

h = depth of flow;

H = stage;

θ = ice cover thickness;

S_i = specific gravity of ice;

S_{fx} = longitudinal boundary friction slope;

S_{fy} = transverse boundary friction slope;

S_{xo} = longitudinal channel bed slope;

S_{yo} = transverse channel bed slope;

x = longitudinal coordinate;

y = transverse coordinate; and

t = temporal coordinate.

After being tested for a theoretical open water surge, the model was used to simulate laboratory tests of ice jam releases using the data collected by Wong *et al.*, (1983, 1985).

To model these laboratory experiments, Saadé *et al.*, (1993) acquired the initial conditions for the simulation using an approach similar to that used by Hicks *et al.*, (1992). The initial conditions were obtained by imposing an ice jam on the flow in the model and then by subsequently running the model until a steady state water surface profile was achieved. This was in contrast to the approach used by Wong *et al.*, (1985), where the measured initial water surface profile from the experiments provided initial conditions for the numerical simulations. The model results agreed well with those from the experimental tests; however, as the laboratory tests were one-dimensional, no verification of the two-dimensional aspect of the computational model could be made.

4.2.2.7 Hicks, McKay, and Shabayek (1997)

Hicks *et al.*, (1997) presented the results of a numerical simulation of the Saint John River ice jam release that is to be modelled in the current investigation (Figure 4.3). The surge propagation analysis was conducted using the same cdg1-D unsteady flow model applied in the Hay River Study, which solves the Saint Venant equations for rectangular channel geometry using the CDG finite element scheme.

This ice jam release event was well documented by Beltaos *et al.*, (1994) and therefore provided an excellent data set with which to assess the applicability of open channel unsteady flow models to ice jam surge release modelling. The day prior to the release, a detailed longitudinal profile was measured along the length of the jam. A stage hydrograph was documented a short distance downstream of the jam, following its release. Hourly discharge data on the Saint John River and on four major tributaries along the study reach were available. In addition, detailed cross section geometry of the reach where the event occurred was also available, which was used to create a geometric database for the cdg1-D model. This database defined the reach in terms of an effective bed profile and channel widths.

Because the flow in the study reach of the Saint John River was subcritical, one boundary condition had to be specified at each end of the modelled reach as well as all tributary inflows. The upstream boundary in the model was taken at a Water Survey of Canada

(WSC) gauge upstream of the location of the jam, as the data from the gauge provided the inflow hydrograph required to define the upstream boundary condition. The downstream boundary was also located at a WSC gauge. The downstream boundary condition was set to a constant stage estimated from the gauge data. As streamflow data were only available on four of the tributaries that flow into the Saint John River within the study reach, only these lateral inflows were input to the model; any ungauged tributaries within the study reach were neglected.

The initial conditions for the model were established in three steps. First, the model was used to compute a steady, gradually varied flow profile for constant incoming and tributary inflows. These constant flows were based on the observed flows at the time when hourly discharge data were first available (specifically, once ice had cleared from the major tributaries and gauges were operational). The gradually varied flow profile was then used as the initial condition for routing the hourly discharge data to the point in time when the jam was observed to release. The measured ice jam profile was then superimposed onto the computed water surface profile to obtain the initial conditions for the ice jam release simulation.

Once the initial and boundary conditions were established, the ice jam release was simulated by the routing upstream and tributary boundary hydrographs down the study reach. It was assumed from the beginning of the simulation that the jam failed instantaneously and that the ice in the jam provided no resistance to the flow once the jam released. Although sheet ice was observed downstream of the jam prior to its release, it was not accounted for in the simulation.

The model results agreed reasonably well with a discharge hydrograph observed at a location downstream of the jam. The model also displayed good wave speed accuracy. The model, however, performed quite poorly with respect to stage, with the predicted peak stage being approximately 1m higher than the observed peak. Hicks *et al.*, (1997) attributed the poor stage accuracy to the approximate geometry, reasoning that detailed channel geometry is necessary to accurately determine water levels. They also attributed the poor stage accuracy to the ungauged tributaries that were neglected in the simulation and the fact that the observed downstream ice cover was not taken into account in the simulation.

4.2.2.8 Khan, Steffler, and Gerard (2000)

Khan *et al.*, (2000) conducted a series of experiments to study the effects of floating debris on dambreak surges. In their experiments, plastic particles were used to simulate the debris. Although the authors believed the results of the experiments to be representative of the whole class of floating debris, the model material in fact has a specific gravity of 0.92 which is most representative of river ice. Unlike the previously mentioned laboratory studies, this series of experiments examined the effects of floating debris (ice) on the resulting surge for the case when the debris is initially on the downstream side of a dam. This situation could be considered analogous to the presence of broken ice downstream of a releasing ice jam.

The experiments were conducted in a 0.411 m wide horizontal flume with a vertical gate located 17.23 m from the downstream end to act as the dam. Dambreak surges were simulated by suddenly lifting the gate. In all, 27 experiments were conducted by varying the downstream and upstream depths and by changing the concentration of debris downstream of the dam. In general, the results of this investigation revealed that the presence of debris slows the resulting surge and increases the surge height with respect to the classic dambreak solution. However, they found that these effects decrease as the downstream to upstream depth ratio increases.

What may be of interest to river ice engineers is the behavior of the debris (ice) depended on the downstream to upstream depth ratio. When low values of depth ratio were tested, the debris stayed ahead of the surge dragging along the bottom of the flume. This is the type of situation that has been observed to initiate a grounded jam in the field (Beltaos, 1995). For higher values of the depth ratio, the downstream depth provided more vertical room for the debris and therefore the surge was able to get ahead of the debris. This observation is similar to those made by Jasek (1996) of an ice jam release event on the Porcupine River, NWT. For that event, at a gauge approximately 200 km downstream of an observed jam release, 80% of the surge height had arrived before the first ice from the jam reached the gauge.

4.2.3 Need for Further Studies

While the above mentioned studies are important contributions toward understanding the ice jam release problem, the numerical methods employed have only had limited verification. Therefore, as mentioned previously, the analysis described herein was conducted to further verify the application of one-dimensional unsteady flow models to the problem of ice jam releases. Furthermore, this analysis was conducted to improve the current understanding of ice jam releases by examining the effects of ice in the jam and of ice in the receiving channel on the resulting surge, which have been assumed negligible in the previous numerical investigations. Finally, the simulation of the 1993 Saint John River jam release presented here represents an improvement over the one conducted by Hicks *et al.*, (1997), as in this analysis, fewer assumptions were made. Specifically, the rectangular channel approximation was not used, as it is not required for the cdg1-Dn model; ice in the downstream channel was not neglected; the available stage data were used as the downstream boundary condition, instead of assuming a constant stage throughout the simulation; and the ice jam profile was adjusted to account for differences in flow between the time of the profile measurement and the time of the final release, rather than using the measured profile.

4.3 DESCRIPTION OF THE STUDY REACH

Figure 4.3 shows the location of the Saint John River. Its basin is one of the largest river basins in Eastern Canada with a drainage area of 55 320 km^2 (Zufelt, 1999). Approximately two-thirds of the basin lies in Canada (Quebec and New Brunswick) and one-third lies in the state of Maine, U.S.A. (Zufelt, 1999). Approximately half of the total basin area is in New Brunswick (Ismail and Davies, 1992). The river's headwaters originate in Little Saint John Lake in Maine and travel for approximately 700 km before emptying into the Bay of Fundy at Saint John, New Brunswick. Along the river, there are three large hydroelectric plants: Grand Falls, Beechwood, and Mactaquac (Humes and Dublin, 1988).

Figure 4.3 also illustrates the study reach of the Saint John River. In this reach, the river flows east and then southeast along the international border between Canada and the United States, from Fort Kent, Maine to the dam at Grand Falls, New Brunswick for a distance of approximately 100 km. The Grand Fall Dam creates a head for run-of-river hydropower operation and has essentially no ability to create backwater effects on the upstream reach (Ismail and Davies, 1992). The river changes character along the study reach from "steep and shallow" in the upper portion of the reach to "flat and deep" near St Leonard (Beltaos *et al.*, 1994). Near St. Leonard, the bed material is comprised mostly of gravel with a median size of 2 cm, while the banks and the tributaries of the St. John are composed of more clayey material (Beltaos *et al.*, 1994). Table 4.1 presents the location of key sites along the study reach measured in kilometers (along the channel centreline) downstream of Fort Kent.

Table 4.1 Location of key sites along the Saint John River (adapted from Hicks *et al.*, 1997).

Location	Station (km)
Fort Kent WSC gauge (01AD002)	1.3
Edmundston WSC gauge (01AD004)	32.6
Ste-Anne-de-Madawaska	62.0
Head of Jam, April 14, 1993	60.9
Toe of Jam, April 14, 1993	69.0
Saint Leonard	74.3
Grand Falls WSC gauge (01AF002)	95.3

4.4 DETAILS OF THE DOCUMENTED ICE JAM RELEASE EVENT

The 1993 ice jam release event modelled in this study was well documented by Beltaos *et al.*, (1994). On April 12, 1993 an ice jam formed near Ste-Anne-de-Madawaska, and the high water levels upstream of the jam caused the closure of the Trans-Canada Highway at Riviere Verte, 15 km upstream of Ste-Anne-de-Madawaska. On the April 13 the jam released and reformed a few kilometres downstream (toe at km 69.0) and remained in place for approximately two days. Water surface profiles measured along the length of the new jam on April 13 and 14 extended upstream to km 50.2. All through April 13 and 14 the flooding worsened, requiring more closures of the Trans-Canada Highway.

The final jam release occurred at approximately 09:00 h on April 15, 1993. The surge peak water level arrived at Saint Leonard, approximately 5 km downstream of the jam toe, 48 minutes after the jam release. Ice from the jam was first documented passing Saint Leonard 35 minutes after the ice jam released and ice floes continued to pass through the town for 90 minutes. Water levels were monitored at Saint Leonard during the event to document the magnitude and shape of the resulting surge wave. During this period, two Water Survey of Canada (WSC) gauges on the Saint John River, Fort Kent and Grand Falls, and WSC gauges on four major tributaries were all operational.

At the time of the release, the channel upstream of the ice jam was free of ice, although there was likely remnant ice along the banks. This was not the situation downstream of the ice jam. On April 13, 1993, sheet ice was observed extending from the jam toe downstream to 'about km 72.6'; broken ice from 'about km 76.6 to km 77.6'; and sheet ice again from 'about km 77.6 to km 83.7'.[4] It is believed that no significant decreases in the extent of ice coverage downstream of the ice jam occurred between the time of these observations and the time the ice jam released.

---

[4] Obtained through personal communications with Dr. Spyros Beltaos in 1996.

4.5 MODEL DATA REQUIREMENTS

4.5.1 Introduction

In order to simulate an ice jam release surge using the cdg-1Dn model, a number of data requirements must be satisfied. The channel geometry along the reach of interest is required to define the computational domain. The hydraulic resistance, which may be treated as a calibration parameter, must be defined along the length of the channel. To solve the non-linear partial differential equations in the cdg1-Dn model, the upstream, downstream and lateral inflow boundary conditions must all be specified. The model also requires initial conditions throughout the computational domain. Verification data are needed to evaluate the model's performance in simulating the ice jam release surge.

4.5.2 Geometric Data

The available cross-section surveys were supplied by the National Water Research Institute (NWRI) and New Brunswick (N.B.) Power. The abundance of available surveys is shown in Figure 4.4. The cross section data cannot be presented explicitly as, at this time, there is an impending court case regarding the 1993 ice jam release event. As mentioned previously, all the sections have been referenced in terms of their location, in river km, downstream of the town of Fort Kent. The computational domain starts at the WSC gauge at Fort Kent (km 1.32) and ends at the WSC gauge at Grand Falls (km 95.3).

For better accuracy, evenly spaced nodes and/or gradual changes in geometry are preferred. For this analysis, an even nodal spacing of 0.4 km was used. This was chosen by considering the spacing of the surveyed cross sections and the computation time step increment (since this is a dynamic problem it was desirable to ensure that the Courant number did not exceed 0.5). The surveyed data consist of 79 cross sections, defining the main channel only. Within these data, the maximum distance between two sections is 7.35 km and the minimum distance is 0.01 km. In trial model tests, a time step of 1 second had to be used in order to ensure stability of the cdg1-Dn model when only the original surveyed sections were used. This is because the time step increment is a function of the smallest space increment in the computational domain (0.01 km). Therefore, it was decided that a uniform spacing of the nodes would be more practical with a spacing greater than 0.01 km. In order to obtain a uniform spacing for the computation domain, cross sections must be removed or interpolated depending on the spacing in the surveyed sections. As it was desirable to use as many of the surveyed sections as possible in the computational domain, a nodal spacing of 0.4 km was chosen as this value only required the removal of 13 of the 79 survey sections. This spacing permitted a computational time increment of 5 second (which corresponds to a Courant number of 0.12 based on the speed of the wave between the toe of the jam and Saint Leonard).

The model geometry was developed from the available cross sections in two steps. The first step involved obtaining the desired spacing of 0.4 km between computational nodes. As previously stated, some of the original sections had to be removed where the spacing was less than 0.4 km and new sections had to be linearly interpolated where the spacing was greater than 0.4 km. In total, 198 cross sections were used to define the computational domain.

The second step involved converting the cross section *x-y* coordinates into the form of a table of topwidths, required by the cdg1-Dn model. The available cross sections define the main channel only. Therefore, they were converted into topwidth table defined by 8 topwidths, as per the recommendations presented in Appendix C.

4.5.3 Resistance

In hydraulic models, channel resistance is the only calibration parameter. As a first approximation, Mannings *n* was taken as 0.025 upstream of Edmundston and 0.020 downstream of Edmundston, based on information supplied by N.B. Power[5] for open water conditions. However, downstream of the head of the jam channel resistance was handled in a number of ways in this analysis in order to account for the effects of ice in and downstream of the jam on the resulting surge.

---

[5] Obtained through personal communications with Dr. Sayed Ismail in 1996.

4.5.4 Boundary Conditions

4.5.4.1 Upstream boundary condition

As in previous studies (Hicks *et al.*, 1997; Beltaos and Krishnappan, 1982), the initial conditions for the ice jam release surge were obtained by superimposing the measured ice jam profile on a computed flow profile. Therefore, it was important to choose an upstream boundary that extended far enough upstream to include the backwater effects of the jam. Furthermore, the model requires an inflow boundary condition that typically consists of a discharge hydrograph. Therefore, the upstream boundary in the model was taken at the WSC gauge 01AD002 (km 1.32) on the Saint John River immediately downstream of Fort Kent. This location was approximately 30 km upstream of the effects of any backwater created by the jam and hourly discharge data were available at this gauge through the entire simulation period.

4.5.4.2 Downstream boundary condition

In order to compare computed and measured hydrographs, it was essential to choose a downstream boundary that extended past Saint Leonard, the location where a hydrograph was measured capturing the release surge as it passed. The model requires a computational outflow boundary condition that may be a stage or discharge hydrograph, or a stage-discharge relationship. However, if this sort of relationship is unavailable, the downstream boundary can be chosen far enough downstream of the study area such that the influence, backwater or drawdown, of an estimated constant stage is not felt. In this analysis, the downstream boundary in the model was taken as the upstream face of the Grand Falls Dam (km 95.3). In addition to the fact that the actual dam structure would prevent surge propagation, this location was chosen as the downstream boundary because the model has no way of handling hydraulic structures such as dams. At this location, hourly stage data measured at Grand Falls by N.B. Power provided the downstream boundary condition for the model. A sensitivity analysis revealed that the water levels downstream of the jam are sensitive to the downstream boundary water level, justifying the use of the hourly data rather than a constant stage at the downstream boundary.

4.5.4.3 Lateral inflows

Within the study reach, hourly discharge data were available for four of the tributaries which flow into the Saint John River namely: the Madawaska River; the Iroquois River; the Green River (Riviere Verte); and, the Grand River. The locations of these tributaries are illustrated on the map in Figure 4.3 and in the profile of Figure 4.4.

4.5.5 Initial Conditions

Prior to any unsteady flow simulation, initial conditions of stage and discharge must be specified at every node within the computational domain. When Hicks *et al.*, (1997) simulated this event on the Saint John River, the initial conditions for the simulation were established by superimposing a measured jam profile onto a computed profile that reflected the flow conditions at the time of release. This approach relies on the assumption that the ice jam profile does not change significantly between the time it was measured and the time of the ice jam release.

In this investigation, the approach used by Hicks *et al.*, (1997) for obtaining the initial condition was re-examined. At the time the jam released, the flows were lower than they had been at the time when the jam profile was measured, based on the WSC gauge data at Fort Kent. Therefore, it was felt that the measured jam profile should be adjusted to reflect the changes in flow conditions that occurred during this period. Consequently, the initial conditions for the Saint John River jam release simulation were established as follows.

The model was first used to calculate a gradually varied flow profile for constant incoming and tributary inflows, based on the time the simulation began, April 14, 1993 at 0:00 h. At this point time, hourly discharge data were available for all inflow boundaries except for the Rivière Verte for which hourly data were not available until April 15, 1993 at 0:00 h. Therefore, for this intervening period, the required hourly data on the Green River were estimated based on mean *daily* flows for this river obtained from published WSC records.

Once the gradually varied profile was established for April 14, 1993 at 0:00 h, it was used as the initial condition to route the hourly discharge data (Saint John River and the four tributaries) to the time of the last jam profile measurement, approximately 14:30 h on April 14, 1993. It was necessary to obtain the computed water surface profile at this time in order to adjust the measured jam profile. The routing was then continued to the time when the ice jam released, which was at approximately 9:00 h on April 15, 1993. The difference between these two computed profiles was then used to adjust every point in the measured ice jam profile. This resulted in a new profile that is lower than the measured one (since discharge was increasing). The adjusted profile was then superimposed onto the computed water surface profile at 9:00 h on April 15, 1993, as shown in Figure 4.4. Since the measured ice jam profile only extended from the toe to the head of the jam, the backwater profile (M1) created by the jam was again approximated by a horizontal line. It should be noted that this is the methodology used to obtain the initial conditions for all the simulations; however, those presented in Figure 4.4 are for the case when the open water values of roughness were used.

4.5.6 Verification Data

When an ice jam release simulation is performed, it is ideal to have stage and discharge hydrographs at numerous points along the channel downstream of the point of release in order to assess the performance of the numerical model. In this investigation, the surge was only capable of propagating the short distance from the location of the jam toe to Grand Falls due to the presence of the dam. However, within this 25 km reach, water levels were measured at the bridge in Saint Leonard (5.3 km downstream of the ice toe location) as the surge passed. Also, estimated inflows to the Grand Falls hydropower plant were made available by N.B. Power.

4.6 MODEL APPLICATION

4.6.1 Introduction

In previous simulations of actual ice jam releases (Hick *et al.*, 1997; Beltaos and Krishnappen, 1982), the investigators:

1. assumed that the ice jam released instantaneously along its length;
2. assumed that that the ice in the jam provided no resistance to the flow after the time of the release; and
3. neglected the effect of any ice that was observed in the downstream channel.

Wong *et al.*, (1985) have illustrated that these assumptions are reasonable in the numerical simulation of experimental ice jam releases. However, in nature, friction between the ice and the banks may cause a more gradual release and resistance to the surge as it propagates downstream. In addition, if an ice jam releases upstream of an undisturbed or a deteriorating ice sheet, the arrival of the surge will cause to ice sheet to lift and break apart, which may also retard the advancing surge. This phenomenon is known as a breaking front (Beltaos, 1995).

Previous investigators (Hicks *et al.*, 1997; Henderson and Gerard, 1981) have suggested that the inability to correctly model the surge that results from an ice jam release is a result of neglecting the effects of ice in the modelling effort. Therefore, in the current investigation, it was desirable to attempt to account for the presence of ice in order to determine whether the ice does indeed have any significant effect on the propagating surge.

At present, there are no equations to describe the effects of ice, in or downstream of an ice jam, on the propagation of an ice jam release surge. Therefore, in the current investigation, various approaches were tried in an attempt to account for these effects. To study the effects of the ice observed in the channel downstream of the ice jam, two approaches were considered. The first approach simply involved varying the channel bed roughness downstream of the ice jam to account for both broken and intact ice. In the second approach, the observed intact ice cover was accounted for in the simulation by doubling the wetted perimeter. The justification for this is described below.

The presence of an ice cover affects the hydraulics of the flow in a number of ways. One, the wetted perimeter is increased due to the underside of the ice in contact with the flow. Two, the channel flow area is reduced since ice floats with about 90% of its thickness submerged. Three, the channel resistance is increased due to the roughness of the underside of the ice. In channels with large aspect ratios (width to depth), the wetted perimeter is approximately equal to the channel topwidth. Therefore, if an ice cover extends across the entire width of a channel, it will essentially double the wetted perimeter. In the case of the Saint John River ice jam release, no measurements were obtained regarding the thickness of the observed ice cover downstream of the ice jam. Therefore, it was decided to neglect the effect that ice thickness has on flow area rather than to incorporate this effect and speculate on the ice thickness.

Two approaches were also considered to account for the effects of the ice in the jam. In the first approach, channel bed roughness was increased in the reach where the ice jam was observed in an attempt to account for any resistive effects that the ice jam may have provided during its release. In the second approach, the possibility of a gradual release was considered more explicitly by introducing a significant resistance to the flow along the length of the ice jam for a short period following the release. This temporary resistance was created by doubling the wetted perimeter and introducing a roughness value representative of the ice jam roughness. The details of implementing all four of the approaches are discussed in the model results.

4.6.2 Model Results

Although four different approaches were considered to account for the effects of the ice in the simulation of the Saint John River ice jam release, they were not all considered separately. Therefore, the results are presented in terms of the various runs that were performed. In total four runs were performed. In all of these runs, a time step increment of 5 seconds was used in order to ensure model stability.

4.6.2.1 Run No. 1

In run No.1, all of the ice effects were neglected and the event was simulated using the open water roughness values throughout the entire domain, based on information provided by N.B. Power. Therefore, Manning's *n* was taken as 0.025 upstream of Edmundston and 0.020 in the reach downstream of Edmundston. This simulation provided a basis for assessing the effects of attempting to incorporate the ice into the simulation.

Figure 4.5 presents the results of this simulation in comparison with the available verification data. Water levels at Saint Leonard are presented in Figure 4.5 (a) where it is seen that the computed peak stage matches the timing and the magnitude of the observed values quite well. The computed peak stage over-predicted the observed by only 16 cm (17 % error based on the ratio between the difference of the measured and computed peaks and the measured stage increase for the event). However, the computed stage decreased much quicker than the observed stage. Figure 4.5 (b) presents the computed discharge hydrographs at various locations along the channel downstream of the ice jam. Results at Grand Falls are consistent with the inflows observed at the power plant with respect to peak discharge and wave speed accuracy. The computed peak discharge was only 52 m^3/s less (-2.7 % error) than the observed peak discharge.

It was thought that the rapid drop in computed stage might be due, in part, to neglecting the attenuating effects of ice in the channel. Therefore, the following three runs were made in an attempt to account for the shape of the observed hydrograph by incorporating the effects of ice into the simulation.

4.6.2.2 Run No. 2

The observations indicate that the head of the ice jam was at km 60.9 just before the ice jam released and that there was ice (broken and intact) in the channel between the toe of the jam and km 83.7. Also, it is likely that there was remnant ice in the remaining reach downstream of km 83.7. Therefore, an attempt was made to account for the possible resistive effects of the ice, in and downstream of the ice jam, by increasing the channel bed roughness along the reach between km 60.9 and the end of the reach (Grand Falls). For run No.2, this increase in channel bed roughness was from the open channel value of 0.020 to 0.025. Upstream of km 60.9 the open water values of roughness were used.

Figure 4.6 presents the results of this simulation in comparison with the observed data. In comparison to Figure 4.5 (a), Figure 4.6 (a) illustrates that the increase in the channel bed roughness mainly produced an increase in the stage at Saint Leonard throughout the entire simulation. For this run, the computed peak stage overestimated the observed by 55 cm (59 % error). It also reduced the peak stage relative to the pre-release stage (just before the release); however, this effect is marginal. For example, in run No. 1, the difference between the peak and pre-release stages is 2.7 m, while in run No.2, the difference is 2.5 m. The computed water levels from run No. 2 provide a better visual fit to the observed water levels at Saint Leonard that those of run No. 1. This suggests that either the ice in the jam or the ice in the channel upstream of Saint Leonard may have provided resistance to the surge, though it not possible to distinguish between these two effects in this run. Nevertheless the shape of the shape of the observed stage hydrographs could not be accounted for entirely by simply using the bed roughness to describe the effects of ice in and downstream of the ice jam.

Figure 4.6 (b) presents the computed discharge hydrographs at various locations along the channel downstream of the ice jam. The results indicate that the increase in channel bed roughness produced a decrease in the peak discharge along the channel downstream of the ice jam in comparison to the results obtained in run No.1. In particular it is important to notice that in run No.1, the computed peak discharge was in good agreement with the observed peak discharge at Grand Falls, while in run No.2 this computed peak discharge was about 640 m^3/s less (-33 % error) than the observed. The fact that the discharge results were better using the open water values in run No. 1 suggests that the remnant ice probably did not provide much resistance to the flow.

4.6.2.3 Run No. 3

Prior to the release, sheet ice and broken ice were observed downstream of the ice jam. Although both broken ice and sheet ice both have the effect of increasing the wetted perimeter, the broken ice may provide little resistance to the flow if it is free to move downstream with the flow. Therefore, in run No. 3, only the observed sheet ice was considered in the simulation. Because the shape of the observed hydrograph could not be accounted for by simply increasing the channel roughness, it was decided to model the observed sheet ice by considering its specific effects on this hydraulics of the flow. As mentioned previously, this was accomplished solely through doubling the wetted perimeter, as the reduction in the flow area was unknown due to a lack of ice thickness data. In the model, the wetted perimeter was doubled at locations along the channel corresponding with the sheet ice observations on April 13, 1993. Specifically, these locations were from km 69.0 to km 72.6 and again from km 77.6 to km 83.7. Although the presence of the ice cover could affect the Manning's roughness values of the channel, as a first approximation, the values were based on those supplied by N.B. Power. That is, Manning's *n* was taken as 0.025 upstream of Edmundston and 0.020 in the reach downstream of Edmundston.

It is likely that the arrival of the surge caused the sheet ice to lift and break apart. However, it would be very complicated to model this sort of breaking front. Therefore, in modelling the ice jam release with the ice sheet remaining intact for the entire simulation, it was thought that perhaps the results from this run could be compared to those from the 'no ice' situation in run No. 1 to provide some insight into the resistance provided by a breaking front.

Figure 4.7 presents the results from run No. 3. In Figure 4.7 (a), water levels at Saint Leonard are presented in comparison with the measured stage hydrograph. The computed water levels for this run are visually very similar to those obtained in run No.2, Figure 4.7 (b) presents the computed discharge hydrographs at various locations along the channel. Again, these results are visually very similar to those obtained in run No.2. The discharge and stage results indicate that both approaches to the ice in the receiving channel produce similar effects to the shape of the computed stage and discharge hydrographs. The results also suggest that, if the shape of the wave is indeed attributable to the resistive forces produced by the breaking front, these forces must be much greater than those provided by an intact ice cover.

4.6.2.4 Run No. 4

In run No. 4, the possibility of a gradual release of the ice jam was considered by introducing a roughness, representative of the ice jam roughness, along the length of the ice jam for a short period following the release. This temporary resistance was achieved by doubling the wetted perimeter and introducing a roughness value representative of the ice jam roughness. Although, the ice in the jam would also have the effect of reducing the flow area, as a first approximation, only the increase in the wetted perimeter was considered.

In a comparison of the ICEJAM and RIVJAM steady state ice jam profile models, Healy and Hicks (1997) applied these two models to the 1993 Saint John River ice jam studied in this investigation. The measured ice jam profile was calibrated for two discharge estimates of 2250 m^3/s and 3000 m^3/s, corresponding to composite (ice and bed) roughness values of 0.040 and 0.030, respectively. Based the computed discharge hydrograph at the toe of the ice jam in run No.1, the discharge at the time of the ice jam profile was measured is 2370 m^3/s. Therefore, a composite roughness value of 0.040 was used in this part of the analysis to represent the resistance provided by the jam and the bed at the onset of release.

The gradual release was simulated as follows. Using the initial conditions established for run No.1, along the length of the ice jam between km 60.9 to km 69.0 the wetted perimeter was doubled and the roughness was increased from the open water value of 0.020 to 0.040. With these modified initial conditions, the incoming and tributary inflows were routed for 15 minutes. After this time, the ice was removed and the roughness was returned to 0.020 for the rest of the simulation. A time of 15 minutes was chosen as it was felt that this was a generous estimate of the time required if the ice jam did release in a gradual manner.

The results of this simulation are presented in Figure 4.8. As Figures 4.5 (a) and 4.8 (a) illustrate, the introduction of a temporary resistance as a means of modelling a gradual release of the ice jam does not affect the computed water levels in Saint Leonard. The effect of the temporary resistance is only apparent immediately downstream of the ice jam as shown in Figure 4.8 (b). At this location, the discharge hovered around 5000 m^3/s before rising to its ultimate peak of about 8500 m^3/s. However, by the time the surge had arrived at Saint Leonard this step in the discharge is visually negligible. The effect of the gradual release on the discharge is further illustrated through a comparison of the computed discharge profiles in the vicinity encompassing the jam for both the gradual release (run No. 4) and instantaneous release (run No.1). These are presented in Figure 4.9. For the case of the instantaneous release, presented in Figure 4.9 (a), the discharge has exceeded 8000 m^3/s, 5 minutes after the release. For the case of the gradual release, after 5 minutes the discharge is still under 5000 m^3/s, as presented in Figure 4.9 (b). The effect of the gradual release is far less dramatic for the computed water levels, as shown in Figure 4.10. After 5 minutes, the water surface profiles for both the instantaneous release, Figure 4.10 (a), and the gradual release, Figure 4.10 (b), are visually very similar. The results (particularly Figure 4.9(a)) suggest that the instantaneous release may be closer to reality as they are in agreement with the commonly reported observation that the velocity within the ice jam increases significantly prior to any increase in depth associated with the release (Henderson and Gerard, 1981).

4.6.3 Discussion of Results

The main objective of this chapter was to assess whether a hydraulic flood routing model based on detailed natural geometry could be used to route an ice related flood event effectively. To accomplish this objective, a documented ice jam release event was simulated, which occurred on the Saint John River upstream of Grand Falls Dam in the spring of 1993.

As mentioned previously, this event was also simulated by Hicks *et al.*, (1997). In their simulations, an approximate geometry of the reach was used and all of the effects of the ice were neglected. In this investigation, the event was simulated using available natural geometry of the reach. In run No.1, the effects of the ice were neglected as they were in the simulation by Hicks *et al.*, (1997). Therefore, this run provided a means of evaluating the use of the natural channel geometry instead of the approximate geometry. At Saint Leonard, the approximate geometry model (cdg1-D) displayed good wave speed accuracy; however, the computed peak stage was about 1 m higher (106 % error) than the observed peak (Hicks *et al.*, 1997). In run No.1, the natural channel geometry model (cdg1-Dn) produced both good wave speed and peak stage accuracy at Saint Leonard, with the computed peak stage within 16 cm (17 % error) of the observed. There were other differences between the two simulations, including 1) the use of a variable stage downstream boundary condition in instead of a constant stage and 2) the use of an adjusted ice jam profile instead of the measured profile. Although these two changes may have also played a role in improving the simulation in run No.1 (compared to Hicks *et al.*, 1997), preliminary model runs suggested that that the improvements are mainly attributable to the implementation of the natural geometry.

Despite these improvements, the natural geometry model was unable to reproduce the shape of the observed stage hydrograph at Saint Leonard. Three additional runs were made in an attempt to improve those results by using roughness and an ice cover approximation to consider the effects of ice in the simulation. None of these was able to reproduce the shape of the observed stage hydrograph. This suggests that the effects of the ice on the surge were too complex to be modelled by the simple approaches used in this investigation. However, it is possible that the poor shape accuracy in all of the runs may be due to the ungauged tributaries. It is important to recognize that this event was a dynamic event. By the time the surge arrived at Saint Leonard it was still quite dynamic (McKay, 1997). Therefore, it is likely that the inertial terms in the Saint Venant equations were still dominant over the friction terms, providing a possible explanation as to why the approaches to the ice effects had little effect on the simulation results.

Another objective of this chapter was to further verify the use of 1-D unsteady open channel flow models to simulate ice jam release surge propagations. In the current investigation, the natural channel geometry model was able to accurately predict the magnitude and timing of the observed peak stage although no considerations were taken for the ice in and downstream of the jam. Therefore, it is felt that 1-D unsteady flow models, such as cdg1-Dn, can be used quite effectively for the purpose of flood forecasting where the timing and location of peak water levels is of concern. The 1-D model used in this investigation could not account for the shape of the stage hydrograph which is possibility attributable to the effects of the ice. However, there is no point in using a more complex model (2-D or 3-D) until the field data describing ice jam releases are more complete.

Although the data set used in the current investigation is very good, there are a number of pieces of information that would be ideal to know for future modelling efforts. The first thing would be to have hydrographs at numerous points downstream of the jam toe location in for model verification. This was not possible in this reach as the extent of the surge propagation was limited by the Grand Falls Dam. Second, these hydrographs should describe the stage before and after the wave has passed in addition to the shape of the wave itself. Water levels obtained before the wave has passed could be used to calibrate the roughness before the release event is to be simulated. Third, it would also be ideal to have a record of an event where the downstream ice is minimal so that the effects of ice in the jam could be separated from the effects of the downstream ice.

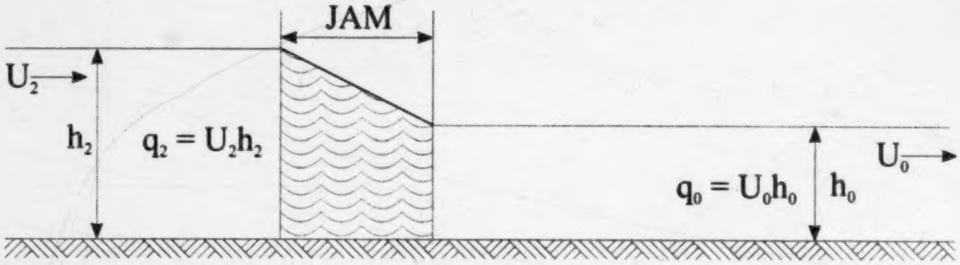

(a) Assumed initial situation prior to ice jam release, adapted from Henderson and Gerard (1981).

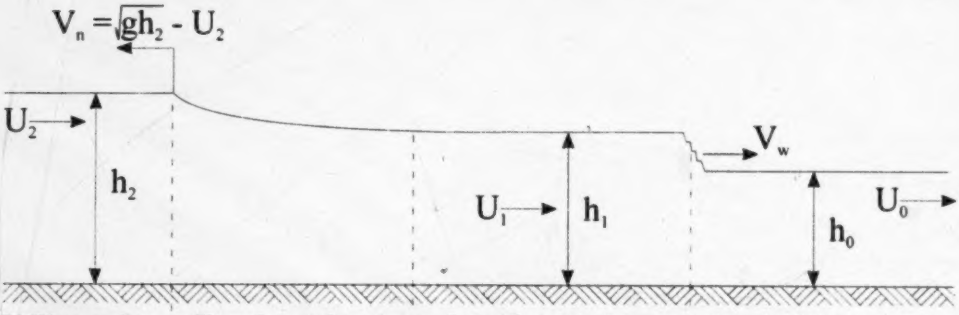

(b) Water surface profile at time t_1 after release, adapted from Henderson and Gerard (1981).

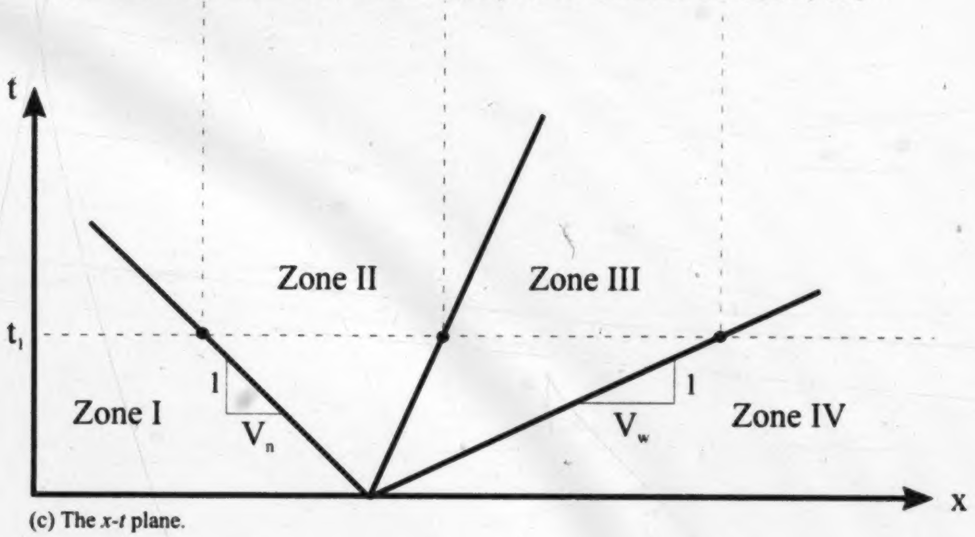

(c) The *x-t* plane.

Figure 4.1. The ice jam release problem treated as a classic dam break.

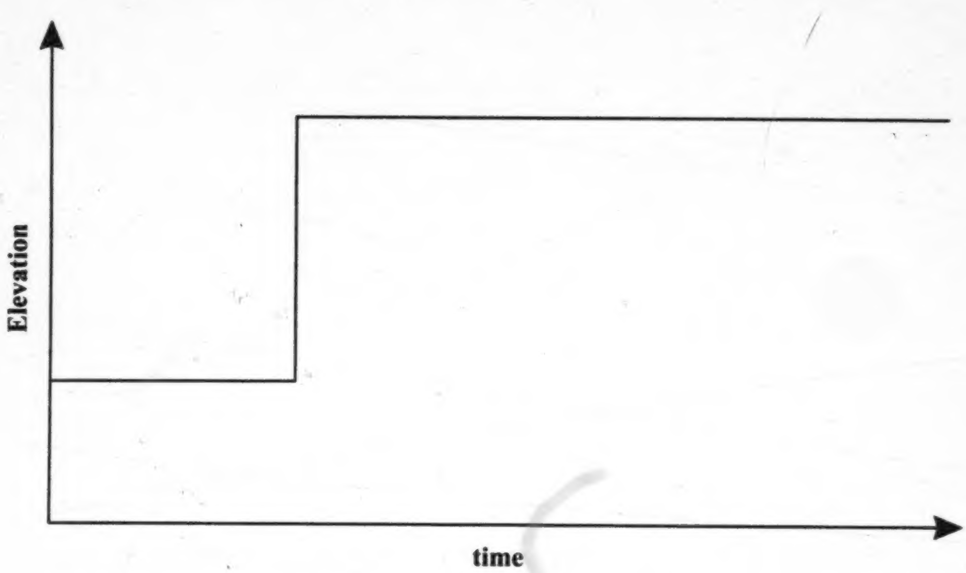

a)A hydrograph produced downstream of an ice jam release, based on the analytical solution of Henderson and Gerard (1981).

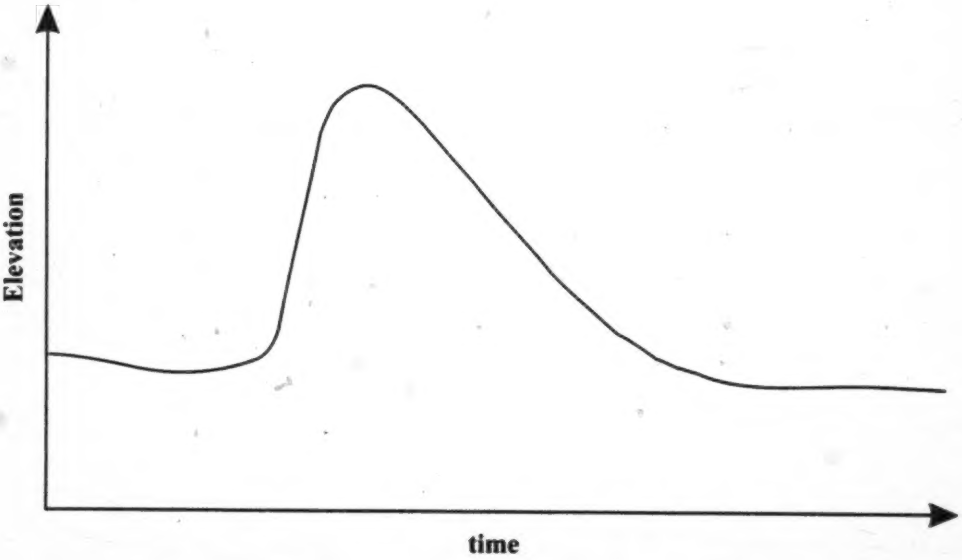

b)A hypothetical hydrograph produced downstream of an actual ice jam release.

Figure 4.2 Comparison of hydrographs produced downstream of an ice jam release.

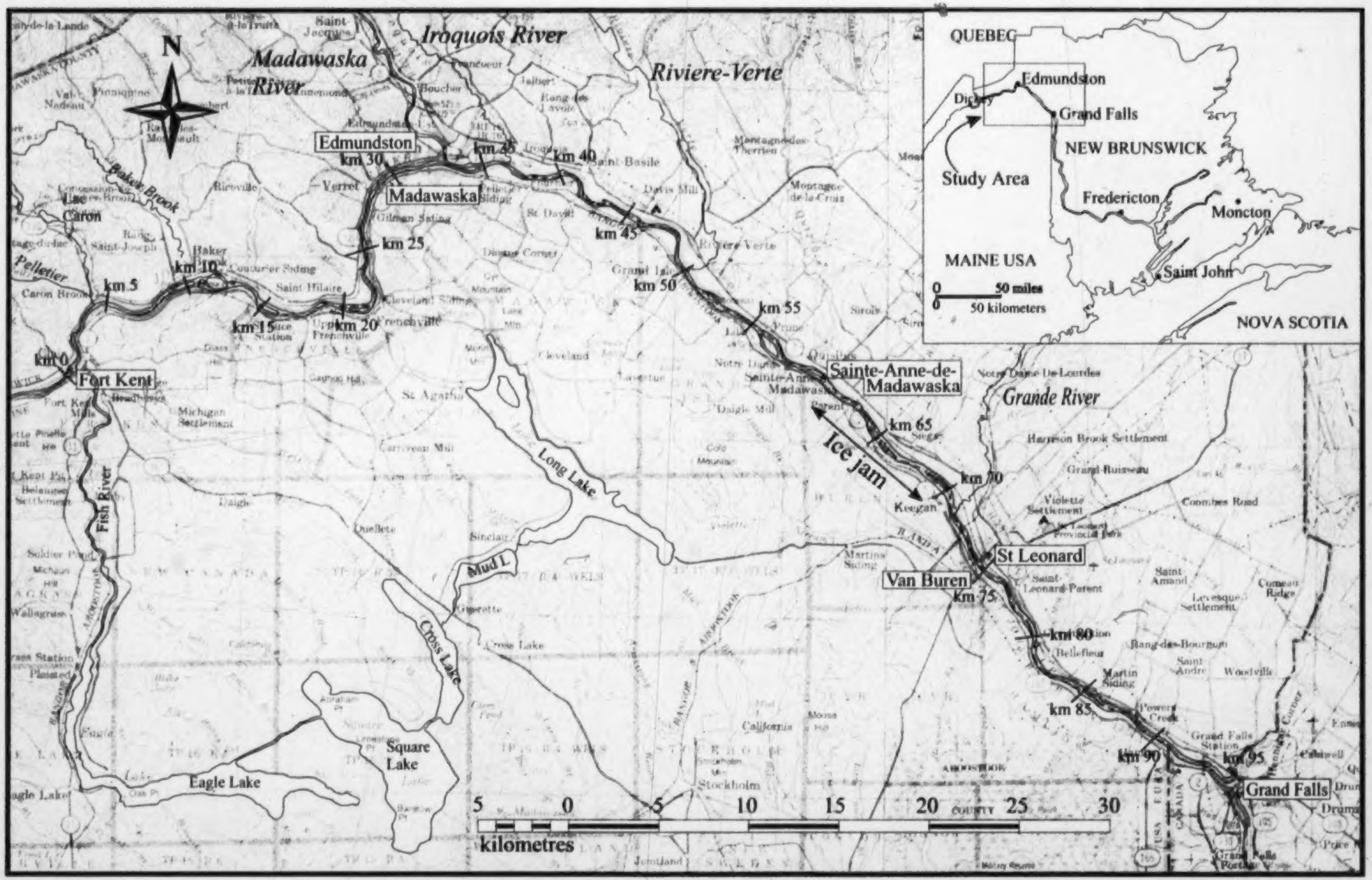

Figure 4.3 Location map of the study reach along the Saint John River

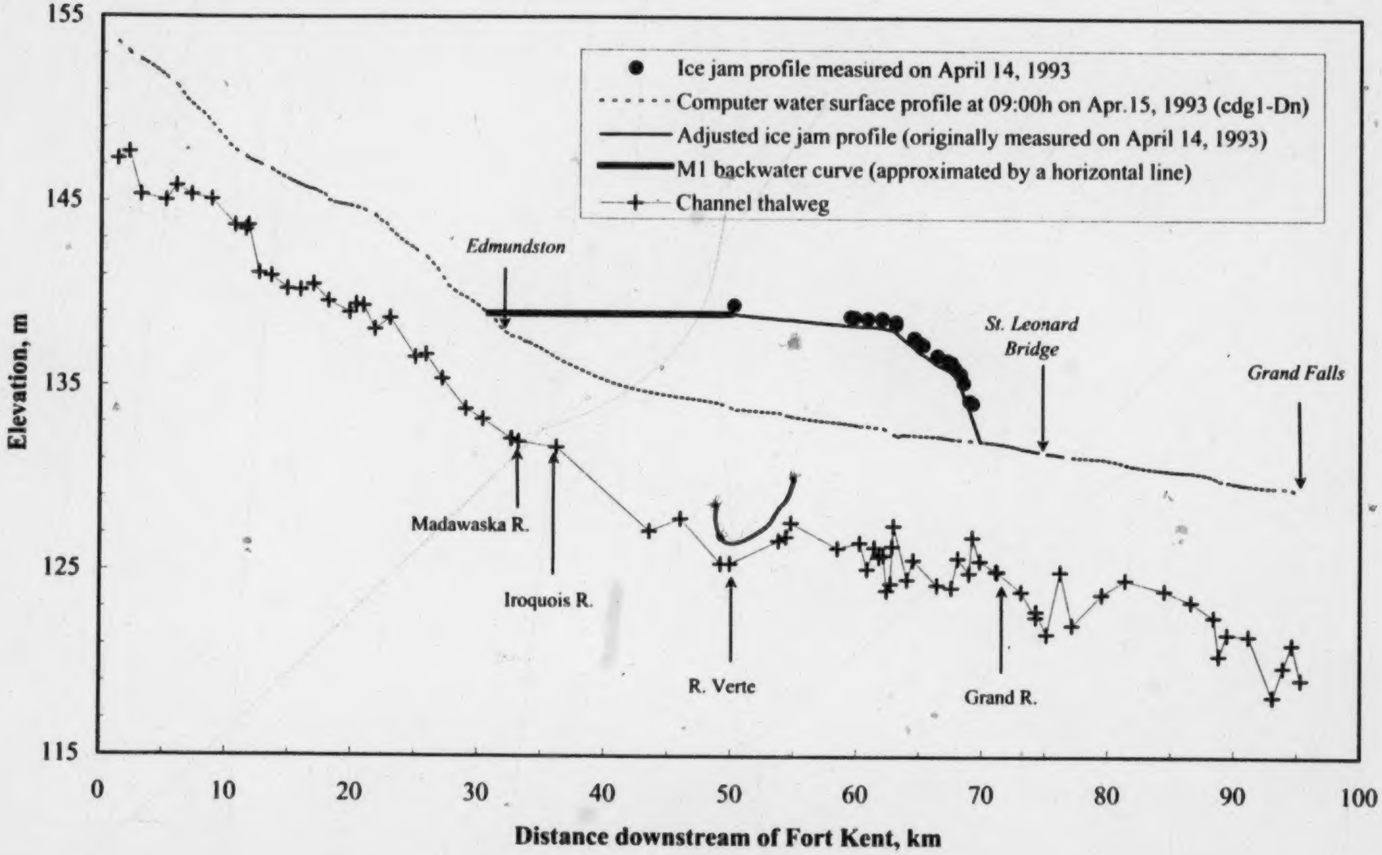

Figure 4.4 Measured ice jam profile and an example of the water levels used in one of the ice jam release simulations.

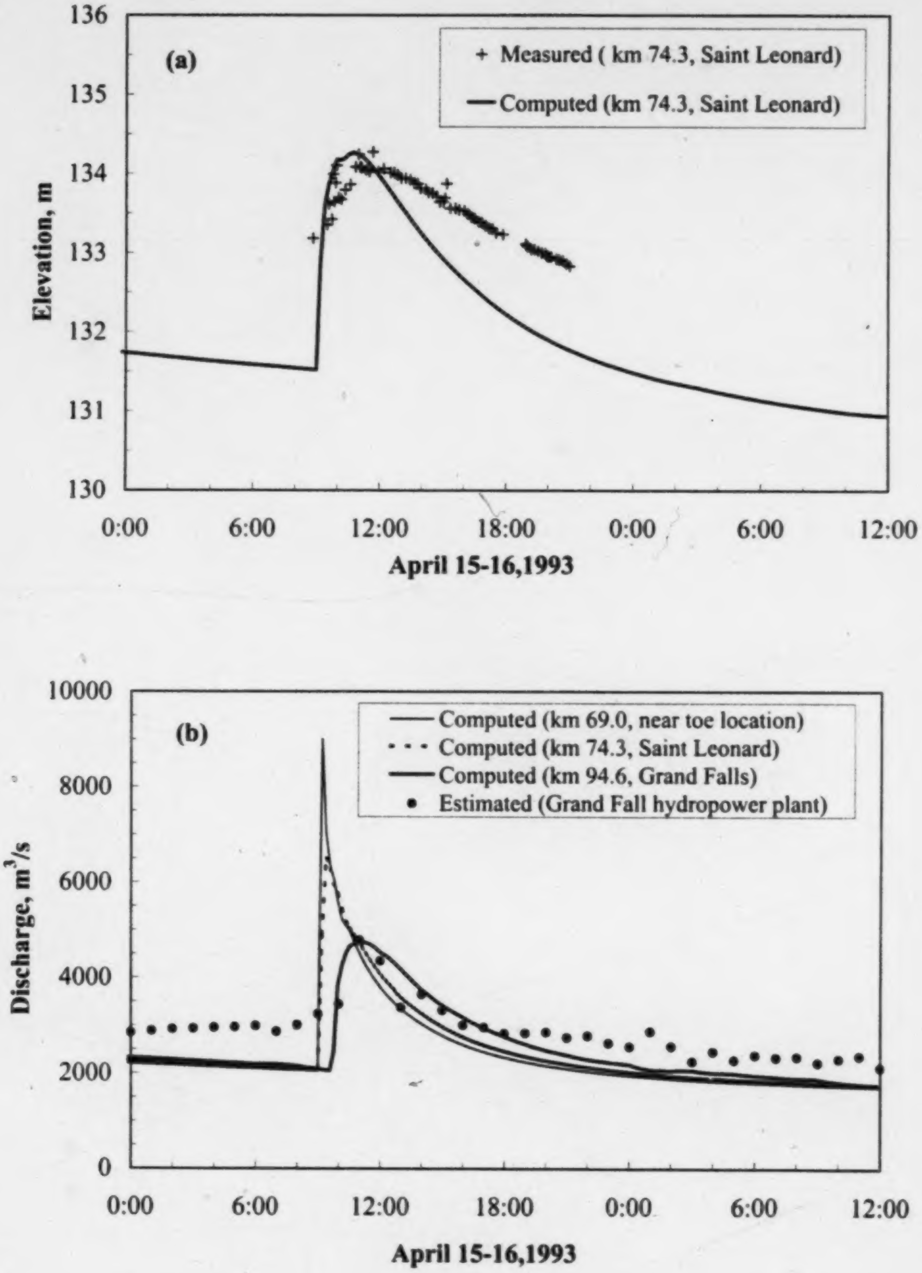

Figure 4.5 Comparison of measured and computed flows and stages for run No.1.

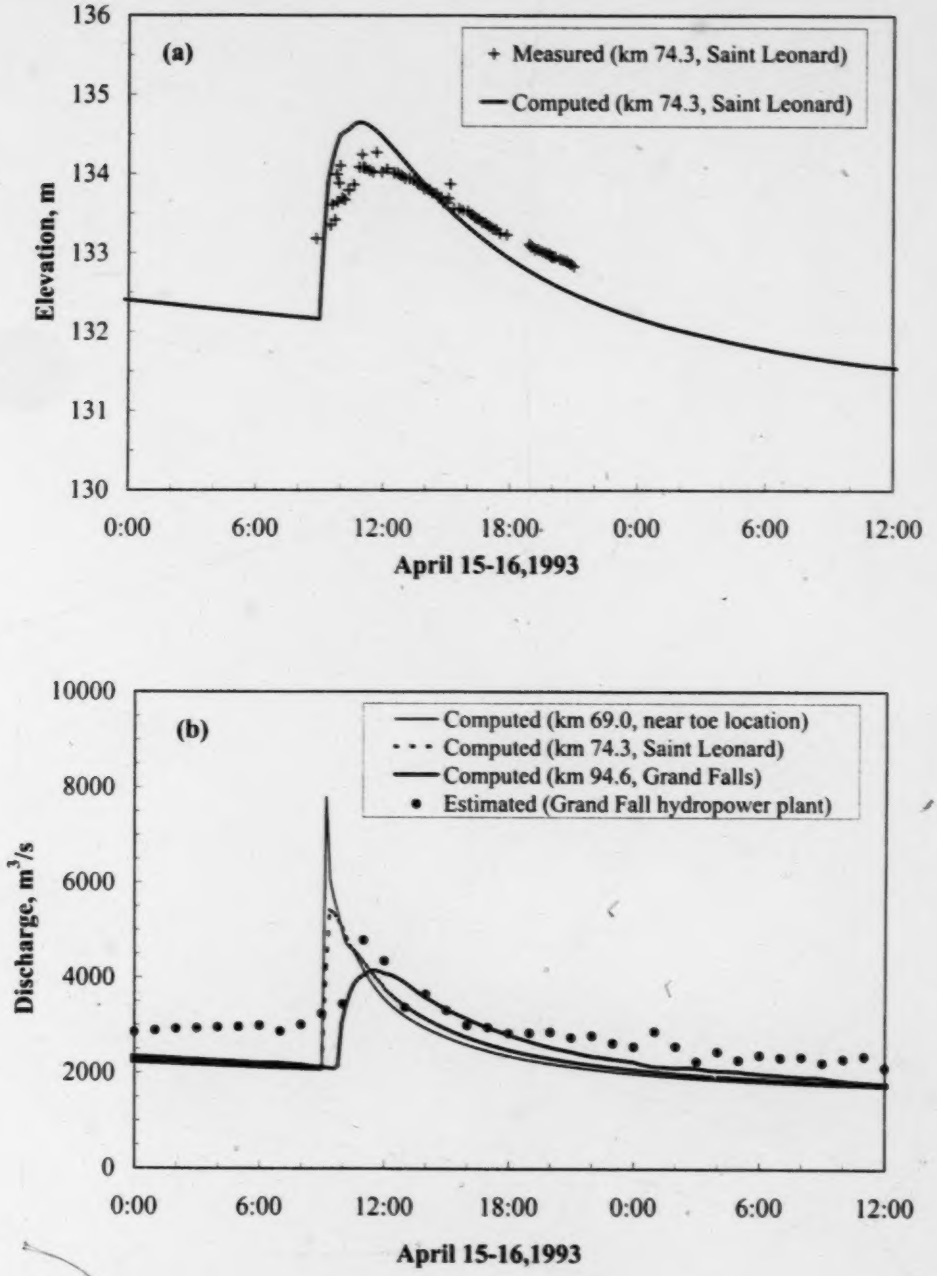

Figure 4.6 Comparison of measured and computed flows and stages for run No.2.

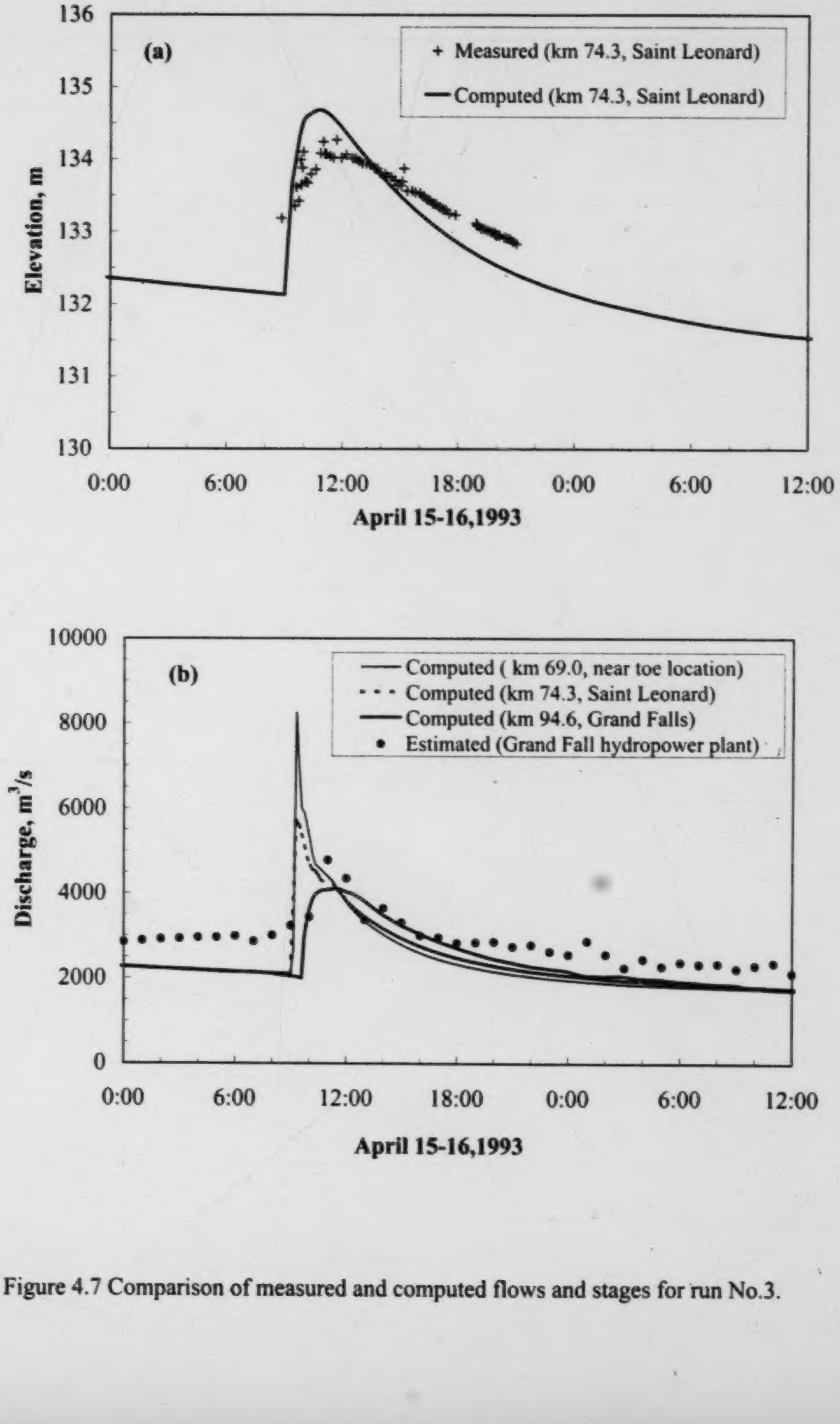

Figure 4.7 Comparison of measured and computed flows and stages for run No.3.

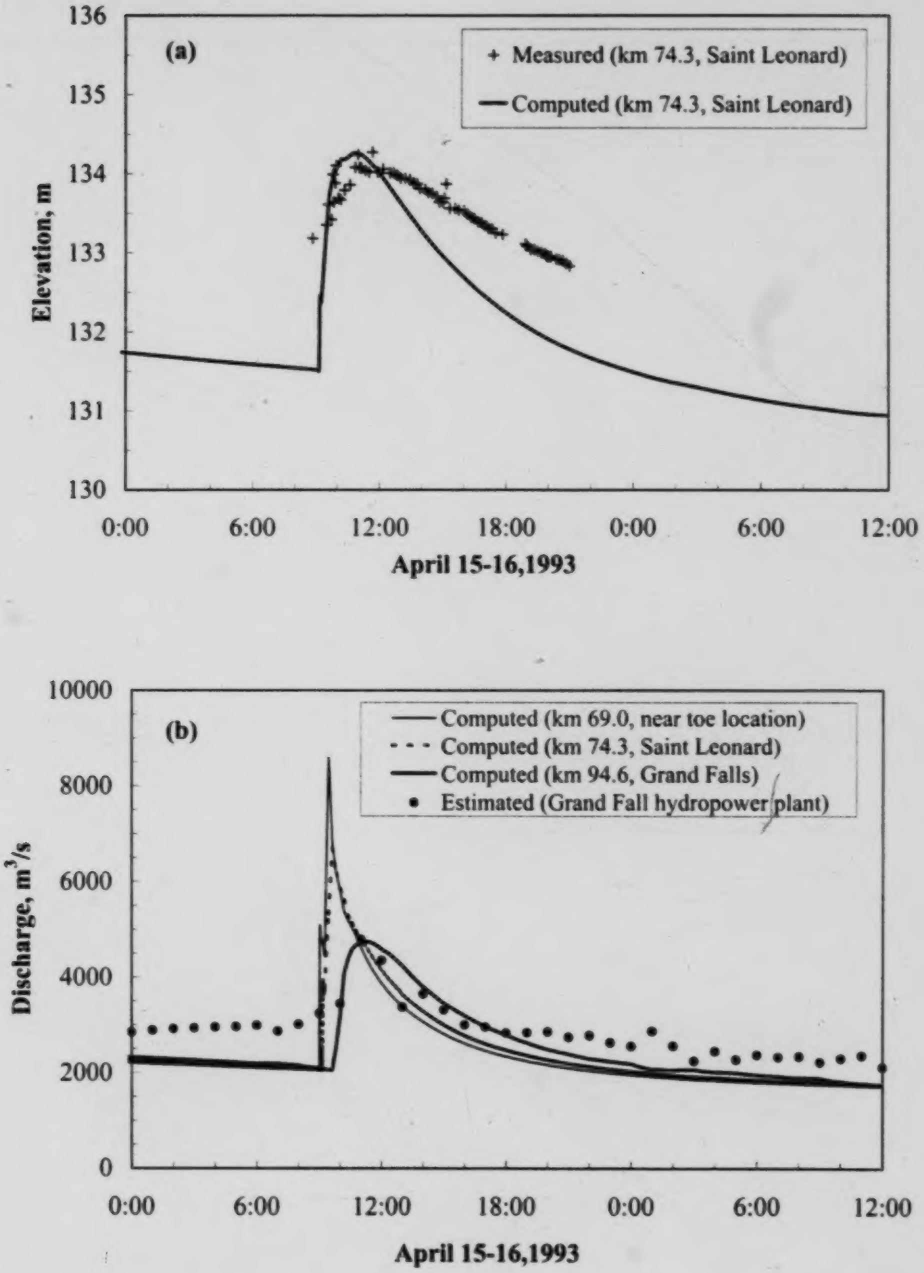

Figure 4.8 Comparison of measured and computed flows and stages for run No.4.

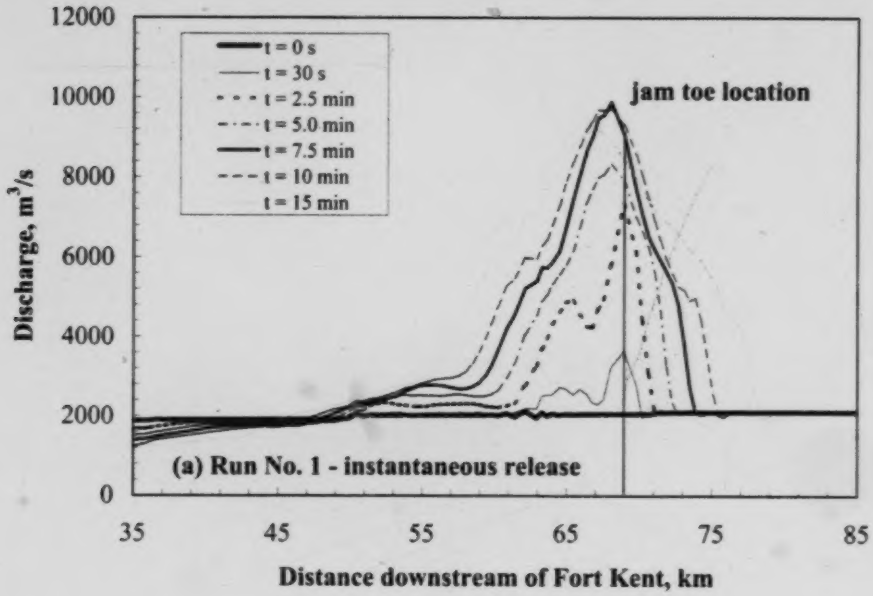

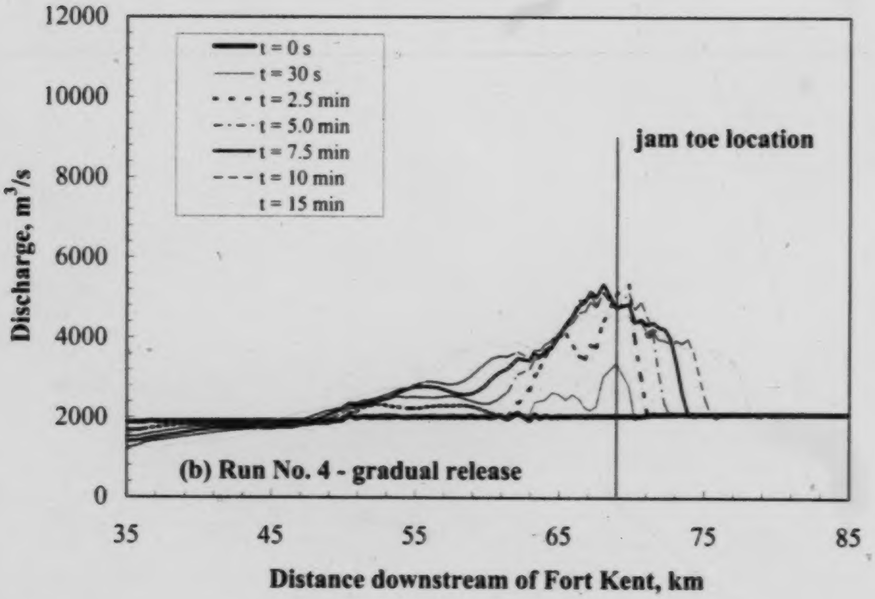

Figure 4.9 Computed discharge profiles for (a) run No.1 and (b) run No.4.

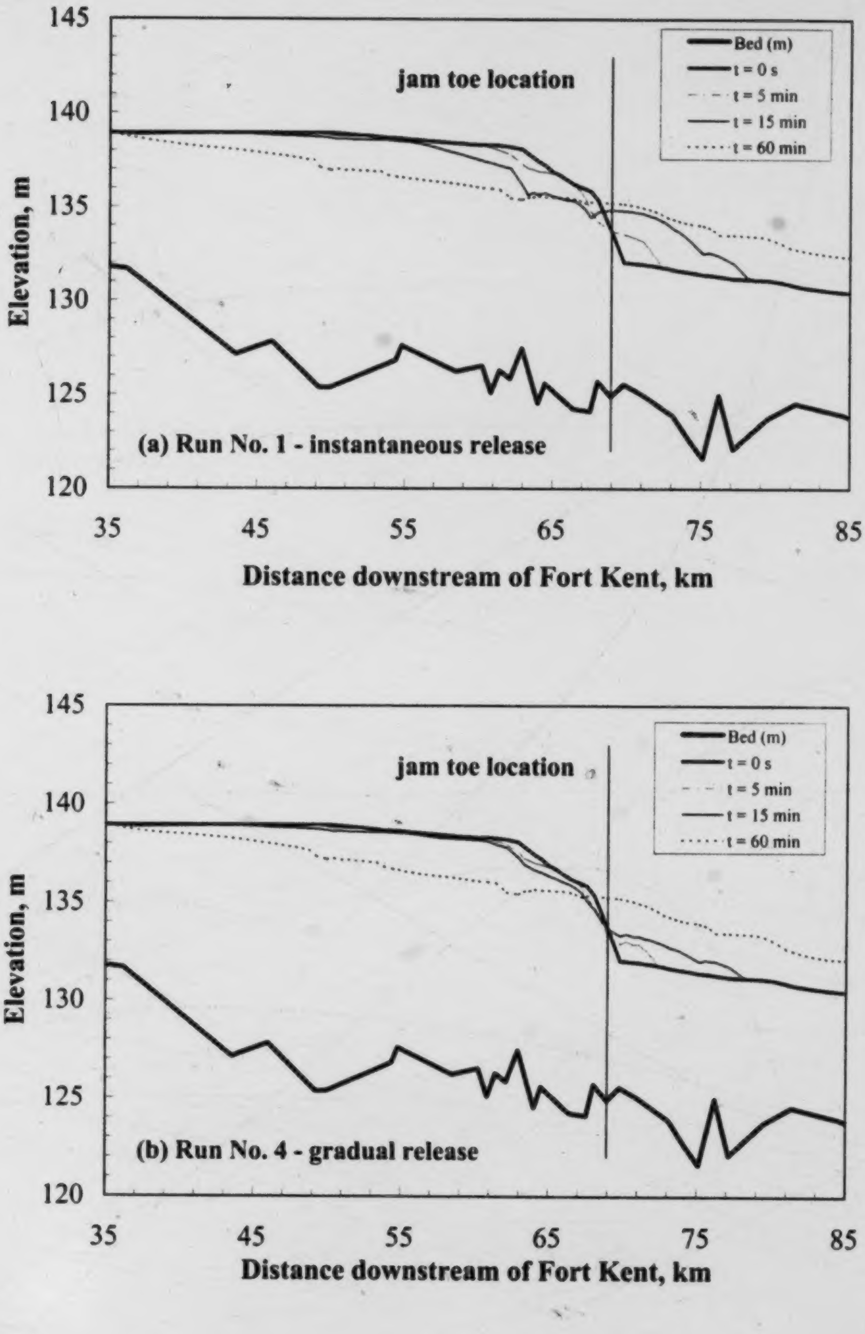

Figure 4.10 Computed water level profiles for (a) run No.1 and (b) run No.4.

CHAPTER 5

CONCLUSIONS AND RECOMMENDATIONS

There were two main objectives to this study. The first was to determine whether it is possible to combine flood forecasting and flood level determination using hydraulic flood routing techniques. The second was to assess whether a hydraulic flood routing model based on detailed natural geometry could be used to effectively route an ice related flood event. To accomplish these objectives two flood events were modelled: a summer flood event on the Peace River, Alberta and an ice jam release surge on the Saint John River, New Brunswick. For the purpose of this study, the cdg1-Dn hydraulic flood routing model was developed based on the Saint Venant equations for natural channels.

5.1 MODEL IMPLEMENTATION

The cdg1-D model (Hicks and Steffler, 1990) uses the CDG finite element scheme to solve the conservation form of the Saint Venant equations for rectangular channels. Because of the proven solution accuracy and numerical stability of the CDG scheme and the successful application of the cdg1-D model in previous flood routing investigations, it was decided to employ the CDG scheme to develop the natural channel flood routing model in the current investigation. The resulting model was named the cdg-1Dn model. Unfortunately, due to the form of the natural channel equations, it was not possible to develop the cdg1-Dn model based on a conservation formulation. Consequently, the cdg1-Dn model cannot perfectly conserve both mass and longitudinal momentum under all circumstances. This was demonstrated through a supercritical dam break test where the cdg1-D model was able to conserve mass and momentum to 5 decimal places while the cdg1-Dn model was only to conserve mass and momentum to 2 decimal places. In the Peace River case study, the mass conservation of both the cdg1-D and cdg1-Dn models was compared again, where it was discovered that, in practical situations, the cdg1-D model is at least twice as good at conserving mass. Nevertheless, the errors in mass conservation displayed by the cdg1-Dn model are considered small.

The form of the natural channel equations, particularly the convection matrix, prevented the proper implementation of the upwinding component of the CDG scheme. Therefore, the upwinding matrix in the cdg1-Dn model is the same as that in the cdg1-D model. The fact that the upwinding matrix is not based upon the natural channel equations that are solved by the cdg1-Dn model may be preventing the appropriate damping of the numerical oscillations that lead to numerically generated instabilities. The instability of the cdg1-Dn model was illustrated in the Peace River case study where the cdg1-D model could be run using a time step increment of 6 hours while for the same situation the cdg1-Dn model could only be run using a maximum time step increment of 1 minute without instabilities arising.

The stability issues of the cdg-1Dn were attributed mainly to the inability to properly implement the upwinding component of the CDG scheme but also partly due to the fact that the cdg1-Dn model is not based a fully conservation formulation of the Saint Venant equations for natural channels. However, the stability problems of the cdg1-Dn model are possibly exacerbated by the use of an approximate Jacobian matrix in the iterative solution technique employed in the cdg1-Dn model. These problems are more of an inconvenience at this stage; improvements would make the model more operationally practical.

5.2 OPEN CHANNEL FLOOD EVENT

The objective in the Peace River case study was to determine whether it is possible to combine flood forecasting and flood level determination using hydraulic flood routing techniques. In particular, it was desirable to determine if it was possible to route an open channel flood using natural channel geometry in the short subreaches where flood levels are required (at cities and town sites) and using approximate geometry in between these sites. Therefore, the 1987 summer flood event on the Peace River was routed through the long approximate subreaches using the cdg1-D model and through the short natural channel subreaches using the cdg-1Dn model. This method of flood routing improved the peak stage accuracy considerably. When only the approximate geometry was used to model the reach, there was a –31 % error in modelled peak stage at the Town of Peace River gauge. This error was reduced to –18% when the natural channel geometry was used. It is significant to note that these results were based on estimates of channel resistance. Calibration would reduce these errors.

Water levels along the Town of Peace River subreach were also determined using a steady, gradually varied flow program (HEC-RAS) based on peak discharges entering the subreach for the event. These results were visually very similar to those obtained using the cdg1-Dn model.

The results of this case study indicated that flood forecasting and flood level determination can be combined. However, in order to produce accurate water levels, natural channel subreaches must be sufficiently defined. It is not possible to conclude what is required for a subreach to be 'sufficiently defined' except that of the three subreaches, namely, Dunvegan (6 cross sections), Fort Vermilion (10 cross sections), and the Town of Peace River (28 cross sections), only the Town of Peace River subreach was well defined. The comparison of the cdg1-Dn results with those obtained using HEC-RAS, illustrate that the natural channel hydraulic flood routing approach produces results that are at least as good as those obtained by using the more conventional approach involving a routing model followed by a gradually varied flow model. In addition, the results demonstrate the validity of using a steady, gradually varied flow approximation for delineating 'non-dynamic' open water flood events.

5.3 ICE RELATED FLOOD EVENT

In the Saint John River case study the objective was to assess whether a hydraulic flood routing model based on detailed natural geometry could be used to route an ice related flood event effectively. When a river is covered with ice, the relationship between stage and discharge is not unique since stage is also dependent on the thickness and roughness of the ice cover. Since there is no way to safely measure the discharge during an ice related event, only water levels are known.

The 1993 ice jam release event on the Saint John River was chosen in particular to assess this objective because it is the type of dynamic ice jam release event that flood forecasters may encounter. In run No.1, the ice jam release event was modelled using the available natural channel geometry and open water roughness values, assuming that the ice jam released instantaneously and that the ice in and downstream of the ice jam had no effect on the resulting surge. These results were compared to those obtained in an investigation by Hicks *et al.*, (1997) where the same event was modelled with approximate geometry using the assumptions described above. Using the natural channel geometry, the computed peak level at Saint Leonard (~5 km downstream of the toe of the ice jam) was within 16 cm (17 %) of the observed, while it was about 1 m (106 %) higher when the approximate geometry was used. Although the natural channel model displayed good peak stage accuracy, it could not reproduce the shape of the stage hydrograph. This illustrates the necessity of natural channel geometry when modelling ice related events.

Additional runs were made in an attempt to improve on the initial results using four different approaches to account for the effects of the observed ice in the simulation. The first approach involved increasing the roughness downstream of the toe of the ice jam to account for all of the types of ice observed downstream of the jam prior to its release (remnant, broken and sheet ice). In the second approach, an ice cover approximation (doubled wetted perimeter) was used to specifically account for the resistance provided by the observed sheet ice. The third approach involved increasing the roughness along the length of the ice jam to account for the effects of the ice in the ice jam on the resulting surge. In the last approach, the possibility of a gradual release was considered by introducing a significant resistance to the flow along the length of the ice jam for a short period following the release.

The first and the third approaches were combined in run No.2. In this run, the roughness was increased between the head of the jam and the downstream end of the study reach to account for the presence of ice in and downstream of the jam. The increased roughness had the effect of translating the stage hydrograph vertically upwards, resulting in a 59 % overestimation in the peak stage with no improvements to the shape of the stage hydrograph in comparison to the observed data.

The second approach was incorporated into the simulation in run No.3. In this run, the wetted perimeter was doubled in the model at all the locations where sheet ice was observed in the receiving channel. The stage and discharge results of this simulation were visually very similar to those obtained when the ice was accounted for using roughness (run No.2).

In the last run, run No.4, the fourth approach was considered. The stage results of the gradual release were visually very similar to those obtained in run No.1 (where the ice jam was assumed to release instantaneously). However, the gradual release produced a considerable effect on the discharge. In run No.1, the discharge exceeded 8000 m^3/s, in the vicinity of the toe of the jam, just 5 minutes after the release in comparison to run No.4 where, after 5 minutes, the discharge was still under 5000 m^3/s. The comparison of the results from run No.4 and run No.1 suggests that the instantaneous release may be more realistic, as the results from run No.1 are in agreement with the commonly reported observation that the velocity within the ice jam increases significantly prior to any increase in depth associated with the release (Henderson and Gerard, 1981).

None of the four approaches for handling ice effects considered in this investigation could be used to reproduce the shape of the observed stage hydrograph at Saint Leonard. It is possible that the difference in shape between the observed and computed stage hydrographs was not produced by ice effects; instead it might be due to ungauged tributaries which were neglected in simulation. However, it is also possible that effects of the ice in the ice jam release event on the Saint John River were too complex to be modelled using these simple approaches. At this time, there are no mathematical equations to describe the effects ice in and downstream of an ice jam on the resulting surge if the jam releases. In order to be able to develop such equations, more field data describing ice jam release events are a necessity.

5.4 RECOMMENDATIONS TO FIELD RESEARCHERS

Field researchers should focus on acquiring better data describing ice jam release events. The data describing the Saint John River ice jam release are currently considered to be some of the best available. However, these data only captured the water levels associated with the release at one location. This location was so close to the toe of the jam that the surge was still dynamic where inertial effects are dominant over friction effects. In this case, additional stage hydrographs could not be measured to capture the transition from dynamic to diffusive due to the presence of the dam at Grand Falls. Therefore, field researchers should focus particularly on acquiring water level data describing the resulting surge at numerous locations downstream of the toe of the jam. These hydrographs should describe the stage before and after the surge passed so that pre-event water levels could be used to calibrate channel roughness before the release event is to be simulated. It might be possible to assess the effects of the ice which was in the channel before the ice jam released, by comparing pre-release calibration roughness values to post-release calibration values (obtained using the post-event water levels). In addition, it would be ideal if an event could be measured from an ice jam with negligible ice in the channel downstream of the jam so that the effects of ice in the jam could be separated from those in the receiving channel.

5.5 RECOMMENDATIONS TO NUMERICAL MODELLERS

The natural channel hydraulic flood routing model used in this investigation, the cdg1-Dn, is too unstable to be an operationally useful tool to the flood forecaster at this time. Future investigators may want to start with improving the Jacobian matrix in the cdg1-Dn model. This could take the form of a full analytical Jacobian matrix or a numerical Jacobian matrix. However, the problems associated with inability to manipulate the natural channel equations into a fully conservation formulation or into a non-conservation formulation with a convection matrix based on the characteristic velocities suggest that, perhaps a different numerical approach is required.

REFERENCES

Beltaos, S. 1995. River Ice Jams. Water Resources Publications, U.S., 372 pp.

Beltaos, S. 1983. River ice jams: theory, case studies, and application. Journal of Hydraulic Engineering, Vol. 109, pp. 1338-1359.

Beltaos, S., Burell, B.C. and Ismail, S. 1994. Ice and Sedimentation Processes in the Saint John River, Canada. Proceedings, 12th International Association for Hydraulic Research, Symposium on Ice, Trondheim, Norway, pp.11-21.

Beltaos, S. and Krishnappan, B.G. 1982. Surges from ice jam releases: a case study. Canadian Journal of Civil Engineering, Vol. 9, No. 2, pp. 276-284.

Chandrupatla, T.R. and Belegundu, A.D. 1997. Introduction to Finite Elements in Engineering, Second Edition. Prentice-Hall, Inc., Upper Saddle River, New Jersey, 461 pp.

Chow, V.T. 1959. Open Channel Hydraulics. McGraw-Hill Book Company, New York, New York, 680 pp.

Chow, V.T., Maidment, D. R. and Mays, L. W. 1987. Applied Hydrology, McGraw-Hill Book Company, New York, New York, 572 pp.

Doyle, P.F. and Andres, D.D. 1979. 1979 spring breakup and jamming on the Athabasca River near Fort McMurray. Report SWE-79-05, Transportation and Surface Water Engineering Division, Alberta Research Council, Edmonton, Alberta. 44 pp.

Fread, D.L. 1988. The NWS DAMBRK Model: Theoretical Background/User Documentation. Office of Hydrology, National Weather Service (NWS), Maryland, U.S.A.

Healy, D. and Hicks, F.E. 1997. A Comparison of the ICEJAM and RIVJAM Ice Jam Profile Models. Water Resources Engineering Report No. 97-H1, Department of Civil and Environmental Engineering, University of Alberta, Edmonton 177 pp.

Henderson, F. M. 1966. Open Channel Flow. MacMillan Publishing Co., Inc., New York, N. Y., pp. 522.

REFERENCES (continued)

Henderson, F.M. and R. Gerard. 1981. Flood waves caused by ice jam formation and failure. Proceedings, International Association for Hydraulic Research, International Symposium on Ice, Quebec City, Quebec, Vol. 1, pp. 277-287.

Hicks, F.E. 1996. Hydraulic flood routing with minimal channel data: Peace River, Canada. Canadian Journal of Civil Engineering, Vol. 23, No. 2, pp. 524-535.

Hicks, F.E. and McKay, K. 1995. Peace/Slave River Flow Modelling. Water Resources Engineering Report No. 95-H3 (Northern River Basins Study Project 1154-D1), Department of Civil Engineering, University of Alberta, Edmonton, AB.

Hicks, F.E., McKay, K. and Shabayek, S. 1997. Modelling an Ice Jam Release Surge on the St. John River, New Brunswick, Proceedings of the 9th Workshop on the Hydraulics of Ice Covered Rivers, Fredericton, NB, pp.303-314.

Hicks, F.E. and Steffler, P.M. 1995. Comparison of finite element method for the St. Venant equations. International Journal for Numerical Methods in Fluids, Vol. 20, pp. 99-113.

Hicks, F.E. and Steffler, P.M. 1992. A characteristic-dissipative-Galerkin Scheme for open channel flow. ASCE Journal of Hydraulic Engineering, Vol. 118, No.2, pp. 337-352.

Hicks, F.E. and Steffler, P.M. 1990. Finite Element Modelling of Open Channel Flow. Water Resources Engineering Report No. 90-6, Department of Civil Engineering, University of Alberta, Edmonton, Alberta, 356 pp.

Hicks, F.E., Steffler, P.M. and Gerard, R. 1992. Finite element modelling of surge propagation and an application to the Hay River, NWT. Canadian Journal of Civil Engineering, Vol. 19, No. 3, pp. 454-462.

Hicks, F.E., Yasmin, N. and Chen, X.. 1994. Peace River Flow Analysis. (NRBS Project 1154-C1) Water Resources Engineering Report No. 94-H2, Civil Engineering Department, University of Alberta, Edmonton, Canada.

Humes, T.M. and Dublin, J. 1988. A Comparison of the 1976 and the 1987 Saint John River Ice Jam Flooding with Emphasis on Antecedent Conditions. Proceedings, 5th Workshop on Hydraulics of River Ice/Ice jams, Winnipeg, Canada, pp. 43-61.

Ismail, S. and Davis, J.L. 1992. Ice Jam Thickness Profiling on the the Saint John River, New Brunswick. Proceedings, 11th International Association for Hydraulic Research, Symposium on Ice, Banff, Canada, pp.383-394.

REFERENCES (continued)

Jasek, M. 1996. Break-up of the Porcupine River, Yukon Territory. Proceedings of the Hydro-Ecology Workshop on the Arctic Environment Strategy, Canadian Geophysical Union – Hydrology Section Annual Meeting, Banff, Alberta, NHRI Symposium No.16, pp 95-114.

Joliffe, I. and Gerard, R. 1982. Surges released by ice jams. Proceedings of the Workshop on the Hydraulics of Ice Covered Rivers, Edmonton, Alberta, pp. 253-259.

Khan, A.A., Steffler, P.M. and Gerard, R. 2000. Dam-break surges with floating debris. Journal of Hydraulic Engineering, Vol. 126, No.5, May 2000, pp. 375-379.

Kellerhals, R., Neill, C.R. and Bray, D. I. 1972. Hydraulic and Geomorphic Characteristics of Rivers in Alberta. Research Council of Alberta, River Engineering and Surface Hydrology Report 72-1, Edmonton, Alberta, 54 pp.

Krishnappan, B.G. and Snider, N. 1977. Mathematical modelling of sediment-laden flow in natural streams. Scientific Series No. 81, Inland Waters Directorate, Canada Centre for Inland Waters, Burlington, Ontario, 48 pp.

Liggett, J.A. 1975. Basic Equations of Unsteady Flow. Unsteady Flow in Open Channels, K. Mahmood and V. Yerjevich, Editors, Vol. 1, Water Resources Publications, Fort Collins, Colorado, pp. 29-62.

McKay, K. 1997. Hydraulic Flood Routin with Minimal Channel Data. M.Sc. Thesis, Department of Civil and Environmental Engineering, University of Alberta, Edmonton, Alberta, 179 pp.

McKay, K., Mikolajczyk, S., and Hicks, F.E. 1996. Application of hydraulic flood routing techniques to the 1995 flood in Southern Alberta. Proceeding, Canadian Society of Civil Engineering Annual Conference, Edmonton, Alberta, pp. 132-142.

Mercer, A.G. and Cooper, R.H. 1977. River bed scour related to the growth of a major ice jam. Proceedings, 3rd National Hydrotechnical Conference, Quebec City, Quebec, pp. 291 – 308.

Ponce, V. M. 1989. Engineering Hydrology Principles and Practices, Prentice-Hall, Inc. Englewood Cliffs, New Jersey, 640 pp.

Saade, R.G., Sarraf, S. and El-Jabi, N. 1993. Numerical modelling of surges resulting from ice jam releases. Proceedings, Canadian Society for Civil Engineering 11th Annual Conference, Frederiction, New Brunswick, pp.633-641.

REFERENCES (continued)

Taggart, J. 1995. The Peace River Natural Flow and Regulated Flow Scenarios - Daily Flow Data Report. Surface Water Assessment Branch, Alberta Environmental Protection, Edmonton, Alberta.

Water Survey Canada. 1998. HYDAT CD-ROM. (Suface water and sediment data) Version 96-1.04. Atmospheric Environmental Service, Environment Cananda.

Watt, W.E. (ed.) 1989. Hydrology of Floods in Canada: A Guide to Planning and Design. National Research Council of Canada, Ottawa, Ontario, 245 pp.

Wong, J., Beltaos, S. and Krishnappan, B.G. 1985. Laboratory tests on surges created by ice jam releases. Canadian Journal of Civil Engineering, Vol. 12, No.4, pp. 930-933.

Wong, J., Beltaos, S. and Krishnappan, B.G. 1983. Laboratory tests on ice jam dynamics. National Water Research Institute, Burlington, Ontario, Unpublished Report.

Xiaobing, C. 1993. Effects of Ice on the Hydraulics of the Mackenzie River at the Outlet of Great Slave Lake, NWT. M.Sc. Thesis, Department of Civil and Environmental Engineering, University of Alberta, Edmonton, Alberta, 173 pp.

Zufelt, J.E. 1999. Breakup on the Upper Saint John River. Cold Regions Engineering Putting Research into Practice, Proceedings, 10th International Conference, Lincoln, New Hampshire, pp. 561-575.

APPENDIX A

IMPLEMENTATION OF THE CDG SCHEME TO THE SAINT VENANT EQUATIONS FOR NATURAL CHANNELS

A.1 INTRODUCTION

In this investigation, the Characteristic-Dissipative-Galerkin (CDG) finite element scheme was employed to develop the natural channel flood routing model called the cdg1-Dn model. In this appendix, the CDG scheme is presented. This is followed by the specifics of implementing the CDG scheme in both the cdg1-D and cdg1-Dn models. The details of the cdg1-D model area presented here to illustrate the difficulties that arose in applying the CDG scheme to the Saint Venant equations for natural channels. Lastly, the handling of boundary condition, tributary inflow, and the selection of appropriate numerical parameters, for both the cdg1-D and cdg1-Dn models are discussed.

A.2 THE CHARACTERISTIC-DISSIPATIVE-GALERKIN FINITE ELEMENT SCHEME (HICKS AND STEFFLER, 1990)

Introduced by Hicks and Steffler in 1990, the Characteristic-Dissipative-Galerkin (CDG) scheme is based on the Petrov-Galerkin finite element method. For this method, the test functions are upwind weighted to introduce numerical diffusion in order to damp numerical oscillations associated with instabilities. Implementation of the Petrov-Galerkin method to the one-dimensional unsteady open channel flow equations is equivalent to a Bubnov-Galerkin formulation of the following system of equations,

$$\begin{bmatrix} f_i & 0 \\ 0 & f_i \end{bmatrix} \begin{Bmatrix} C_c \\ M_c \end{Bmatrix} + \omega \frac{\Delta x}{2} [\mathrm{W}] \frac{d}{dx} \begin{bmatrix} f_i & 0 \\ 0 & f_i \end{bmatrix} \begin{Bmatrix} C_{nc} \\ M_{nc} \end{Bmatrix} = \{0\} \qquad \text{[A.1]}$$

where:

f_i = interpolation function;

ω = upwinding coefficient;

Δx = length of an element;

[W] = upwinding matrix;

C_c = conservation form of the continuity equation;

M_c = conservation form of the momentum equations;

C_{nc} = non-conservation form of the continuity equation; and

M_{nc} = non-conservation form of the momentum equation.

For the CDG scheme, the upwinding matrix is used to introduce selective dissipation based on the characteristic velocities of a propagating disturbance (Hicks and Steffler, 1995), such that,

$$[\mathbf{W}] = \frac{[\mathbf{A}]}{|[\mathbf{A}]|} = [\mathbf{M}] \begin{bmatrix} \lambda_1 / |\lambda_1| & 0 \\ 0 & \lambda_2 / |\lambda_2| \end{bmatrix} [\mathbf{M}]^{-1} \qquad [A.2]$$

where:

[A] = convection matrix for non-conservation form;

λ_i = eigenvalues of **[A]**; and

[M] = matrix having as its columns, the eigenvectors of **[A]**.

The components of the upwinding matrix can be expressed as:

$$[\mathbf{W}]=\begin{bmatrix} w_{aq} & w_{aq} \\ w_{qa} & w_{qq} \end{bmatrix} \qquad [A.3]$$

such that equation system [A.1] can be separated as

$$f_i C_c + \omega\frac{\Delta x}{2}\left(w_{aa}\frac{df_i}{dx}\right)C_{nc} + \omega\frac{\Delta x}{2}\left(w_{aq}\frac{df_i}{dx}\right)M_{nc} = 0 \qquad [A.4]$$

for the continuity equation of this system, and

$$f_i M_c + \omega\frac{\Delta x}{2}\left(w_{qa}\frac{df_i}{dx}\right)C_{nc} + \omega\frac{\Delta x}{2}\left(w_{qq}\frac{df_i}{dx}\right)M_{nc} = 0 \qquad [A.5]$$

for the momentum equation of this system.

In the upwinding matrix, the first letter in the component subscript denotes the equation from which it is derived (a for continuity or 'area' equation, q for momentum or 'discharge' equation), while the second denotes the equation on which the component operates (Hicks and Steffler, 1990, 1992).

Forming the ‘finite element’ weak statement for equations [A.4] and [A.5],

$$\int_0^L \left\{ f_i C_c + \omega\frac{\Delta x}{2}\left(w_{aa}\frac{df_i}{dx}\right)C_{nc} + \omega\frac{\Delta x}{2}\left(w_{aq}\frac{df_i}{dx}\right)M_{nc} \right\} dx = \{0\} \qquad [A.6]$$

is the contribution from the continuity equation; and

$$\int_0^L \left\{ f_i M_c + \omega\frac{\Delta x}{2}\left(w_{qa}\frac{df_i}{dx}\right)C_{nc} + \omega\frac{\Delta x}{2}\left(w_{qq}\frac{df_i}{dx}\right)M_{nc} \right\} dx = \{0\} \qquad [A.7]$$

is the contribution from the momentum equation.

The above may also be written in matrix notation as:

$$[S]\left\{\frac{\partial \Phi}{\partial t}\right\} + [K]\{\Phi\} = \{0\} \qquad [A.8]$$

where:

$$\{\Phi\} = \text{nodal values of the solution} \equiv \begin{Bmatrix} A_j \\ Q_j \end{Bmatrix} \qquad [A.9]$$

$$[S] = \text{mass matrix} \equiv \begin{bmatrix} S_{aa} & S_{aq} \\ S_{qa} & S_{qq} \end{bmatrix} \qquad [A.10]$$

$$[K] = \text{stiffness matrix (dependent on } \Phi) \equiv \begin{bmatrix} K_{aa} & K_{aq} \\ K_{qa} & K_{qq} \end{bmatrix} \qquad [A.11]$$

In equations [A.10] and [A.11], the component subscripts in the mass and stiffness matrix have a slightly differently meaning than in the upwinding matrix. The first letter in the component subscript describes from which part of the weak statement the component is derived ('a' for continuity contribution or 'q' for momentum contribution). The second denotes the variable on which the component operates ('a' for area or 'q' for discharge).

Equation [A.8] is called the semi-discrete form of the problem, as it is only discretized in space. The problem is discretized in time using a semi-implicit finite difference approximation:

$$\left[[S] + \theta\Delta t\left[K\left(\Phi^{n+1}\right)\right]\right]\left\{\Phi^{n+1}\right\} = \left[[S] - (1-\theta)\Delta t\left[K\left(\Phi^{n}\right)\right]\right]\left\{\Phi^{n}\right\} \qquad [A.12]$$

where θ denotes the level of implicitness. To solve this non-linear system, a Newton-Raphson iteration is employed in both the cdg1-D and cdg1-Dn models. The Jacobian for the Newton-Raphson iteration is given by:

$$[J] = \left[\frac{\partial\{R\}}{\partial\{\Phi\}}\right] \qquad [2.84]$$

where:

$$\{R\}=\left[[S]+\theta\Delta t\left[K\left(\Phi^{n+1}\right)\right]\right]\left\{\Phi^{n+1}\right\}-\left[[S]-(1-\theta)\Delta t\left[K\left(\Phi^{n}\right)\right]\right]\left\{\Phi^{n}\right\} \qquad [A.13]$$

or

$$\{R\}=[K']\left\{\Phi^{n+1}\right\}-\{F'\} \qquad [A.14]$$

for a more general form. In both the cdg1-D and cdg1-Dn models, the Jacobian matrix is solved analytically, rather than numerically. Therefore, the above expression is used to expand equation [2.84] as follows:

$$\begin{aligned}[J]=\left[\frac{\partial\{R\}}{\partial\{\Phi\}}\right]&=\frac{\partial\left[[K']\{\Phi\}\right]}{\partial\{\Phi\}}-\frac{\partial\{F'\}}{\partial\{\Phi\}}=\frac{\partial[K']}{\partial\{\Phi\}}\{\Phi\}+\frac{\partial\{\Phi\}}{\partial\{\Phi\}}[K'] \\ &=[K']+\frac{\partial[K']}{\partial\{\Phi\}}\{\Phi\}=[K']+[J']\end{aligned} \qquad [A.15]$$

where:

$$[K']=\left[[S]+\theta\Delta t[K]\right] \qquad [A.16]$$

$$[J']=\frac{\partial[K']}{\partial\{\Phi\}}\{\Phi\}=\begin{bmatrix}J_{aa} & J_{aq}\\ J_{qa} & J_{qq}\end{bmatrix} \qquad [A.17]$$

In both the cdg1-D and cdg1-Dn models, convergence at every time step is assessed based on:

$$\frac{\sum\left[(\delta\Phi)^2\right]}{\sum\left(\Phi^2\right)}\leq \text{tolerance} \qquad [A.18]$$

A.3 WEAK STATEMENT, UPWINDING MATRIX AND JACOBIAN FOR THE cdg1-D MODEL (HICKS AND STEFFLER, 1990)

The cdg1-D model solves the Saint Venant equations for the case when the channel can be approximated by a rectangle. Again, in conservation form the equations are:

$$\frac{\partial A}{\partial t}+\frac{\partial Q}{\partial x}=0 \qquad [2.1]$$

$$\frac{\partial Q}{\partial t}+\frac{\partial (Q^2/A)}{\partial x}+\frac{\partial}{\partial x}\left(\frac{gAh}{2}\right)-\frac{gAh}{2B}\frac{dB}{dx}-gAS_o+gAS_f=0 \qquad [2.5]$$

Considering

$$Q = AU \qquad [2.7]$$

The conservation formulation can be written in matrix form as

$$\frac{\partial\{\Phi\}}{\partial t}+\frac{\partial\{F\}_r}{\partial x}+\{f\}_{r,c}=\{0\} \qquad [A.19]$$

where:

$$\{\Phi\}\equiv\begin{Bmatrix} A \\ Q \end{Bmatrix} \qquad [2.12]$$

$$\{F\}_r=\begin{Bmatrix} Q \\ QU+\dfrac{ghA}{2} \end{Bmatrix} \qquad [A.20]$$

$$\{f\}_{r,c}=\begin{Bmatrix} 0 \\ gA\left(S_f-S_o-\dfrac{h}{2B}\dfrac{dB}{dx}\right) \end{Bmatrix} \qquad [A.21]$$

where $\{F\}_r$ is called the flux vector.

The non-conservation form in matrix notation is:

$$\frac{\partial\{\Phi\}}{\partial t}+[\mathbf{A}]_r\frac{\partial\{\Phi\}}{\partial x}+\{f\}_{r,nc}=\{0\} \qquad [2.11]$$

where:

$$[\mathbf{A}]_r = \begin{bmatrix} 0 & 1 \\ gh - U^2 & 2U \end{bmatrix} = \begin{bmatrix} 0 & 1 \\ c^2 - U^2 & 2U \end{bmatrix} = \begin{bmatrix} a_{aa} & a_{aq} \\ a_{qa} & a_{qq} \end{bmatrix} \qquad [2.13]$$

$$\{f\}_{r,nc} = \left\{ \begin{matrix} 0 \\ gA\left(S_f - S_o - \frac{h}{B}\frac{dB}{dx} \right) \end{matrix} \right\} \qquad [2.15]$$

In the above equations, considering

$$\psi = \frac{g|Q|n^2}{\varphi^2 AR^{4/3}} = \frac{gA}{Q} S_f \qquad [A.22]$$

then,

$$gAS_f = \psi Q \qquad [A.23]$$

The continuity contribution to the weak statement is:

$$\int_0^L \left\{ \begin{matrix} f_i \left[\frac{\partial A}{\partial t} + \frac{\partial Q}{\partial x} \right] + \omega \frac{\Delta x}{2} w_{aa} \frac{df_i}{dx} \left[\frac{\partial A}{\partial t} + \frac{\partial Q}{\partial x} \right] + \\ \omega \frac{\Delta x}{2} w_{aq} \frac{df_i}{dx} \left[\frac{\partial Q}{\partial t} + a_{qq} \frac{\partial Q}{\partial x} + a_{qa} \frac{\partial A}{\partial x} - gA\left(S_0 + \frac{h}{B}\frac{dB}{dx} \right) + \psi Q \right] \end{matrix} \right\} dx = \{0\} \qquad [A.24]$$

Substitution of the interpolation functions and integration by parts of the flux term in the conservation form yields:

$$\int_0^L \left\{ \begin{matrix} f_i f_j \frac{dA_j}{dt} - \frac{df_i}{dx} f_j Q_j + \omega \frac{\Delta x}{2} w_{aa} \frac{df_i}{dx} \left[f_j \frac{dA_j}{dt} + \frac{df_j}{dx} Q_j \right] \\ + \omega \frac{\Delta x}{2} w_{aq} \frac{df_i}{dx} \left[\begin{matrix} f_j \frac{dQ_j}{dt} + a_{qq} \frac{df_j}{dx} Q_j + a_{qa} \frac{df_j}{dx} A_j \\ - gf_j \left(S_0 + \frac{h}{B}\frac{dB}{dx} \right) A_j + \psi f_j Q_j \end{matrix} \right] \end{matrix} \right\} dx + [f_i(Q)]_0^L = \{0\} \qquad [A.25]$$

f_i = interpolation function;

f_j = interpolation function; and

L = length of the domain.

The momentum contribution to the weak statement is:

$$\int_0^L \left\{ \begin{array}{l} f_i\left[\dfrac{\partial Q}{\partial t}+\dfrac{\partial(QU)}{\partial x}+\dfrac{\partial}{\partial x}\left(\dfrac{gAh}{2}\right)-\dfrac{gAh}{2B}\dfrac{dB}{dx}-gAS_o+\psi Q\right] \\ +\,\omega\dfrac{\Delta x}{2}w_{qa}\dfrac{df_i}{dx}\left[\dfrac{\partial A}{\partial t}+\dfrac{\partial Q}{\partial x}\right] \\ +\,\omega\dfrac{\Delta x}{2}w_{qq}\dfrac{df_i}{dx}\left[\dfrac{\partial Q}{\partial t}+a_{qq}\dfrac{\partial Q}{\partial x}+a_{qa}\dfrac{\partial A}{\partial x}-gA\left(S_0+\dfrac{h}{B}\dfrac{dB}{dx}\right)+\psi Q\right] \end{array} \right\} dx=\{0\} \qquad [A.26]$$

Substitution of the interpolation functions and integration by parts of the flux terms in the conservation form yields:

$$\int_0^L \left\{ \begin{array}{l} f_i f_j\dfrac{dQ_j}{dt}-U\dfrac{df_i}{dx}f_jQ_j-\dfrac{gh}{2}\dfrac{df_i}{dx}f_jA_j \\ -\dfrac{gh}{2B}\dfrac{dB}{dx}f_if_jA_j-gS_of_if_jA_j+\psi f_if_jQ_j \\ +\,\omega\dfrac{\Delta x}{2}w_{qa}\dfrac{df_i}{dx}\left[f_j\dfrac{dA_j}{dt}+\dfrac{df_j}{dx}Q_j\right] \\ +\,\omega\dfrac{\Delta x}{2}w_{qq}\dfrac{df_i}{dx}\left[\begin{array}{l} f_j\dfrac{dQ_j}{dt}+a_{qq}\dfrac{df_j}{dx}Q_j \\ +\,a_{qa}\dfrac{df_j}{dx}A_j+\psi f_jQ_j \\ -\,gf_j\left(S_0+\dfrac{h}{B}\dfrac{dB}{dx}\right)A_j \end{array}\right] \end{array} \right\} dx+\left[f_i\left(QU+\dfrac{gAh}{2}\right)\right]_0^L=\{0\} \qquad [A.27]$$

In the model, integration proceeds on an element by element basis. Therefore, equations [A.25] and [A.27] can be rewritten as:

$$\sum_{e=1}^{E}\left\{\int_{l_e}^{r_e}\left\{\begin{array}{l} f_if_j\frac{dA_j}{dt}-\frac{df_i}{dx}f_jQ_j+\omega\frac{\Delta x}{2}w_{aa}\frac{df_i}{dx}\left[f_j\frac{dA_j}{dt}+\frac{df_j}{dx}Q_j\right] \\ +\omega\frac{\Delta x}{2}w_{aq}\frac{df_i}{dx}\left[\begin{array}{l} f_j\frac{dQ_j}{dt}+a_{qq}\frac{df_j}{dx}Q_j+a_{qa}\frac{df_j}{dx}A_j \\ -gf_j\left(S_0+\frac{h}{B}\frac{dB}{dx}\right)A_j+\psi f_jQ_j\end{array}\right]\end{array}\right\}dx+\left[f_i(Q)\right]_{l_e}^{r_e}\right\}=\{0\} \quad [A.28]$$

$$\sum_{e=1}^{E}\left\{\int_{l_e}^{r_e}\left\{\begin{array}{l} f_if_j\frac{dQ_j}{dt}-U\frac{df_i}{dx}f_jQ_j-\frac{gh}{2}\frac{df_i}{dx}f_jA_j \\ -\frac{gh}{2B}\frac{dB}{dx}f_if_jA_j-gS_of_if_jA_j+\psi f_if_jQ_j \\ +\omega\frac{\Delta x}{2}w_{qa}\frac{df_i}{dx}\left[f_j\frac{dA_j}{dt}+\frac{df_j}{dx}Q_j\right] \\ +\omega\frac{\Delta x}{2}w_{qq}\frac{df_i}{dx}\left[\begin{array}{l} f_j\frac{dQ_j}{dt}+a_{qq}\frac{df_j}{dx}Q_j \\ +a_{qa}\frac{df_j}{dx}A_j+\psi f_jQ_j \\ -gf_j\left(S_0+\frac{h}{B}\frac{dB}{dx}\right)A_j\end{array}\right]\end{array}\right\}dx+\left[f_i\left(QU+\frac{gAh}{2}\right)\right]_{l_e}^{r_e}=\{0\}\right\} \quad [A.29]$$

where E is the number of elements, and l_e and r_e represent the left and right boundaries of the e^{th} element, respectively. The last term in equation [A.28] and the last two terms in equation [A.29] represent the mass flux and momentum flux across the boundaries of each element, respectively. Now, if the conservation of mass and momentum are enforced at each internal element boundary, these terms will only provide contributions to the equations written at the domain boundary nodes ($x = 0$ and $x = L$) (Hicks and Steffler, 1992). These boundary terms are known as natural boundary conditions for the domain (Hicks and Steffler, 1990, 1992).

Grouping the mass and stiffness matrices into their components gives:

$$S_{aa} = \int_e \left[\left(f_i f_j \right) + \left(\omega \frac{\Delta x}{2} w_{aa} \frac{df_i}{dx} f_j \right) \right] dx \tag{A.30}$$

$$S_{aq} = \int_e \left(\omega \frac{\Delta x}{2} w_{aq} \frac{df_i}{dx} f_j \right) dx \tag{A.31}$$

$$S_{qa} = \int_e \left[\left(f_i f_j \right) + \left(\omega \frac{\Delta x}{2} w_{qa} \frac{df_i}{dx} f_j \right) \right] dx \tag{A.32}$$

$$S_{qq} = \int_e \left(\omega \frac{\Delta x}{2} w_{qq} \frac{df_i}{dx} f_j \right) dx \tag{A.33}$$

$$K_{aa} = \int_e \left\{ \omega \frac{\Delta x}{2} w_{aq} \left[a_{qa} \frac{df_i}{dx} \frac{df_j}{dx} - g \left(S_0 + \frac{h}{B} \frac{dB}{dx} \right) \frac{df_i}{dx} f_j \right] \right\} dx \tag{A.34}$$

$$K_{aq} = \int_e \left\{ - \frac{df_i}{dx} f_j + \omega \frac{\Delta x}{2} \left[w_{aa} \frac{df_i}{dx} \frac{df_j}{dx} + w_{aq} a_{qq} \frac{df_i}{dx} \frac{df_j}{dx} + w_{aq} \psi \frac{df_i}{dx} f_j \right] \right\} dx \tag{A.35}$$

$$K_{qa} = \int_e \left\{ \begin{array}{l} - \dfrac{gh}{2} \dfrac{df_i}{dx} f_j - g \left(S_0 + \dfrac{h}{2B} \dfrac{dB}{dx} \right) f_i f_j \\ + \omega \dfrac{\Delta x}{2} w_{qq} \left[a_{qa} \dfrac{df_i}{dx} \dfrac{df_j}{dx} - g \left(S_0 + \dfrac{gh}{B} \dfrac{dB}{dx} \right) \dfrac{df_i}{dx} f_j \right] \end{array} \right\} dx \tag{A.36}$$

$$K_{qq} = \int_e \left\{ \begin{array}{l} - U \dfrac{df_i}{dx} f_j + \psi f_i f_j \\ + \omega \dfrac{\Delta x}{2} \left[w_{qa} \dfrac{df_i}{dx} \dfrac{df_j}{dx} + w_{qq} a_{qq} \dfrac{df_i}{dx} \dfrac{df_j}{dx} + w_{qq} \psi \dfrac{df_i}{dx} f_j \right] \end{array} \right\} dx \tag{A.37}$$

The upwinding matrix is developed by considering the decomposition of the $[\mathbf{A}]_r$ matrix in equation [2.13]:

$$
\begin{aligned}
[\mathbf{A}]_r &= [\mathbf{M}]\begin{bmatrix} \lambda_1 & 0 \\ 0 & \lambda_2 \end{bmatrix}[\mathbf{M}]^{-1} \\
&= \begin{bmatrix} 1/2c & -1/2c \\ (U+c)/2c & -(U+c)/2c \end{bmatrix}\begin{bmatrix} U+c & 0 \\ 0 & U-c \end{bmatrix}\begin{bmatrix} -(U-c) & 1 \\ -(U+c) & 1 \end{bmatrix}
\end{aligned}
\qquad [A.38]
$$

Therefore,

$$
\begin{aligned}
[\mathbf{W}]_r &= \frac{[\mathbf{A}]_r}{|[\mathbf{A}]_r|} = [\mathbf{M}]\begin{bmatrix} \lambda_1/|\lambda_1| & 0 \\ 0 & \lambda_2/|\lambda_2| \end{bmatrix}[\mathbf{M}]^{-1} \\
&= \begin{bmatrix} 1/2c & -1/2c \\ (U+c)/2c & -(U+c)/2c \end{bmatrix}\begin{bmatrix} \dfrac{U+c}{|U+c|} & 0 \\ 0 & \dfrac{U-c}{|U-c|} \end{bmatrix}\begin{bmatrix} -(U-c) & 1 \\ -(U+c) & 1 \end{bmatrix}
\end{aligned}
\qquad [A.39]
$$

which illustrates the use of both characteristic velocities, $U+c$ and $U-c$, in the determination of the upwinding matrix. The above expression can be simplified to:

$$
[\mathbf{W}]_r = \frac{1}{2c}\begin{bmatrix} \left(c^2-U^2\right)\left(\dfrac{1}{|U+c|}-\dfrac{1}{|U-c|}\right) & \dfrac{U+c}{|U+c|}-\dfrac{U-c}{|U-c|} \\ \left(c^2-U^2\right)\left(\dfrac{U+c}{|U+c|}-\dfrac{U-c}{|U-c|}\right) & \dfrac{(U+c)^2}{|U+c|}-\dfrac{(U-c)^2}{|U-c|} \end{bmatrix}
\qquad [A.40]
$$

The analytical Jacobian for this method can be separated into $[K']$ and $[J']$ as defined by equations [A.16] and [A.17]. Since $[K']$ is simply formed from the mass and stiffness matrices, it is not presented here explicitly. The components for $[J']$ are defined as follows.

Equation [A.18] for the Jacobian matrix can be expanded to give:

$$
\begin{aligned}
[J'] = \frac{\partial[K']}{\partial\{\Phi\}}\{\Phi\} &= \frac{\partial}{\partial\{\Phi\}}\begin{bmatrix} K'_{aa} & K'_{aq} \\ K'_{qa} & K'_{qq} \end{bmatrix}\begin{Bmatrix} A \\ Q \end{Bmatrix} \\
&= \begin{bmatrix} \dfrac{\partial[K'_{aa}]}{\partial A}A + \dfrac{\partial[K'_{aq}]}{\partial A}Q & \dfrac{\partial[K'_{aa}]}{\partial Q}A + \dfrac{\partial[K'_{aq}]}{\partial Q}Q \\ \dfrac{\partial[K'_{qa}]}{\partial A}A + \dfrac{\partial[K'_{qq}]}{\partial A}Q & \dfrac{\partial[K'_{qa}]}{\partial Q}A + \dfrac{\partial[K'_{qq}]}{\partial Q}Q \end{bmatrix} \\
&= \begin{bmatrix} J_{aa} & J_{aq} \\ J_{qa} & J_{qq} \end{bmatrix}
\end{aligned}
\qquad [A.41]
$$

Neglecting the dependence of the upwinding matrix on the solution,

$$
\frac{\partial[\mathbf{w}]}{\partial\{\Phi\}} \approx [0] \qquad [2.85]
$$

then:

$$
J_{aa} \equiv \int_e -\theta\Delta t\,\omega\frac{\Delta x}{2}w_{aq}\left(\left(\frac{gh}{2B}\frac{dB}{dx} + 2U\psi - j_a\right)\frac{df_i}{dx}f_j\right)dx \qquad [A.42]
$$

$$
J_{aq} \equiv \int_e \theta\Delta t\,\omega\frac{\Delta x}{2}w_{aq}\left((\psi + j_q)\frac{df_i}{dx}f_j\right)dx \qquad [A.43]
$$

$$
J_{qa} \equiv \int_e \theta\Delta t\begin{pmatrix} -\left(\dfrac{gh}{2} - U^2\right)\dfrac{df_i}{dx}f_j - \left(\dfrac{gh}{2B}\dfrac{dB}{dx} + 2U\psi\right)f_i f_j \\ -\,\omega\dfrac{\Delta x}{2}w_{qq}\left(\dfrac{gh}{2B}\dfrac{dB}{dx} + 2U\psi - j_a\right)\dfrac{df_i}{dx}f_j \end{pmatrix}dx \qquad [A.44]
$$

$$
J_{qq} \equiv \int_e \theta\Delta t\left(-U\frac{df_i}{dx}f_j + \psi f_i f_j + \omega\frac{\Delta x}{2}w_{qq}(\psi + j_q)\frac{df_i}{dx}f_j\right)dx \qquad [A.45]
$$

where:

$$j_a \equiv \frac{1}{A}\left\{\frac{\partial A}{\partial x}\left(c^2 + 2U^2\right) - 2U\frac{\partial Q}{\partial x}\right\} \qquad [A.46]$$

$$j_q \equiv \frac{2}{A}\left\{\frac{\partial Q}{\partial x} - U\frac{\partial A}{\partial x}\right\} \qquad [A.47]$$

A.4 WEAK STATEMENT, UPWINDING MATRIX AND JACOBIAN FOR THE cdg1-Dn MODEL

For this study, the CDG scheme was implemented to solve Saint Venant equations for natural channels, with the resulting model being named 'cdg1-Dn'. Hicks and Steffler (1990, 1992, and 1995) found that CDG scheme produces the best results when it is fundamentally based on the conservation form of the equations. As it is not possible to manipulate the equations for natural channels into a fully conservation form, the following form of the Saint Venant equations for natural channels was chosen for implementation:

$$s\left(1 + \frac{T_o}{T}\right)\frac{\partial A}{\partial t} + \frac{\partial Q}{\partial x} = 0 \qquad [2.46]$$

$$s\frac{\partial Q}{\partial t} + \frac{\partial(\beta QU)}{\partial x} + \frac{\partial(gAH)}{\partial x} - gH\frac{\partial A}{\partial x} + gAS_f = 0 \qquad [2.47]$$

This formulation can be written in matrix form as

$$[\mathbf{B}]\frac{\partial\{\Phi\}}{\partial t} + \frac{\partial\{F\}_n}{\partial x} + \{f\}_{n,c} = \{0\} \qquad [A.48]$$

where:

$$\{\Phi\} \equiv \begin{Bmatrix} A \\ Q \end{Bmatrix} \qquad [2.12]$$

$$[\mathbf{B}] = \begin{bmatrix} s\left(1+\dfrac{T_o}{T}\right) & 0 \\ 0 & s \end{bmatrix} \qquad [2.53]$$

$$\{F\}_n = \begin{Bmatrix} Q \\ \beta QU + gHA \end{Bmatrix} \qquad [A.49]$$

$$\{f\}_{n,c} = \begin{Bmatrix} 0 \\ gA\left(S_f - \dfrac{H}{A}\dfrac{dA}{dx}\right) \end{Bmatrix} \qquad [A.50]$$

This form of the equations is very similar to the conservation formulation in the cdg1-D model. Particularly, in this form, $\{F\}_n$ is very similar to $\{F\}_r$. However, $\{F\}_n$ is not a true flux vector as the momentum component is not the momentum flux for this problem. The momentum flux for a irregular shaped channel is (Henderson, 1966):

$$\beta QU + gA\bar{y} \qquad [A.51]$$

where $\bar{y}$ is the depth from the surface to the centroid of the cross section.

The non-conservation form used for the development of the upwinding terms in the CDG scheme in the cdg1-Dn model is, in matrix form:

$$[\mathbf{B}]\frac{\partial\{\Phi\}}{\partial t} + [\mathbf{A}]_n\frac{\partial\{\Phi\}}{\partial x} + \{f\}_{n,nc} = \{0\} \qquad [2.53]$$

where:

$$\{\Phi\} \equiv \begin{Bmatrix} A \\ Q \end{Bmatrix} \qquad [2.12]$$

$$[\mathbf{A}]_n = \begin{bmatrix} 0 & 1 \\ -\beta U^2 & 2\beta U \end{bmatrix} = \begin{bmatrix} a_{aa} & a_{aq} \\ a_{qa} & a_{qq} \end{bmatrix} \qquad [2.52]$$

$$[\mathbf{B}] = \begin{bmatrix} s\left(1+\frac{T_o}{T}\right) & 0 \\ 0 & s \end{bmatrix} = \begin{bmatrix} b_{aa} & b_{aq} \\ b_{qa} & b_{qq} \end{bmatrix} \qquad [2.53]$$

$$\{f\}_{n,nc} = \begin{Bmatrix} 0 \\ gA\left(\frac{\partial H}{\partial x} + S_f\right) + QU\frac{\partial \beta}{\partial x} \end{Bmatrix} \qquad [2.54]$$

Using the above formulations, the development of the weak statement is as follows.

The continuity contribution to the weak statement is:

$$\int_0^L \left\{ \begin{aligned} & f_i\left[b_{aa}\frac{\partial A}{\partial t} + \frac{\partial Q}{\partial x}\right] + \omega\frac{\Delta x}{2}w_{aa}\frac{df_i}{dx}\left[b_{aa}\frac{\partial A}{\partial t} + \frac{\partial Q}{\partial x}\right] + \\ & \omega\frac{\Delta x}{2}w_{aq}\frac{df_i}{dx}\left[b_{qq}\frac{\partial Q}{\partial t} + a_{qq}\frac{\partial Q}{\partial x} + a_{qa}\frac{\partial A}{\partial x} + gA\frac{dH}{dx} + \psi Q + QU\frac{d\beta}{dx}\right] \end{aligned} \right\} dx = \{0\} \qquad [A.52]$$

Substitution of the interpolation functions and integration by parts of the mass flux term of the non-up-winded terms yields:

$$\int_0^L \left\{ \begin{aligned} & b_{aa}\frac{dA_j}{dt}f_i f_j - \frac{df_i}{dx}f_j Q_j \\ & + \omega\frac{\Delta x}{2}w_{aa}\frac{df_i}{dx}\left[b_{aa}\frac{dA_j}{dt}f_j + \frac{df_j}{dx}Q_j\right] \\ & + \omega\frac{\Delta x}{2}w_{aq}\frac{df_i}{dx}\left[\begin{aligned} & b_{qq}\frac{dQ_j}{dt}f_j + a_{qq}\frac{df_j}{dx}Q_j + a_{qa}\frac{df_j}{dx}A_j \\ & + \left(\psi + U\frac{d\beta}{dx}\right)f_j Q_j + g\frac{dH}{dx}f_j A_j \end{aligned} \right] \end{aligned} \right\} dx + \left[f_i(Q)\right]_0^L = \{0\} \qquad [A.53]$$

The momentum contribution to the weak statement is:

$$\int_0^L \left\{ \begin{aligned} & f_i \left[b_{qq} \frac{\partial Q}{\partial t} + \frac{\partial(\beta QU)}{\partial x} + \frac{\partial(gAH)}{\partial x} - gH \frac{\partial A}{\partial x} + \psi Q \right] \\ & + \omega \frac{\Delta x}{2} w_{qa} \frac{df_i}{dx} \left[b_{aa} \frac{\partial A}{\partial t} + \frac{\partial Q}{\partial x} \right] \\ & + \omega \frac{\Delta x}{2} w_{qq} \frac{df_i}{dx} \left[b_{qq} \frac{\partial Q}{\partial t} + a_{qq} \frac{\partial Q}{\partial x} + a_{qa} \frac{\partial A}{\partial x} + gA \frac{dH}{dx} + \psi Q + QU \frac{d\beta}{dx} \right] \end{aligned} \right\} dx = \{0\} \qquad [A.54]$$

Substitution of the interpolation functions and integration by parts of 'pseudo'momentum flux terms of the non-up-winded terms yields:

$$\int_0^L \left\{ \begin{aligned} & b_{qq} \frac{dQ_j}{dt} f_i f_j - \beta U \frac{df_i}{dx} f_j Q_j - gH \frac{df_i}{dx} f_j A_j \\ & - gH \frac{df_j}{dx} f_i A_j + \psi f_i f_j Q_j \\ & + \omega \frac{\Delta x}{2} w_{qa} \frac{df_i}{dx} \left[b_{aa} \frac{dA_j}{dt} f_j + \frac{df_j}{dx} Q_j \right] \\ & + \omega \frac{\Delta x}{2} w_{qq} \frac{df_i}{dx} \left[\begin{aligned} & b_{qq} \frac{dQ_j}{dt} f_j + a_{qq} \frac{df_j}{dx} Q_j \\ & + a_{qa} \frac{df_j}{dx} A_j + \left(\psi + U \frac{d\beta}{dx} \right) f_j Q_j \\ & + g \frac{dH}{dx} f_j A_j \end{aligned} \right] \end{aligned} \right\} dx + \left[f_i (QU + gAH) \right]_0^L = \{0\} \qquad [A.55]$$

Considering the integration on an element by element basis and grouping the mass and stiffness matrices in their components gives:

$$S_{aa} = \int_e b_{aa} \left[(f_i f_j) + \left(\omega \frac{\Delta x}{2} w_{aa} \frac{df_i}{dx} f_j \right) \right] dx \qquad [A.56]$$

$$S_{aq} = \int_e b_{qq} \left(\omega \frac{\Delta x}{2} w_{aq} \frac{df_i}{dx} f_j \right) dx \qquad [A.57]$$

$$S_{qa} = \int_e b_{aa}\left[\left(f_i f_j\right) + \left(\omega \frac{\Delta x}{2} w_{qa} \frac{df_i}{dx} f_j\right)\right]dx \qquad [A.58]$$

$$S_{qq} = \int_e b_{qq}\left(\omega \frac{\Delta x}{2} w_{qq} \frac{df_i}{dx} f_j\right)dx \qquad [A.59]$$

$$K_{aa} = \int_e \left\{\omega \frac{\Delta x}{2} w_{aq}\left[a_{qa} \frac{df_i}{dx}\frac{df_j}{dx} + g\frac{dH}{dx}\frac{df_i}{dx} f_j\right]\right\}dx \qquad [A.60]$$

$$K_{aq} = \int_e \left\{\begin{matrix} -\dfrac{df_i}{dx} f_j \\ + \omega \dfrac{\Delta x}{2}\left[w_{aa}\dfrac{df_i}{dx}\dfrac{df_j}{dx} + w_{aq} a_{qq}\dfrac{df_i}{dx}\dfrac{df_j}{dx} + w_{aq}\left(\psi + U\dfrac{d\beta}{dx}\right)\dfrac{df_i}{dx} f_j\right]\end{matrix}\right\}dx \qquad [A.61]$$

$$K_{qa} = \int_e \left\{\begin{matrix} -gH\left(\dfrac{df_i}{dx} f_j + \dfrac{df_j}{dx} f_i\right) \\ + \omega \dfrac{\Delta x}{2} w_{qq}\left[a_{qa}\dfrac{df_i}{dx}\dfrac{df_j}{dx} + g\dfrac{dH}{dx}\dfrac{df_i}{dx} f_j\right]\end{matrix}\right\}dx \qquad [A.62]$$

$$K_{qq} = \int_e \left\{\begin{matrix} -\beta U\dfrac{df_i}{dx} f_j + \psi f_i f_j \\ + \omega \dfrac{\Delta x}{2}\left[w_{qa}\dfrac{df_i}{dx}\dfrac{df_j}{dx} + w_{qq} a_{qq}\dfrac{df_i}{dx}\dfrac{df_j}{dx} + w_{qq}\left(\psi + U\dfrac{d\beta}{dx}\right)\dfrac{df_i}{dx} f_j\right]\end{matrix}\right\}dx \qquad [A.63]$$

where:

$$\psi Q = gAS_f \qquad [A.23]$$

The upwinding matrix is developed using the decomposition of the convective matrix of the non-conservation form of the equations; that is, equation [2.52]. This form of the convection matrix, because of the lack of the celerity term, c^2, does not have the characteristic velocities as its eigenvalues. The eigenvalues are instead:

$$\lambda_1 = \frac{\sqrt{\beta} - \sqrt{\beta - 1}}{\sqrt{\beta} U} \qquad \text{[A.64]}$$

$$\lambda_2 = \frac{\sqrt{\beta} + \sqrt{\beta - 1}}{\sqrt{\beta} U} \qquad \text{[A.65]}$$

Use of these eigenvalues, along with a decomposed version of equation [2.52], yields a very complex upwinding matrix of which all the terms are indeterminate if $\beta = 1$ (which is the case if the velocity distribution is uniform). Therefore, in order for the upwinding matrix to be based on the characteristic velocities, the convection matrix must be of the form in equation [2.13], so that the eigenvalues are indeed the characteristic velocities. Because, it is not possible to develop an upwinding matrix that does not produce indeterminate values using the convection matrix defined by equation [2.52], the upwinding matrix for the cdg1-Dn was developed from the convection matrix of equation [2.13]. That is the upwinding matrix in the cdg1-Dn model is the same as that in the cdg1-D model, as defined by equation [A.40]. However, for natural channels, celerity is defined by:

$$c = \sqrt{g \frac{A}{T}} \qquad \text{[2.81]}$$

where A/T is known as the hydraulic depth.

Using the components of the mass and stiffness matrices in equations [A.56] to [A.63], the components of the Jacobian matrix are defined using equation [A.41] as:

$$J_{aa} \equiv \int_e -\theta \Delta t \omega \frac{\Delta x}{2} w_{aq} \left(\left(-gA \frac{d}{dx} \left(\frac{1}{T} \right) + U^2 \frac{d\beta}{dx} + 2U\psi - j_a \right) \frac{df_i}{dx} f_j \right) dx \qquad \text{[A.66]}$$

$$J_{aq} \equiv \int_e \theta \Delta t \omega \frac{\Delta x}{2} w_{aq} \left(\left(f + U \frac{d\beta}{dx} + j_q \right) \frac{df_i}{dx} f_j \right) dx \qquad \text{[A.67]}$$

$$J_{qa} \equiv \int_e \theta\Delta t \begin{pmatrix} -gh\left(\frac{df_i}{dx} f_j + \frac{df_j}{dx} f_i\right) + \beta U^2 \frac{df_i}{dx} f_j - 2U\psi f_i f_j \\ -\omega\frac{\Delta x}{2} w_{qq}\left(-gA\frac{d}{dx}\left(\frac{1}{T}\right) + U^2\frac{d\beta}{dx} + 2U\psi - j_a\right)\frac{df_i}{dx} f_j \end{pmatrix} dx \qquad [A.68]$$

$$J_{qq} \equiv \int_e \theta\Delta t\left(-\beta U\frac{df_i}{dx} f_j + \psi f_i f_j + \omega\frac{\Delta x}{2} w_{qq}\left(\psi + U\frac{d\beta}{dx} + j_q\right)\frac{df_i}{dx} f_j\right) dx \qquad [A.69]$$

where:

$$j_a \equiv \frac{\beta}{A}\left\{2U^2\frac{\partial A}{\partial x} - 2U\frac{\partial Q}{\partial x}\right\} \qquad [A.70]$$

$$j_q \equiv \frac{2\beta}{A}\left\{\frac{\partial Q}{\partial x} - U\frac{\partial A}{\partial x}\right\} \qquad [A.71]$$

A.5 HANDLING OF BOUNDARY CONDITIONS AND TRIBUTARIES IN BOTH THE cdg1-D AND cdg1-Dn MODELS

In the development of the weak statement in the cdg1-Dm model, the mass flux and the 'pseudo' momentum flux were integrated by parts to obtain the natural boundary conditions. However, because integration by parts of the momentum contribution to the weak statement does not produce the actual momentum flux for the problem, it was felt that problems might have arisen if the natural boundary conditions were implemented directly. Therefore, in the cdg1-Dn model the penalty method (Chandrupatla and Belegundu, 1997) was used instead, in which the solution is forced to satisfy the mathematical boundary conditions at the boundary nodes ($x = 0$ and $x = L$). In addition, the penalty method was implemented in the cdg1-Dn model because it functions correctly in the cdg-1D model.

If there are tributary inflows within the computational domain, these must also be specified by the user. Both models handle tributary inflows by applying the increase in discharge directly to the mass equation of the computational node where the tributary confluence occurs. It is assumed that tributary inflows contribute no momentum in the x-direction or that the x-direction tributary momentum is negligible; therefore, the momentum equation at a tributary node remains unchanged in both models.

A.6 SELECTION OF NUMERICAL PARAMETER VALUES

A.6.1 Introduction

To use the cdg1-D and cdg-1Dn models a number of model parameters must be specified. The appropriate values depend on the type of simulation at hand, that is, an unsteady flow simulation or a steady flow simulation. These include convergence tolerance, the level of implicitness θ, and the upwinding coefficient, ω. In the iterative process, the upwinding matrix can be updated at every time step or at every iteration. The selection of these three numerical parameters and the approach to updating the upwinding matrix are discussed below.

A.6.2 Selection of Convergence Tolerance

In an unsteady problem, it is important to converge to the correct answer at every time step, therefore a small tolerance should be used. Based on a series of extensive numerical tests, Hicks and Steffler recommend a strict tolerance of 10^{-5} for unsteady flow problems. When an unsteady flow model is used for a steady flow problem, the time stepping is used to converge to the steady state solution. Since the details of progression of the solution to the final steady state solution are not of concern, the convergence of the solution at every time step is not essential. Therefore, for steady flow problems a coarse convergence tolerance can be used, such as 0.1.

A.6.3 Selection of ω

In a series of extensive tests, Hicks and Steffler (1990 found that for $\omega = 0.25$ that the scheme was the most selective at dampening the numerically generated disturbances ($2\Delta x$ waves) and that for $\omega = 0.5$ the scheme dampened physical disturbances as well (greater than $2\Delta x$). Because the physical disturbances are part of an unsteady flow solution, Hicks and Steffler (1990) recommended $\omega = 0.25$ for unsteady flow problems. When a steady flow problem is being modelled with an unsteady model, the initial conditions are using given such that the water level is in excess of the actual steady state solution. Therefore, the model is run until all of the excess water leaves the system. This typically generates many waves. However, as only the final steady state solution is of concern, it does not matter if these waves are dampened even if they are physical. It is important to recognize that increasing the dissipation increases the model stability. The increased stability allows a larger time step increment. Therefore, the most expedient way to a steady state solution is by using $\omega > 0.25$.

A.6.4 Selection of θ

The level of implicitness, θ, affects the dissipation in a similar way as ω, however θ is not selective of the wavelength. The amount of dissipation increases with increasing θ. In a linear stability analysis, Hicks and Steffler (1990) tested the CDG scheme using $\theta = 0.5$ and $\theta = 1.0$. They found that for $\theta = 1.0$, the CDG scheme has a significant dissipative effect. Therefore, they recommended a $\theta = 0.5$ for unsteady flow problems where only the dampening of numerical disturbances is desired. As explained in the previous section, the dissipation is not of concern for a steady state solution and the greater the dissipation, the greater the allowable time step increment. Therefore, $\theta = 1.0$ can be used for steady state problems.

A.6.5 Approach to Updating the Upwinding Matrix

Through a series of numerical tests Hicks and Steffler (1990) found that for a dambreak tests, the CDG produced the best results when the upwinding matrix was updated at every iteration rather than at every time step. Therefore, for the dam break tests performed in Appendix B, the upwinding matrix was updated every iteration. However, in all other cases (steady state tests in Appendix B and simulations in chapters 3 and 4) in the current investigation, preliminary tests indicated the approach to updating the upwinding matrix did not affect the performance of the cdg-1Dn model. For these cases, the upwinding matrix in the cdg1-Dn model was only updated at every time step.

A.6.6 Summary

Based on the recommendations by Hicks and Steffler (1990) for unsteady flow and the above discussion regarding steady flow, the numerical parameters were selected according to Table A.1 in the current investigation.

Table A.1 Numerical parameter values for unsteady and steady flow.

Parameter	Unsteady problem	Steady problem
θ	0.5	1.0
ω	0.25	0.5
tolerance	10^{-5}	0.1

APPENDIX B

COMPARISON OF THE cdgl-D and cdgl-Dn MODELS

B.1 INTRODUCTION

The cdg1-Dn model was subjected to two numerical tests: one steady flow test and one unsteady flow test. The cdg1-D model has previously undergone an extensive number of rigorous numerical tests by Hicks and Steffler (1990). Since the cdg1-D and cdg1-Dn models both employ the CDG numerical scheme, only a couple of tests are presented here to demonstrate the performance of the cdg1-Dn model relative to the cdg1-D model. As the cdg1-D model can only handle rectangular channel geometry, both of these tests involved flow in a rectangular channel.

B.2 STEADY FLOW TEST

This test, adapted from Hicks and Steffler (1990), involved the calculation of a steady state gradually varied flow profile along a rectangular channel with a mild to steep slope transition. The channel had an upstream slope of 0.0025 and a downstream slope of 0.04 with a width of 10 m and a Manning's roughness, n, or 0.030. Calculated using Manning's equation, the uniform flow depths for the mild and steep parts of the channel were 3.65m and 1.41m respectively. The domain consisted of 200 elements, each 10m long, for a total domain length of 2000m built from 201 nodes. The slope break occurred at 1660 m. Initial conditions for the test included a discharge of 100 m^3/s and a depth of 3.5m at every node in the entire domain. Since there was a flow transition in the domain from subcritical to supercritical, only one upstream boundary condition was required to obtain a unique solution.

The test was performed by each model, cdg1-D and cdg1-Dn, using a time step increment of 0.25 s, 0.50 s, 0.75 s, and 1.00 s. As this test is a steady flow test, the model parameters were set according to Table A.1. In total 8 runs were performed, 4 for each model. The results of these runs are presented in Table B.1. The results of these runs indicate that the cdg1-Dn model is somewhat more sensitive to the time step increment than the cdg1-D model.

Table B. 1 Test results: transition from a mild to a steep channel.

Time step, Δt	Convergence?	
	cdg1-D	cdg1-Dn
1	yes	no
075	yes	no
0.5	yes	yes
0.25	yes	yes

For the cdg1-Dn model, the maximum stable time step increment was 0.5 s as compared to 1 s for the cdg1-D model. Figure B.1 illustrates the results from the cdg1-Dn model for the time step increment of 0.5 s after a time of 2000 s. In this case, the results obtained were very smooth with only a minor discharge oscillation at the slope break (about 0.03 %), with the depths approaching the uniform flow depths asymptotically in the up and downstream directions away from the slope break. Results for the cdg1-D model for the same case are presented in Figure B.2 for comparison. The results obtained for this case are visually very similar to those for the cdg1-Dn model for the same case (maximum discharge oscillation was, again, about 0.03 %).

B.3 UNSTEADY FLOW TEST

This test, reproduced from Hicks and Steffler (1990), involved the simulation of the instantaneous failure of a vertical dam in a horizontal, frictionless, unit width channel.

The domain consisted of 80 elements, each 25 m long, for a total of 81 nodes. As it is not possible to have two nodes in the same location, the vertical dam was approximated over a single element. Initially, the discharge was set to zero throughout the entire domain and the flow depth upstream of the dam, H_0, was set to 10 m. Downstream of the dam, two flow depths, H_l, were studied: $H_l = 5$ m ($H_0/H_l = 0.5$) and $H_l = 0.5$ m ($H_0/H_l = 0.05$). At both ends of the domain, the boundary conditions were specified as a discharge of zero.

For these tests, the model parameters were set according to Table A.1. Hicks and Steffler (1990) found that the CDG scheme produced the best results for these dam break tests when the upwinding matrix is updated at every iteration rather than at every time step. Therefore as mentioned in Appendix A, these tests were only performed with the upwinding matrix updated at every iteration.

Figure B.3 illustrates the initial depth profile for the first test where $H_0/H_l = 0.5$. For this test, both models obtained optimum solutions when the time step increment was set to 1.25 s. This corresponded to a Courant number of 0.47, based on the speed of the progressive wave. Figure B.4 presents the results for both the cdg1-D and cdg1-Dn models at 60 s. The figure illustrates that both models produced visually similar results with the progressive wave front distributed over two elements.

Figure B.5 illustrates the initial depth profile for the second test where $H_0/H_l = 0.05$. The test provided a more challenging situation to the models, as depth oscillations were more likely to cause model failure as a result of the small initial downstream flow depth. Consequently, both models had to be run using time step increments of 0.625 s in order to obtain optimum solutions. This time step corresponded to a Courant number of 0.26, based on the propagation speed of the progressive wave front. Figure B.6 presents the results for both the cdg1-D and cdg1-Dn models using this time step increment after 60 s has elapsed. At a time step increment of 1.25 s (Courant number = 0.52) both models "blew up" before 60 s had passed. As in the first test, the cdg1-Dn model produced visually similar results to the cdg1-D model with the progressive wave front distributed over two elements.

Qualitatively, the models produced identical results for both dam break tests. The models were compared quantitatively by assessing each model's ability to conserve mass and momentum for each dam break test. The percent error in mass conservation was evaluated using Hicks and Steffler (1990):

$$\%\,error = \frac{M_t - M_0}{M_0} \qquad [B.1]$$

where:

M_t = mass in the system at time $t = t$; and

M_0 = mass in the system at time $t = 0$.

For a dambreak, the initial momentum is zero, therefore the percent error in momentum conservation was evaluated by Hicks and Steffler (1990):

$$\%\,error = \frac{\dot{M} - \Delta F}{\Delta F} \qquad [B.2]$$

where:

$$\dot{M} \equiv rate\ of\ change\ of\ momentum = \frac{momentum\ at\ time\ t}{t} \qquad [B.3]$$

and ΔF represents the net force acting on the flow (for these tests it is simply the difference between the up and downstream hydrostatic forces). The percent error in mass and momentum conservation of each model for both dam break tests is presented in Table B.2. For the first test, $H_0/H_1 = 0.5$, both modelS conserved mass and momentum perfectly. In the second test, $H_0/H_1 = 0.05$, the cdg1-D model was able to conserved mass and momentum to 5 decimal places; however, the cdg1-Dn model was only able to conserve mass and momentum to 2 decimal places.

Table B. 2 Comparison of conservation properties of cdg1-D and cdg1-Dn.

Test Description	C	# of time steps	% Error in Mass Conservation		% Error in Momentum Conservation	
			cdg1-D	cdg1-Dn	cdg1-D	cdg1-Dn
dam break $H_l/H_0 = 0.5$	0.47	48	0.0	0.0	0.0	0.0
dam break $H_l/H_0 = 0.05$	0.26	96	0.0	9.42×10^{-4}	8.52×10^{-5}	6.22×10^{-3}

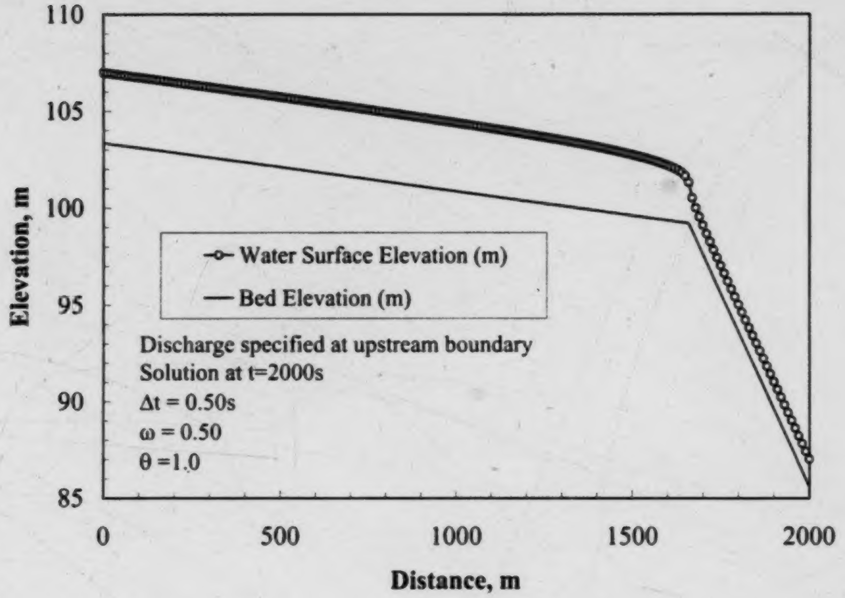

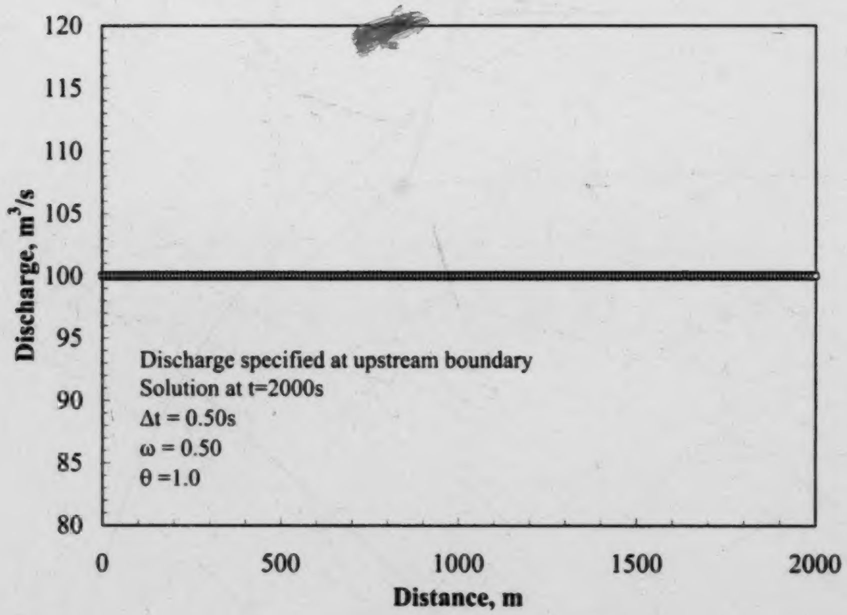

Figure B.1 Transition from a mild to a steep slope, cdg1-Dn, at 4000 time steps.

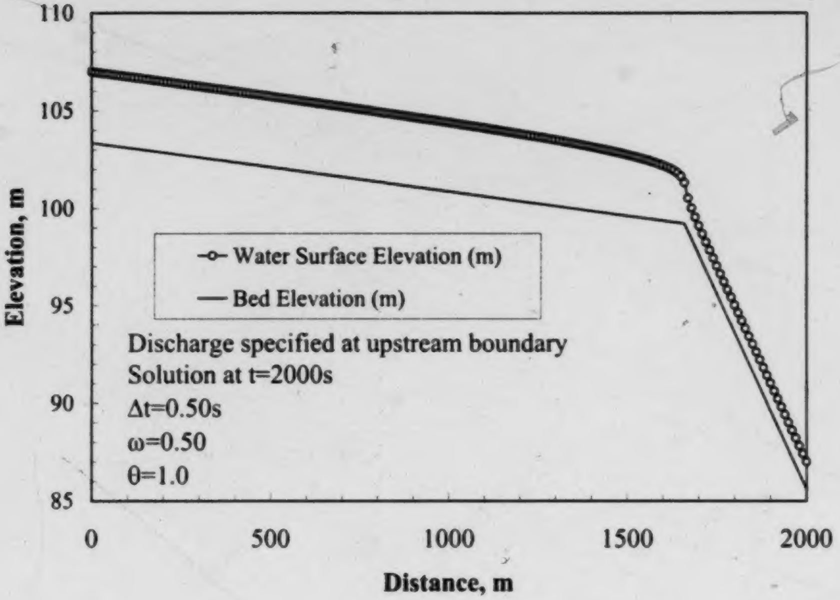

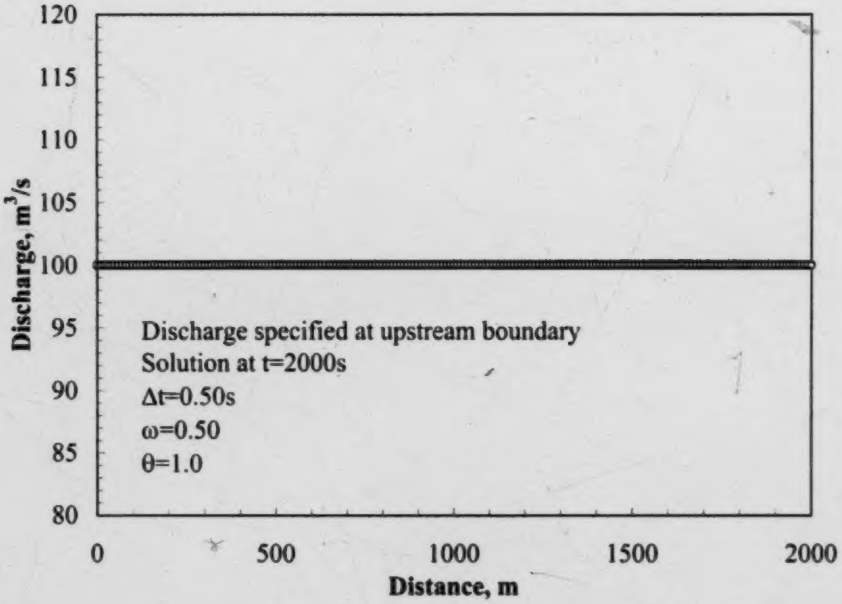

Figure B.2 Transition from a mild to a steep slope, cdg1-D, at 4000 time steps.

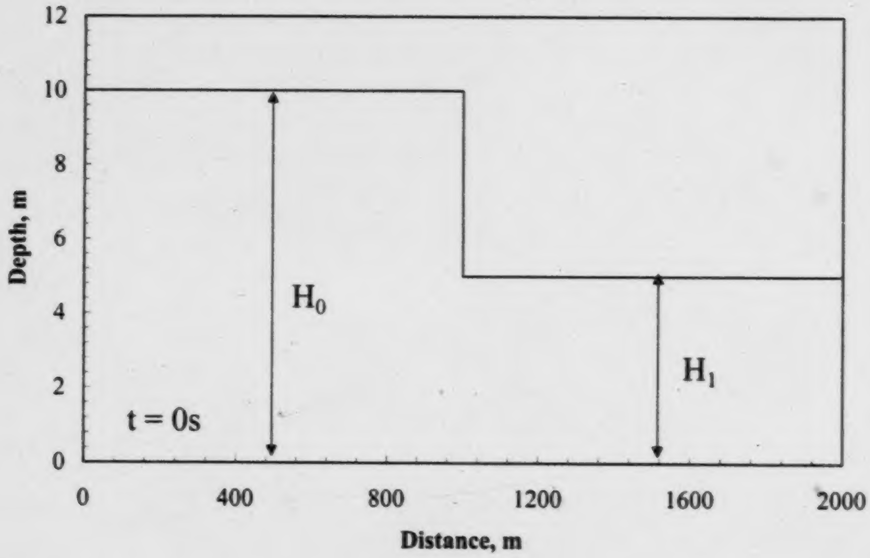

Figure B.3 Dam break, $H_1/H_0 = 0.5$, initial conditions.

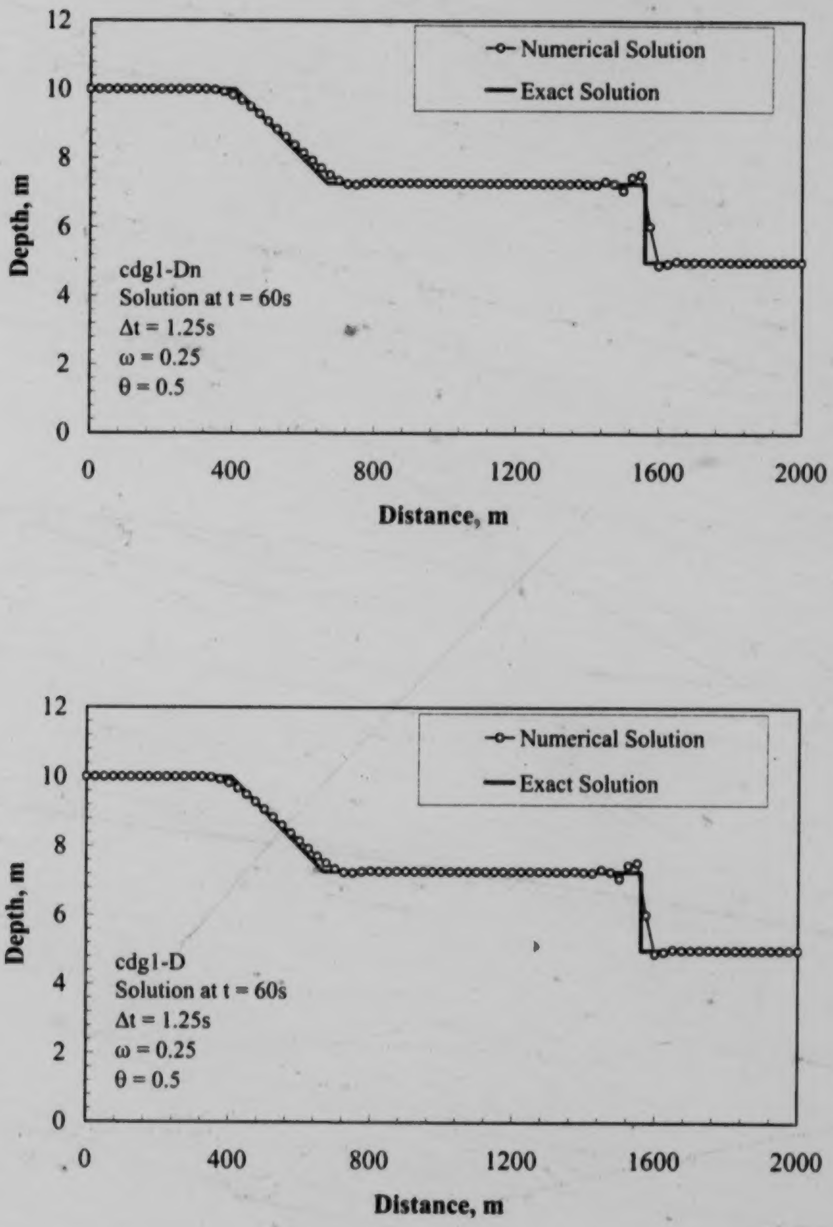

Figure B.4 Dam break , $H_1/H_0 = 0.5$.

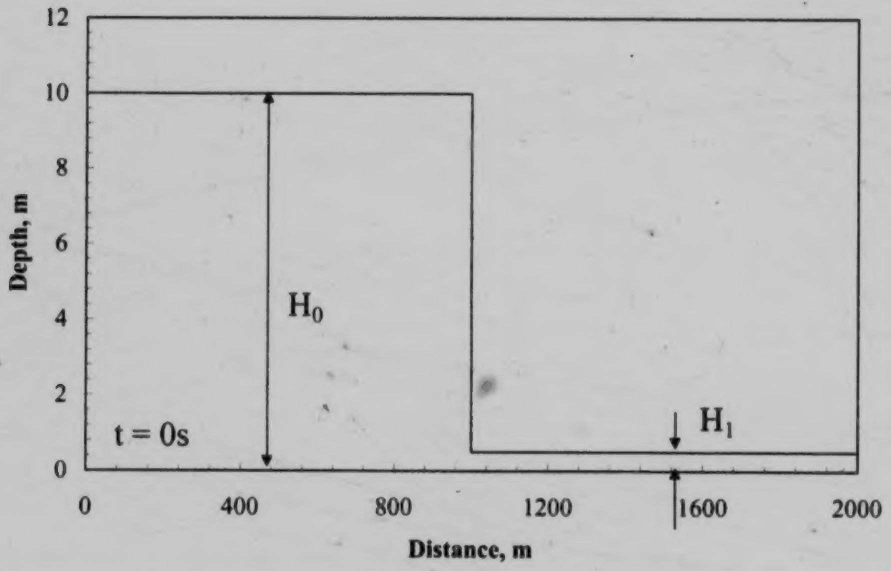

Figure B.5 Dam break $H_1/H_0 = 0.05$, initial conditions.

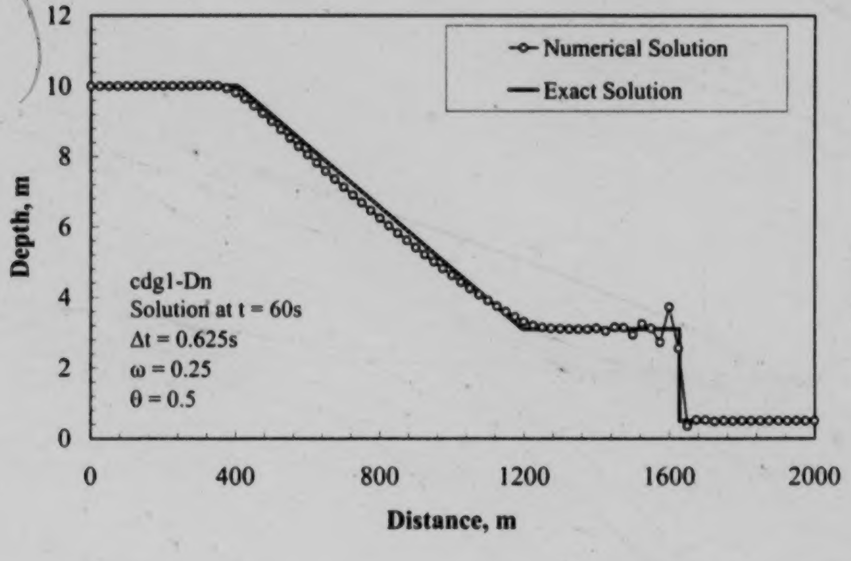

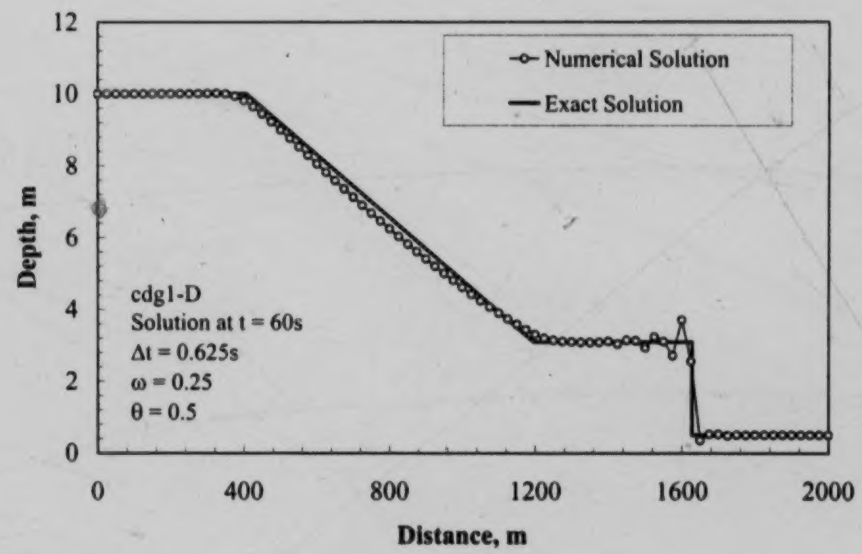

Figure B.6 Dam break, $H_1/H_0 = 0.05$.

APPENDIX C

HANDLING OF NATURAL CHANNEL GEOMETRY IN THE cdg1-Dn MODEL

For computational efficiency, the cdg1-Dn model has been designed to handle individual cross section data in the form a table of topwidths (active and inactive) and corresponding elevations, typically obtained from cross sectional field data. In Chapter 2, the active topwidth is defined as the topwidth corresponding to the active flow area (where water is actively being conveyed rather than stored). The active topwidth, can be a total width if the section is composite, or, in the case of compound channels, it can be separated into left floodplain, right floodplain, and main channel topwidths.

At a given node, the cdg1-Dn model uses a topwidth table to develop a table of cross sectional areas, based on the elevations at which the topwidth table is defined. The cdg1-Dn model uses this table of cross section areas and corresponding elevations to determine the cross sectional area of the flow at any given elevation by linearly interpolation of the values within the table. The question is: how many topwidths are required to adequately define the area-stage relationship for a given cross section? To answer this question, 8 cross sections were used to compare the actual area-stage relationships of the sections with area-elevation tables developed using topwidths, for various numbers of topwidths. Four composite sections and four compound sections were using in this comparison.

The first three composite sections are from the Mackenzie River near Fort Providence, NWT (Xiaobing, 1993), while the fourth composite section was taken from the Peace River at Fort Vermilion, Alberta. These are presented in Figure C.1. Figure C.2 shows the actual area-stage relationship for each cross section in comparison with the area-stage relationships developed using 4, 6, 8, and 10 topwidths. The area-stage relationships are well defined by only 6 topwidths for composite sections 1 and 3; however, 8 topwidths are required to define the area-stage relationships for composite sections 2 and 4.

The four compound sections are all from the Battle River, Alberta (obtained from Alberta Environment). These sections are presented in Figure C.3. Figure C.4 shows the actual area-stage relationship for each cross section in comparison with the area-stage relationships developed using various numbers of topwidths. The area-stage relationships for compound sections 1 and 4 are quite well defined by 8 topwidths. At least 10 topwidths are required to adequately define the stage-area relationship for compound sections 2 and 4.

Based on this small analysis, it recommended that composite sections should be defined by about 8 topwidths, while compound sections should be defined by at least 10 topwidths. These guidelines are used in Chapters 3 and 4 of this study.

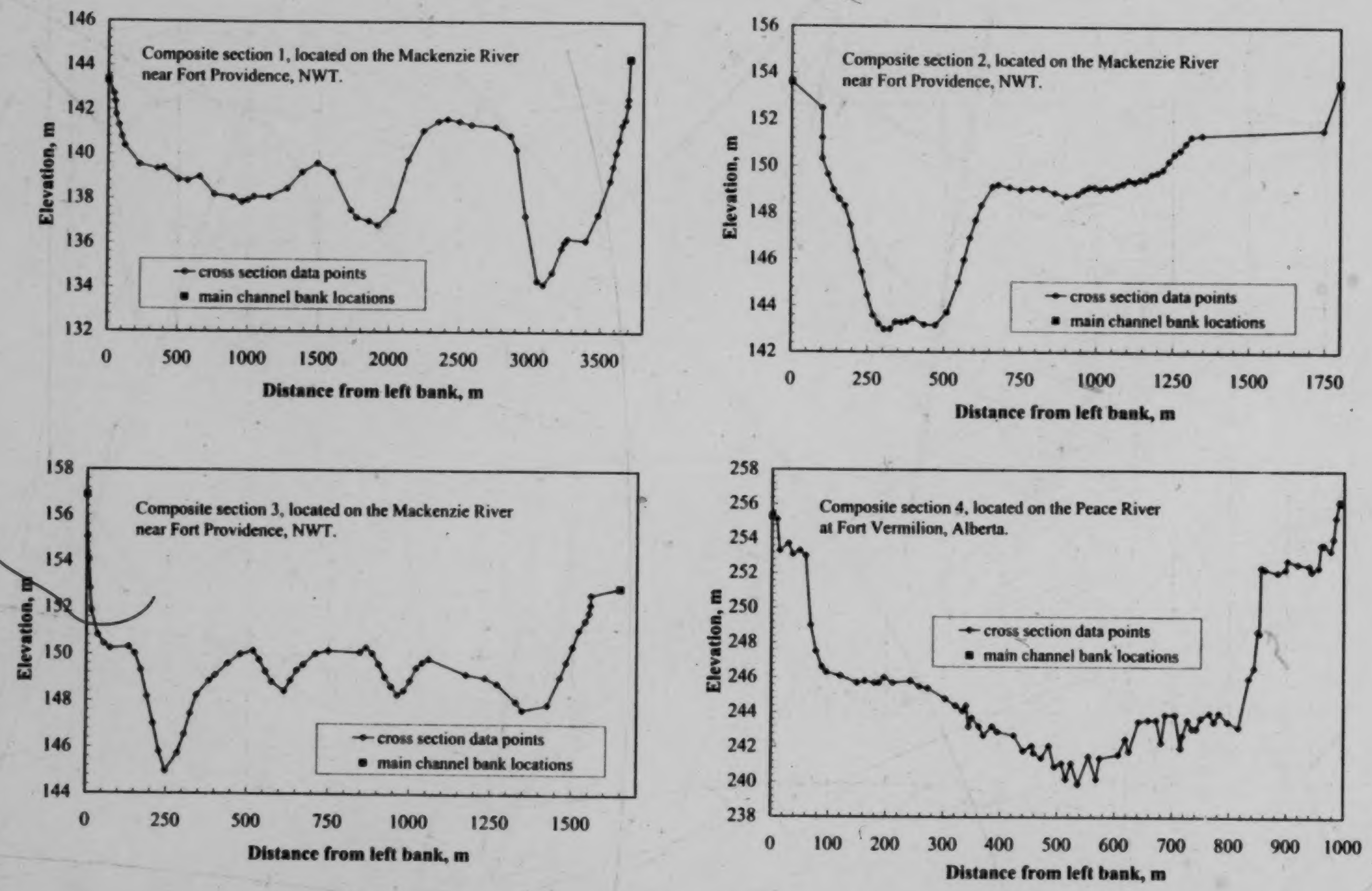

Figure C.1 Composite sections used to determine the number of topwidths required to adequately define a composite section in cdg1-Dn.

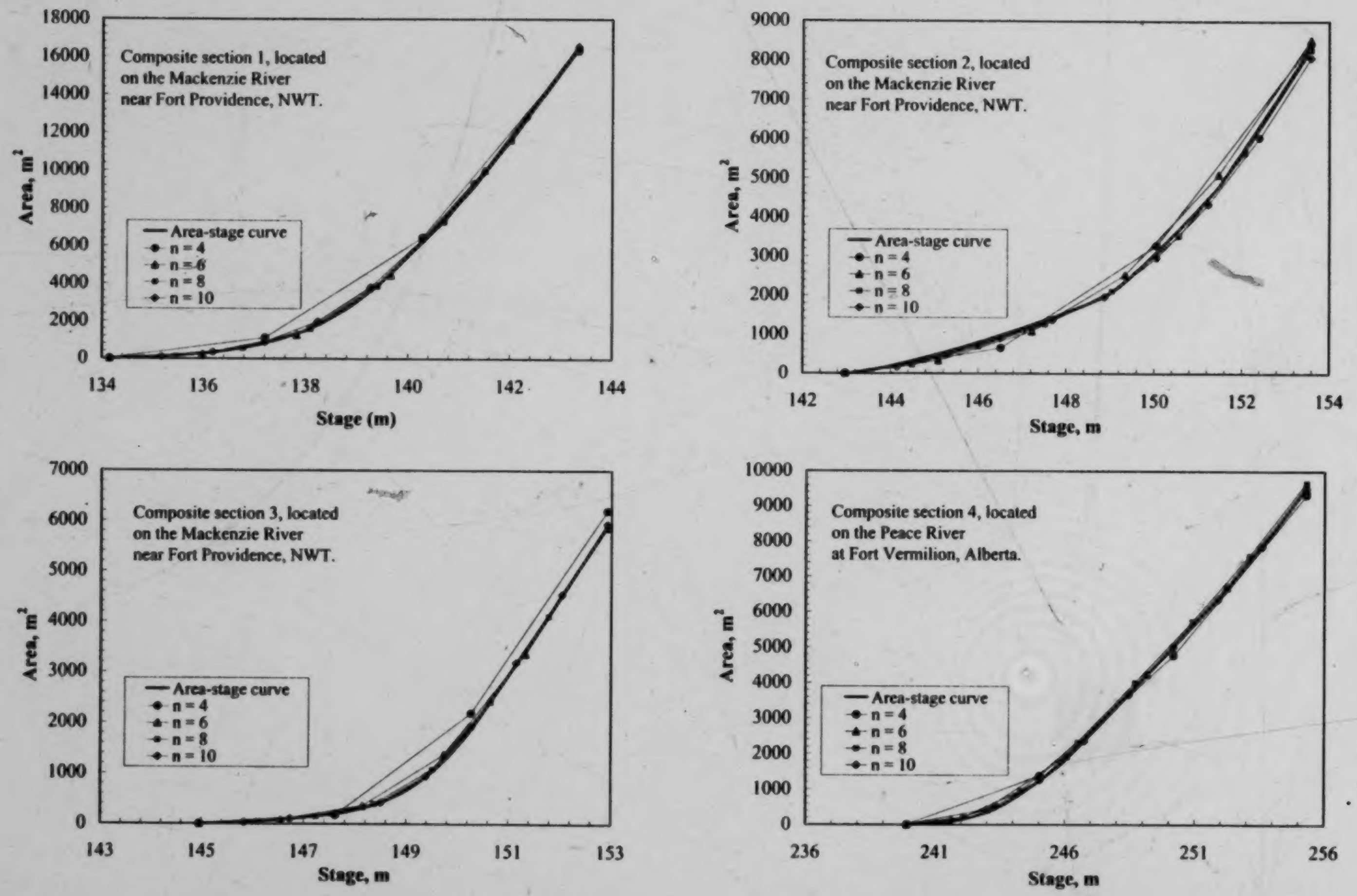

Figure C.2 Area versus stage curves for all four composite sections, where n is the number of topwidths defining a section.

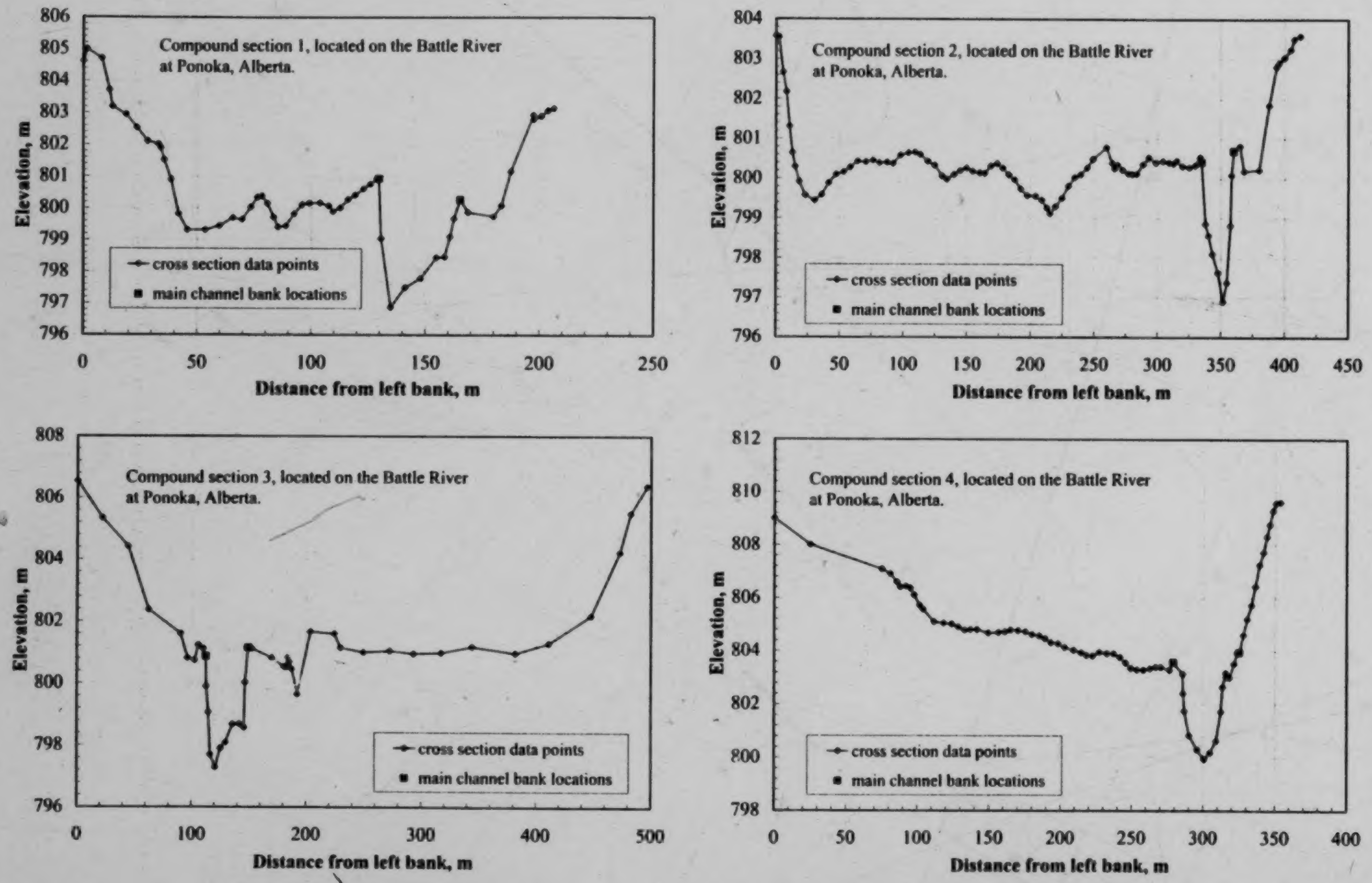

Figure C.3 Compound sections used to determine the number of topwidths required to adequately define a composite section in cdg1-Dn.

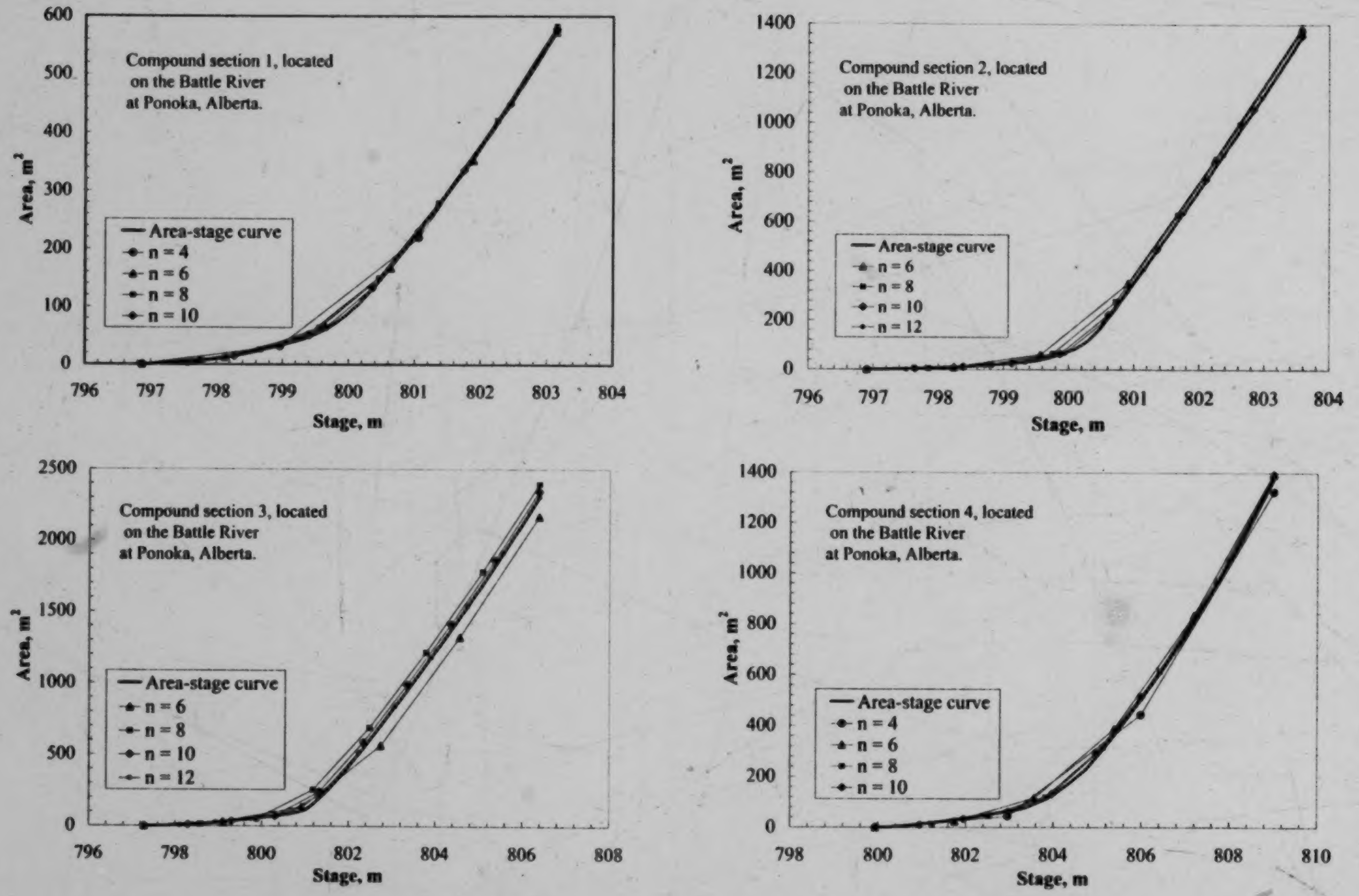

Figure C.4 Area versus stage curves for all four compound sections, where n is the number of topwidths defining a section.

APPENDIX D

CROSS SECTIONS ALONG THE PEACE RIVER

This appendix presents the cross sections that were used to define the three natural channel subreaches in chapter 3. The availability of surveyed cross sections varied in each of the three subreaches: 10 cross sections in Dunvegan; 28 cross sections at Town of Peace River; and 6 at Fort Vermilion. These cross sections are all referenced to the downstream side of the W.A.C. Bennett Dam in British Columbia.

Distance from left bank (m)	Elevation (m)
0.00	355.80
9.00	342.30
24.00	339.00
43.00	338.60
61.00	339.20
91.00	339.50
137.00	339.00
183.00	339.70
204.00	339.10
293.00	339.00
308.00	338.70
354.00	338.90
402.00	336.90
411.00	336.90
448.00	339.00
466.00	355.10

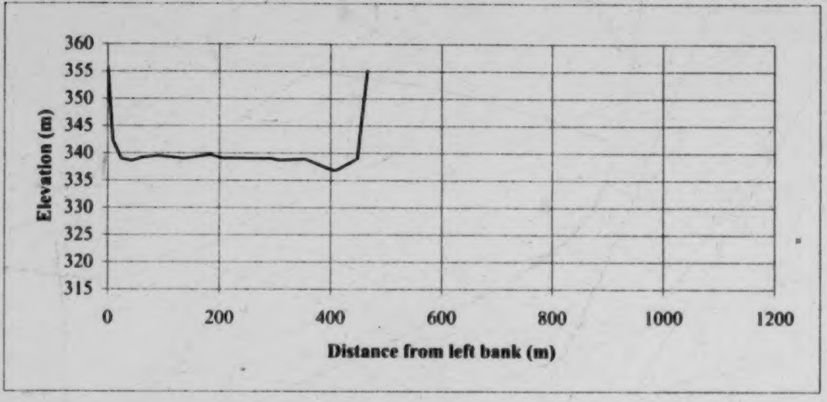

BC Hydro Cross Section No.:	10112
Distance from Bennett Dam:	293.60 km
Provided by:	Alberta Environment

Figure D.1 Cross section on the Peace River at 293.60 km downstream of the Bennett Dam (Dunvegan subreach).

Distance from left bank (m)	Elevation (m)
0.00	355.70
9.00	355.30
88.00	355.80
110.00	355.90
192.00	355.20
300.00	355.70
308.00	340.00
405.00	339.00
506.00	335.60
533.00	335.40
557.00	336.20
582.00	342.00
591.00	355.20

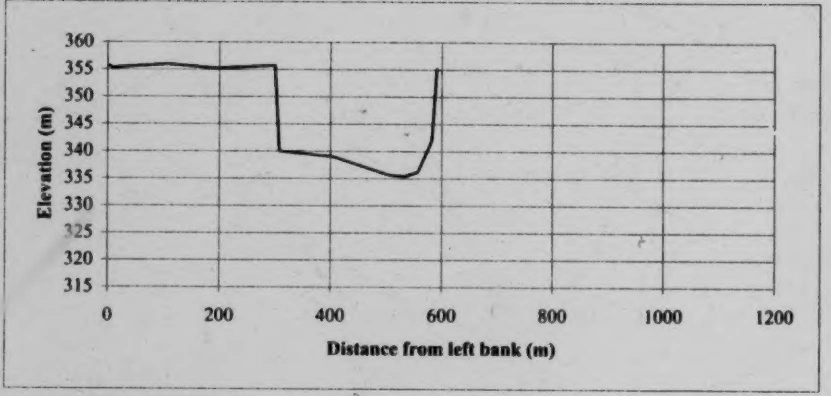

BC Hydro Cross Section No.: 10104

Distance from Bennett Dam: 294.50 km

Provided by: Alberta Environment

Figure D.2 Cross section on the Peace River at 294.50 km downstream of the Bennett Dam (Dunvegan subreach).

Distance from left bank (m)	Elevation (m)
0.00	355.90
11.00	355.30
91.00	355.00
122.00	355.20
134.00	355.10
180.00	355.40
280.00	355.50
290.00	340.30
341.00	338.50
360.00	335.30
366.00	335.30
451.00	337.40
552.00	338.20
567.00	355.40

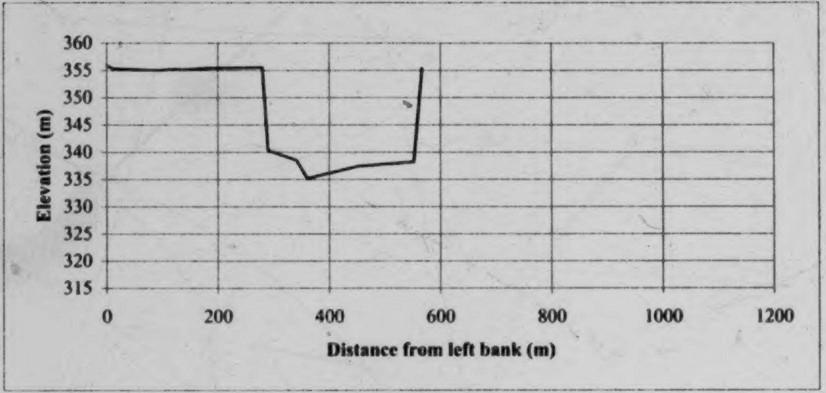

BC Hydro Cross Section No.: 10098

Distance from Bennett Dam: 295.20 km

Provided by: Alberta Environment

Figure D.3 Cross section on the Peace River at 295.20 km downstream of the Bennett Dam (Dunvegan subreach).

Distance from left bank (m)	Elevation (m)
0.00	355.50
17.00	355.40
90.00	355.90
100.00	340.20
168.00	336.80
229.00	336.00
311.00	335.80
323.00	336.10
344.00	335.20
387.00	336.50
411.00	338.10
426.00	355.40

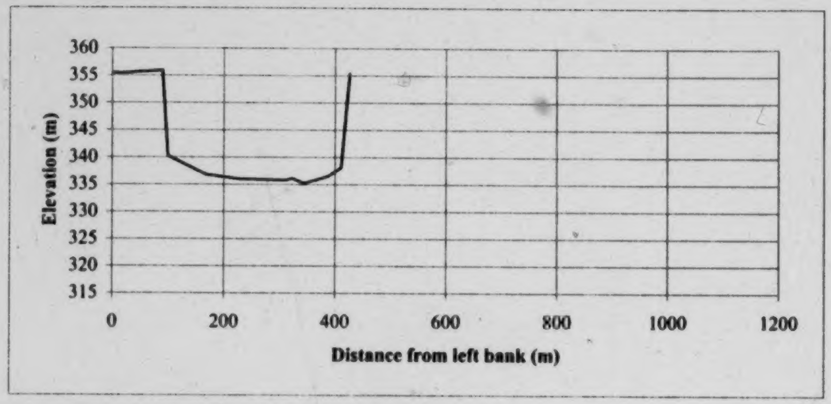

BC Hydro Cross Section No.: 10091

Distance from Bennett Dam: 295.90 km

Provided by: Alberta Environment

Figure D.4 Cross section on the Peace River at 295.90 km downstream of the Bennett Dam (Dunvegan subreach).

Distance from left bank (m)	Elevation (m)
0.00	355.90
27.00	338.20
76.00	337.40
189.00	338.00
283.00	336.90
296.00	337.10
332.00	335.90
354.00	335.90
363.00	335.50
366.00	355.30

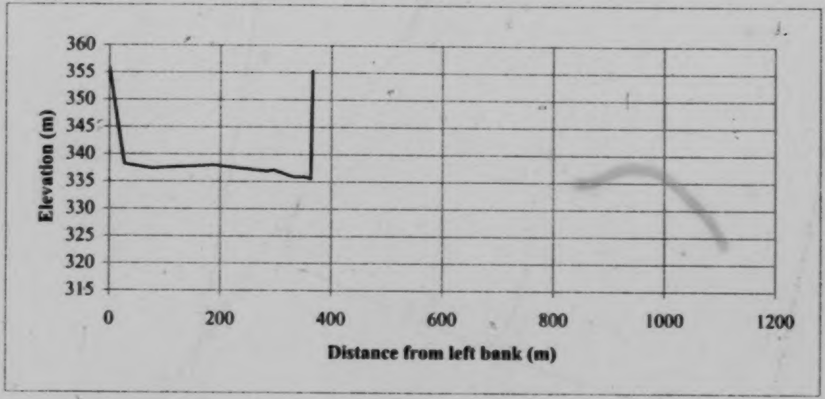

BC Hydro Cross Section No.: 10082

Distance from Bennett Dam: 296.70 km

Provided by: Alberta Environment

Figure D.5 Cross section on the Peace River at 296.70 km downstream of the Bennett Dam (Dunvegan subreach).

Distance from left bank (m)	Elevation (m)
0.00	355.90
14.00	339.50
29.00	338.00
55.00	337.20
216.00	338.40
317.00	337.20
361.00	335.90
384.00	335.70
422.00	338.10
440.00	340.60
448.00	355.80

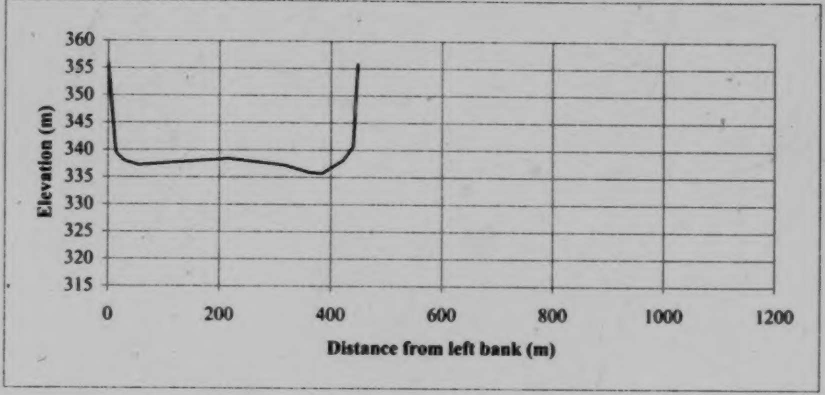

BC Hydro Cross Section No.: 10076

Distance from Bennett Dam: 297.30 km

Provided by: Alberta Environment

Figure D.6 Cross section on the Peace River at 297.30 km downstream of the Bennett Dam (Dunvegan subreach).

Distance from left bank (m)	Elevation (m)
0.00	355.00
12.00	340.60
18.00	340.50
34.00	337.70
58.00	336.80
134.00	337.50
166.00	337.90
222.00	337.90
266.00	337.30
314.00	335.20
436.00	338.10
464.00	339.70
476.00	355.00

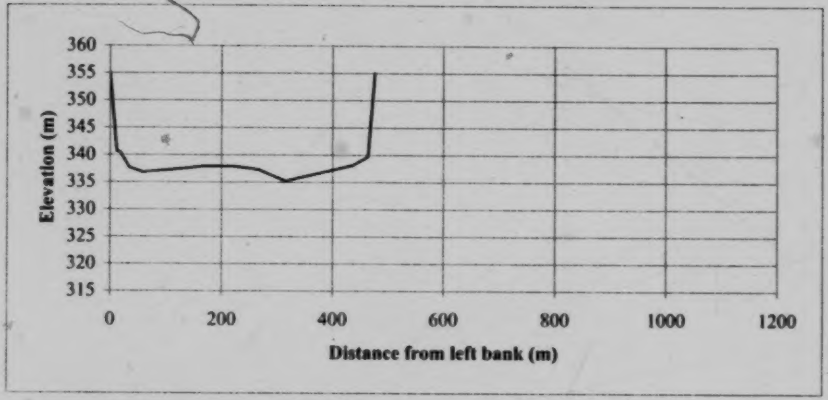

BC Hydro Cross Section No.:	10068
Distance from Bennett Dam:	298.10 km
Provided by:	Alberta Environment

Figure D.7 Cross section on the Peace River at 298.10 km downstream of the Bennett Dam (Dunvegan subreach).

Distance from left bank (m)	Elevation (m)
0.00	355.50
16.80	355.40
22.90	355.50
48.80	355.90
100.60	355.30
170.70	336.80
233.20	336.20
310.90	335.90
323.10	336.10
342.90	335.30
353.60	335.70
374.90	336.80
384.00	336.50
408.40	338.20
420.60	347.30

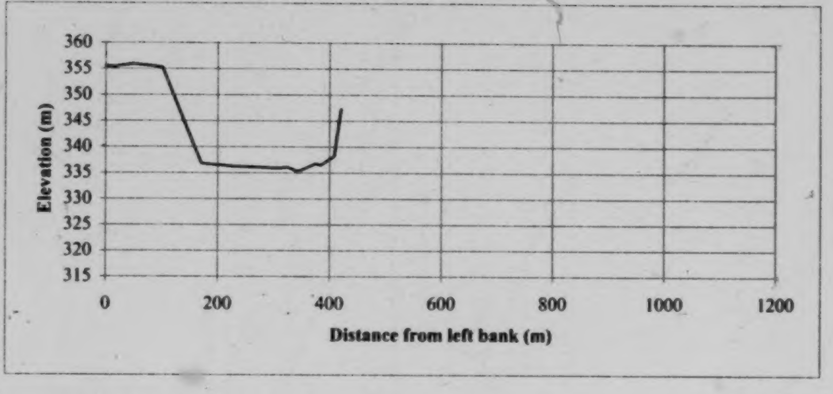

BC Hydro Cross Section No.:	1841
Distance from Bennett Dam:	298.90 km
Provided by:	Alberta Environment

Figure D.8 Cross section on the Peace River at 298.90 km downstream of the Bennett Dam (Dunvegan subreach).

Distance from left bank (m)	Elevation (m)
0.00	355.10
24.00	355.40
50.00	355.70
91.00	337.50
146.00	337.30
172.00	337.70
232.00	337.90
264.00	337.40
294.00	336.50
354.00	333.40
383.00	333.90
424.00	337.30
440.00	355.00

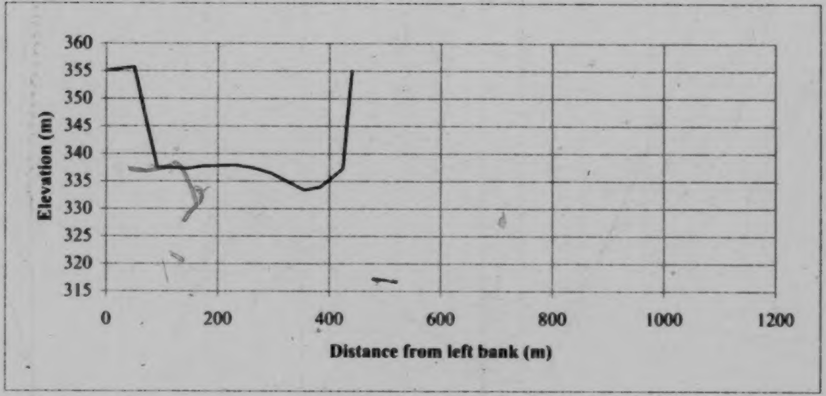

BC Hydro Cross Section No.:	10058
Distance from Bennett Dam:	299.10 km
Provided by:	Alberta Environment

Figure D.9 Cross section on the Peace River at 299.10 km downstream of the Bennett Dam (Dunvegan subreach).

Distance from left bank (m)	Elevation (m)
0.00	354.10
30.50	337.20
79.20	336.40
189.00	337.00
253.00	336.40
280.40	335.90
295.70	336.10
332.20	335.00
353.60	335.00
362.70	334.60
365.80	356.30

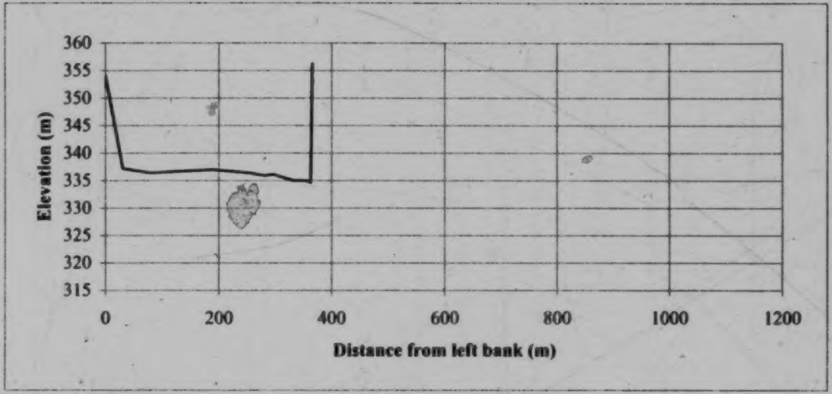

BC Hydro Cross Section No.: 1846

Distance from Bennett Dam: 299.70 km

Provided by: Alberta Environment

Figure D.10 Cross section on the Peace River at 299.70 km downstream of the Bennett Dam (Dunvegan subreach).

Distance from left bank (m)	Elevation (m)
0.00	328.46
1.21	327.73
9.44	327.00
25.93	324.97
35.02	322.28
37.09	321.27
52.26	321.29
58.29	323.05
70.00	323.69
83.93	323.89
95.72	323.97
108.37	324.07
122.94	323.62
133.34	323.00
142.57	322.26
153.50	320.77
164.86	319.35
169.83	318.44
174.34	318.45
183.34	317.20
188.34	317.28
193.34	317.00
199.34	316.80
203.34	316.84
213.34	316.82
215.34	316.80
223.34	316.25
233.34	316.11
243.34	315.73
253.34	315.40
263.34	315.12
273.34	314.90
283.34	314.70
293.34	314.63
303.34	314.55
313.34	314.48
323.34	314.41
333.34	314.30
343.34	314.26
353.34	314.12
363.34	314.02
373.34	314.20
383.34	314.22
393.34	314.32
403.34	314.35
413.34	314.32
423.34	314.12
428.84	314.00
433.34	314.57
436.34	314.23
443.34	314.20
453.34	314.40
462.34	314.25
463.34	314.41
473.34	315.55
478.34	315.38
483.34	315.70
493.34	316.31
498.34	316.60
503.34	317.20
505.34	317.70
506.34	318.02
509.34	318.25
511.46	318.45
516.35	319.34
523.12	321.06
523.62	321.89
532.08	326.08
533.14	328.85
534.23	329.53
535.59	329.93

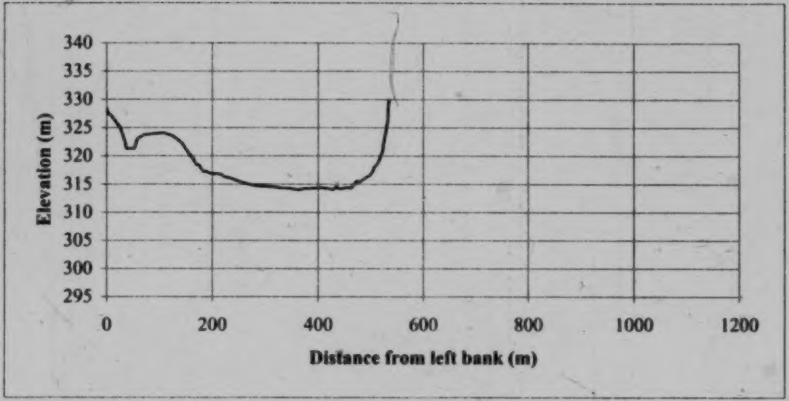

Cross Section Name:	Shaftesbury Ferry
Distance from Bennett Dam:	369.80 km
Year of Survey:	1992
Surveyed by:	Alberta Environment

Figure D.11 Cross section on the Peace River at 369.80 km downstream of the Bennett Dam (Town of Peace River subreach).

Distance from left bank (m)	Elevation (m)
0.00	325.07
222.83	324.17
238.51	324.16
250.95	323.69
260.38	323.28
265.00	323.49
268.88	323.65
272.32	322.74
276.51	320.15
286.36	319.88
290.30	320.26
298.08	320.42
308.13	320.00
310.78	318.99
311.33	318.26
312.98	317.90
315.14	317.31
320.00	317.24
322.00	317.12
335.00	317.00
345.00	316.70
350.00	316.48
355.00	316.38
365.00	316.30
375.00	316.42
385.00	316.45
395.00	316.40
405.00	316.48
415.00	316.40
435.00	316.38
445.00	316.25
455.00	316.12
465.00	315.92
475.00	315.80
485.00	315.70
495.00	315.62
505.00	315.48
525.00	315.48
531.50	315.83
535.00	315.92
545.00	316.10
555.00	316.20
565.00	316.33
575.00	316.42
585.00	316.48
595.00	316.60
605.00	316.72
615.00	316.68
625.00	316.62
635.00	316.62
645.00	316.52
665.00	316.50
695.00	316.48
705.00	316.57
710.00	316.52
715.00	316.40

Distance from left bank (m)	Elevation (m)
725.00	316.30
735.00	316.18
740.00	316.02
745.00	316.20
755.00	315.90
765.00	315.52
770.00	315.30
775.00	315.55
780.00	315.70
783.00	315.85
785.00	315.75
790.00	315.70
795.00	314.85
805.00	314.94
820.00	315.00
825.00	315.35
830.00	315.85
840.00	316.62
848.00	316.56
855.00	316.48
865.00	316.44
875.00	316.32
878.00	316.15
885.00	316.15
895.00	315.73
905.00	315.30
915.00	314.90
925.00	314.62
935.00	314.31
938.50	314.30
941.50	314.54
955.00	314.48
960.00	315.02
965.50	315.30
967.50	316.69
971.50	316.70
972.64	316.91
975.59	317.71
978.79	318.40
982.30	320.37
991.83	321.45
997.99	323.63
1000.00	325.07
1002.48	324.98

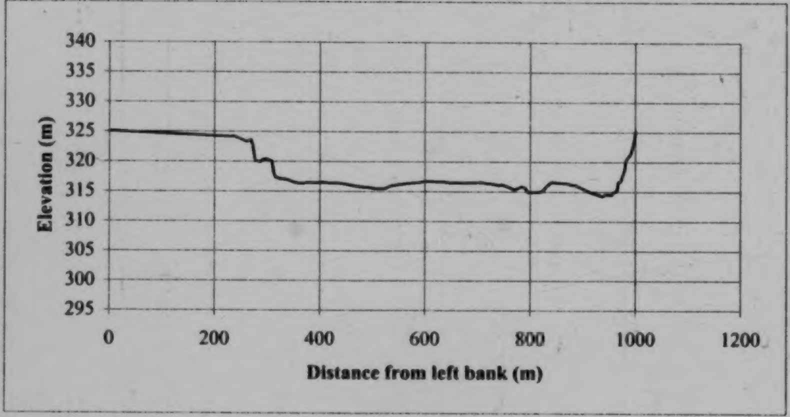

Cross Section Name:	Simpsons's Residence
Distance from Bennett Dam:	375.20 km
Year of Survey:	1992
Surveyed by:	Alberta Environment

Figure D.12 Cross section on the Peace River at 375.20 km downstream of the Bennett Dam (Town of Peace River subreach).

Distance from left bank (m)	Elevation (m)
0.00	331.55
15.67	331.23
18.17	331.23
22.07	328.68
24.28	327.51
30.50	322.44
32.95	322.26
38.70	319.85
40.98	318.60
41.89	317.74
48.75	316.91
51.43	316.06
58.67	315.42
65.67	314.90
75.67	314.52
85.67	314.12
91.67	313.84
100.67	313.88
105.67	313.70
115.67	312.48
125.67	311.48
128.17	311.28
135.67	311.50
145.67	311.90
152.17	312.45
155.67	312.70
165.67	313.20
170.67	313.20
175.67	313.40
179.17	313.20
182.17	313.40
185.67	313.62
195.67	314.40
205.67	314.78
215.67	314.90
227.67	314.56
235.67	314.56
245.67	314.70
255.67	314.70
265.67	314.68
275.67	314.58
285.67	314.40
295.67	314.20
305.67	314.04
315.67	313.74
325.67	313.58
335.67	313.30
345.67	312.92
355.67	312.55
360.67	312.48
365.67	312.50
370.67	312.80
379.67	312.40
390.67	312.50
395.67	312.90
405.67	313.11
415.67	313.30
425.67	313.50
435.67	313.70
445.67	313.80
450.67	314.13
455.67	315.10
460.17	315.68
465.35	316.31
468.64	317.05
473.40	318.13
475.08	319.25
478.81	321.09
485.53	322.44
486.20	323.39
487.72	323.96

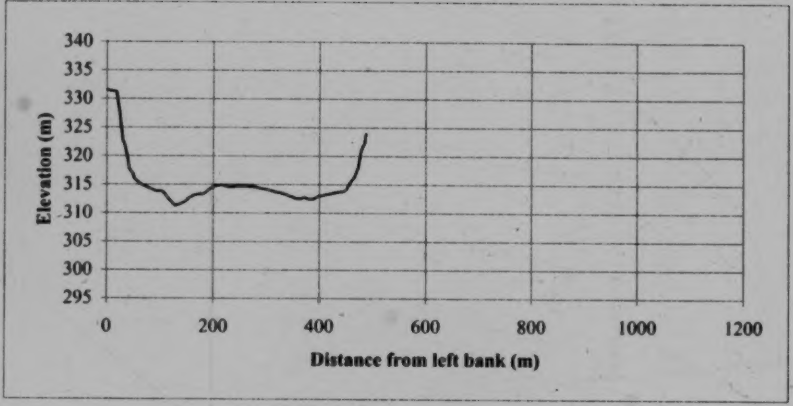

Cross Section Name:	Mackenzie's Cairn
Distance from Bennett Dam:	377.90 km
Year of Survey:	1992
Surveyed by:	Alberta Environment

Figure D.13 Cross section on the Peace River at 377.90 km downstream of the Bennett Dam (Town of Peace River subreach).

Distance from left bank (m)	Elevation (m)
0.00	325.77
5.74	324.24
10.99	324.15
22.37	324.26
24.87	324.05
29.10	321.60
29.97	320.45
31.94	319.61
33.38	317.83
35.79	317.64
38.26	316.55
40.87	315.66
45.37	315.30
52.37	314.56
62.37	313.50
72.37	312.90
82.37	312.88
92.37	312.88
102.37	312.88
112.37	312.88
122.37	312.90
132.37	313.06
142.37	312.90
152.37	313.00
162.37	312.92
172.37	313.00
182.37	313.18
192.37	313.30
202.37	313.42
212.37	313.52
222.37	313.62
232.37	313.80
242.37	313.90
252.37	314.08
262.37	314.22
272.37	314.50
282.37	314.70
292.37	314.88
302.37	315.06
312.37	315.12
322.37	315.26
332.37	315.25
342.37	315.38
352.37	315.44
362.37	315.46
372.37	315.40
376.87	314.52
378.37	314.42
382.37	313.92
392.37	313.32
402.37	313.00
412.37	312.90
422.37	312.90
432.37	312.70
442.37	313.06
452.37	313.06
462.37	313.50
474.37	314.46
482.37	314.70
483.37	315.06
486.43	315.48
486.87	315.80
490.78	316.55
495.14	317.78
505.78	321.06
506.22	322.05
510.26	322.72
511.91	323.57

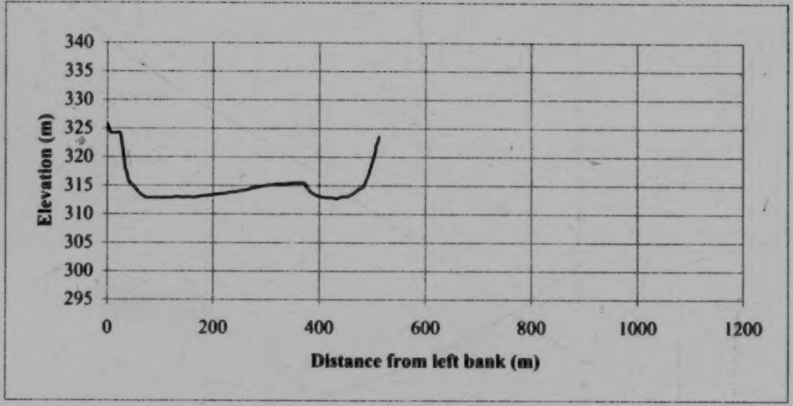

Cross Section Name: Correctional Institute (or Jail)

Distance from Bennett Dam: 380.85 km

Year of Survey: 1992

Surveyed by: Alberta Environment

Figure D.14 Cross section on the Peace River at 380.85 km downstream of the Bennett Dam (Town of Peace River subreach).

Distance from left bank (m)	Elevation (m)
0.00	324.20
8.61	323.97
14.70	323.30
16.87	322.67
22.08	322.48
27.27	319.20
35.84	318.36
37.70	317.80
39.17	316.77
48.80	315.96
54.08	315.50
56.08	314.70
56.47	314.92
67.08	313.72
72.08	313.52
82.08	313.20
92.08	312.62
102.08	312.20
112.08	311.72
122.08	311.40
132.08	311.02
142.08	310.88
152.08	310.52
162.08	310.58
172.08	310.50
182.08	310.45
192.08	310.48
202.08	310.52
212.08	310.60
222.08	310.72
232.08	310.84
242.08	310.89
252.08	311.10
262.08	311.22
272.08	311.42
282.08	311.78
292.08	312.10
302.08	312.52
312.08	312.70
322.08	312.98
332.08	313.20
342.08	313.52
352.08	313.56
362.08	313.85
372.08	314.08
382.08	314.32
392.08	314.38
402.08	314.12
406.08	314.96
411.08	315.04
413.93	315.27
430.81	315.83
432.51	317.77
443.08	318.71
458.47	320.14
464.56	321.40
469.80	321.37
471.27	321.63

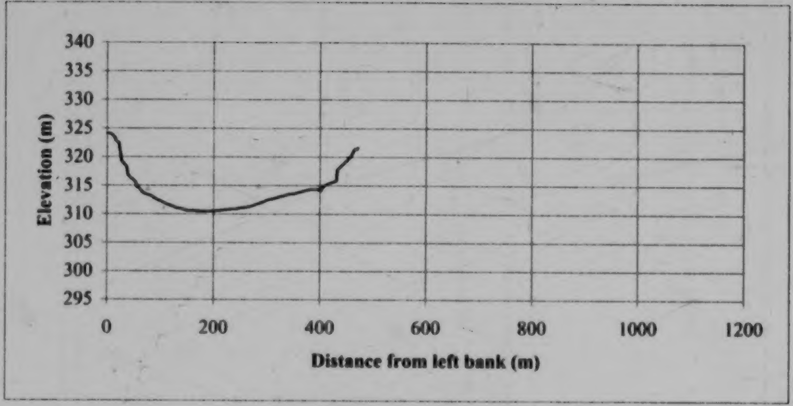

Cross Section Name: Purcell's

Distance from Bennett Dam: 382.35 km

Year of Survey: 1992

Surveyed by: Alberta Environment

Figure D.15 Cross section on the Peace River at 382.35 km downstream of the Bennett Dam (Town of Peace River subreach).

Distance from left bank (m)	Elevation (m)
0.00	326.46
2.26	324.55
3.91	324.60
6.24	325.02
12.34	319.61
17.34	316.41
20.43	315.62
24.47	314.61
27.25	314.54
31.24	313.84
36.24	313.14
41.24	312.72
46.24	313.14
50.74	313.27
56.24	312.79
66.24	312.94
76.24	313.14
86.24	313.22
96.24	313.42
106.24	313.52
116.24	313.64
126.24	313.74
136.24	313.92
146.24	314.00
156.24	314.04
166.24	314.12
176.24	314.04
186.24	313.94
196.24	313.92
206.24	313.74
216.24	313.62
226.24	313.42
236.24	312.83
246.24	312.82
256.24	312.54
266.24	312.34
276.24	312.10
281.24	311.98
296.24	311.64
306.24	311.57
316.25	311.42
326.25	311.44
336.25	311.52
341.25	311.34
366.25	311.22
376.25	311.24
386.25	311.32
396.25	311.46
406.25	311.60
416.25	311.74
426.25	311.94
436.25	312.04
446.25	312.12
456.25	312.18
461.25	312.28
476.25	312.62
486.25	312.87
496.25	313.14
506.25	313.44
516.24	313.74
518.74	314.22
521.24	314.26
523.44	314.37
528.06	315.61
539.46	319.55
539.59	320.84
541.06	321.69
543.43	322.34

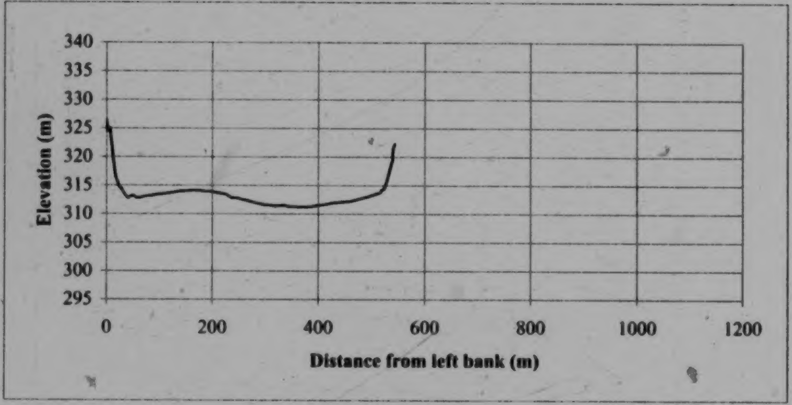

Cross Section Name: Old Highway

Distance from Bennett Dam: 384.85 km

Year of Survey: 1992

Surveyed by: Alberta Environment

Figure D.16 Cross section on the Peace River at 384.85 km downstream of the Bennett Dam (Town of Peace River subreach).

Distance from left bank (m)	Elevation (m)
0.00	326.37
4.75	325.30
9.15	325.25
11.44	325.62
13.19	325.62
13.35	324.65
22.16	318.50
25.31	316.34
29.01	315.45
32.33	314.66
36.44	314.47
41.44	313.98
51.44	313.70
55.44	313.80
61.44	313.30
68.44	313.78
71.44	313.72
81.44	313.90
91.44	314.00
101.44	313.86
111.44	313.42
119.44	313.00
121.44	312.62
130.44	310.80
141.44	310.66
151.44	310.98
159.44	310.82
167.94	310.80
171.44	310.62
181.44	310.02
191.44	309.72
194.44	309.66
201.44	309.78
211.44	310.33
221.44	311.22
231.44	311.84
241.44	312.18
251.44	312.75
261.44	312.97
271.44	313.00
291.44	313.40
301.44	313.46
311.44	313.70
321.44	313.78
331.44	313.70
341.44	313.90
351.44	313.90
361.44	313.78
371.44	313.80
381.44	313.95
391.44	313.80
401.44	314.00
411.44	313.98
421.44	314.00
441.44	313.90
451.44	313.58
454.44	313.52
461.94	314.02
471.44	313.22
480.94	313.02
483.44	313.40
487.44	313.60
491.44	313.25
501.44	313.12
511.94	312.70
521.44	313.45
529.44	313.74
531.44	313.48
536.44	312.80
541.44	312.70
551.44	312.45
561.44	312.48
566.44	312.62
571.44	312.45
573.44	312.90
581.44	313.07
584.94	313.42
586.44	313.90
587.94	313.60
591.44	314.28
594.44	314.52
596.71	314.79
601.76	315.44
607.81	316.05
614.79	317.70
619.48	318.91
621.69	320.62
624.09	320.92

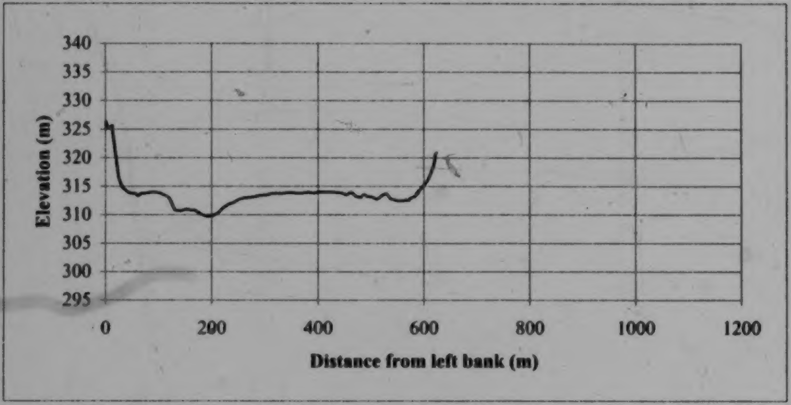

Cross Section Name: Macloed Cairn

Distance from Bennett Dam: 386.05 km

Year of Survey: 1992

Surveyed by: Alberta Environment

Figure D.17 Cross section on the Peace River at 386.05 km downstream of the Bennett Dam (Town of Peace River subreach).

Distance from left bank (m)	Elevation (m)
0.00	337.68
57.57	321.84
60.51	321.21
65.70	319.22
72.82	319.24
78.07	319.86
79.07	319.86
83.92	316.84
88.54	315.34
90.95	314.14
93.19	313.35
98.08	312.78
103.08	311.90
108.08	311.48
120.08	311.38
123.08	310.97
128.08	310.90
130.58	310.82
134.58	311.08
138.08	310.63
145.58	310.33
148.08	310.68
153.08	310.31
168.08	310.43
178.08	310.43
188.08	310.57
198.08	310.76
208.08	310.88
218.08	311.00
228.08	311.16
238.08	311.20
248.08	311.24
258.08	311.42
268.08	311.43
278.08	311.53
288.08	311.50
298.08	311.58
318.08	311.66
328.08	311.70
358.08	311.70
368.08	311.79
378.08	311.83
388.08	311.88
398.08	311.98
408.08	312.09
418.08	311.88
428.08	311.68
438.08	312.16
448.08	312.18
458.08	312.13
468.08	312.07
478.08	311.80
488.08	311.68
498.08	311.90
508.08	312.43
518.08	312.70

Distance from left bank (m)	Elevation (m)
528.08	312.76
538.08	312.70
548.08	312.80
558.08	312.70
568.08	312.70
578.08	312.66
588.08	312.50
598.08	312.46
608.08	312.30
618.08	312.30
628.08	312.56
638.08	312.78
648.08	312.83
651.08	313.12
656.08	313.20
660.08	313.60
663.09	313.16
664.72	313.80
672.90	314.06
684.45	314.20
715.41	314.11
730.91	314.03
763.04	313.18
776.83	313.14
789.72	313.39
806.60	313.70
819.91	314.06
846.83	314.31
856.11	314.07
866.12	313.74
877.69	313.88
880.89	314.02
887.84	314.29
916.93	314.17
929.08	313.77
937.45	313.13
947.28	312.96
955.51	312.94
958.45	313.79
961.51	314.60
966.37	317.89
970.85	321.69
972.24	323.52
976.43	325.87

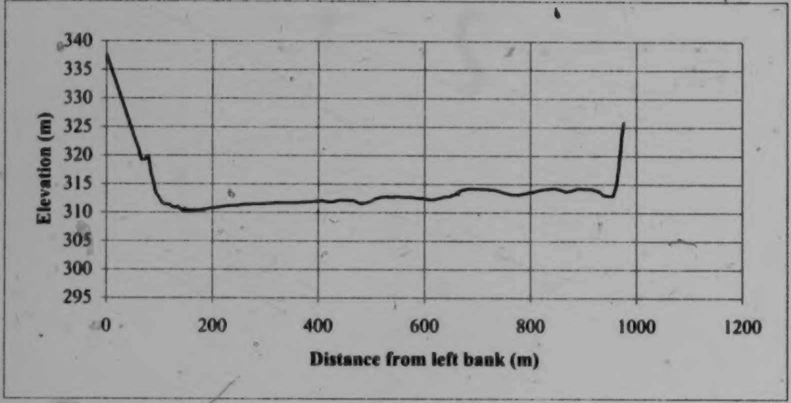

Cross Section Name:	Sawchuck's (near Pumphouse)
Distance from Bennett Dam:	390.00 km
Year of Survey:	1992
Surveyed by:	Alberta Environment

Figure D.18 Cross section on the Peace River at 390.00 km downstream of the Bennett Dam (Town of Peace River subreach).

Distance from left bank (m)	Elevation (m)
0.00	333.66
12.21	322.73
13.78	318.39
15.33	317.26
16.66	315.78
29.85	313.83
37.09	313.21
41.35	312.92
51.20	312.18
55.70	312.18
60.22	312.71
62.61	313.22
67.81	315.12
74.77	315.69
96.25	316.01
147.79	316.48
190.78	317.37
215.07	318.12
225.01	317.80
244.33	317.02
274.15	316.20
284.85	315.69
290.46	313.30
298.90	312.43
303.96	311.98
318.01	310.90
321.51	310.38
325.01	310.30
335.01	310.30
345.01	310.02
350.01	309.90
355.01	310.00
365.01	310.40
370.01	310.50
375.01	310.74
385.01	311.20
395.01	311.50
398.63	311.43
407.97	311.70
420.78	312.08
437.37	312.18
450.45	312.00
457.01	312.00
465.01	311.55
475.01	310.90
485.01	310.60
495.01	310.55
505.01	310.40
515.01	310.38
525.01	310.38
535.01	310.42
545.01	310.76
555.01	311.40
559.50	311.57
560.01	311.72
565.89	312.40

Distance from left bank (m)	Elevation (m)
582.62	312.86
601.28	313.82
616.77	314.12
640.64	313.63
669.36	313.72
696.57	313.74
719.63	313.64
726.09	313.10
739.29	312.99
769.15	313.19
793.00	313.10
827.72	312.89
848.43	312.72
860.81	312.30
862.40	312.27
875.01	311.68
885.01	311.28
895.01	310.80
905.01	310.78
915.01	310.80
925.01	310.70
935.01	310.68
945.01	310.60
955.01	310.58
965.01	310.15
975.01	309.90
985.01	309.70
995.01	309.58
1005.01	309.26
1015.01	309.42
1025.01	309.58
1027.01	309.60
1045.01	310.35
1055.00	310.28
1065.00	310.53
1075.00	311.42
1075.50	311.78
1080.84	312.00
1081.21	313.05
1082.77	314.99
1084.83	315.06
1088.30	318.87
1090.59	323.18
1091.68	323.62

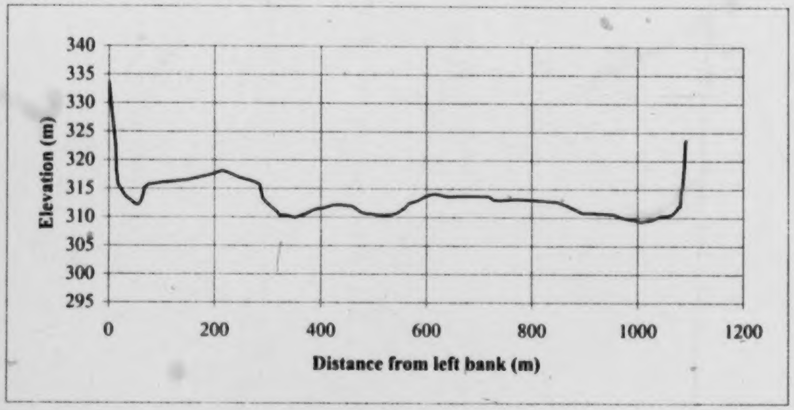

Cross Section Name:	Sisson's
Distance from Bennett Dam:	391.80 km
Year of Survey:	1992
Surveyed by:	Alberta Environment

Figure D.19 Cross section on the Peace River at 391.80 km downstream of the Bennett Dam (Town of Peace River subreach).

Distance from left bank (m)	Elevation (m)
0	320.98
2.99	321.09
5.44	320.47
17.59	314.61
26.71	313.88
43.53	312.04
51.22	311.52
60.14	311.56
63.28	312.09
68.87	312.44
71.65	312.09
75.32	311.47
83.19	311.6
84.52	311.43
84.99	311.22
92.99	311.31
102.99	311.22
112.99	311.42
122.99	311.32
132.99	311.28
142.99	311.12
152.99	310.98
162.99	310.83
172.99	310.7
182.99	310.5
192.99	310.2
202.99	309.84
212.99	309.7
222.99	309.62
242.99	309.46
252.99	309.33
262.99	309.22
272.99	309.12
287.99	309
302.99	308.7
322.99	308.88
332.99	308.7
342.99	308.62
352.99	308.4
362.99	308.25
372.99	308.32
382.99	308.42
392.99	308.38
402.99	308.4
412.99	308.4
422.99	308.58
432.99	308.52
442.99	308.5
452.99	308.5
462.99	308.5
472.99	308.7
476.99	308.5
482.99	308.7
492.99	308.7
497.99	308.5
502.99	308.8
512.99	309.32
517.99	309.7
522.99	309.98
543.39	310.35
544.26	310.5
549.59	312.16
549.9	312.45
554.01	313.34
557.48	323.31
567.1	323.54
568.03	323.78
568.74	323.88

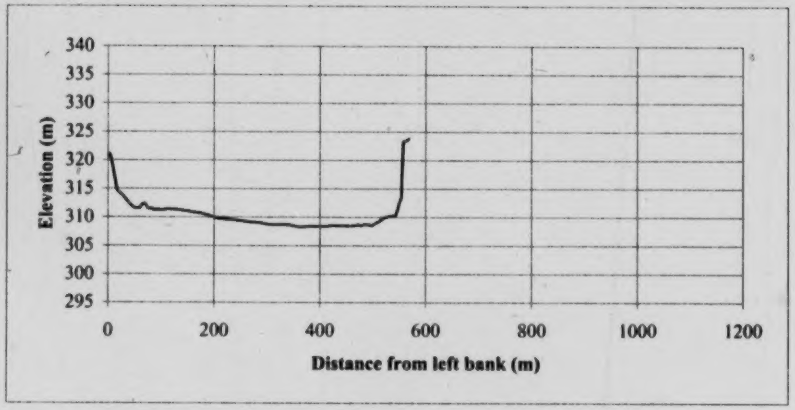

Cross Section Name:	West Peace
Distance from Bennett Dam:	393.50 km
Year of Survey:	1992
Surveyed by:	Alberta Environment

Figure D.20 Cross section on the Peace River at 393.50 km downstream of the Bennett Dam (Town of Peace River subreach).

Distance from left bank (m)	Elevation (m)
0	320.3
2.91	320.37
16.68	315.16
22.14	314.88
23.47	313.6
49.13	313.29
62.14	311.98
76.54	311.47
78.5	311.54
82.91	311.4
84.41	311.17
92.91	311.01
102.91	310.82
112.91	310.6
122.91	310.44
132.91	310.02
142.91	309.7
152.91	309.4
162.91	309.22
172.91	308.8
182.91	308.5
192.91	308.12
202.91	307.65
212.91	307.12
222.91	306.88
232.91	306.45
252.91	306.1
262.91	306.2
282.91	306.42
292.91	306.32
302.91	306.42
312.91	306.62
322.91	306.75
332.91	307.15
342.91	307.12
352.91	307.52
359.41	307.55
362.91	307.92
382.91	308.98
402.91	309.65
412.91	310
417.91	310.42
422.91	310.48
427.91	310.84
432.91	310.92
436.41	311.2
441.04	311.09
448.88	312
450.89	312.34
459.82	312.38
477.95	312.85
482.75	313.5
489.49	316.4
497.64	320.39
497.77	320.41
502.3	320.32

Distance from left bank (m)	Elevation (m)
504.5	319.44

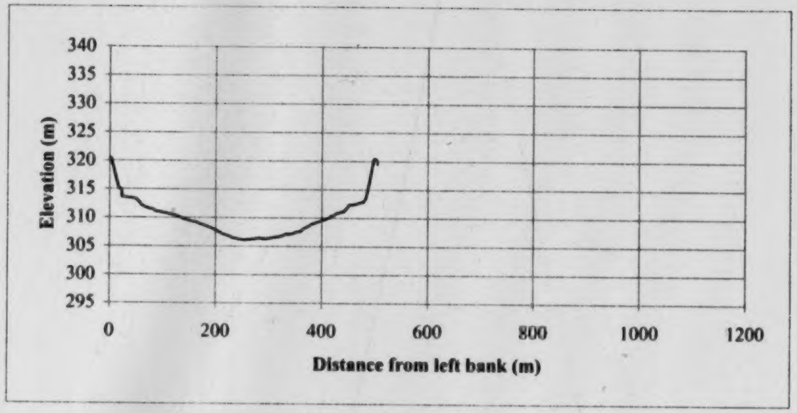

Cross Section Name: Boat Launch

Distance from Bennett Dam: 394.40 km

Year of Survey: 1992

Surveyed by: Alberta Environment

Figure D.21 Cross section on the Peace River at 394.40 km downstream of the Bennett Dam (Town of Peace River subreach).

Distance from left bank (m)	Elevation (m)
0.00	318.16
9.85	317.72
13.15	317.53
18.87	314.25
29.57	313.69
31.64	314.06
36.84	313.94
37.66	313.07
50.16	312.98
67.39	312.37
77.32	312.09
93.64	311.40
106.02	310.90
115.52	310.61
121.02	310.22
126.02	310.02
136.02	309.60
146.02	309.27
156.02	308.75
166.02	308.40
171.02	308.30
176.02	308.00
186.02	307.40
206.02	306.45
216.02	306.20
226.02	306.02
236.02	305.90
246.02	305.82
256.02	305.80
257.02	305.96
276.02	305.90
286.02	306.20
306.02	306.90
316.02	307.28
326.02	307.38
336.02	307.50
346.02	307.92
353.52	308.50
361.02	308.64
371.02	308.90
376.02	309.18
386.02	309.22
396.02	309.70
406.02	310.45
421.02	311.02
426.02	311.11
430.02	311.55
432.12	311.37
442.06	312.03
463.90	312.85
468.72	312.81
479.20	312.80
481.17	313.61
487.53	314.38
521.06	316.16
527.89	318.73
532.48	319.19
534.92	319.52
536.01	320.44
539.36	320.47
543.01	319.33
548.32	318.32

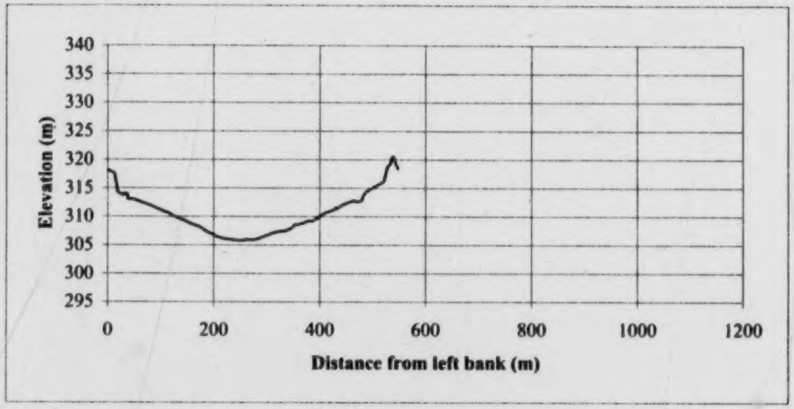

Cross Section Name:	Pat's Creek
Distance from Bennett Dam:	394.72 km
Year of Survey:	1992
Surveyed by:	Alberta Environment

Figure D.22 Cross section on the Peace River at 394.72 km downstream of the Bennett Dam (Town of Peace River subreach).

Distance from left bank (m)	Elevation (m)
0.00	326.32
3.12	324.04
7.09	321.58
14.75	312.82
17.92	312.44
19.37	311.72
23.89	310.87
25.48	310.90
34.47	309.85
44.47	308.80
54.47	308.02
59.47	307.87
64.47	308.02
74.47	307.32
84.47	306.72
89.47	306.42
90.47	306.07
94.47	306.00
104.47	305.25
114.47	305.30
124.47	305.22
134.47	305.30
144.47	305.32
154.47	305.54
164.47	305.80
184.47	305.98
194.47	306.00
204.47	306.02
214.47	305.98
224.47	305.90
234.47	306.02
244.47	306.40
254.47	306.50
257.47	306.75
264.47	306.80
267.47	306.92
274.47	307.10
294.47	307.50
304.47	307.80
314.48	308.10
319.48	308.48
327.48	308.50
334.48	308.80
335.98	308.52
344.48	309.06
354.48	309.52
364.48	310.02
374.48	310.52
384.48	310.84
392.48	311.22
397.32	311.35
400.08	311.74
409.20	312.97
410.99	314.43
415.55	316.47
424.48	319.96

Distance from left bank (m)	Elevation (m)
427.48	320.10
431.43	319.01

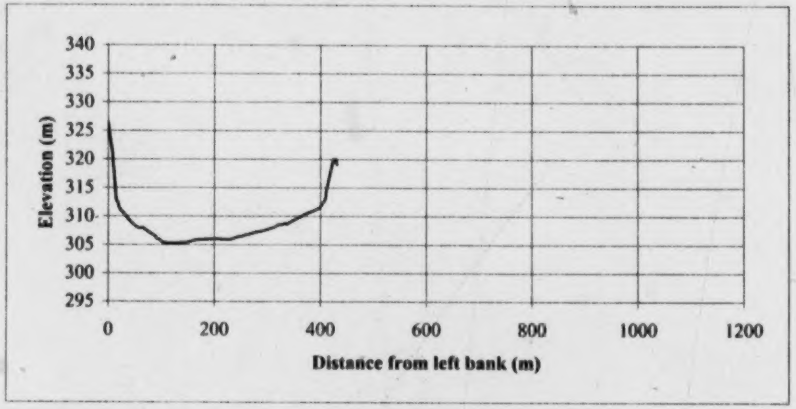

Cross Section Name:	W.H. Wood's
Distance from Bennett Dam:	395.10 km
Year of Survey:	1992
Surveyed by:	Alberta Environment

Figure D.23 Cross section on the Peace River at 395.10 km downstream of the Bennett Dam (Town of Peace River subreach).

Distance from left bank (m)	Elevation (m)
0.00	322.38
0.31	312.66
4.76	311.63
7.04	310.60
13.07	309.62
19.07	309.42
30.07	308.72
36.57	308.72
38.07	308.20
48.07	308.28
50.57	307.70
52.07	308.20
60.07	307.92
65.07	308.17
67.57	308.00
71.07	307.90
75.07	307.02
80.07	306.50
86.07	306.22
92.07	304.80
100.07	304.38
105.07	304.02
110.07	304.22
117.07	304.28
122.57	305.30
126.07	304.88
130.07	304.92
134.07	304.42
150.07	304.48
153.57	304.82
160.07	304.80
170.07	304.90
175.07	305.20
179.07	305.85
181.07	305.86
183.07	306.30
185.07	307.12
187.07	306.65
190.07	306.20
200.07	305.60
210.07	305.62
220.07	305.70
225.07	305.52
230.07	305.72
234.07	305.78
238.07	305.12
247.07	307.20
250.07	307.12
251.07	305.62
257.07	305.60
260.07	306.78
280.07	307.14
292.07	307.52
298.07	308.60
300.07	308.98
304.07	309.00
310.07	309.02
312.07	308.40
315.07	308.32
319.47	308.58
319.57	309.38
330.07	309.58
340.07	309.70
342.07	309.70
347.07	310.42
350.07	310.40
360.07	310.62
362.07	311.10
368.07	311.38
372.64	310.69
374.24	311.62
391.43	311.12
400.59	311.42
408.48	311.75
416.66	313.06
424.47	313.98
435.33	315.54
441.33	316.95
446.13	320.10
450.07	320.24
454.61	320.06
461.65	319.67

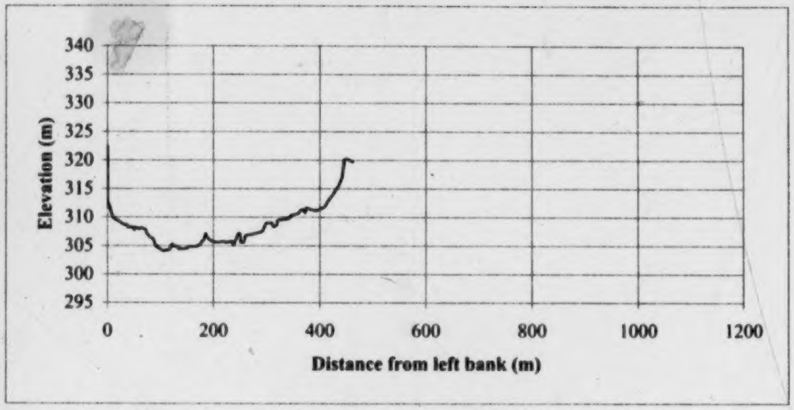

Cross Section Name: Rail Bridge (downstream side)

Distance from Bennett Dam: 395.58 km

Year of Survey: 1992

Surveyed by: Alberta Environment

Figure D.24 Cross section on the Peace River at 395.58 km downstream of the Bennett Dam (Town of Peace River subreach).

Distance from left bank (m)	Elevation (m)
0.00	321.19
3.62	314.12
8.41	311.71
10.24	310.94
14.11	310.40
18.11	310.00
28.09	309.34
35.59	310.20
53.09	308.45
58.09	308.28
61.59	308.30
66.09	307.80
68.09	307.30
76.59	306.12
78.09	307.02
88.09	307.80
98.09	304.90
105.09	303.56
108.09	303.45
118.09	303.62
123.09	303.75
128.10	304.12
138.10	304.52
148.10	305.08
158.10	305.42
163.10	305.52
173.10	305.38
178.10	305.50
185.10	305.75
188.10	306.10
190.60	305.90
193.10	305.50
195.60	304.70
198.10	304.95
208.10	305.25
218.10	305.95
223.10	306.05
228.10	306.52
233.10	306.72
238.10	307.44
244.10	307.56
248.10	308.12
258.10	308.30
268.10	308.02
278.10	308.42
288.10	308.95
298.10	309.26
303.10	309.12
308.10	309.30
316.61	309.56
318.11	310.12
319.11	310.18
320.11	309.88
323.11	309.92
328.11	309.80
335.61	309.72
338.11	309.90
339.11	310.22
341.11	309.92
346.11	310.90
353.11	310.60
358.11	310.70
364.11	310.80
368.11	311.18
375.61	311.35
376.34	311.13
386.50	311.75
394.00	312.16
410.28	312.07
436.05	311.94
443.76	313.00
448.51	314.64
458.73	317.99
466.91	321.01
468.11	321.01
469.67	321.05
471.71	320.22
474.06	320.09

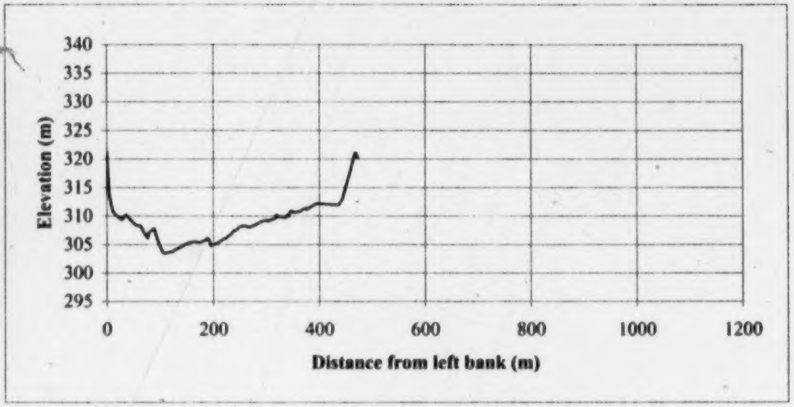

Cross Section Name:	Highway #2 bridge (downstream side)
Distance from Bennett Dam:	395.65 km
Year of Survey:	1992
Surveyed by:	Alberta Environment

Figure D.25 Cross section on the Peace River at 395.65 km downstream of the Bennett Dam (Town of Peace River subreach).

Distance from left bank (m)	Elevation (m)
0.00	327.86
6.60	327.95
8.30	327.62
11.77	324.99
17.74	319.41
22.89	315.50
26.89	312.80
33.46	311.58
35.38	310.95
36.58	310.87
43.32	310.64
56.18	309.80
72.18	308.50
77.18	308.82
87.18	308.14
95.68	307.92
100.46	307.34
103.88	307.82
107.18	307.52
117.18	307.62
127.18	307.62
129.18	307.50
132.18	305.80
137.18	305.46
147.18	305.42
157.18	305.32
167.18	305.14
177.18	305.11
187.18	305.02
197.18	305.09
207.18	305.32
217.18	305.64
227.18	305.65
232.18	305.82
237.18	306.22
242.18	306.52
247.18	306.60
252.18	306.59
257.18	306.72
267.18	306.82
277.18	306.98
287.18	307.12
295.18	307.22
303.18	307.52
307.18	307.84
317.18	307.86
327.18	308.17
337.18	308.33
347.18	308.50
357.18	308.71
367.18	309.00
377.18	309.32
387.18	309.64
397.18	310.17
417.18	310.34
427.18	310.54

Distance from left bank (m)	Elevation (m)
429.18	310.60
429.68	311.32
430.68	311.34
431.18	310.62
437.18	310.64
449.18	311.03
451.79	310.93
454.86	311.03
466.99	311.64
490.86	311.81
509.99	313.05
519.54	314.46
533.18	315.59
542.31	319.66
545.34	320.07
547.18	320.57
548.68	320.57
550.59	319.65
553.09	319.39
567.41	319.49
568.37	319.55

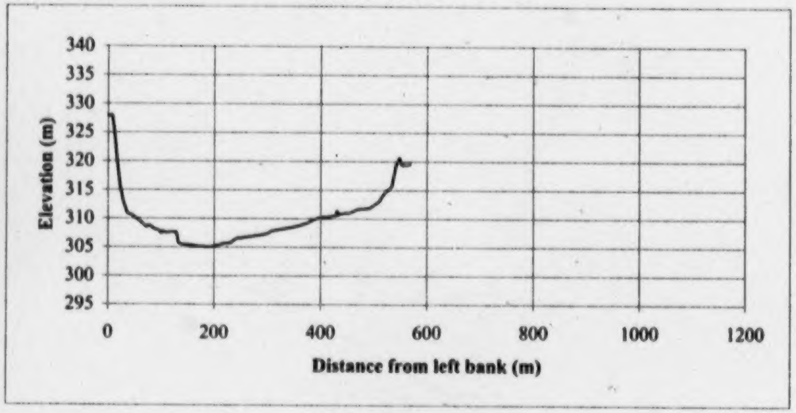

Cross Section Name:	WSC gauging section
Distance from Bennett Dam:	395.95 km
Year of Survey:	1992
Surveyed by:	Alberta Environment

Figure D.26 Cross section on the Peace River at 395.95 km downstream of the Bennett Dam (Town of Peace River subreach).

Distance from left bank (m)	Elevation (m)
0.00	321.29
5.50	317.09
12.09	312.84
16.92	311.53
19.66	310.72
24.77	310.36
26.77	310.58
28.77	309.79
31.77	308.63
38.76	308.71
41.27	308.65
48.77	309.53
53.77	309.99
58.77	310.19
61.77	310.58
66.77	310.45
75.77	310.33
78.77	310.05
88.77	309.74
98.77	309.51
108.77	309.38
118.77	309.33
128.77	309.35
138.77	309.35
148.77	309.55
158.77	309.57
168.77	309.36
173.77	309.13
178.77	309.11
188.77	309.23
198.77	309.08
208.77	309.05
218.77	308.91
228.77	308.73
238.77	308.74
248.77	308.83
258.77	308.83
268.77	308.73
278.77	308.73
288.77	308.65
298.77	308.65
318.77	308.65
328.77	308.75
338.77	309.01
348.77	309.13
358.77	309.35
378.77	309.53
388.77	309.53
398.77	309.53
408.77	309.65
418.77	309.65
428.77	309.67
438.77	309.69
448.77	309.63
468.77	309.58
478.77	309.73

Distance from left bank (m)	Elevation (m)
488.77	309.82
508.77	309.93
518.77	310.07
528.77	310.33
548.77	310.41
568.77	310.41
578.77	310.43
588.77	310.53
598.77	310.65
608.77	310.75
628.77	310.83
638.77	310.93
648.77	310.83
658.77	310.41
668.77	310.31
673.77	310.33
678.77	310.63
688.77	310.75
698.77	311.23
701.77	311.38
702.30	311.09
713.19	310.69
727.23	310.66
728.48	310.83
730.46	311.51
735.22	312.74
746.77	319.94
748.77	319.94
752.29	319.89
756.99	318.67
757.32	318.35
783.26	318.41
783.44	318.41

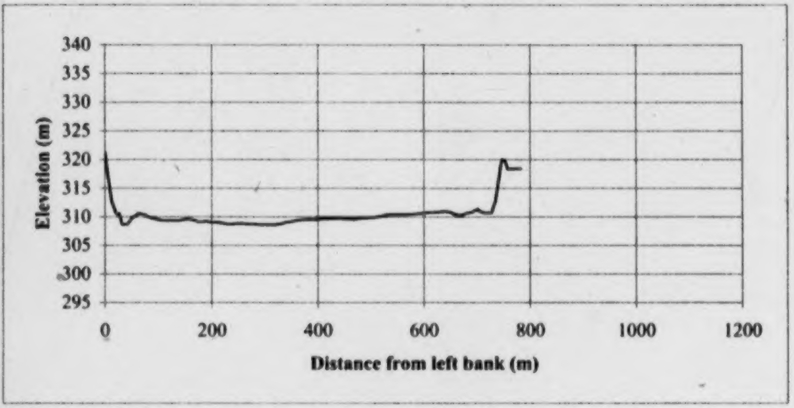

Cross Section Name:	WSC gauge
Distance from Bennett Dam:	396.35 km
Year of Survey:	1992
Surveyed by:	Alberta Environment

Figure D.27 Cross section on the Peace River at 396.35 km downstream of the Bennett Dam (Town of Peace River subreach).

Distance from left bank (m)	Elevation (m)
0.00	323.42
2.83	322.66
7.02	320.09
18.12	313.82
23.03	312.86
25.38	311.32
26.52	310.85
28.86	310.11
30.00	310.12
35.00	309.76
40.00	308.92
45.00	308.28
50.00	307.74
55.00	307.42
56.50	307.18
60.00	307.04
70.00	307.37
80.00	307.70
90.00	307.97
100.00	308.72
110.00	309.48
115.00	309.88
120.00	309.94
130.00	309.98
137.00	310.32
140.00	310.34
148.00	310.20
150.00	310.20
161.00	310.07
170.00	309.70
180.00	309.70
190.00	309.50
200.00	309.42
210.00	309.34
220.00	309.29
230.00	309.12
240.00	309.10
250.00	309.16
260.00	309.35
264.00	309.46
270.00	309.66
280.00	309.84
285.04	309.76
288.00	310.07
296.79	310.18
315.94	310.44
334.21	310.50
351.72	310.58
372.04	310.80
388.51	310.84
409.73	311.28
428.67	311.74
433.46	312.56
443.62	313.19
454.24	313.58
472.80	314.27
484.67	315.45
499.74	315.63
510.90	317.00
513.82	319.62
664.00	319.62
668.00	316.95
678.27	314.04
688.08	313.75
700.30	312.65
706.13	312.81
718.78	311.80
743.83	311.44
760.61	311.12
769.61	310.93
780.18	310.67
792.33	310.45
797.47	310.45
799.47	310.35
809.47	310.15
819.47	309.93
829.47	309.92
839.47	309.73
849.47	309.57
859.47	309.31
869.47	309.12
879.47	308.98
889.47	308.93
899.47	308.81
909.47	308.63
919.47	308.73
929.47	308.72
936.47	309.03
939.47	308.73
949.47	308.63
959.47	308.86
969.47	308.06
972.97	308.07
979.47	308.48
989.47	309.05
993.47	309.41
996.63	310.39
998.53	310.60
1001.28	311.19
1003.43	311.82
1013.08	312.71
1022.31	314.79
1031.19	314.84
1036.40	314.91
1049.42	317.08
1055.47	319.00
1057.70	319.48
1059.47	319.55
1060.97	319.62
1066.87	318.73
1069.84	318.52
1089.90	318.50

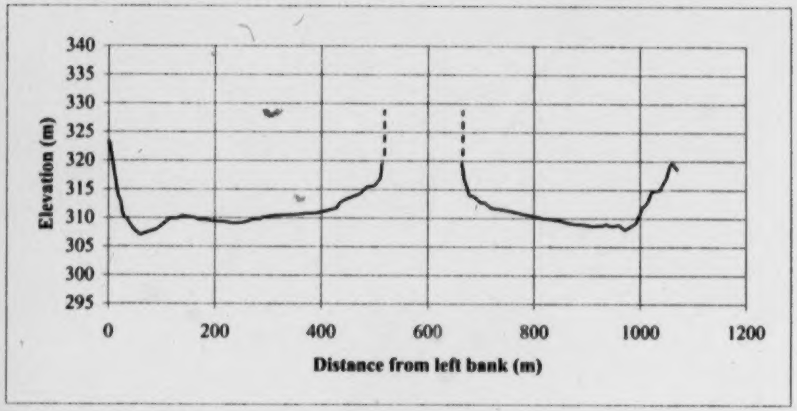

Cross Section Name:	Bewley Island
Distance from Bennett Dam:	396.95 km
Year of Survey:	1992
Surveyed by:	Alberta Environment

Figure D.28 Cross section on the Peace River at 396.95 km downstream of the Bennett Dam (Town of Peace River subreach).

Distance from left bank (m)	Elevation (m)
0.00	323.42
0.78	314.20
2.63	313.58
4.56	312.85
7.59	311.81
16.63	311.44
26.63	310.66
36.63	310.41
41.63	310.12
45.13	309.54
51.63	309.42
56.70	308.54
66.63	308.09
69.13	308.16
76.63	307.34
79.63	307.18
86.63	307.44
96.63	307.82
106.63	308.32
116.63	308.66
126.63	308.96
136.63	309.35
146.63	309.71
156.13	310.14
166.63	310.14
176.63	310.20
186.63	310.58
196.63	311.02
206.63	311.52
216.63	312.08
222.84	312.13
223.63	312.34
225.69	312.30
233.78	312.88
244.83	313.57
255.22	313.92
275.65	315.16
295.20	316.23
301.50	317.78
306.63	318.14
312.88	319.71
762.00	319.71
763.58	317.70
764.73	316.51
771.73	315.77
776.14	313.76
787.48	312.56
802.82	311.77
816.74	310.96
825.83	310.21
835.96	309.89
836.96	309.81
844.96	309.71
854.96	309.61
864.96	309.64
874.96	309.63

Distance from left bank (m)	Elevation (m)
884.96	309.62
894.96	309.52
904.96	309.54
914.96	309.41
924.96	309.41
934.96	309.30
944.96	309.31
954.96	309.26
964.96	309.20
967.96	309.09
974.96	309.16
989.96	309.16
994.96	309.23
1004.96	309.24
1014.96	309.29
1024.96	309.33
1034.96	309.43
1044.96	309.49
1054.96	309.51
1064.96	309.49
1074.96	309.39
1084.96	309.44
1089.96	309.47
1094.96	309.64
1099.46	310.15
1102.13	310.19
1103.56	310.33
1106.93	310.95
1121.47	312.24
1134.14	313.39
1143.90	314.32
1147.64	316.07
1152.77	319.47
1154.98	319.69
1161.10	319.71
1166.77	318.96
1173.24	318.68
1174.04	318.68

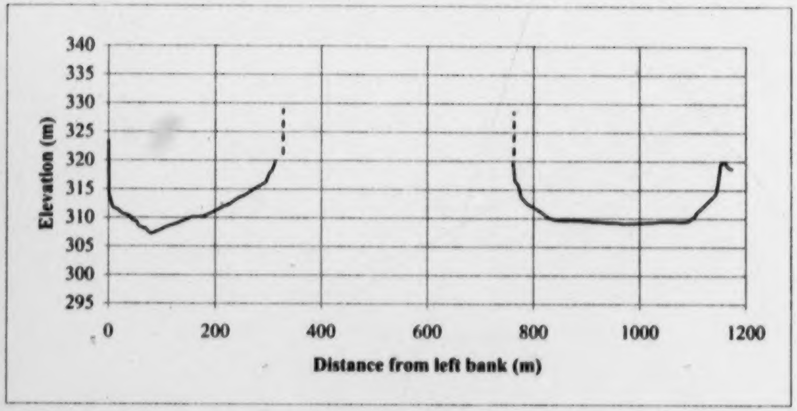

Cross Section Name: Centre of Bewley Island

Distance from Bennett Dam: 397.65 km

Year of Survey: 1992

Surveyed by: Alberta Environment

Figure D.29 Cross section on the Peace River at 397.65 km downstream of the Bennett Dam (Town of Peace River subreach).

Distance from left bank (m)	Elevation (m)
0.00	323.42
2.26	313.86
7.81	313.56
7.87	313.60
16.12	311.41
18.65	309.63
23.68	309.20
25.76	308.75
28.16	308.30
30.10	308.05
31.65	308.49
33.65	307.94
38.65	307.91
41.65	307.12
46.65	306.79
51.65	306.92
61.65	306.77
71.65	306.39
77.65	306.04
81.65	305.00
83.65	304.47
91.65	304.59
101.65	304.79
111.65	304.92
121.65	305.01
131.65	305.12
141.65	305.24
151.65	305.34
161.65	305.47
171.65	305.74
181.65	305.86
191.65	306.09
201.65	306.29
211.65	306.48
221.65	306.64
231.65	306.79
241.65	306.86
251.65	306.96
261.65	306.99
271.65	307.01
281.65	307.14
291.65	307.28
301.65	307.50
311.65	307.77
316.65	307.92
321.65	308.26
323.42	308.25
327.49	308.79
333.93	309.62
338.31	311.74
347.51	315.70
348.97	316.78
351.65	318.84
356.02	319.95
705.00	319.95
710.26	316.86

Distance from left bank (m)	Elevation (m)
711.35	316.58
716.31	314.56
721.94	313.47
729.62	311.58
744.13	311.34
764.78	311.28
785.28	311.20
799.60	311.20
807.14	310.90
817.76	310.41
830.10	310.42
847.55	310.50
869.54	310.33
884.87	310.19
899.26	309.94
903.99	310.08
907.99	310.07
917.99	310.00
927.99	309.98
937.99	309.82
944.99	309.78
947.99	309.56
957.99	309.55
967.99	309.45
977.99	309.38
987.99	309.33
997.99	309.32
1007.99	309.18
1017.99	309.15
1027.99	309.08
1037.99	309.12
1047.99	309.17
1057.99	309.30
1067.99	309.45
1077.99	309.65
1087.99	309.92
1097.99	310.04
1107.99	309.93
1114.99	310.03
1119.83	310.21
1130.61	310.83
1136.42	310.86
1156.36	311.34
1167.73	315.07
1172.66	317.04
1177.99	317.94
1181.85	318.65
1185.05	319.89
1187.26	319.95
1188.83	319.44
1190.18	319.40

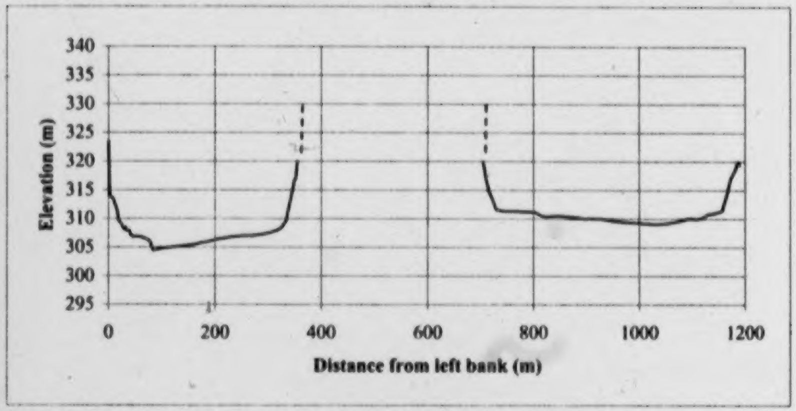

Cross Section Name: Czuy House (near treatment plant)

Distance from Bennett Dam: 398.40 km

Year of Survey: 1992

Surveyed by: Alberta Environment

Figure D.30 Cross section on the Peace River at 398.40 km downstream of the Bennett Dam (Town of Peace River subreach).

Distance from left bank (m)	Elevation (m)
0.00	314.35
5.93	313.79
7.23	312.72
9.25	312.29
22.88	311.54
36.88	310.77
50.88	310.63
64.91	310.50
84.02	310.41
103.17	310.22
123.27	310.22
143.40	310.14
162.26	309.95
181.63	309.66
209.91	309.64
230.50	309.65
248.50	309.15
266.76	309.22
300.12	308.67
309.10	307.86
310.93	308.12
315.93	307.86
321.93	307.32
325.93	307.36
330.93	307.38
335.93	307.19
345.93	306.99
355.93	306.82
365.93	306.89
375.93	306.97
385.93	307.14
395.93	307.46
409.93	307.87
414.82	307.84
423.48	308.08
437.62	308.39
452.47	308.49
465.26	308.36
480.40	308.37
493.90	308.43
510.80	308.38
529.12	308.48
546.97	308.37
564.07	308.12
572.93	308.14
575.93	307.99
585.93	307.41
595.93	307.01
605.93	306.76
615.93	306.54
625.93	306.23
635.93	305.79
645.93	305.41
655.93	305.16
665.93	305.21
675.93	305.67

Distance from left bank (m)	Elevation (m)
685.93	306.61
692.93	307.61
695.93	307.64
705.93	307.66
715.93	307.66
725.93	307.71
735.93	307.77
745.93	307.79
755.93	307.78
765.93	307.78
775.93	307.81
785.93	307.79
795.93	307.67
805.93	307.77
815.93	307.71
825.93	307.69
835.93	307.74
845.93	307.71
865.93	307.82
875.93	307.84
885.93	307.91
895.93	307.91
903.07	307.56
905.93	308.01
908.87	307.72
915.93	308.09
916.93	308.04
916.98	307.67
927.64	307.83
936.39	307.98
946.46	308.29
977.53	307.48
982.35	308.19
984.80	308.64
987.56	309.39
991.83	309.76
996.50	310.77
1003.35	311.39
1009.37	313.08
1015.41	315.46
1023.90	317.87
1028.74	318.84
1029.18	319.52

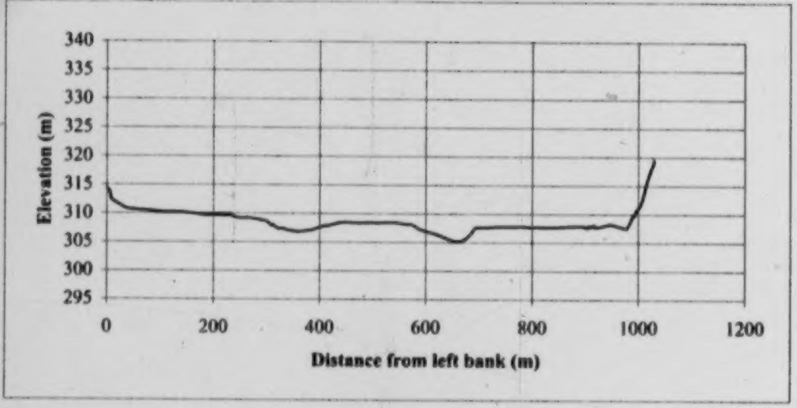

Cross Section Name:	Dick's Diving
Distance from Bennett Dam:	400.40 km
Year of Survey:	1992
Surveyed by:	Alberta Environment

Figure D.31 Cross section on the Peace River at 400.40 km downstream of the Bennett Dam (Town of Peace River subreach).

Distance from left bank (m)	Elevation (m)
0.00	317.22
3.50	317.14
11.25	315.39
14.24	315.33
15.64	314.01
23.57	310.59
28.83	309.23
33.39	307.24
37.86	306.89
45.72	306.05
53.45	305.61
62.36	304.52
72.94	305.67
74.89	307.03
77.86	308.19
98.54	309.14
117.08	309.77
123.59	307.86
144.59	307.45
154.19	307.23
168.79	306.81
177.36	306.54
186.51	307.07
200.13	307.24
229.86	307.74
256.32	307.52
266.20	307.22
278.02	306.89
285.24	306.69
288.14	306.53
290.24	306.44
291.24	306.50
301.24	306.21
311.24	305.91
321.24	305.79
331.24	305.56
341.24	305.41
351.24	305.25
361.24	305.11
371.24	304.84
381.24	304.81
391.24	304.69
401.24	304.61
411.24	304.51
421.24	304.39
431.24	304.39
441.24	304.51
451.24	304.59
461.24	304.71
471.24	304.85
481.24	304.91
491.24	304.97
501.24	304.99
511.24	305.03
521.23	305.07
531.23	305.07

Distance from left bank (m)	Elevation (m)
541.23	305.03
551.23	304.90
561.23	305.09
571.23	304.89
581.23	304.69
591.23	304.72
601.23	304.66
611.23	304.68
621.23	304.74
631.23	304.91
641.23	305.22
651.23	305.69
661.24	306.03
671.24	306.17
676.24	306.47
679.14	306.39
683.41	307.22
689.19	309.25
692.81	310.87
700.24	312.41
706.62	313.66
717.28	317.33
725.78	318.25
733.30	319.87
734.64	320.76

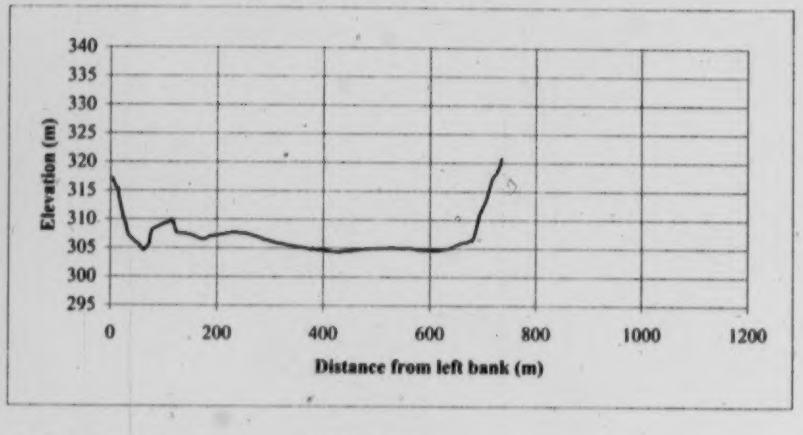

Cross Section Name:	Six Mile Farm
Distance from Bennett Dam:	404.00 km
Year of Survey:	1992
Surveyed by:	Alberta Environment

Figure D.32 Cross section on the Peace River at 404.00 km downstream of the Bennett Dam (Town of Peace River subreach).

Distance from left bank (m)	Elevation (m)
0.00	317.21
11.31	316.00
24.42	313.72
39.14	311.13
47.39	307.95
50.35	307.71
52.35	306.60
53.33	305.00
55.31	305.27
61.31	304.10
66.31	304.08
71.31	303.28
81.31	301.32
91.31	301.34
101.31	301.45
111.31	301.88
121.31	302.52
131.31	303.05
141.31	303.68
151.31	304.18
161.31	304.45
171.31	304.22
181.31	304.03
201.31	304.37
211.31	304.48
221.31	304.68
231.31	304.78
241.31	304.82
251.31	304.94
261.31	305.00
271.31	304.96
281.31	304.94
291.31	304.92
301.31	304.92
311.31	304.90
321.31	304.82
331.31	304.82
341.31	304.82
351.31	304.80
361.31	305.38
371.31	305.38
376.31	305.08
381.31	305.22
391.31	305.50
401.31	305.62
411.31	305.85
418.91	306.02
420.00	305.94
426.26	306.20
436.25	306.59
448.02	307.02
474.35	307.69
510.91	307.86
555.58	307.90
586.07	308.05
607.60	307.84
617.90	309.66
625.55	310.75
635.08	311.57
643.31	313.49
645.42	313.92
647.51	313.90
651.31	313.84
658.96	313.82
662.68	312.35
674.63	309.22
689.15	308.07
700.41	307.77
704.76	309.57
718.13	312.89
723.16	313.89
730.93	314.82
736.88	315.62

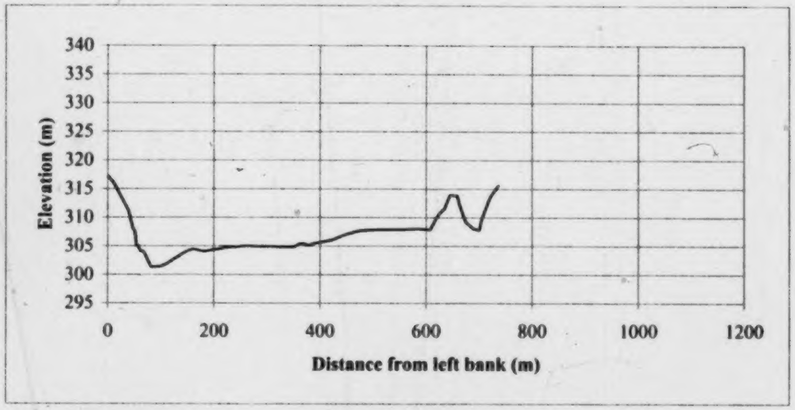

Cross Section Name:	Seven Mile Bend
Distance from Bennett Dam:	405.95 km
Year of Survey:	1992
Surveyed by:	Alberta Environment

Figure D.33 Cross section on the Peace River at 405.95 km downstream of the Bennett Dam (Town of Peace River subreach).

Distance from left bank (m)	Elevation (m)
0.00	329.14
4.77	328.44
18.32	327.89
19.82	327.79
27.40	323.58
46.74	314.08
58.59	313.19
71.89	309.58
81.77	306.30
85.40	305.61
88.32	305.48
93.32	305.22
98.32	304.88
105.32	304.52
108.32	304.65
118.32	305.22
123.32	305.30
128.32	304.02
138.32	304.75
148.32	304.32
158.32	303.98
168.32	304.00
178.32	304.03
188.32	304.12
198.32	304.38
208.32	304.50
218.32	304.40
228.32	304.32
238.32	304.24
248.32	304.20
258.32	304.20
268.32	304.27
278.32	304.32
288.32	304.35
298.32	304.30
308.32	304.40
318.32	304.32
328.32	304.30
338.32	304.25
348.32	304.03
358.32	303.82
368.32	303.44
378.32	303.10
388.32	302.88
398.32	302.66
408.32	302.50
418.32	302.37
428.32	302.38
438.32	302.38
448.32	302.49
458.32	302.67
468.32	302.85
478.32	303.08
488.32	303.52
498.32	303.94
508.32	304.00
518.32	304.20
528.32	304.30
538.32	305.00
542.82	305.36
546.10	305.35
549.65	305.60
556.32	306.22
567.51	307.38
579.09	308.55
591.73	309.18
599.73	310.55
604.73	311.69
613.39	314.27
615.45	314.32

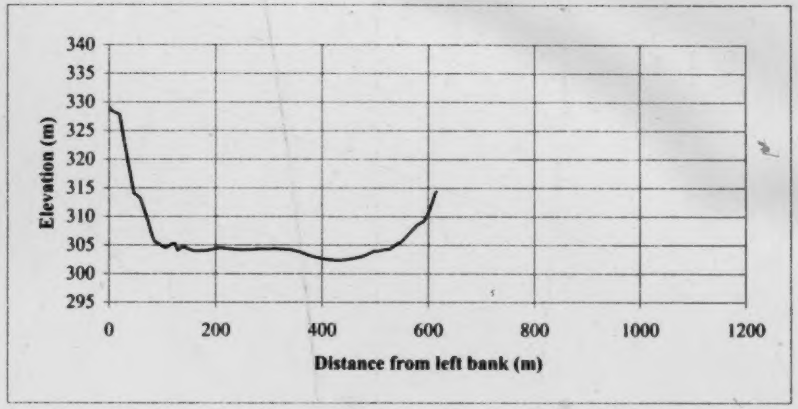

Cross Section Name:	Island 'A'
Distance from Bennett Dam:	408.58 km
Year of Survey:	1992
Surveyed by:	Alberta Environment

Figure D.34 Cross section on the Peace River at 408.58 km downstream of the Bennett Dam (Town of Peace River subreach).

Distance from left bank (m)	Elevation (m)
0.00	314.56
0.94	313.89
3.93	312.21
13.92	309.24
24.82	308.07
29.68	307.43
40.37	306.05
66.14	305.15
78.19	305.00
85.43	305.14
98.29	305.45
110.10	305.17
128.09	304.89
146.45	305.17
162.68	305.22
175.17	304.98
185.68	304.62
189.68	304.57
196.44	304.34
199.68	304.35
209.68	304.22
219.68	303.86
229.68	303.45
239.68	303.43
249.68	303.09
259.68	302.84
269.68	302.63
279.68	302.32
289.68	302.09
299.68	301.85
309.68	301.53
319.68	301.40
327.68	301.43
329.68	301.28
339.68	301.03
349.68	300.90
359.68	300.97
369.68	300.93
379.68	300.95
389.68	301.15
399.68	301.03
409.68	301.03
419.68	301.43
429.68	301.56
439.68	301.83
449.68	302.23
459.68	302.25
469.68	302.93
480.68	303.37
484.68	304.05
489.68	304.23
490.73	304.20
493.93	305.05
498.24	305.82
500.68	307.03
508.04	311.22

Distance from left bank (m)	Elevation (m)
511.25	314.28
512.23	315.01
514.62	316.35

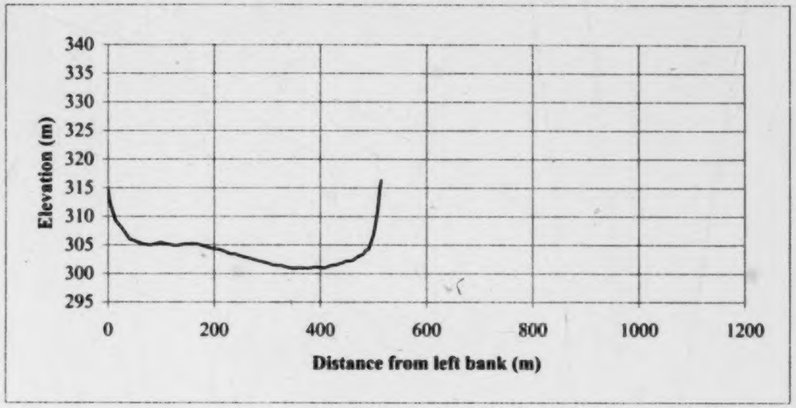

Cross Section Name: Birch Island

Distance from Bennett Dam: 411.20 km

Year of Survey: 1992

Surveyed by: Alberta Environment

Figure D.35 Cross section on the Peace River at 411.20 km downstream of the Bennett Dam (Town of Peace River subreach).

Distance from left bank (m)	Elevation (m)
0.00	315.37
7.59	313.52
26.38	308.36
33.56	308.14
40.84	305.98
55.72	304.81
57.78	304.12
70.00	304.60
72.50	304.36
80.00	302.85
85.00	302.02
90.00	301.90
96.50	301.30
100.00	301.60
102.00	302.30
107.50	300.62
110.00	301.12
120.00	301.02
130.00	302.10
132.50	302.22
140.00	301.27
150.00	300.68
160.00	300.42
170.00	299.95
175.00	299.60
180.00	299.82
185.00	300.38
190.00	300.56
198.00	298.75
200.00	298.75
205.00	298.98
210.00	298.62
215.00	298.62
218.00	298.65
219.50	297.72
220.00	297.98
230.00	298.98
240.00	299.18
250.00	300.70
256.50	301.75
260.00	301.00
262.50	300.12
270.00	300.32
273.00	300.60
280.00	300.20
290.00	300.00
300.00	300.26
305.00	300.86
310.00	301.30
316.00	302.62
320.00	302.52
325.00	303.00
330.00	303.18
331.50	304.08
340.00	302.50
341.00	302.20
342.50	302.35
347.50	300.85
350.00	300.90
360.00	301.38
366.00	300.96
370.00	301.18
372.50	301.32
380.00	301.03
390.00	300.92
400.00	300.92
410.00	301.02
420.00	301.38
426.50	301.82
430.00	301.60
437.00	300.98
440.00	301.62
445.00	303.85
450.00	303.63
460.00	304.48
492.00	304.58
501.78	304.65
509.53	304.85
517.29	306.00
524.52	308.23
538.04	312.17
549.76	312.38

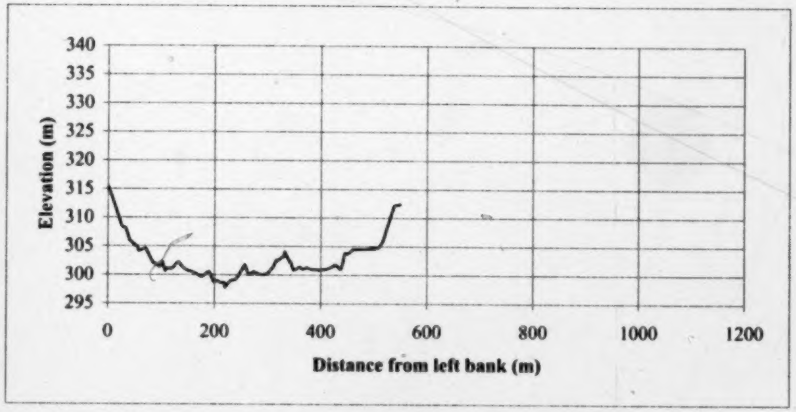

Cross Section Name:	Daishowa bridge (downstream side)
Distance from Bennett Dam:	412.39 km
Year of Survey:	1992
Surveyed by:	Alberta Environment

Figure D.36 Cross section on the Peace River at 412.39 km downstream of the Bennett Dam (Town of Peace River subreach).

Distance from left bank (m)	Elevation (m)
0.00	314.60
15.84	310.24
22.27	308.78
34.99	306.05
64.17	305.84
64.18	304.80
64.30	298.60
80.00	300.53
86.50	300.80
90.00	300.50
100.00	300.15
110.00	300.22
120.00	299.85
124.00	299.58
130.00	299.82
140.00	300.26
150.00	300.82
160.00	301.40
166.00	301.85
170.00	301.90
180.00	301.76
190.00	301.38
200.00	301.28
210.00	301.31
220.00	301.45
230.00	301.50
240.00	301.45
247.00	301.22
260.00	300.68
270.00	300.38
280.00	300.50
290.00	300.63
300.00	300.97
310.00	301.43
320.00	301.87
330.00	302.43
340.00	302.67
350.00	302.78
360.00	302.76
370.00	302.72
375.00	302.74
390.00	302.99
410.00	303.12
420.00	303.20
430.00	303.25
440.00	303.32
450.00	303.32
460.00	303.18
470.00	303.58
473.00	304.18
476.57	304.45
477.30	304.84
479.71	305.59
483.90	306.57
488.24	309.42
496.26	312.78
497.63	313.95

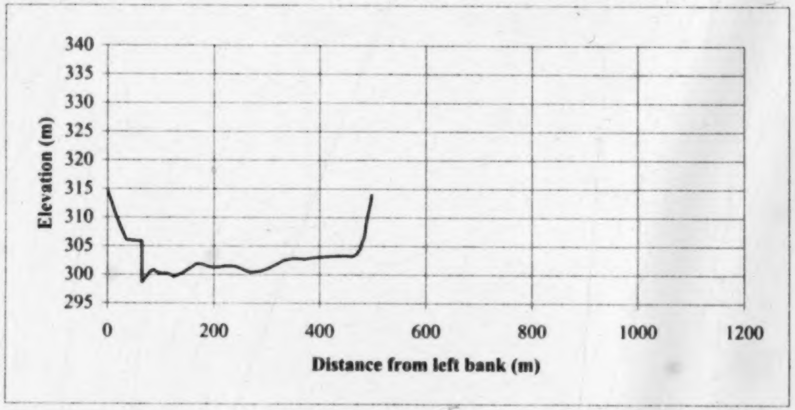

Cross Section Name:	Daishowa Intake
Distance from Bennett Dam:	412.84 km
Year of Survey:	1992
Surveyed by:	Alberta Environment

Figure D.37 Cross section on the Peace River at 412.84 km downstream of the Bennett Dam (Town of Peace River subreach).

Distance from left bank (m)	Elevation (m)
0.00	311.81
7.26	311.84
11.44	311.27
25.63	306.70
54.64	305.97
73.01	306.44
96.23	307.30
116.10	307.24
145.94	307.33
171.45	307.30
210.72	307.19
247.89	306.30
287.23	305.35
316.98	304.23
331.08	303.56
338.95	302.88
341.26	302.79
347.26	302.29
357.26	301.86
377.26	300.64
387.26	300.66
397.26	300.49
407.26	300.22
417.26	300.04
427.26	299.92
437.26	299.64
447.26	299.64
457.26	299.56
467.26	299.71
477.26	299.84
487.26	300.02
497.26	300.16
507.26	300.42
517.26	300.42
527.26	300.40
537.26	300.37
547.26	300.37
557.26	300.32
567.26	300.49
577.26	300.48
587.26	300.34
597.26	300.62
607.26	301.19
617.26	301.92
619.76	302.92
622.26	302.86
622.73	302.76
624.55	303.12
626.00	303.63
626.61	304.08
635.46	307.28
642.26	309.79
652.13	312.20
679.26	312.02
699.46	312.06

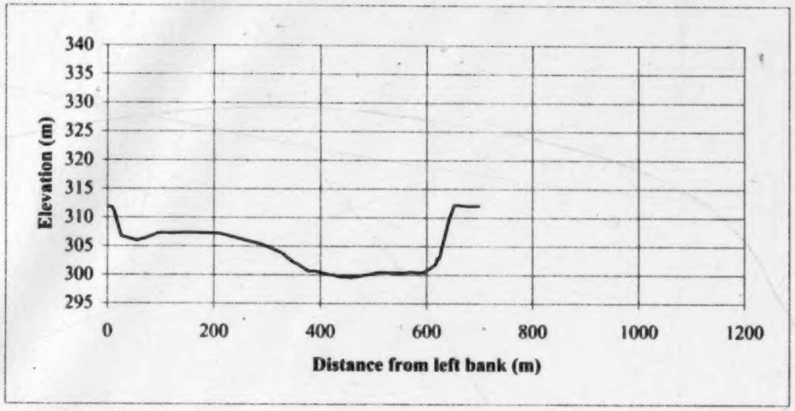

Cross Section Name:	Shell Intake
Distance from Bennett Dam:	415.65 km
Year of Survey:	1992
Surveyed by:	Alberta Environment

Figure D.38 Cross section on the Peace River at 415.65 km downstream of the Bennett Dam (Town of Peace River subreach).

Distance from left bank (m)	Elevation (m)
0.00	265.20
13.70	262.70
18.30	259.70
24.40	256.60
27.40	254.20
36.60	251.60
53.30	248.40
57.90	246.00
64.00	245.10
73.20	244.10
91.40	242.80
103.60	241.60
111.30	240.20
120.40	238.20
128.00	237.80
134.10	237.70
138.70	236.20
146.30	235.90
155.40	236.80
163.10	237.10
167.60	236.40
178.30	237.10
189.00	236.50
204.20	236.60
225.60	238.20
249.90	240.20
265.20	240.20
277.40	240.80
289.60	241.10
303.30	242.00
323.10	243.20
350.50	243.70
361.20	243.80
388.60	244.30
402.30	244.20
428.20	244.80
445.00	244.90
454.20	244.40
469.40	244.90
476.10	244.00
481.60	245.10
484.60	245.10
493.80	244.80
502.90	245.10
506.00	244.80
522.10	246.90
524.30	248.70
539.50	250.80
548.60	252.20
579.10	253.10
591.30	253.00
618.70	254.20
649.20	254.40
667.50	254.00
682.80	254.40
707.10	254.20

Distance from left bank (m)	Elevation (m)
731.50	254.80
774.20	255.60

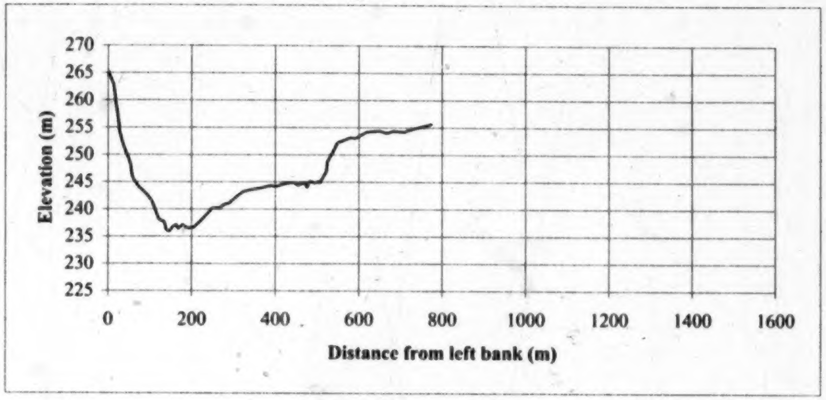

ARC Peace River IFN-Fisheries Cross Section No.: F

Distance from Bennett Dam: 804.30 km

Provided by: Alberta Environment

Figure D.39 Cross section on the Peace River at 804.30 km downstream of the Bennett Dam (Fort Vermilion subreach).

Distance from left bank (m)	Elevation (m)
0.00	263.50
30.50	262.70
51.80	260.80
70.10	260.20
79.20	257.90
86.90	255.40
91.40	252.40
94.50	251.30
106.70	250.40
109.70	249.30
128.00	247.20
134.10	245.20
140.20	244.60
147.20	243.80
164.60	242.70
179.80	243.20
210.30	238.40
225.20	236.80
225.60	237.50
237.70	237.70
256.00	238.40
271.30	237.60
286.50	237.40
298.40	236.80
299.30	237.70
318.20	238.40
326.40	238.00
338.30	238.40
347.50	240.20
359.70	240.70
367.30	240.80
371.90	241.10
376.40	240.80
387.10	240.50
392.60	240.50
399.30	239.00
406.90	240.20
429.80	241.20
450.50	242.40
481.60	243.50
512.10	244.20
527.30	245.00
556.30	245.40
562.40	245.40
573.00	245.70
580.60	245.70
602.00	246.50
621.80	246.70
630.90	247.00
658.40	247.50
676.70	248.70
688.80	249.40
694.90	250.70
697.70	253.30
713.20	252.60
725.40	252.70
734.60	253.40
737.60	254.60
743.70	254.70
755.90	254.50

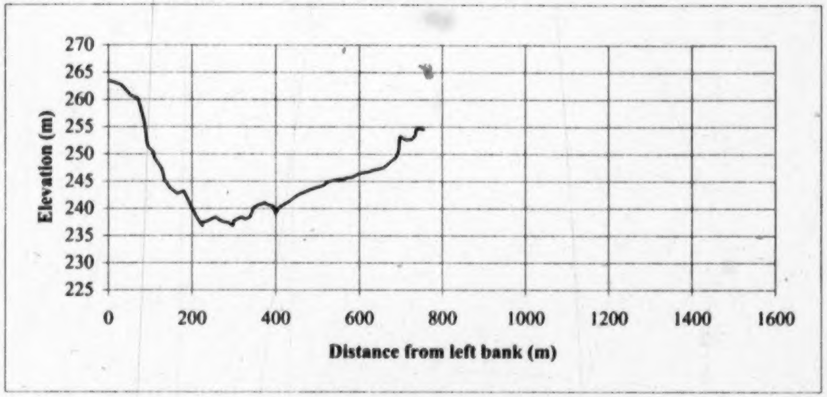

ARC Peace River IFN-Fisheries Cross Section No.: A

Distance from Bennett Dam: 806.00 km

Provided by: Alberta Environment

Figure D.40 Cross section on the Peace River at 806.00 km downstream of the Bennett Dam (Fort Vermilion subreach).

Distance from left bank (m)	Elevation (m)
0.00	255.30
8.50	255.10
13.70	253.30
29.00	253.70
36.60	253.10
48.80	253.30
59.40	253.00
68.60	249.00
77.70	247.50
88.40	246.60
96.00	246.30
120.40	246.10
149.40	245.70
163.10	245.80
179.80	245.70
187.50	245.70
196.60	246.00
211.80	245.70
242.30	245.80
257.60	245.50
272.80	245.40
303.30	244.80
321.60	244.40
333.80	244.10
339.90	244.40
344.40	243.20
349.60	243.70
362.70	243.20
370.30	242.70
385.60	243.20
394.70	242.90
423.70	242.70
440.40	241.80
455.70	242.10
458.70	241.70
472.40	241.40
485.50	242.10
495.30	240.90
507.50	241.10
515.10	240.80
524.30	241.10
536.40	239.90
554.70	241.50
568.50	240.20
574.50	241.40
606.60	241.60
618.70	242.50
624.80	241.80
641.60	243.50
658.40	243.60
672.10	243.60
681.20	242.30
687.90	243.90
705.00	243.90
714.80	242.00
717.80	242.70
726.90	243.60
734.60	243.10
742.20	243.10
749.80	243.70
765.00	244.00
772.70	243.50
781.80	244.00
797.10	243.50
815.90	243.20
833.60	246.00
842.80	246.60
848.90	248.70
851.90	248.60
855.00	252.40
861.10	252.30
883.90	252.10
897.60	252.30
900.70	252.80
919.00	252.60
938.80	252.50
943.40	252.20
955.50	252.40
960.10	253.70
964.70	253.70
976.90	253.40
981.50	254.10
986.00	255.30
991.50	256.20
995.20	256.20

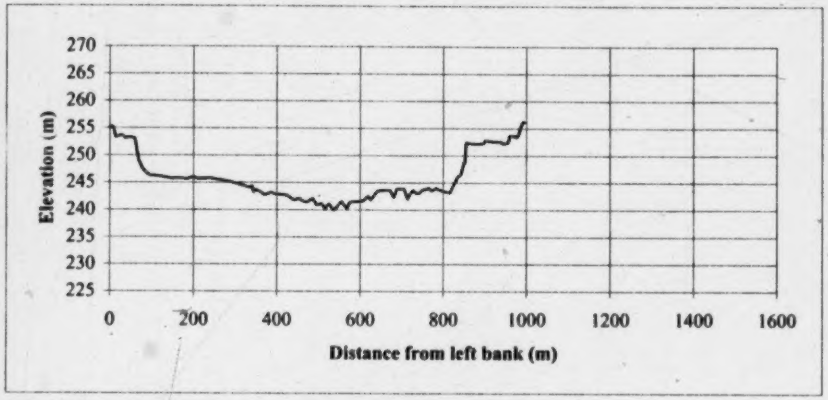

ARC Peace River IFN-Fisheries Cross Section No.: U - 1

Distance from Bennett Dam: 807.00 km

Provided by: Alberta Environment

Figure D.41 Cross section on the Peace River at 807.00 km downstream of the Bennett Dam (Fort Vermilion subreach).

Distance from left bank (m)	Elevation (m)
0.00	254.40
3.00	255.30
9.80	255.20
15.80	253.40
28.00	251.90
73.80	251.50
95.10	251.40
110.30	251.50
125.60	250.10
165.20	248.00
195.70	244.30
201.80	244.60
220.10	245.10
226.20	244.40
238.40	245.20
253.60	244.90
271.90	245.40
284.10	245.70
313.00	245.80
332.80	246.10
363.30	246.20
387.70	246.10
406.00	245.80
424.30	245.30
436.50	245.20
445.60	246.10
448.70	248.30
455.40	251.60
456.30	252.70
564.50	251.60
704.70	254.70
811.40	254.80
848.00	254.20
854.00	253.60
863.20	253.30
866.20	251.20
872.30	249.60
890.60	249.30
922.60	249.90
957.70	250.70
969.00	250.90
982.10	250.90
994.30	250.70
1006.40	250.50
1033.90	249.10
1046.10	249.00
1056.70	248.70
1067.40	248.10
1081.10	247.50
1100.90	246.00
1116.20	245.70
1128.40	244.90
1131.40	245.20
1166.50	242.60
1189.30	241.40
1216.80	240.30
1255.80	238.20
1262.50	237.50
1268.60	237.90
1283.80	236.50
1289.90	236.50
1299.10	236.70
1314.30	238.50
1326.50	239.00
1344.80	240.30
1355.40	242.00
1361.50	243.20
1369.20	243.40
1393.50	243.20
1405.70	243.30
1414.90	243.80
1436.20	246.90
1457.60	251.30
1463.00	253.60
1463.60	255.70
1467.00	257.90
1471.30	258.60
1488.00	259.10

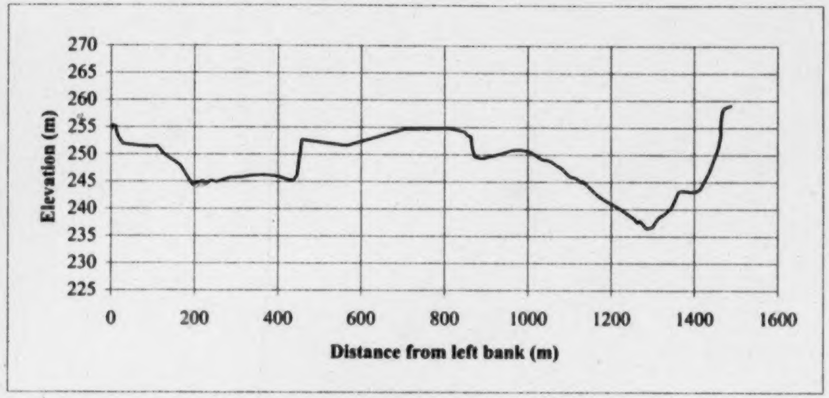

ARC Peace River IFN-Fisheries Cross Section No.: G

Distance from Bennett Dam: 809.50 km

Provided by: Alberta Environment

Figure D.42 Cross section on the Peace River at 809.50 km downstream of the Bennett Dam (Fort Vermilion subreach).

Distance from left bank (m)	Elevation (m)
13.70	253.70
21.90	253.90
30.50	251.20
33.50	248.10
36.60	246.90
64.00	245.70
112.80	247.20
125.00	248.10
131.10	252.50
143.30	250.90
153.90	251.00
167.60	250.90
184.40	250.30
198.10	250.90
228.60	250.90
237.10	251.50
238.40	252.80
262.10	253.40
609.60	254.80
847.30	253.40
865.60	253.00
870.80	252.20
877.80	252.50
880.90	251.20
881.20	249.90
890.00	248.30
896.10	246.90
908.30	246.30
932.70	245.70
972.30	244.20
993.60	243.70
1002.80	243.40
1011.90	242.60
1024.10	240.80
1036.30	239.90
1054.60	237.70
1066.80	236.50
1072.90	236.20
1088.10	236.20
1106.40	236.80
1115.60	236.90
1121.70	236.70
1130.80	236.90
1136.90	236.50
1140.00	235.90
1149.10	237.10
1153.70	237.20
1158.20	237.10
1165.90	236.80
1173.50	237.10
1178.10	237.20
1185.70	237.70
1202.40	236.50
1213.10	237.10
1225.30	237.00
1229.90	236.40
1240.50	236.40
1243.60	235.90
1250.30	235.90
1261.90	238.00
1271.60	241.40
1277.10	242.90
1283.50	243.60
1292.40	243.80
1310.60	243.70
1316.70	243.30
1322.80	243.80
1335.00	246.60
1347.80	249.30
1356.40	250.90
1359.40	252.50
1371.60	255.40
1374.60	255.50
1377.70	256.30
1389.90	256.40

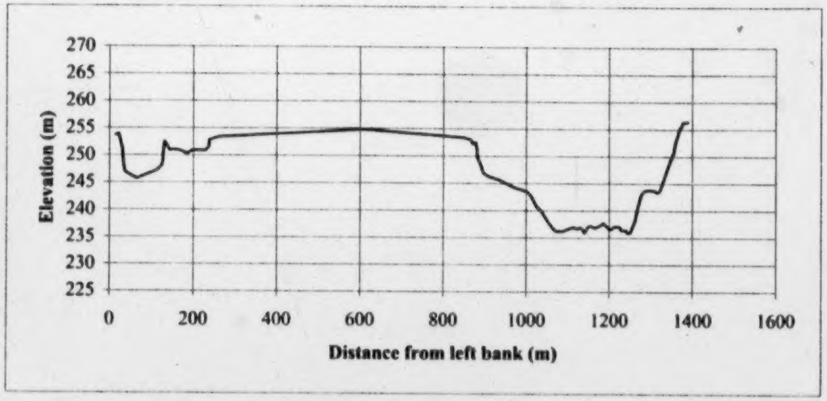

ARC Peace River IFN-Fisheries Cross Section No.: D 1

Distance from Bennett Dam: 810.80 km

Provided by: Alberta Environment

Figure D.43 Cross section on the Peace River at 810.80 km downstream of the Bennett Dam (Fort Vermilion subreach).

Distance from left bank (m)	Elevation (m)
27.40	251.90
38.10	251.40
39.60	249.90
47.50	249.50
57.90	244.40
61.30	243.20
78.00	240.80
91.40	239.60
106.70	238.80
121.90	238.50
170.10	239.50
176.80	238.80
185.30	239.80
201.20	239.70
215.80	238.90
216.70	240.20
225.60	240.80
231.60	240.20
237.70	240.10
243.50	240.20
243.80	240.80
256.60	240.80
271.30	241.50
277.40	241.00
288.30	241.10
304.80	240.60
308.20	240.30
315.80	241.20
322.80	240.60
332.20	240.20
337.70	240.50
341.40	240.30
345.00	239.90
352.00	240.10
353.90	240.40
375.20	241.60
382.50	241.60
402.30	241.00
426.70	241.10
437.40	241.00
446.50	241.10
466.00	241.00
469.40	241.40
470.90	241.40
475.50	241.10
506.00	241.10
518.20	241.50
536.40	242.00
552.00	242.10
554.70	242.60
566.90	244.60
576.10	245.70
590.10	246.90
592.80	247.50
597.40	249.50
606.60	249.90
609.60	250.70
618.70	250.80
621.80	252.10

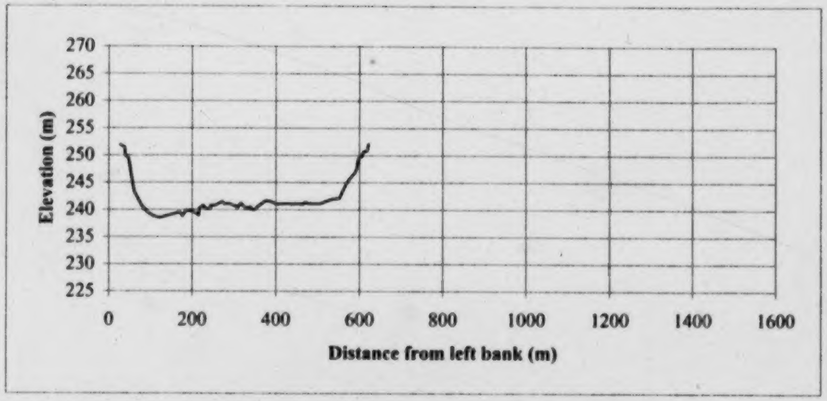

ARC Peace River IFN-Fisheries Cross Section No.: D 2

Distance from Bennett Dam: 812.00 km

Provided by: Alberta Environment

Figure D.44 Cross section on the Peace River at 812.00 km downstream of the Bennett Dam (Fort Vermilion subreach).